Enlightening the properties of the Higgs boson with the ATLAS Experiment using full Run-2 LHC data

Gaetano Αθανάσιος Barone

Brookhaven National Laboratory

BNL,

January 2021

Matter

Fermions

$s = 1/2$

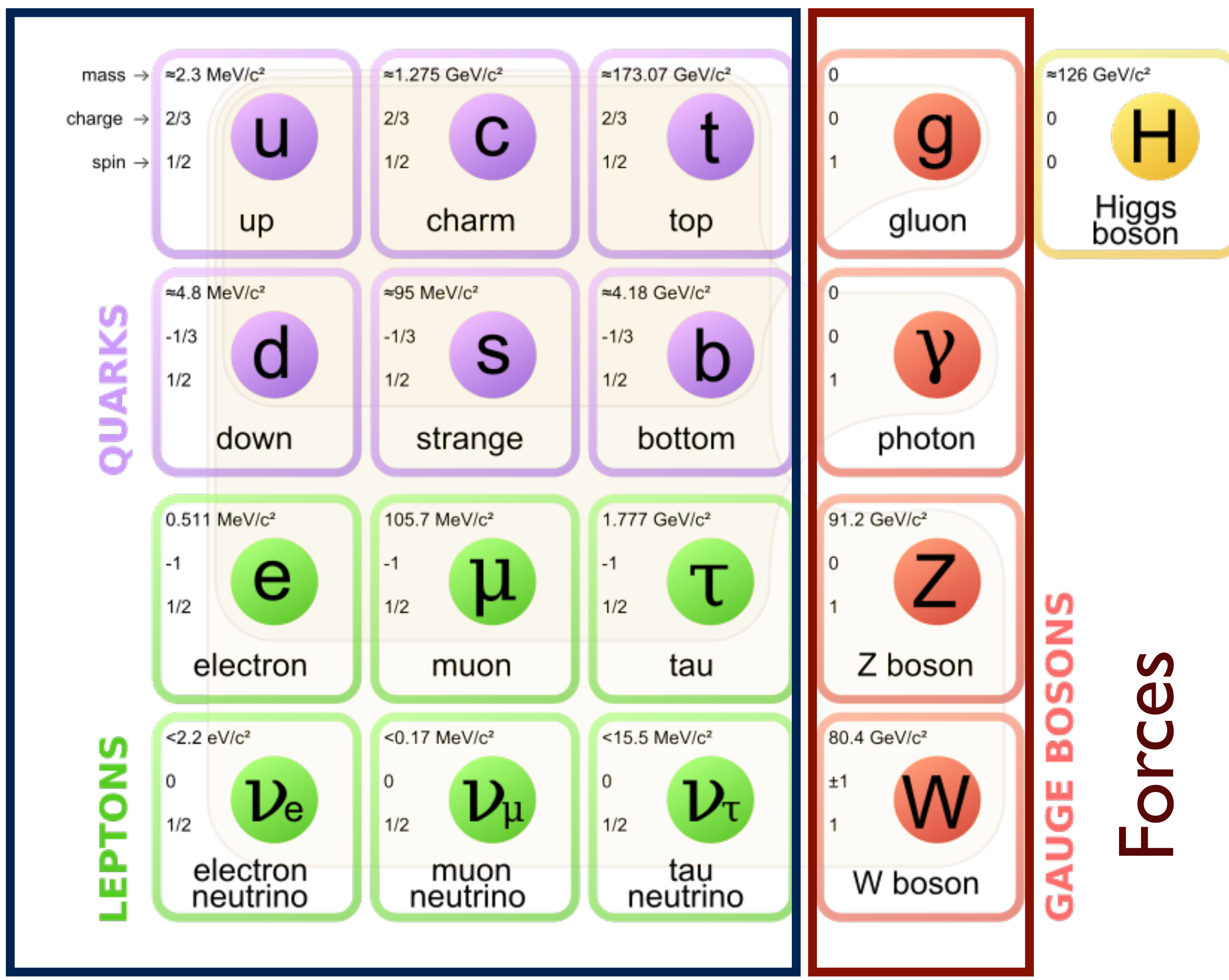

Forces

Fields

Higgs boson kinematics

- Higgs boson kinematics:
  - $p_{T,4\ell}$: Lagrangian structure of H interactions.

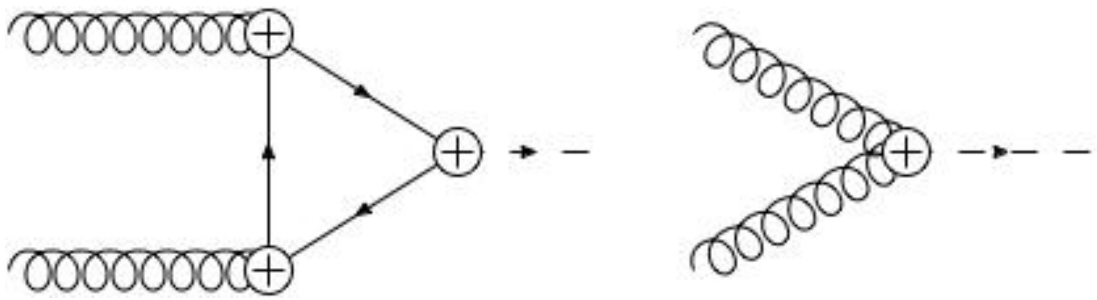

- Sensitivity to phenomena resonant at higher energies → changes in observables at lower energies.

$$\frac{c_1}{\Lambda^2}\mathcal{O}_1 \to \frac{\alpha_S}{\pi v} c_g h G^a_{\mu\nu} G^{a,\mu\nu}\,,$$

c_g: ggH contact interaction

$$\frac{c_2}{\Lambda^2}\mathcal{O}_2 \to \frac{m_t}{v} c_t h\bar{t}t\,,$$

$$\frac{c_3}{\Lambda^2}\mathcal{O}_3 \to \frac{m_b}{v} c_b h\bar{b}b\,,$$

c_t: t and b Yukawa couplings

$$\frac{c_4}{\Lambda^2}\mathcal{O}_4 \to c_{tg}\underbrace{\frac{g_S m_t}{2v^3}(v+h)G^a_{\mu\nu}(\bar{t}_L\sigma^{\mu\nu}T^a t_R + h.c)}_{}$$

c_{tg}: dipole-moment, g-t interaction

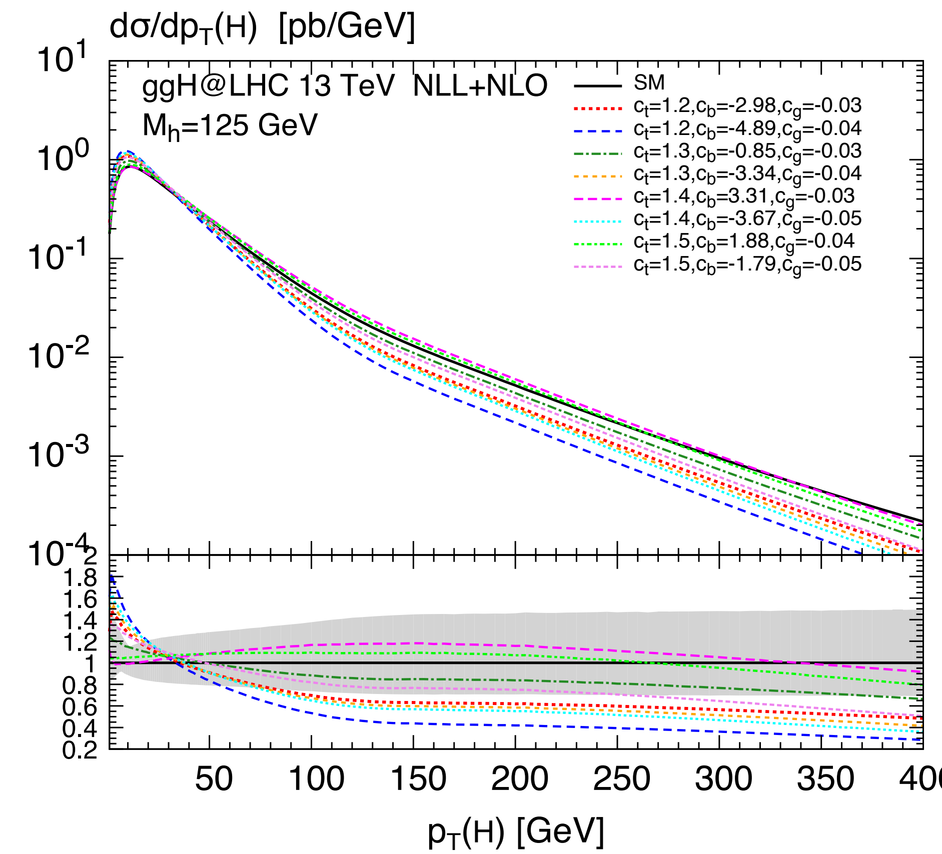

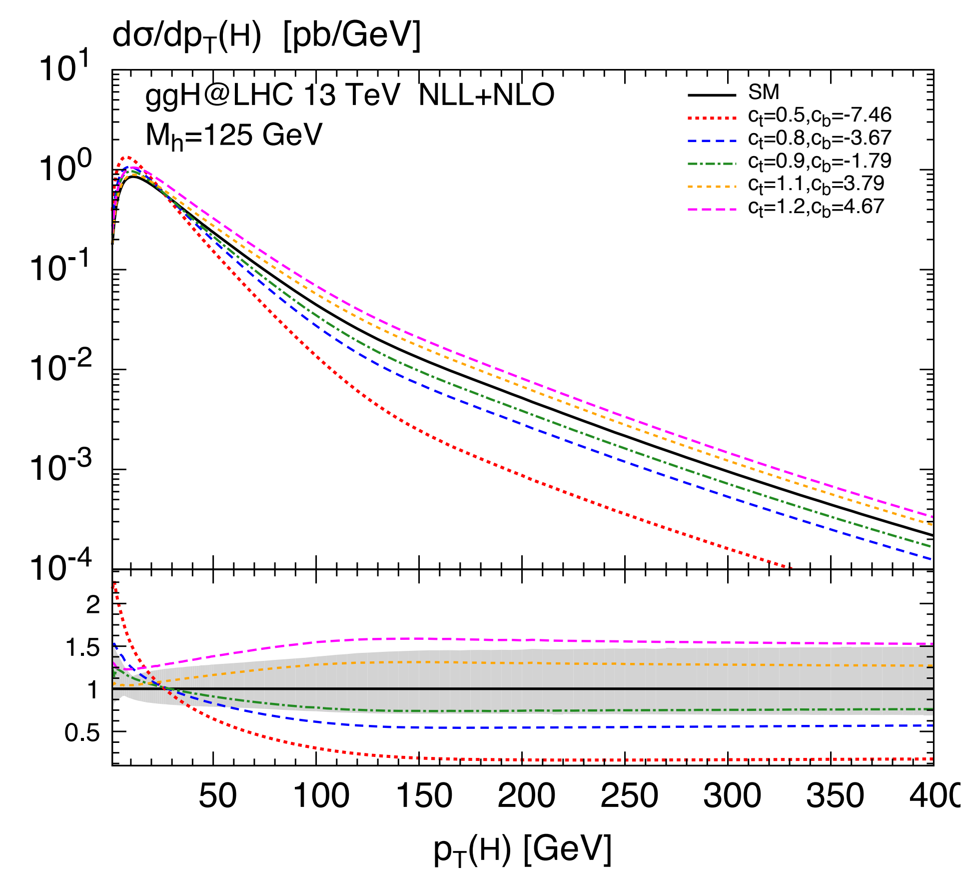

Grazzini *et al.* `arXiv:1612.00283`

Introduction

- Higgs boson (*H*) main production in proton-proton collisions:
  - Predominant production gluon-gluon fusion (87%) and VBF (6.8)
  - W, Z associated production (4%) and $t\bar{t}H$ (<1%)

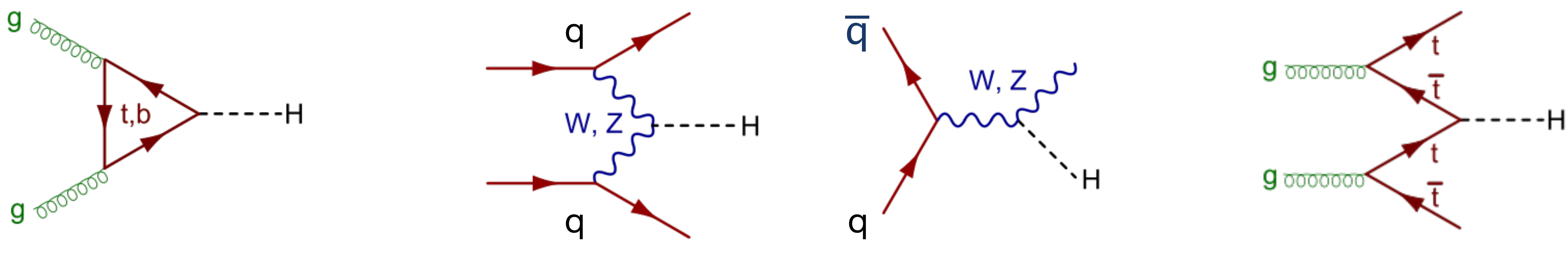

ggF VBF WH, ZH $t\bar{t}H$

- Experimentally challenging final states
  - In association with additional jets, same final state of many other processes
  - forward jets with large rapidity gap, small rates

Introduction

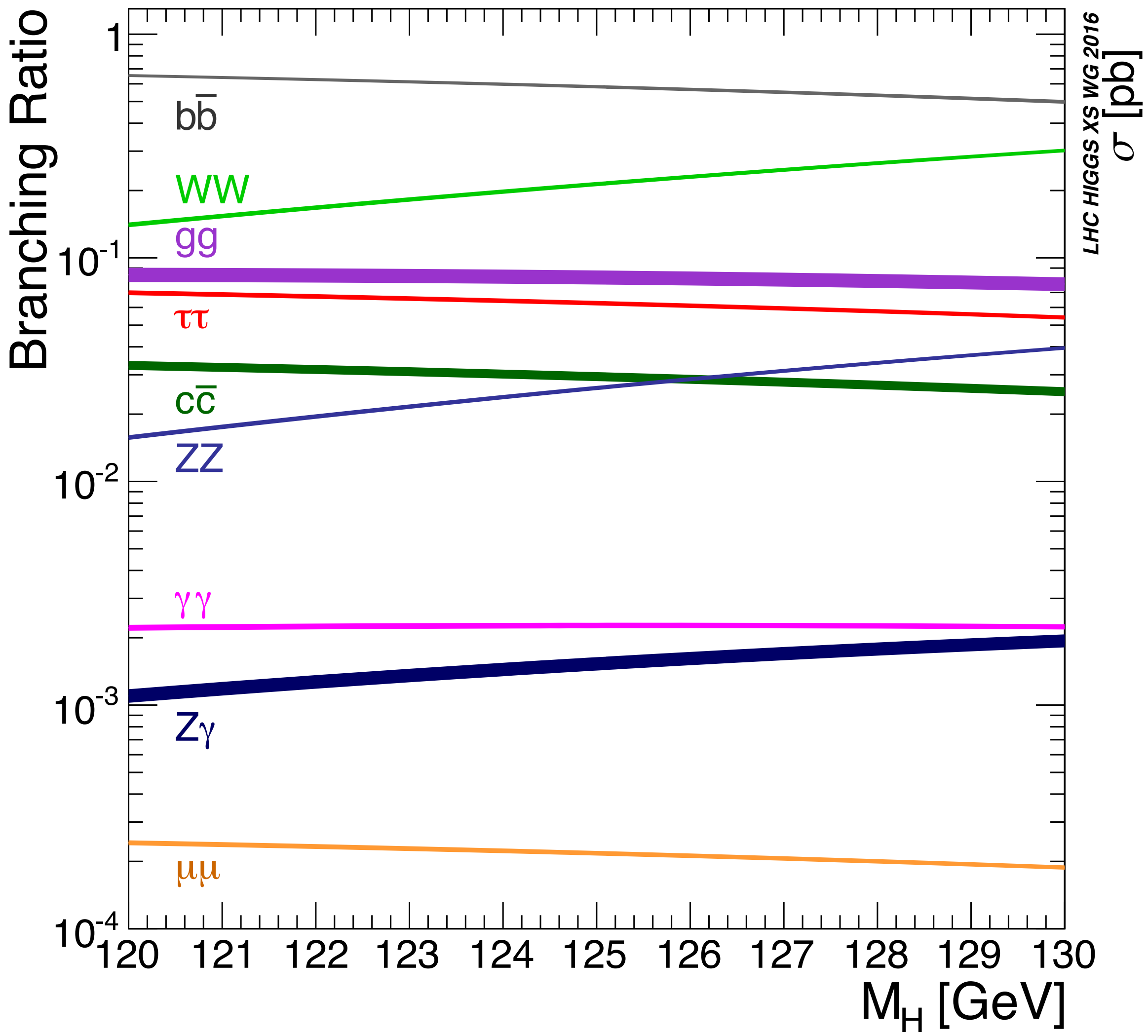

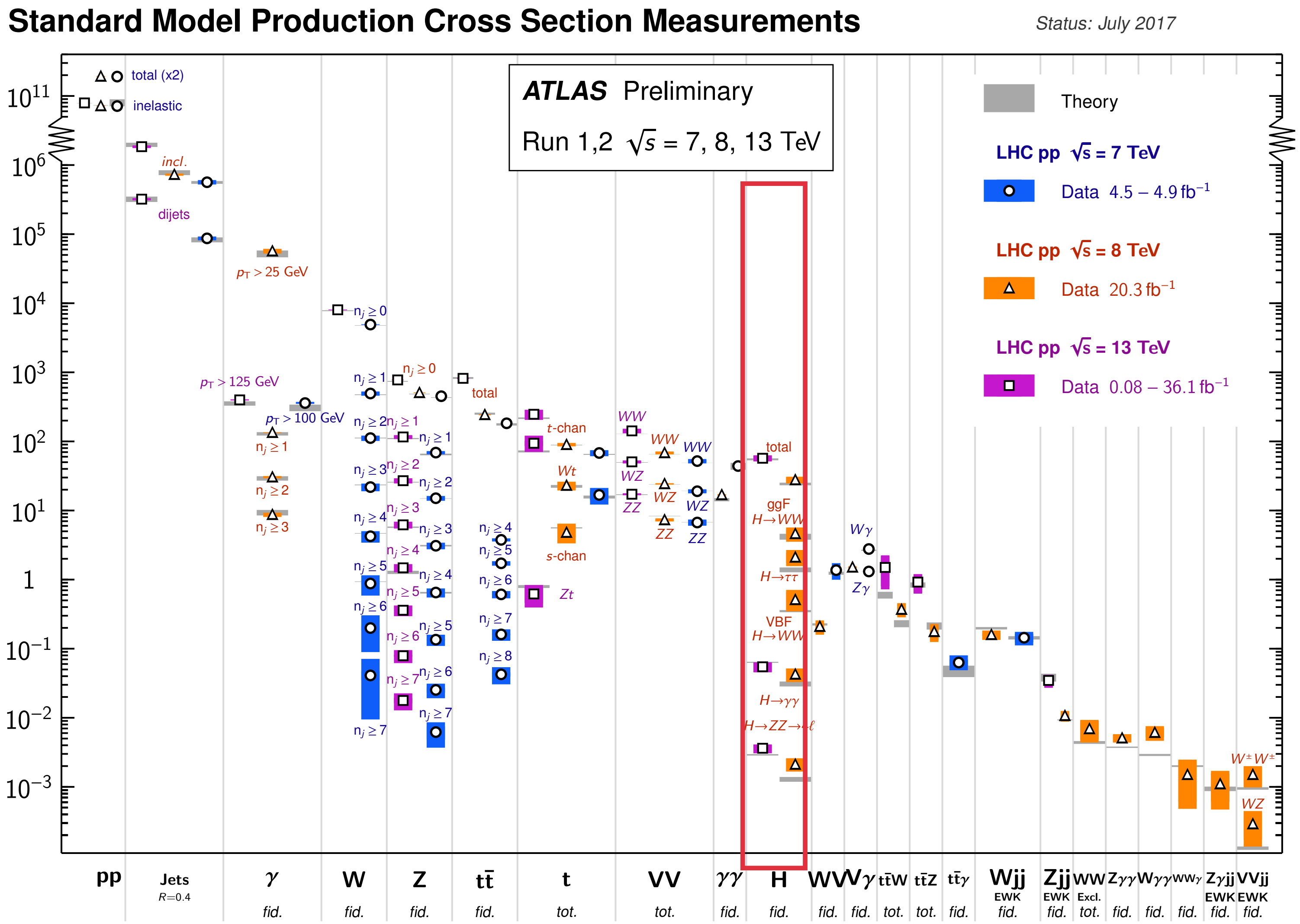

- Channels considered in this talk :

  (i) $H \rightarrow$ Dibosons ($ZZ^* \rightarrow 4\ell$, $WW^* \rightarrow \ell\bar{\nu}\bar{\ell}\nu$), and $\gamma\gamma$

  (ii) $H \rightarrow$ light leptons (ee,$\mu\bar{\mu}$)

Run 1 Legacy

- Run-1 featured *in primis* the discovery
  - First properties measurements
  - Programme largely limited by statistical accuracy.

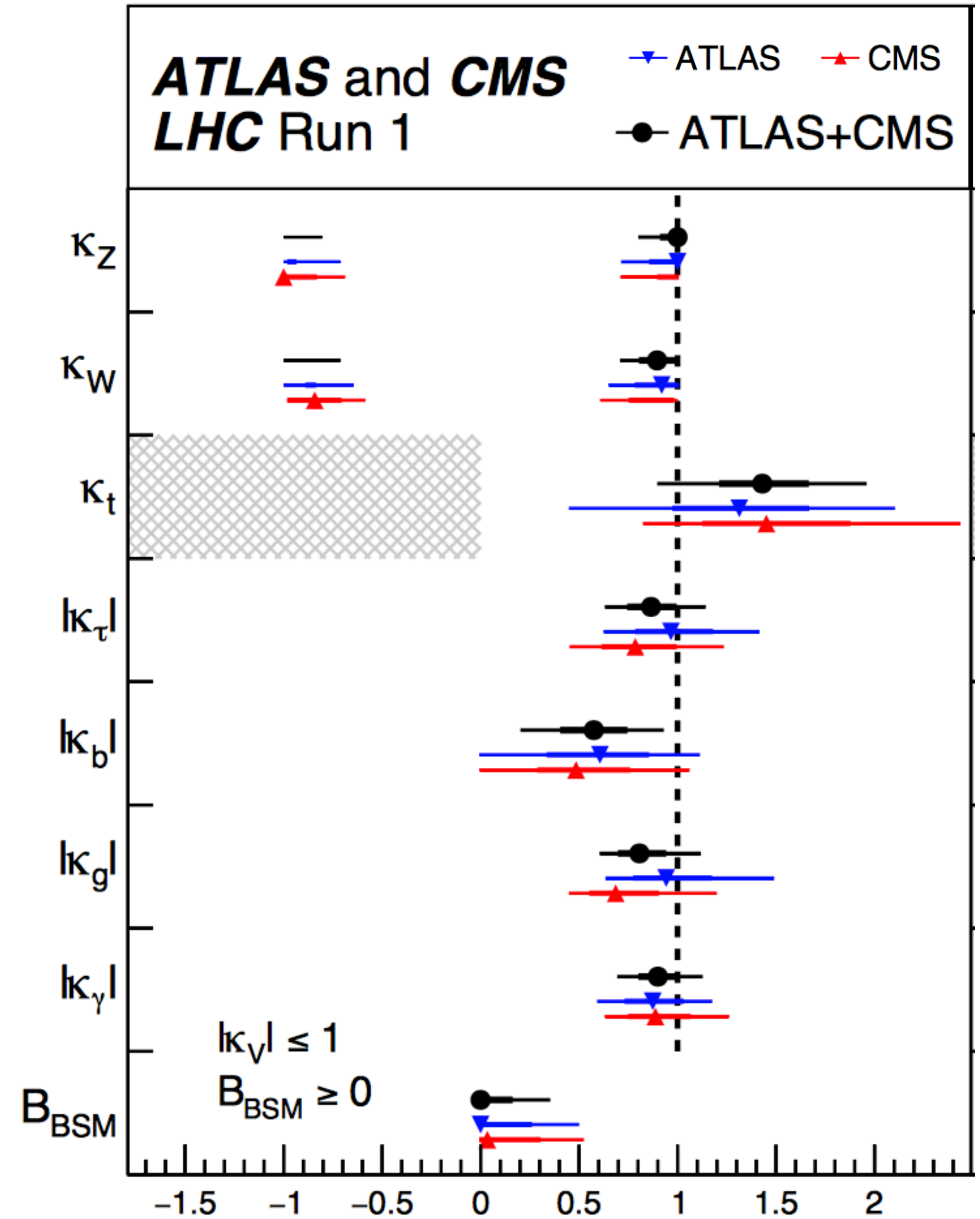

- Properties:
  - ATLAS precision in m_H of 0.33%:
  - Couplings measured to 10% to 25% precision
  - $H \to \text{inv.}$ constrained to < 30%
  - First studies of $J^{PC} = 0^{++}$, (indirect) width $\Gamma_H < 14.4$ MeV (15.2 MeV)

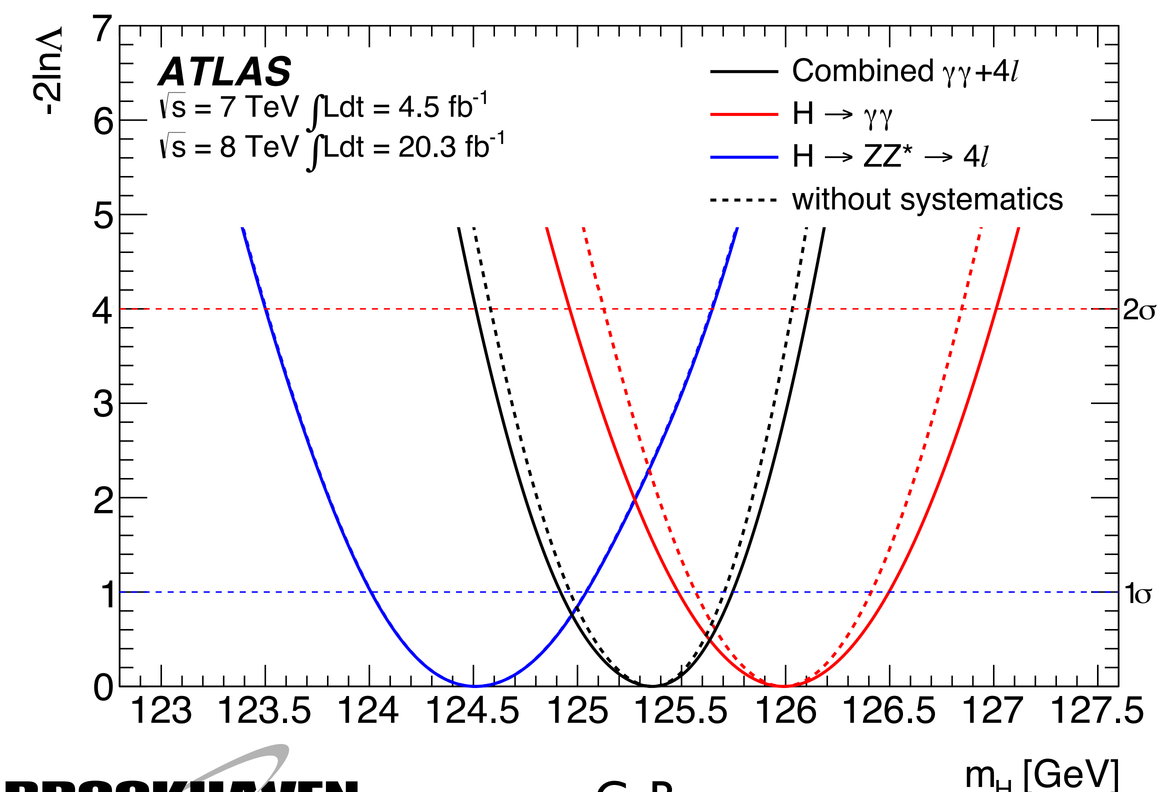

Channel	Mass measurement [GeV]
$H \to \gamma\gamma$	$125.98 \pm 0.42\,(\text{stat}) \pm 0.28\,(\text{syst}) = 125.98 \pm 0.50$
$H \to ZZ^* \to 4\ell$	$124.51 \pm 0.52\,(\text{stat}) \pm 0.06\,(\text{syst}) = 124.51 \pm 0.52$
Combined	$125.36 \pm 0.37\,(\text{stat}) \pm 0.18\,(\text{syst}) = 125.36 \pm 0.41$

Overview

- ATLAS collected 139 fb^{-1} in Run 2
  - Sufficient statistics for precision-level measurements.
  - Path open to exploration of SM Lagrangian in the Eelectro-Weak symmetry braking sector.
  - Probe to couplings to bosons and fermions
  - Understand structure of its potential.

$$\begin{aligned}\mathcal{L} &= -\frac{1}{4}F_{\mu\nu}F^{\mu\nu} \\ &+ i\bar{\Psi}\not{D}\psi \\ &+ D_\mu\Phi^\dagger D^\mu\Phi - V(\Phi) \\ &+ \bar{\Psi}_L\hat{Y}\Phi\Psi_R + h.c.\end{aligned}$$

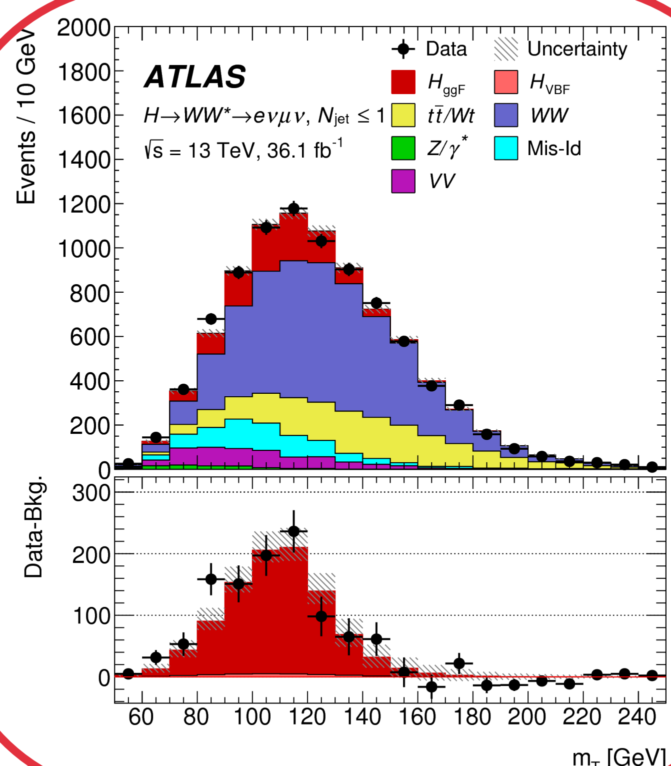

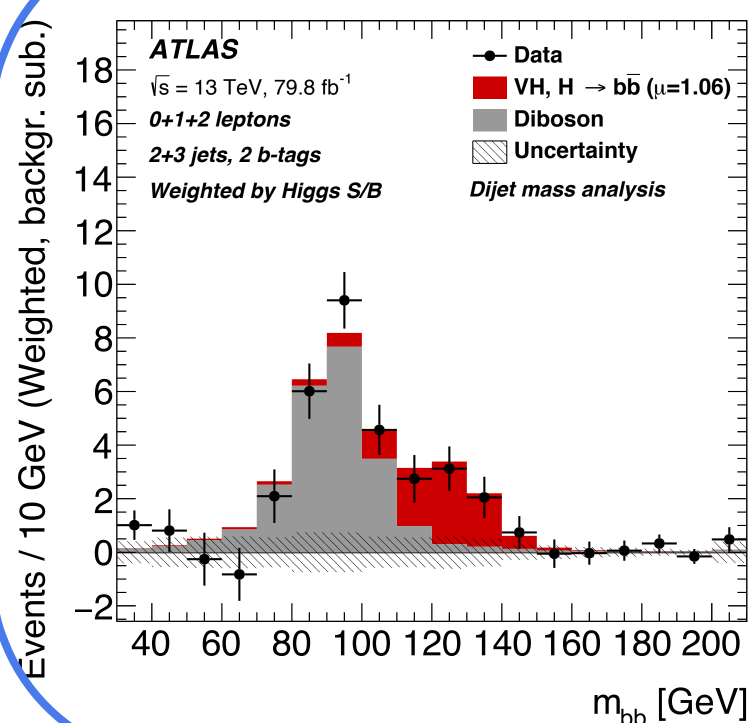

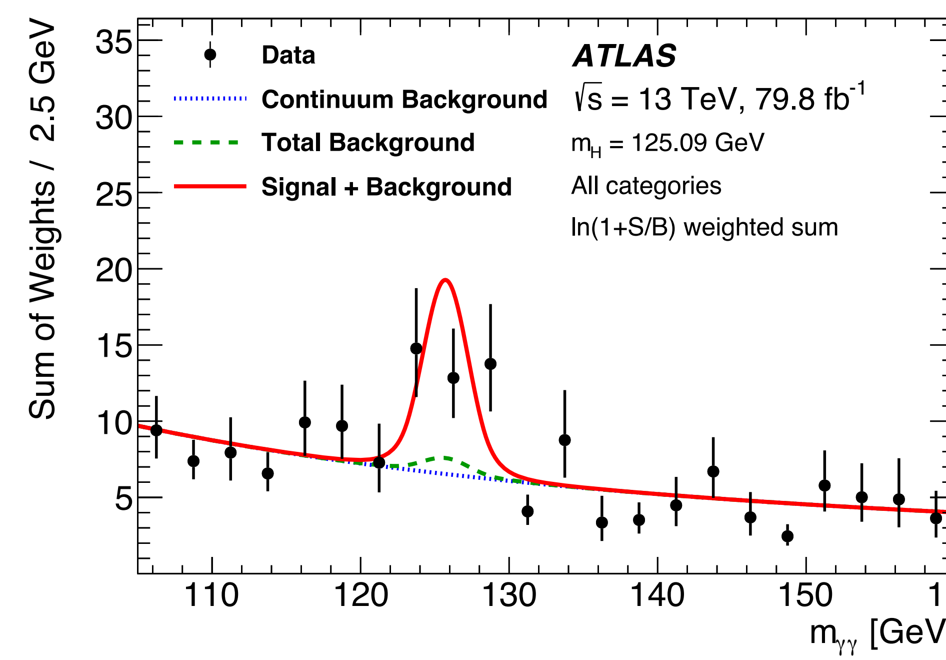

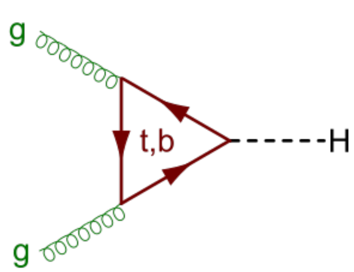

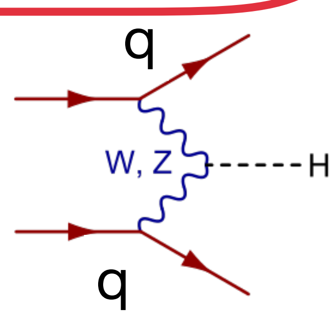

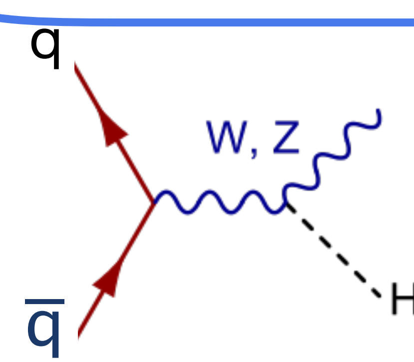

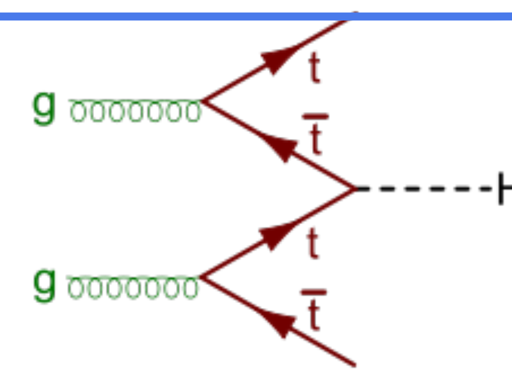

ggF VBF: 6.5 σ

VH: 5.3 σ

$t\bar{t}H$: 5.8 σ

2. Mass measurement

Introduction

Mass measurement

- The Higgs boson mass (m_H) is a fundamental free parameter of the Standard Model.

$$V(h) \quad = \quad \frac{1}{4}\lambda h^4 + \lambda v h^3 + \lambda v^2 h^2$$

  - Understanding the perturbative expansion of its potential ($\lambda v^2 h^2$)
  - Precision determination allows for evermore precise higher order corrections to the cross section.
  - Sensitivity to new physics in higher order corrections.
  - Input to precision Electro Weak global fit.
  - Key measurement of the LHC program.

- Aim in improving significantly on δm_H

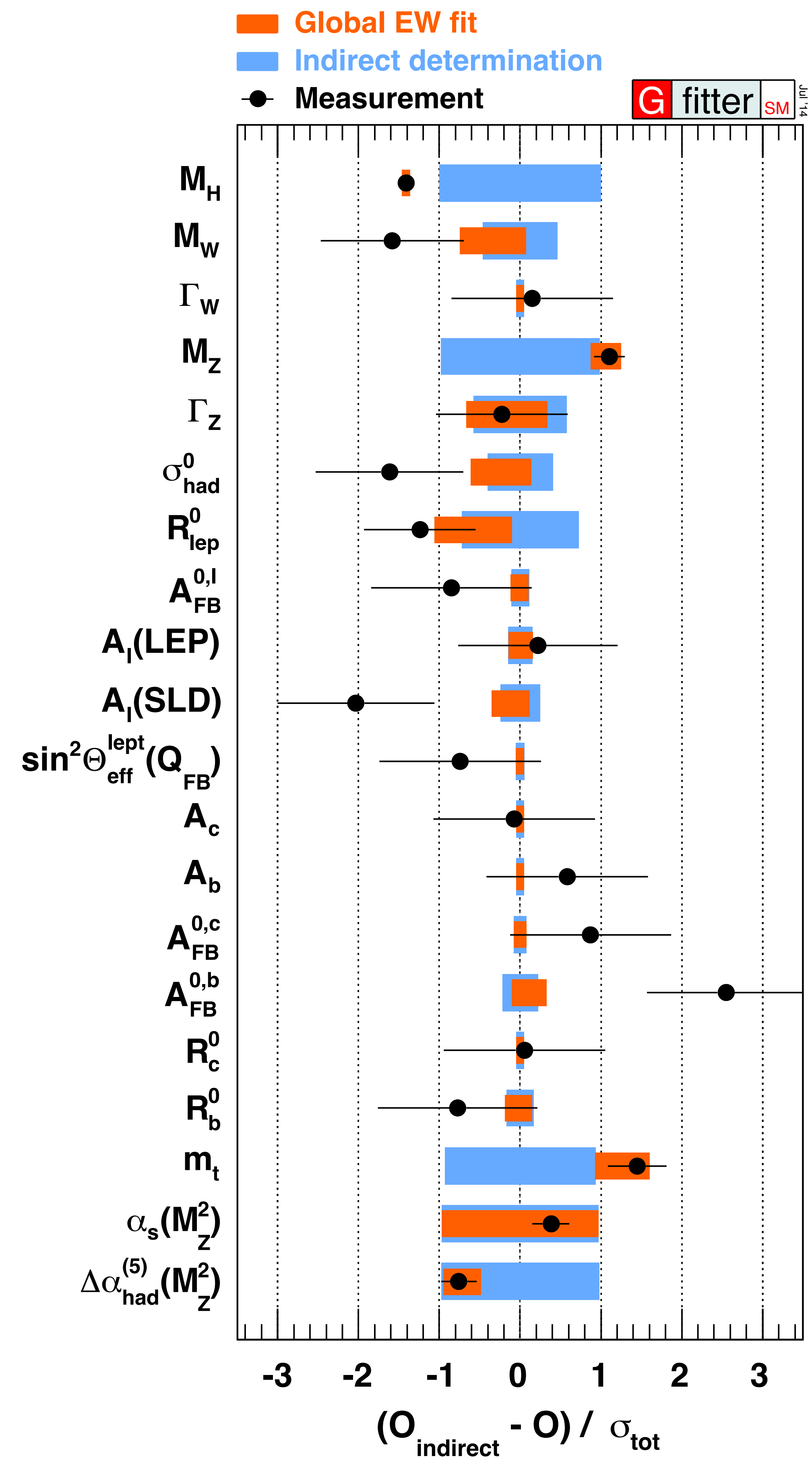

- For γγ and 4ℓ, signal is narrow resonant peak above a background continuum
  - Allows for precise Higgs boson mass measurement
  - Minimises the model dependency.
- Ingredients for optimal measurement of Higgs boson mass:
  - Detector performance driven measurement

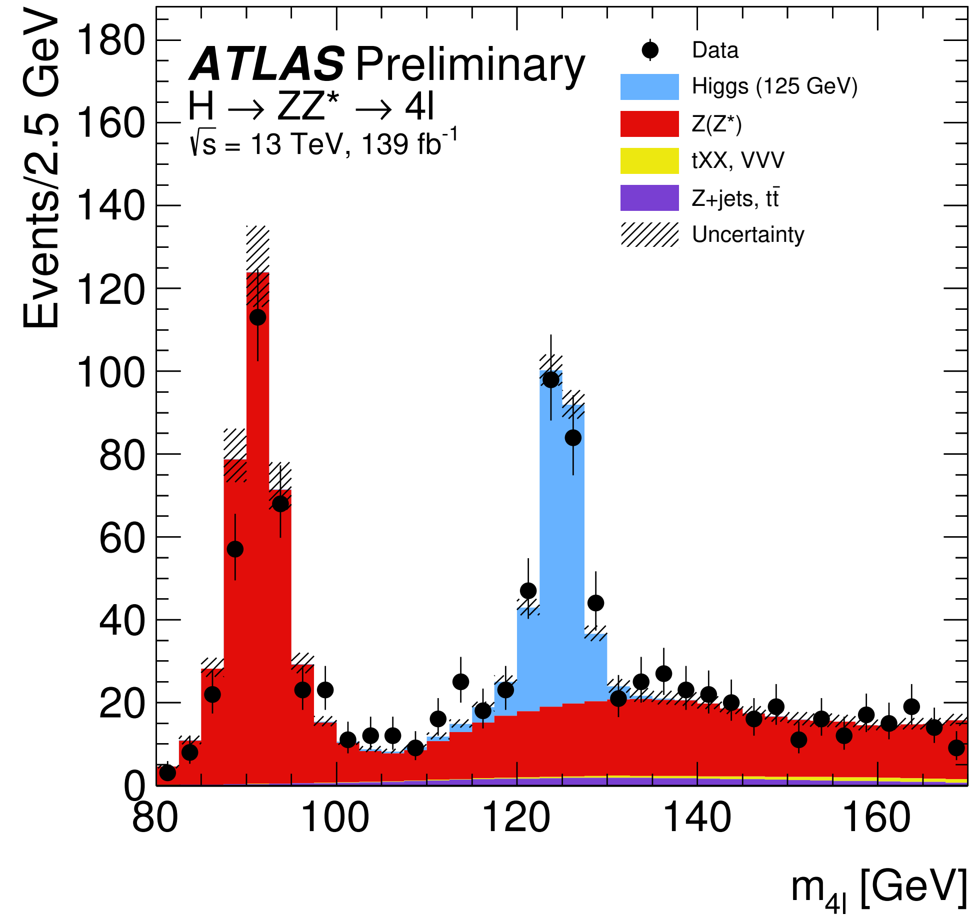

$$\delta m_H \simeq \frac{\sigma(m_{4\ell,\gamma\gamma})}{\sqrt{N - N_\mathrm{b}}}$$

(I) Statistical precision precision depends upon:
- resolution of the reconstructed final state,
- number of signal events.

(II) Systematic uncertainty from understanding of detector performance:
- energy and momentum scale,
- resolution uncertainty.

Muon p_T resolution

- Resolution muon channels (4μ, 2e2μ and 4μ) crucial for m_H uncertainty:
  - Excellent momentum resolution of about 1% at about p_T 45 ~GeV.
- Momenta calibrated to J/ψ and Z samples in data
  - for residual mis modelling of E^{loss} in calorimeters, alignment precision etc.
  - Including corrections to data accounting for alignment weak modes.
  - Precision down to 0.5 per mille for |η|<1.0

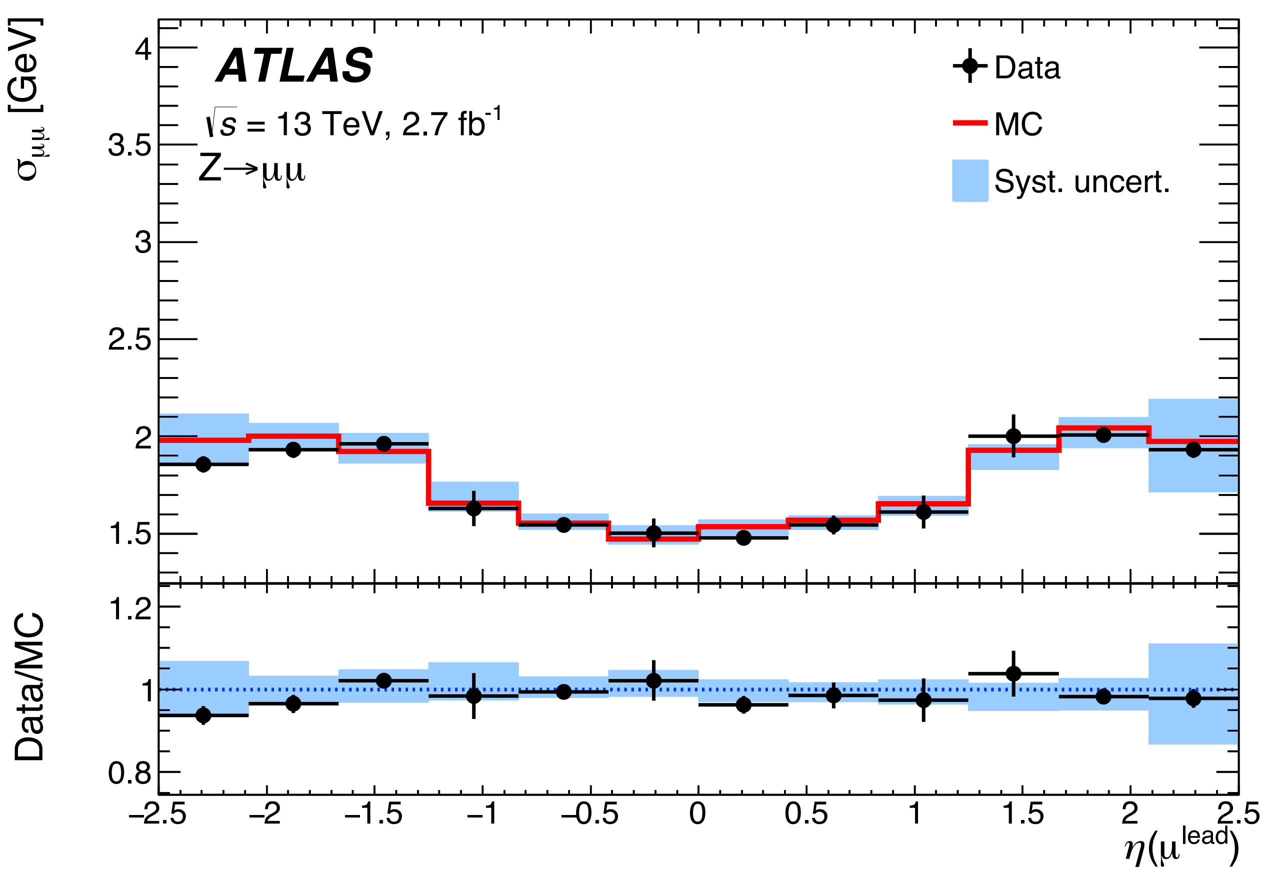

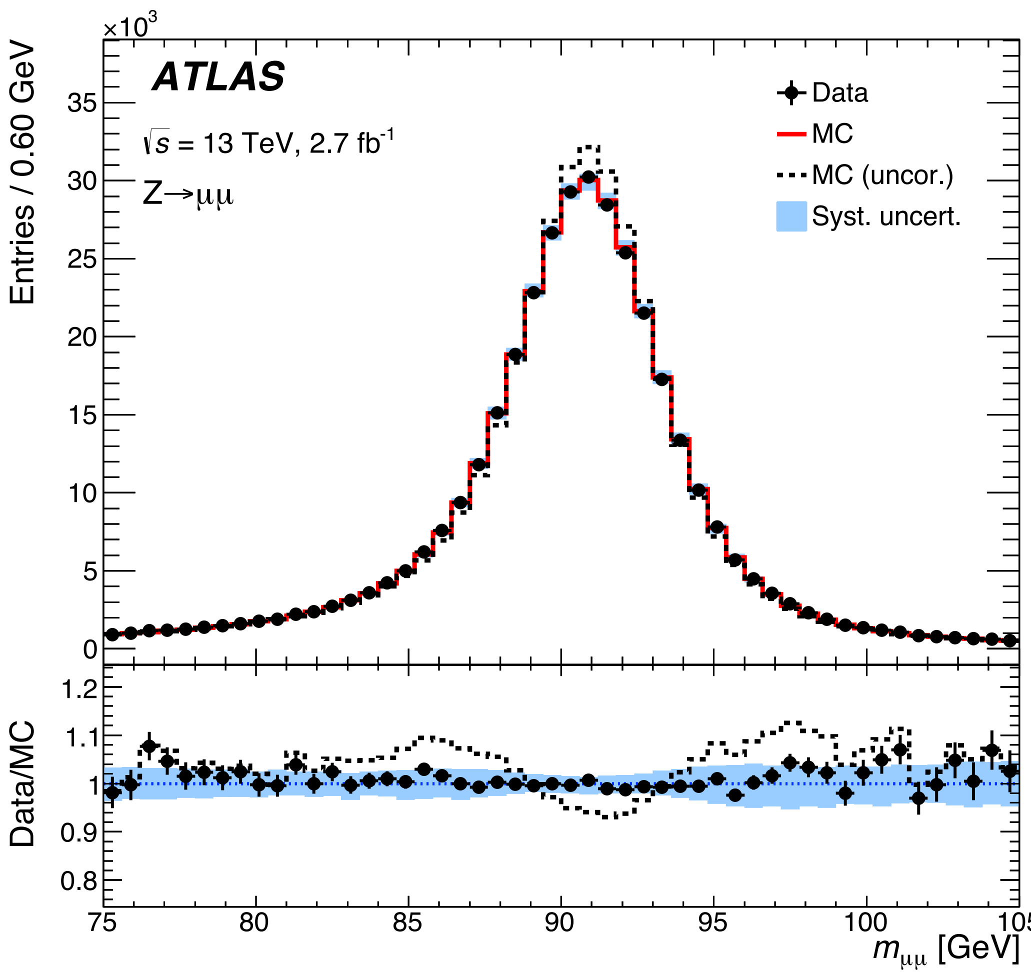

Muon p_T resolution

- Resolution muon channels (4μ, 2e2μ and 4μ) crucial for m_H uncertainty:
  - Excellent momentum resolution of about 1% at about p_T 45 ~GeV.

- Simulated momenta calibrated to J/ψ and Z samples in data
  - for residual mis modelling of E^{loss} in calorimeters, alignment precision etc.
  - Uncertainty of about 10% on the resolution and 0.5% on the momentum scale.

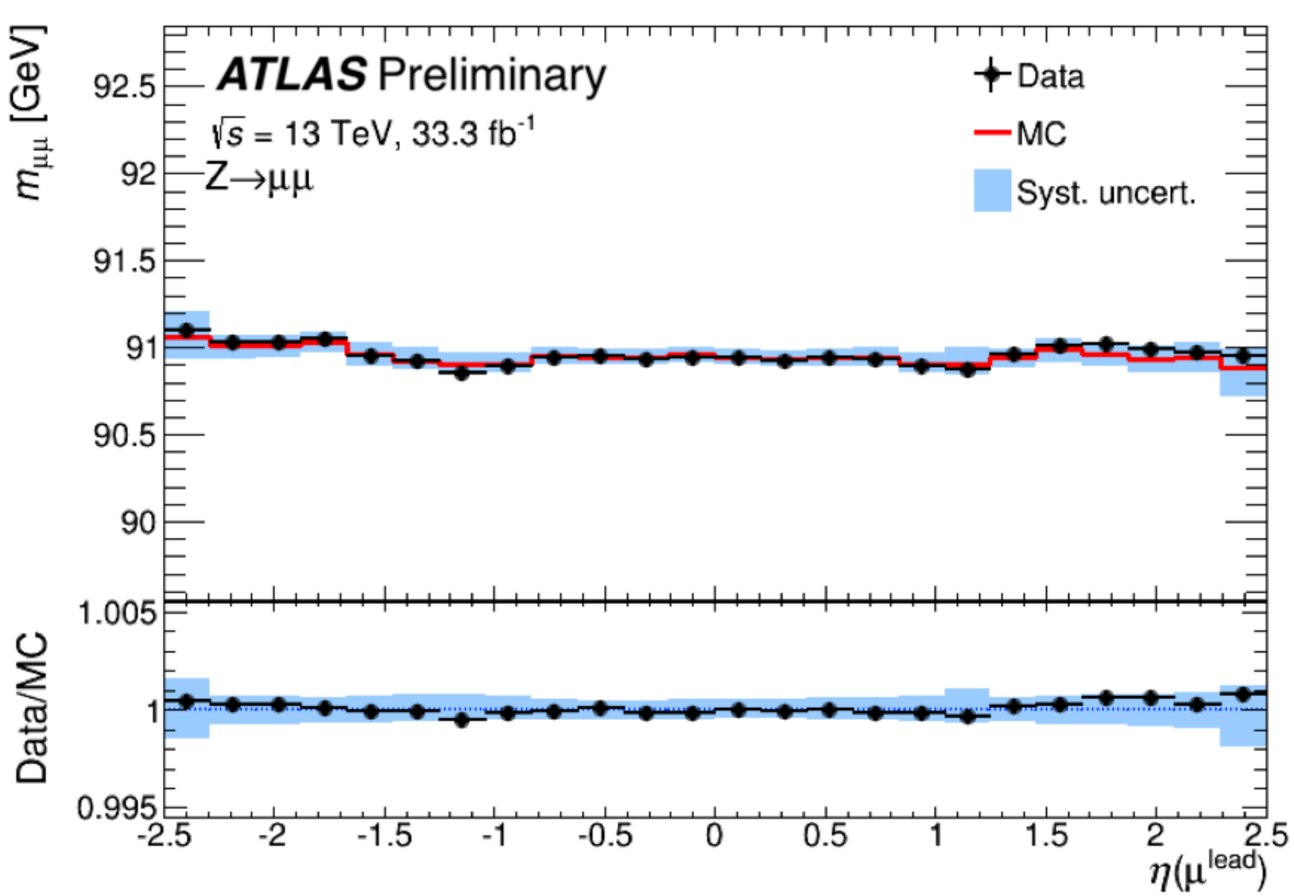

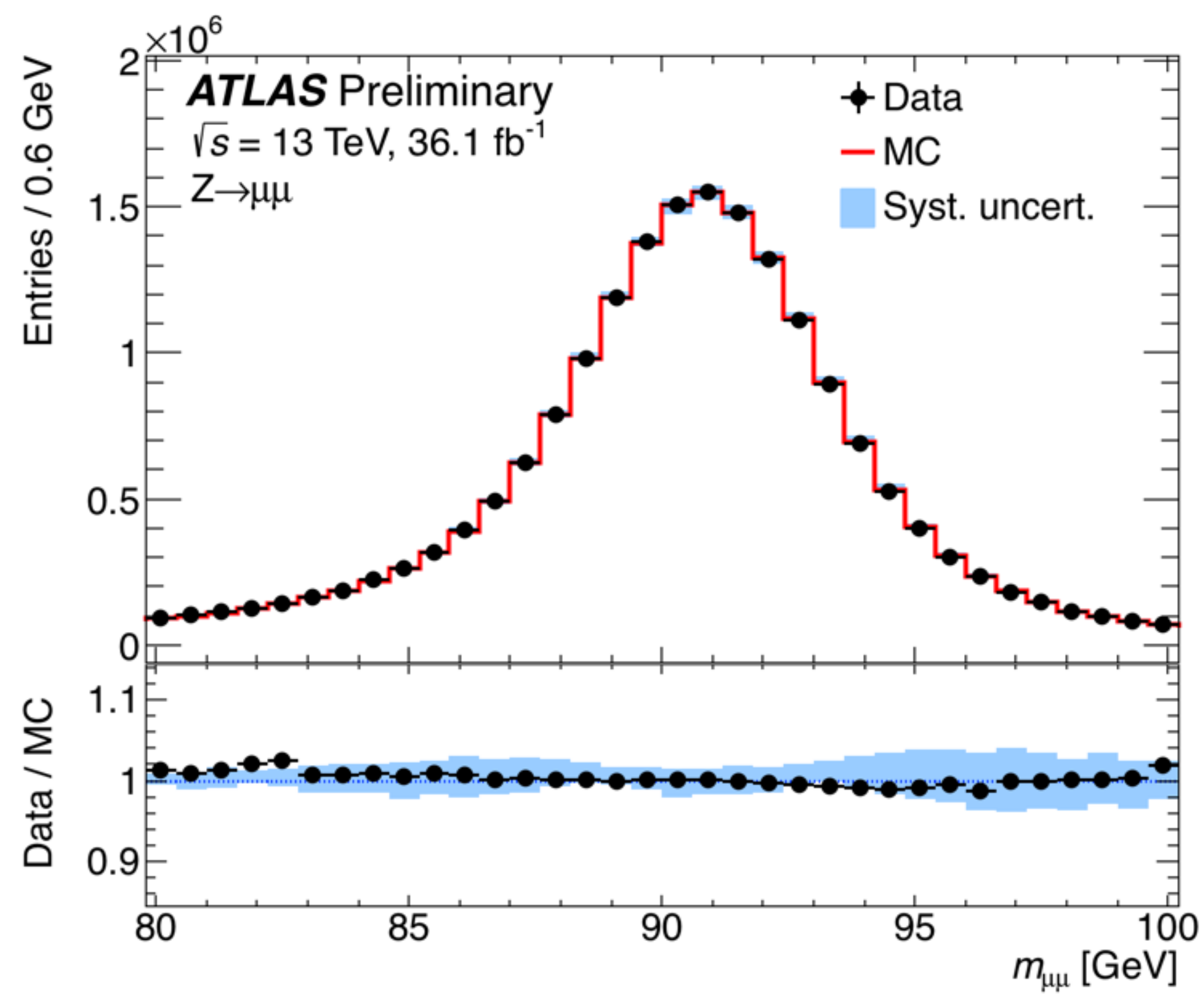

- Local misalignments and second order effects:
  - Charge dependent sagitta bias, with net effect of worsening resolution
  - In-situ correction based on $Z \rightarrow \mu\mu$ data, recovers up to 5% in resolution.

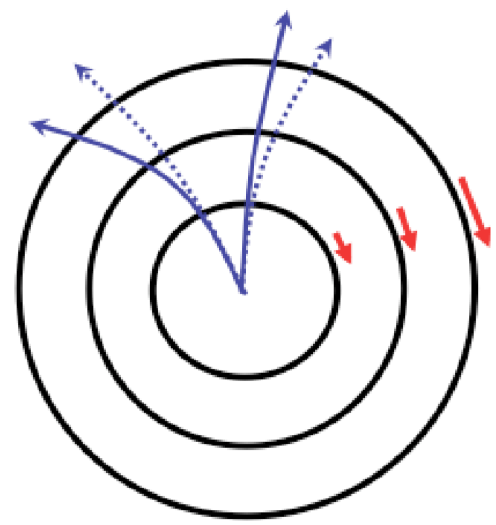

- Momentum scale understood down to the per mille level
  - Precision down to 0.5 per mille for $|\eta|<1.0$

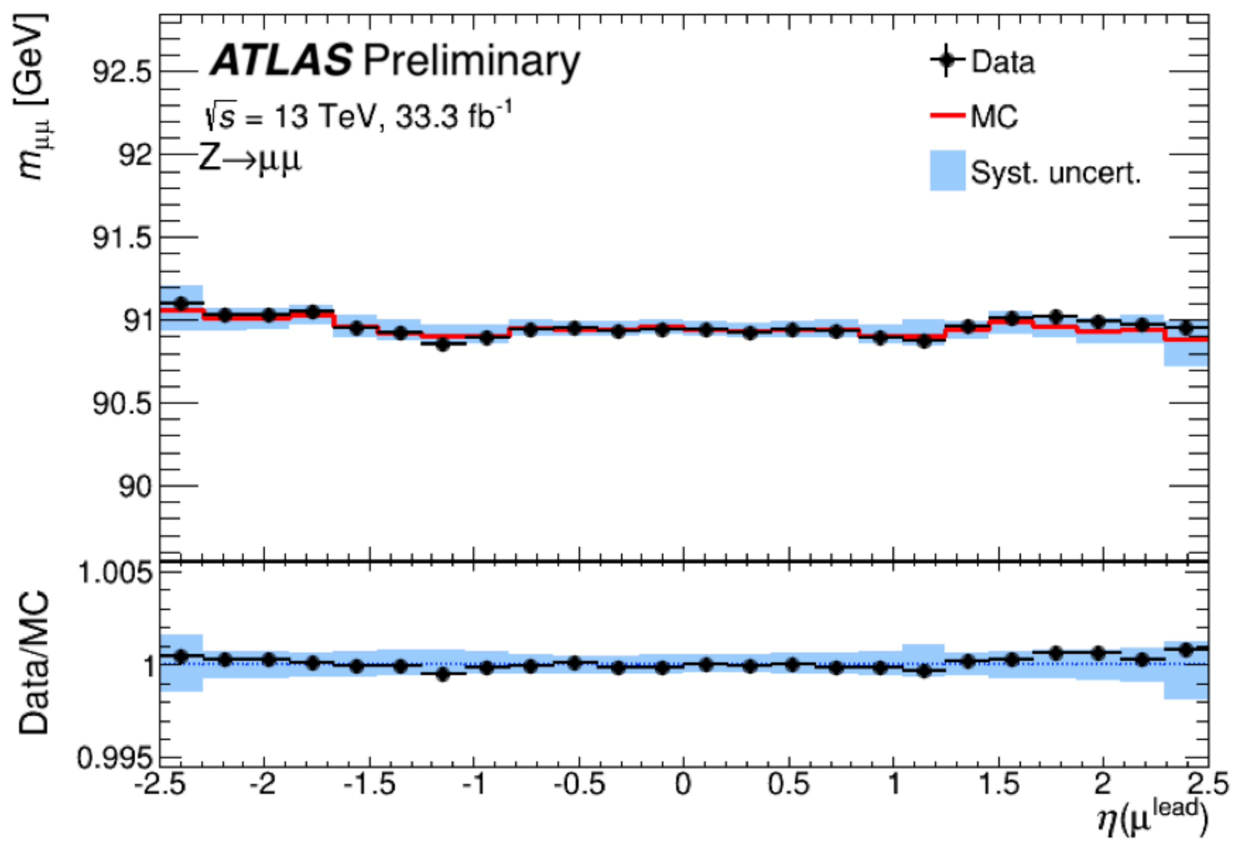

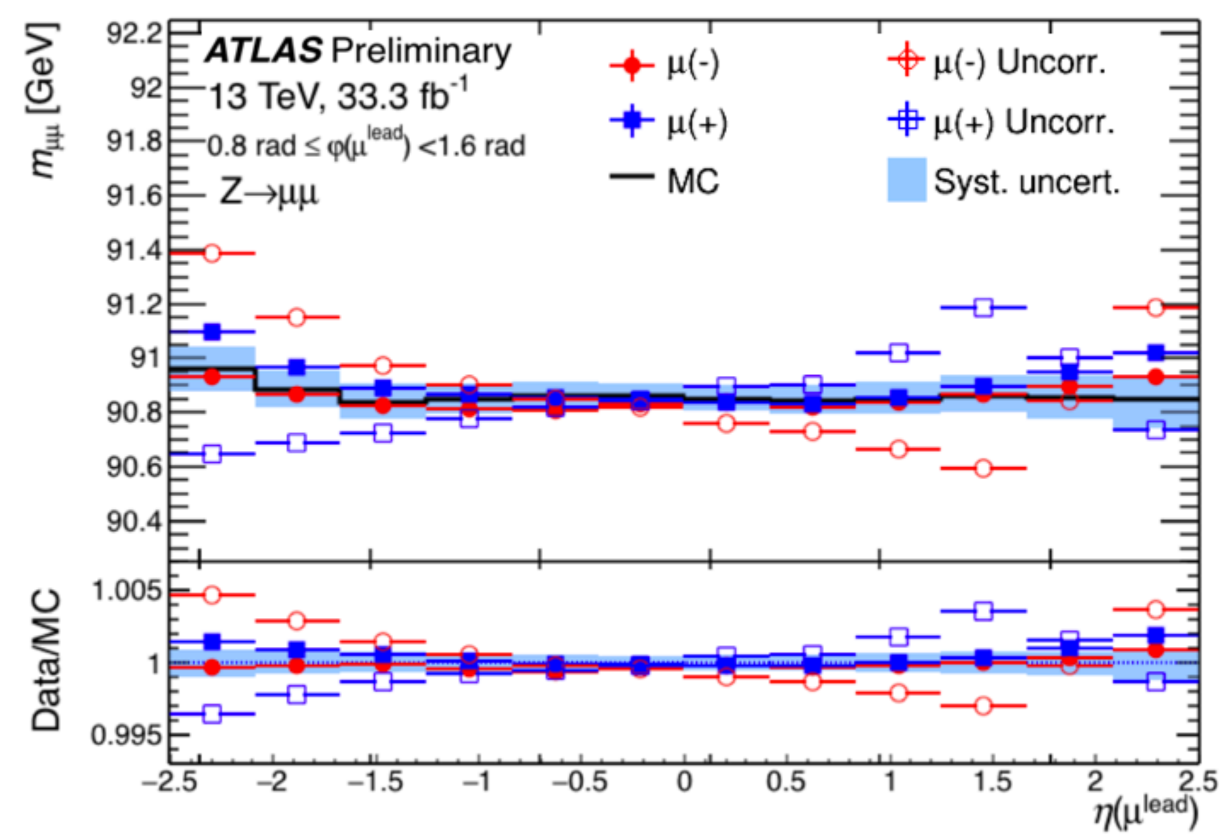

- Three-prong approach to reduce uncertainty at analysis level: arXiv:1806.00242

(i) ~15% from m_{12} constraint to m_Z with kinematic fit and m_Z constraints on alignment weak modes.

(i) ~2% from kinematic discriminant selecting signal and background events

- Boosted Decision Tree on $p_T(4\ell)$, $y(4\ell)$ and $\log(|\mathcal{M}_H|^2/|\mathcal{M}_{ZZ^*}|^2)$

(ii) ~5% from multivariate per-event resolution likelihood.

- Neural network to solve uncertainty correlations induced by kinematic discriminant.

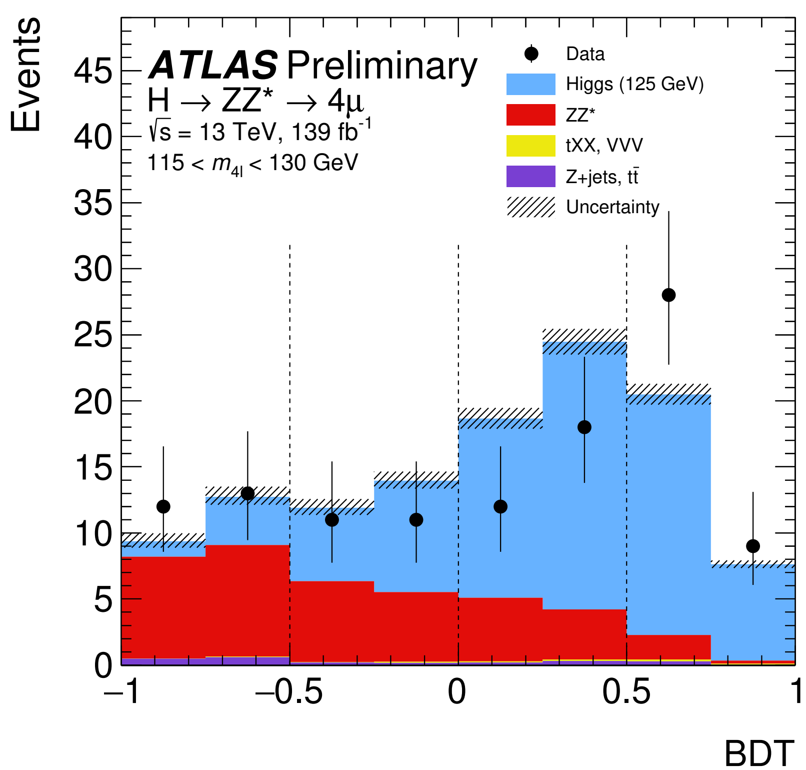

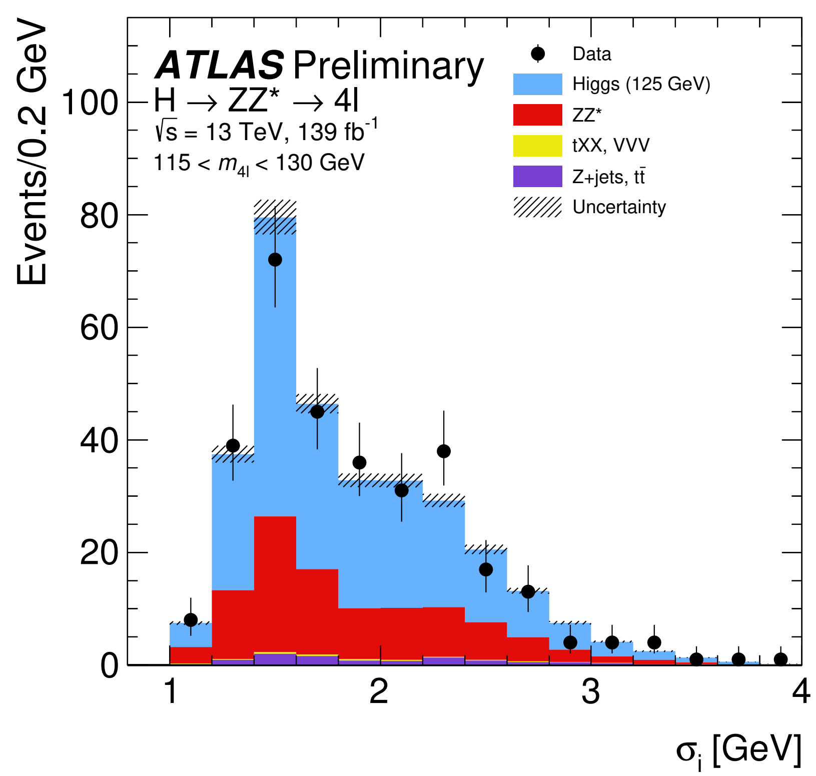

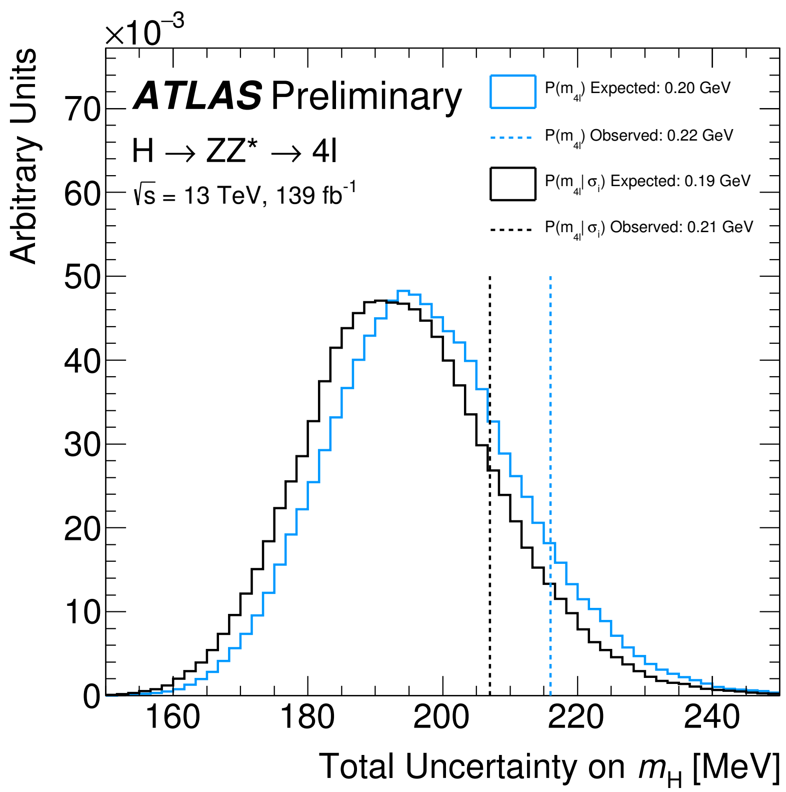

$H \to ZZ \to 4\ell$ results — Mass measurement

- Three-prong approach to reduce uncertainty at analysis level: arXiv:1806.00242

(i) ~15% from m_{12} constraint to m_Z with kinematic fit and m_Z constraints on alignment weak modes.

(i) ~2% from kinematic discriminant selecting signal and background events

- Boosted Decision Tree on $p_T(4\ell)$, $y(4\ell)$ and $\log(|\mathcal{M}_H|^2/|\mathcal{M}_{ZZ^*}|^2)$

(ii) ~2% from multivariate per-event resolution likelihood.

- Neural network to solve uncertainty correlations induced by kinematic discriminant.

- Systematic uncertainty of ~70 MeV

Systematic Uncertainty	Impact (GeV)
Muon momentum scale	+0.08, −0.06
Electron energy scale	±0.02
Muon momentum resolution	±0.01
Muon sagitta bias correction	±0.01

- 61% improvement w.r.t $m_H^{H \to ZZ,\text{Run1}}$
- 15% improved precision w.r.t $m_H^{\text{ATLAS+CMS,Run1}}$

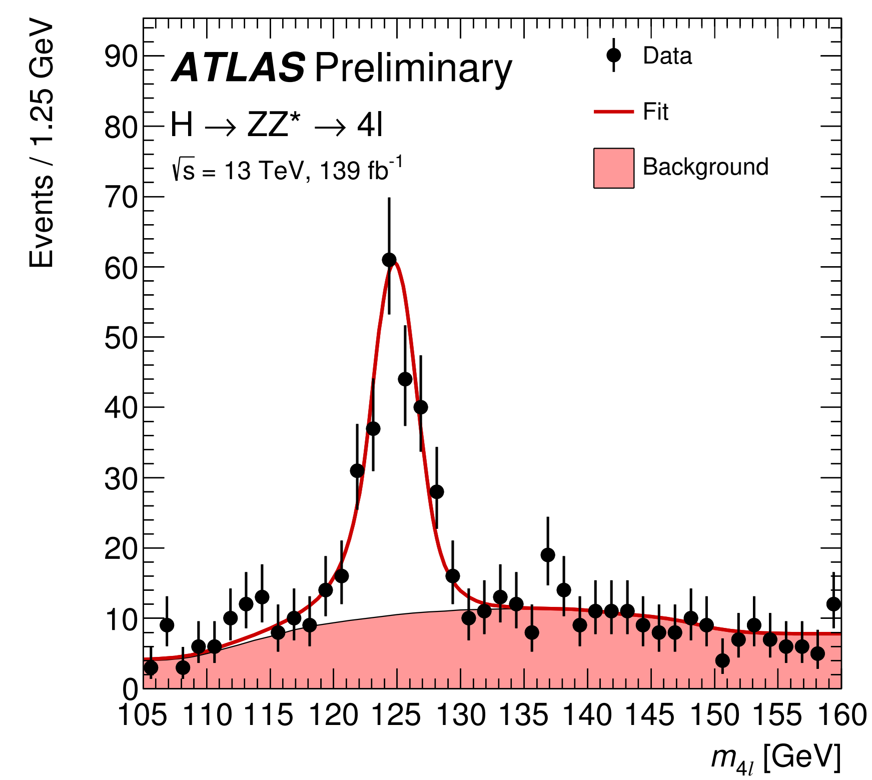

$$m_H = 124.92^{+0.21}_{-0.20}\ \text{GeV}$$

- 4ℓ and $\gamma\gamma$ measurements are combined with ATLAS Run 1 result arXiv:1806.00242

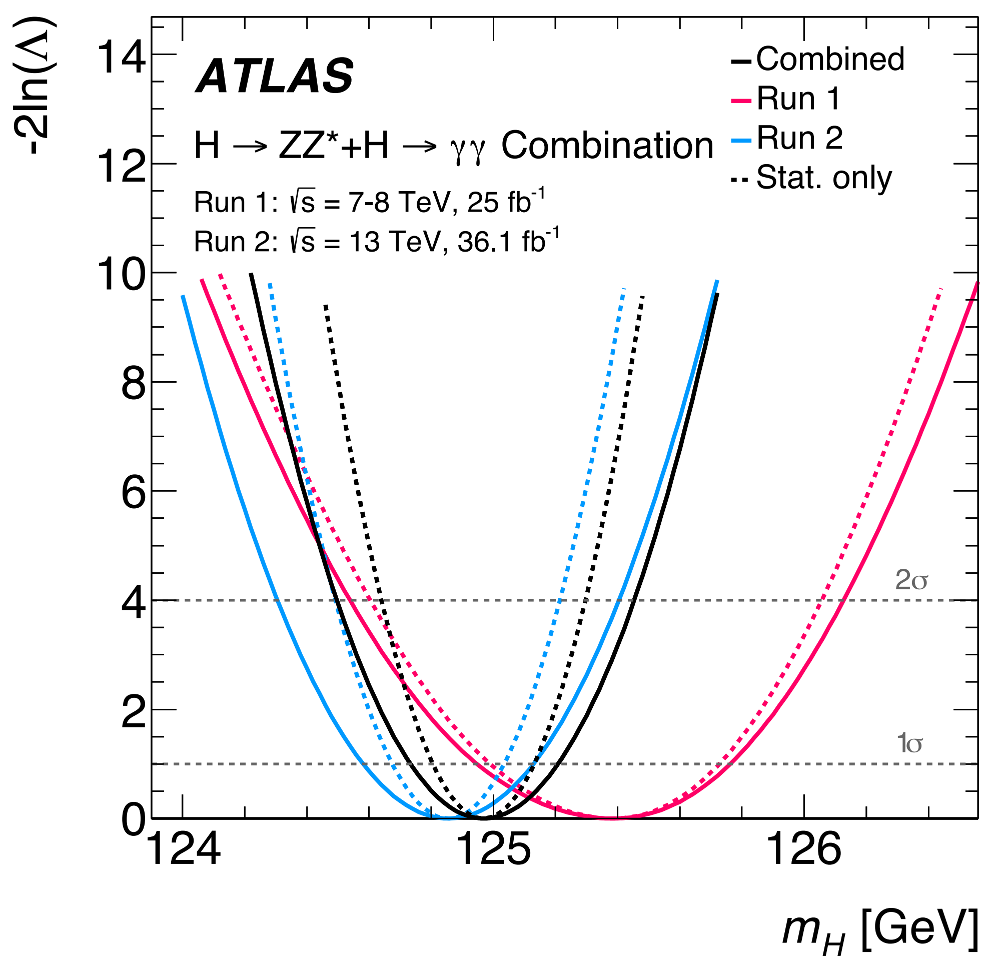

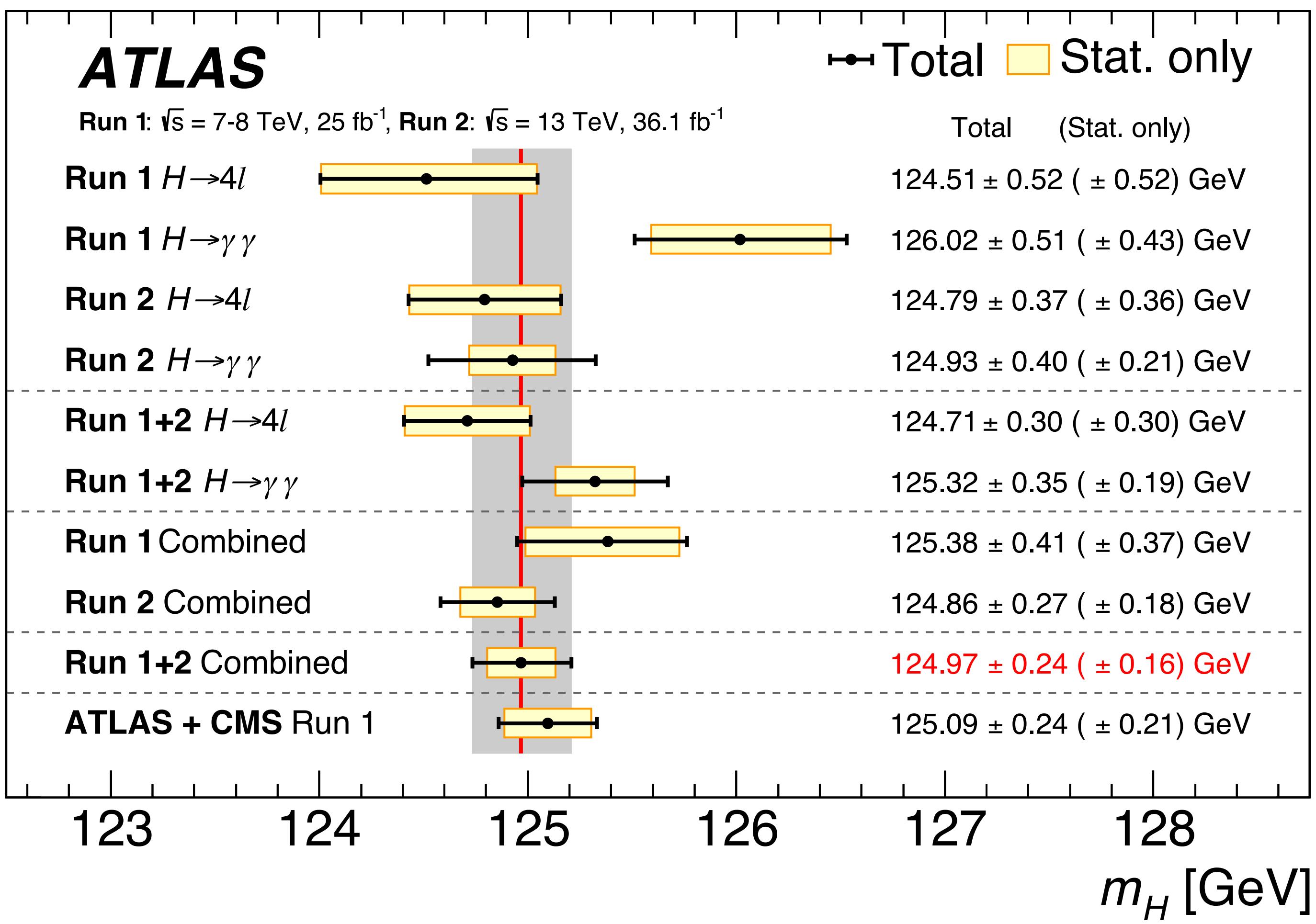

- Run 2 precision improved w.r.t Run 1.

$$m_H = 124.86 \ \pm \ 0.27(\pm 0.18 \text{ stat only}) \text{ GeV}$$

- ATLAS Run 1 + 2 comparable precision to LHC Run 1 combination.

$$m_H = 124.97 \ \pm \ 0.24(\pm 0.16 \text{ stat only}) \text{ GeV}$$

3.Decays to light leptons.

Second generation fermions

- Fermions acquire mass through Yukawa interactions with the Higgs field.

$$\mathcal{L} = -\frac{1}{4}F_{\mu\nu}F^{\mu\nu} + i\bar{\Psi}\not{D}\psi + D_\mu\Phi^\dagger D^\mu\Phi - V(\Phi) + \bar{\Psi}_L\hat{Y}\Phi\Psi_R + h.c.$$

  - Remains an elusive sector not probed by EWK precision tests.
  - LHC successfully probed couplings to third generation fermions ($t\bar{t}H,\ H\rightarrow\tau\tau$)

- Next milestone, probe couplings to second and first generation fermions.
  - $H\rightarrow\mu\mu$ and ee offer unique insight.
  - Fully reconstructed final states with low hadronic activity.
  - Very rare processes:
    - $\mathscr{B}(H\rightarrow\mu\mu)$ ~ $(2.17 \pm 0.04)\times10^{-4}$
    - Large backgrounds from Drell-Yann production Z→ μμ, ee

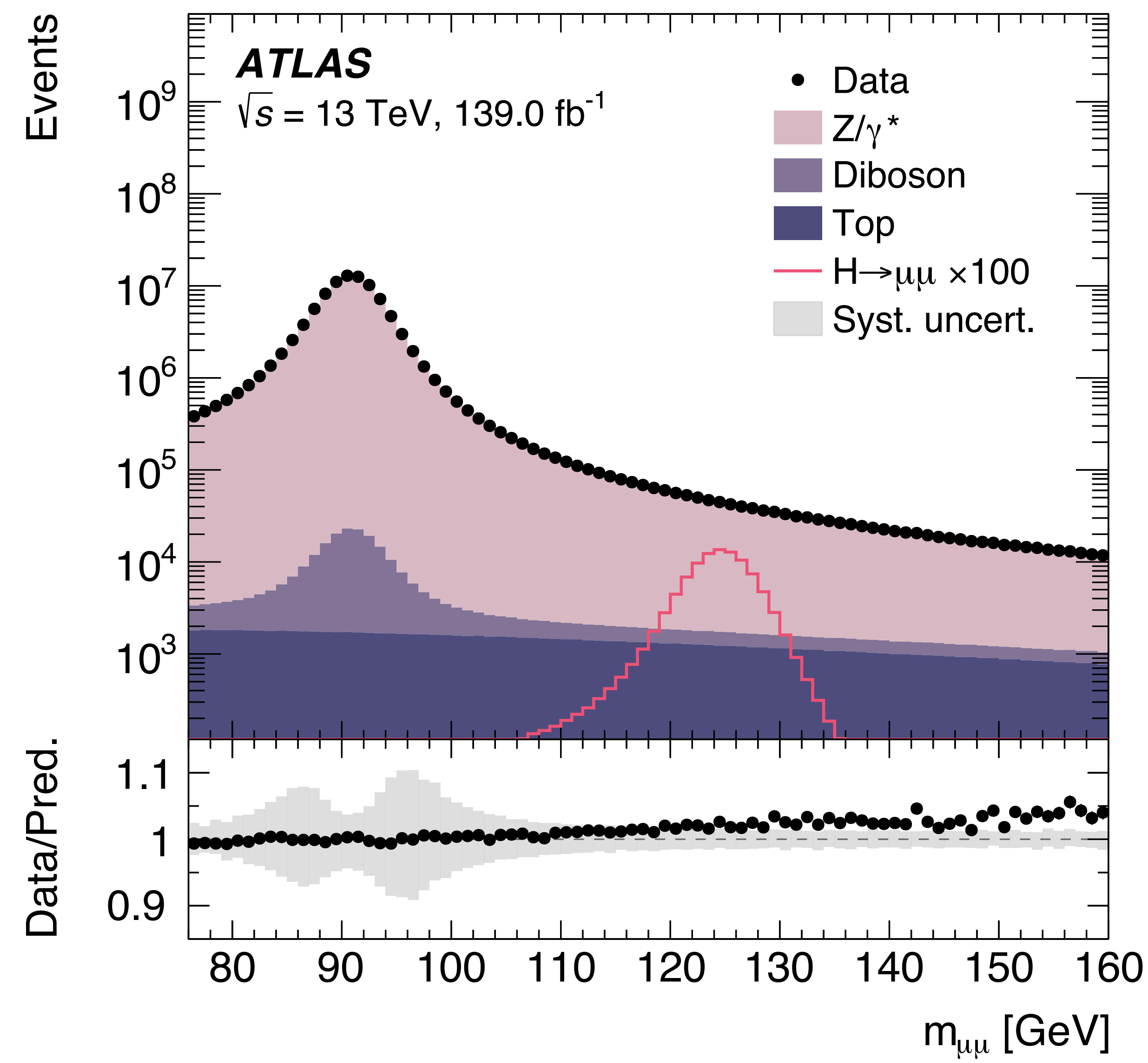

- Mutually exclusive categories
  - Targeting the various Higgs production modes, to increase s/b.
  - $H \to \mu\mu$, further splitting according process-specific multivariate boosted decision tree.
    - s/b ranging from 0.1% (0-jet Low) to 18% (VBF Very High)

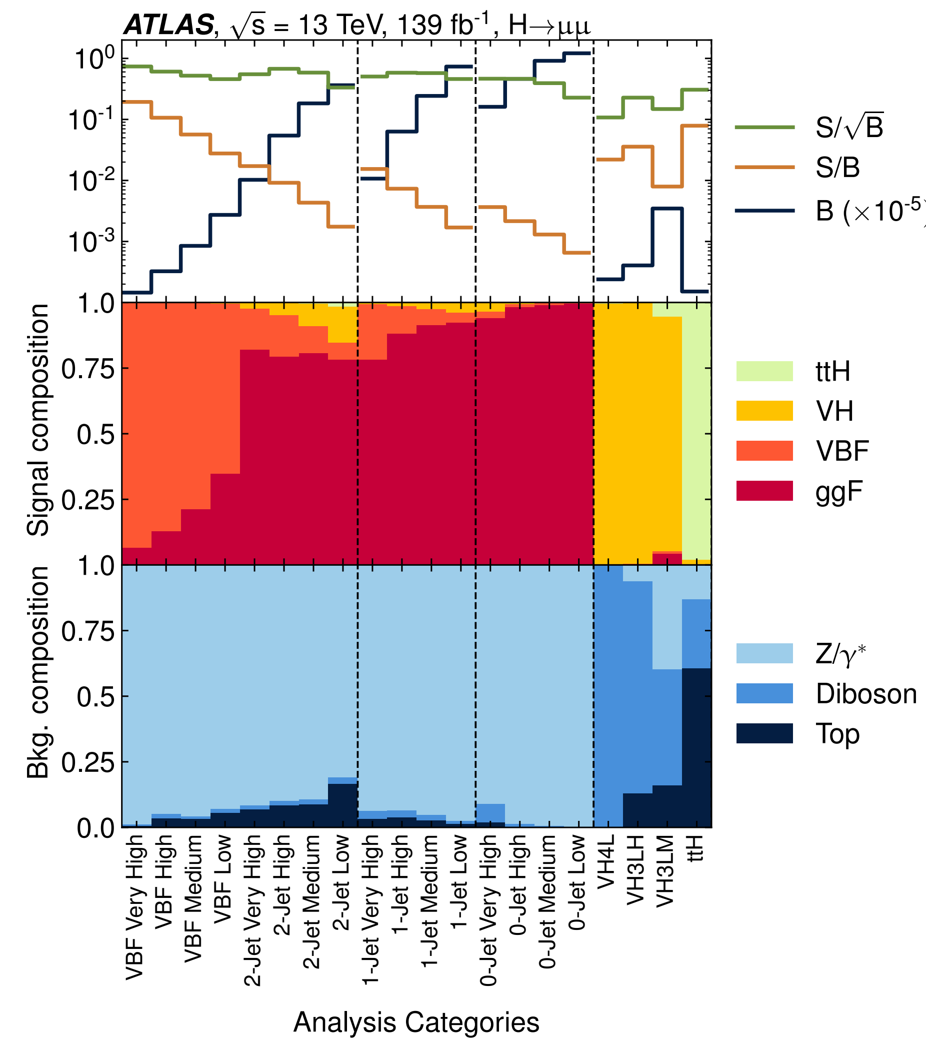

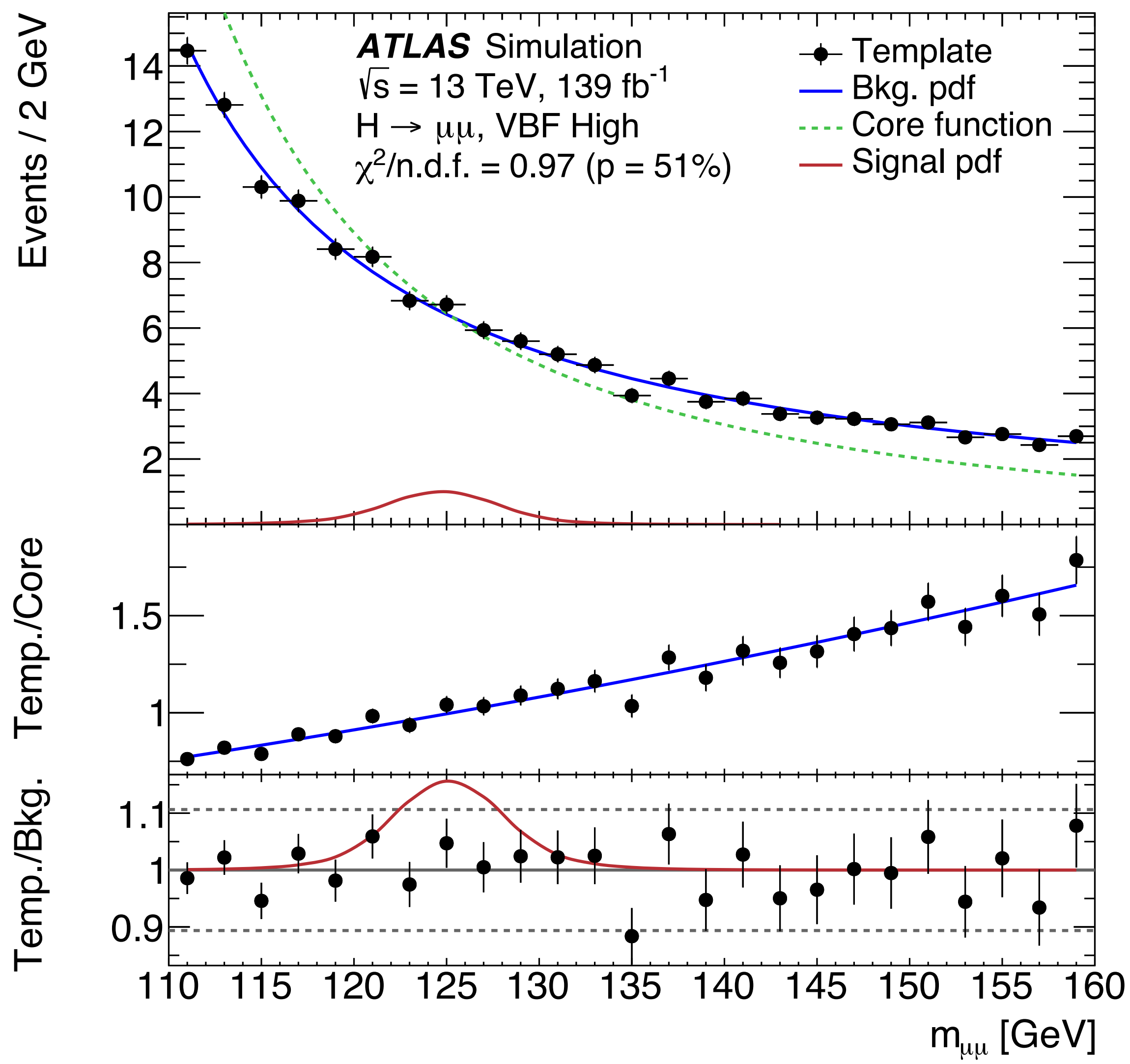

- Empirical background modelling in both analyses.
  - $F(m_{\mu\mu})$ = Rigid core($m_{\mu\mu}$) × Flexible Empirical($m_{\mu\mu}$)
  - Per-mille precision reached with two *ad-hoc* high statistics fast simulation ~10 ab^{-1} per category.

- $\mathscr{B}(H\rightarrow ee) < 3.6 \times 10^{-4}$ **at 95%CL.**
  - Expected limit at 3.5×10^{-4}
  - Improvement of a factor of 5 w.r.t previous results.

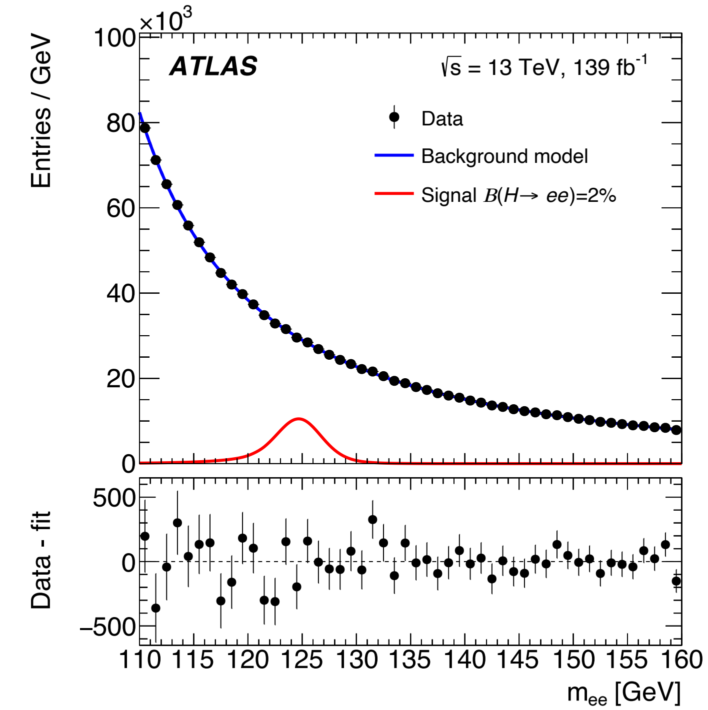

- $H\rightarrow\mu\mu$: observed significance 2.0σ, $\mu = 1.2 \pm 0.5$.
  - Expected 1.7σ.
  - $\sigma(H\rightarrow\mu\mu)\ /\sigma^{SM}(H\rightarrow\mu\mu) < 2.2$ at 95%CL.
  - Improvement of a factor 2.5, with 25% from the methods used.

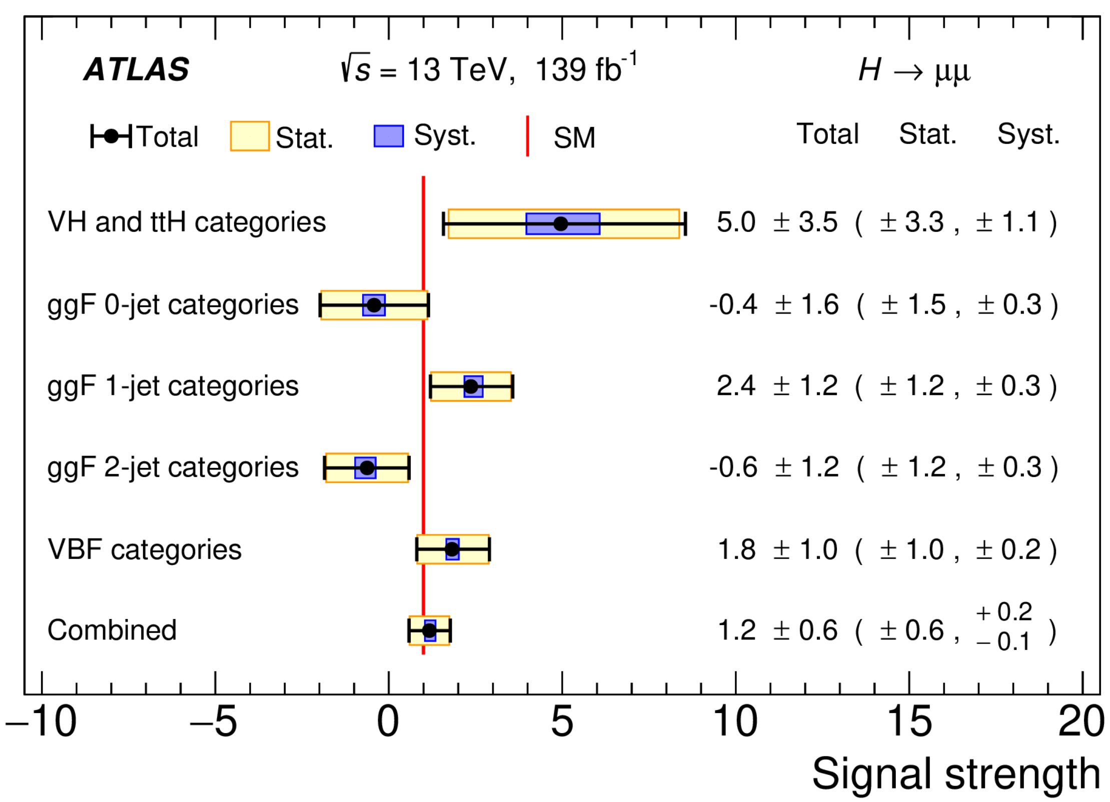

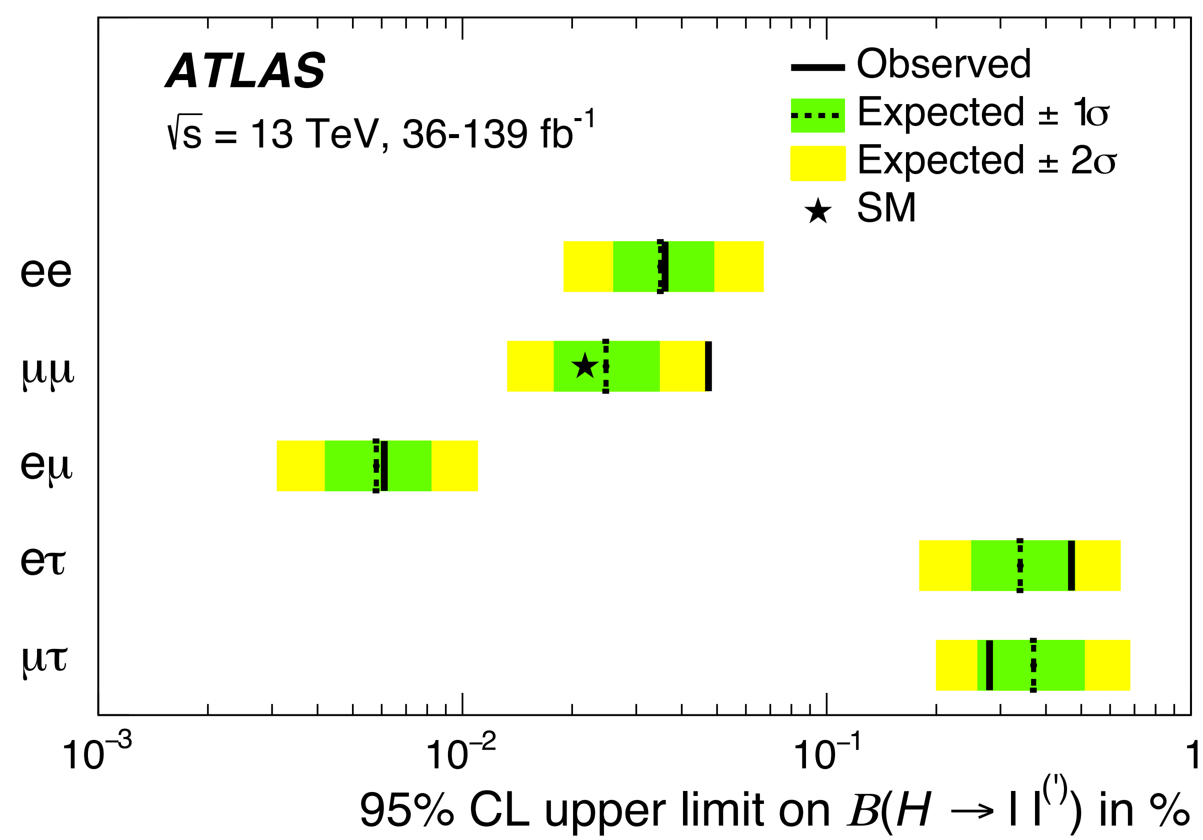

4. Production mode measurements

- ATLAS full Run-2 combination

ATLAS-CONF-2020-027

  - Combined sensitivity of all channels to increase the precision of the Higgs productions.

Analysis decay channel	Target Prod. Modes	$\mathcal{L}$ [fb^{-1}]
$H \to \gamma\gamma$	ggF, VBF, WH, ZH, $t\bar{t}H$, tH	139
$H \to ZZ^*$	ggF, VBF, WH, ZH, $ttH(4\ell)$	139
	$t\bar{t}H$ excl. $H \to ZZ^* \to 4\ell$	36.1
$H \to WW^*$	ggF, VBF	36.1
	$t\bar{t}H$	
$H \to \tau\tau$	ggF, VBF	36.1
	$t\bar{t}H$	
	VBF	24.5 – 30.6
$H \to b\bar{b}$	WH, ZH	139
	$t\bar{t}H$	36.1
$H \to \mu\mu$	ggF, VBF, VH, $t\bar{t}H$	139
$H \to inv$	VBF	139

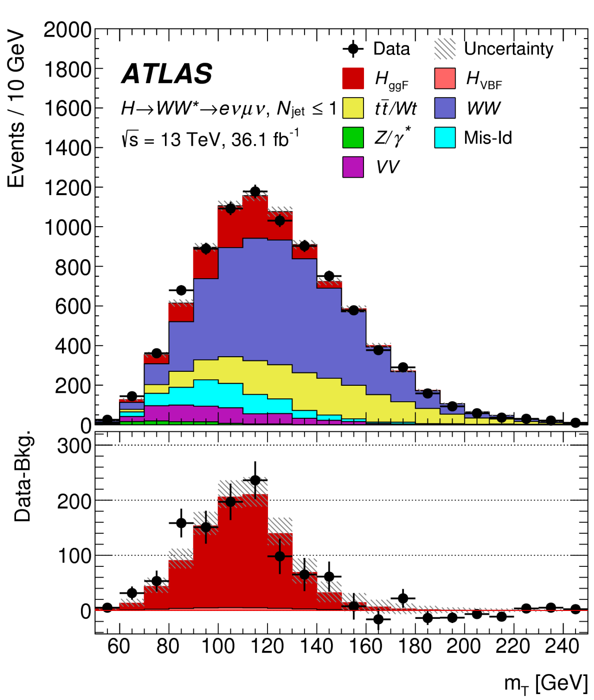

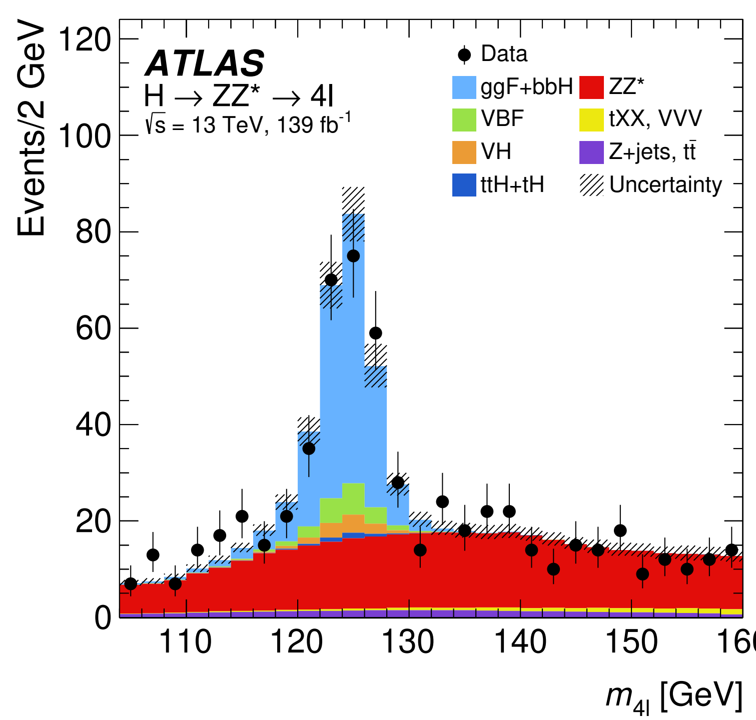

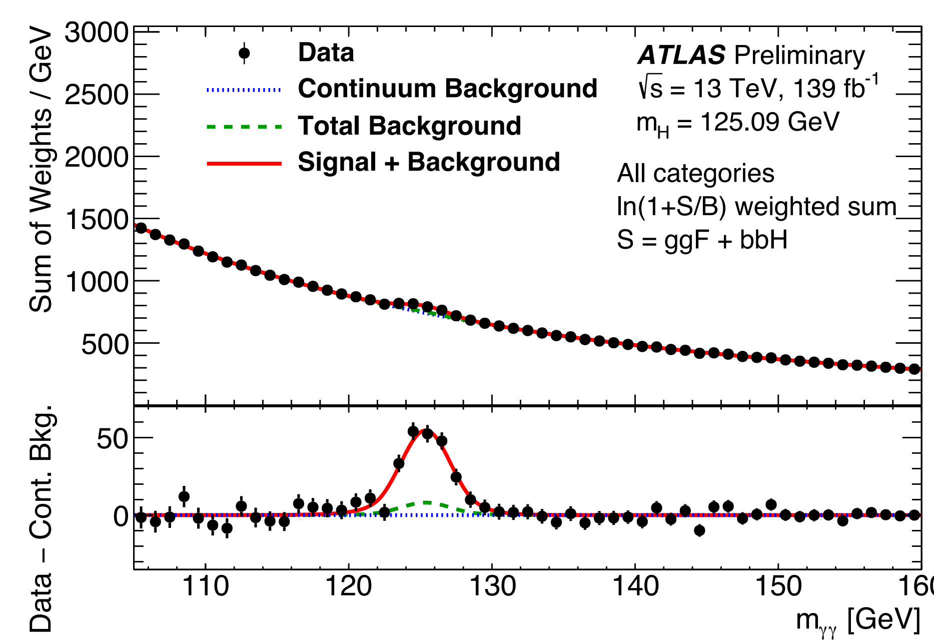

- Simultaneous fit to all template cross sections

ATLAS-CONF-2019-005

  - Extraction of global signal strength ($\mu=\sigma^{obs}/\sigma^{exp}$).
  - Experimental sensitivity of the same oder as of theory (up to N^{3}LO for ggF)

$$\mu = 1.06 \pm 0.07 = 1.06 \pm 0.04\,(\text{stat.}) \pm 0.03\,(\text{exp.})\,^{+0.05}_{-0.04}\,(\text{sig. th.}) \pm 0.02\,(\text{bkg. th.})$$

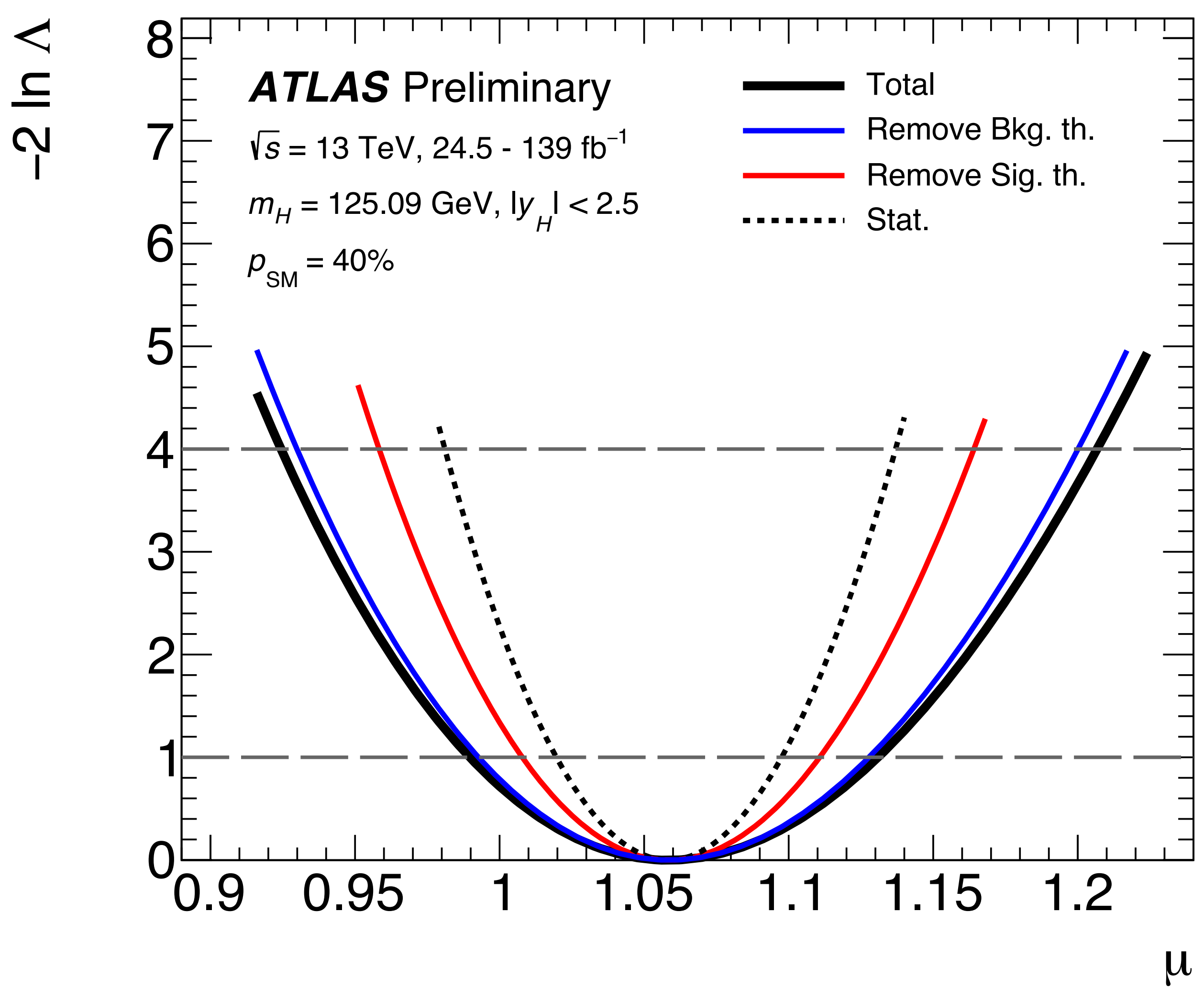

Uncertainty source	$\Delta\mu/\mu$ [%]
Luminosity	2.0
Background modeling	1.6
Jets, E_T^{miss}	1.4
Flavour tagging	1.1
Electrons, photons	2.2
Muons	0.2
τ-lepton	0.4
Other	1.6
MC statistical uncertainty	1.7

Production modes

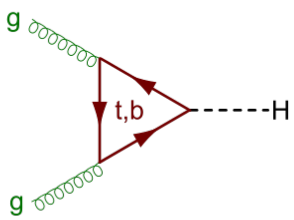

ggF

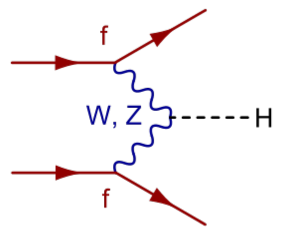

VBF: 6.5 σ

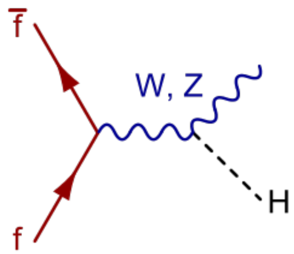

VH: 5.3 σ

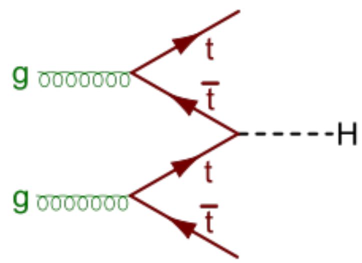

$t\bar{t}H$: 5.8 σ

- In the first Run-2 data observed all SM production modes at the LHC.
  - With current precision uncertainties from 20% to 7% on production cross section.
  - Sufficient for more in-depth investigations into the couplings

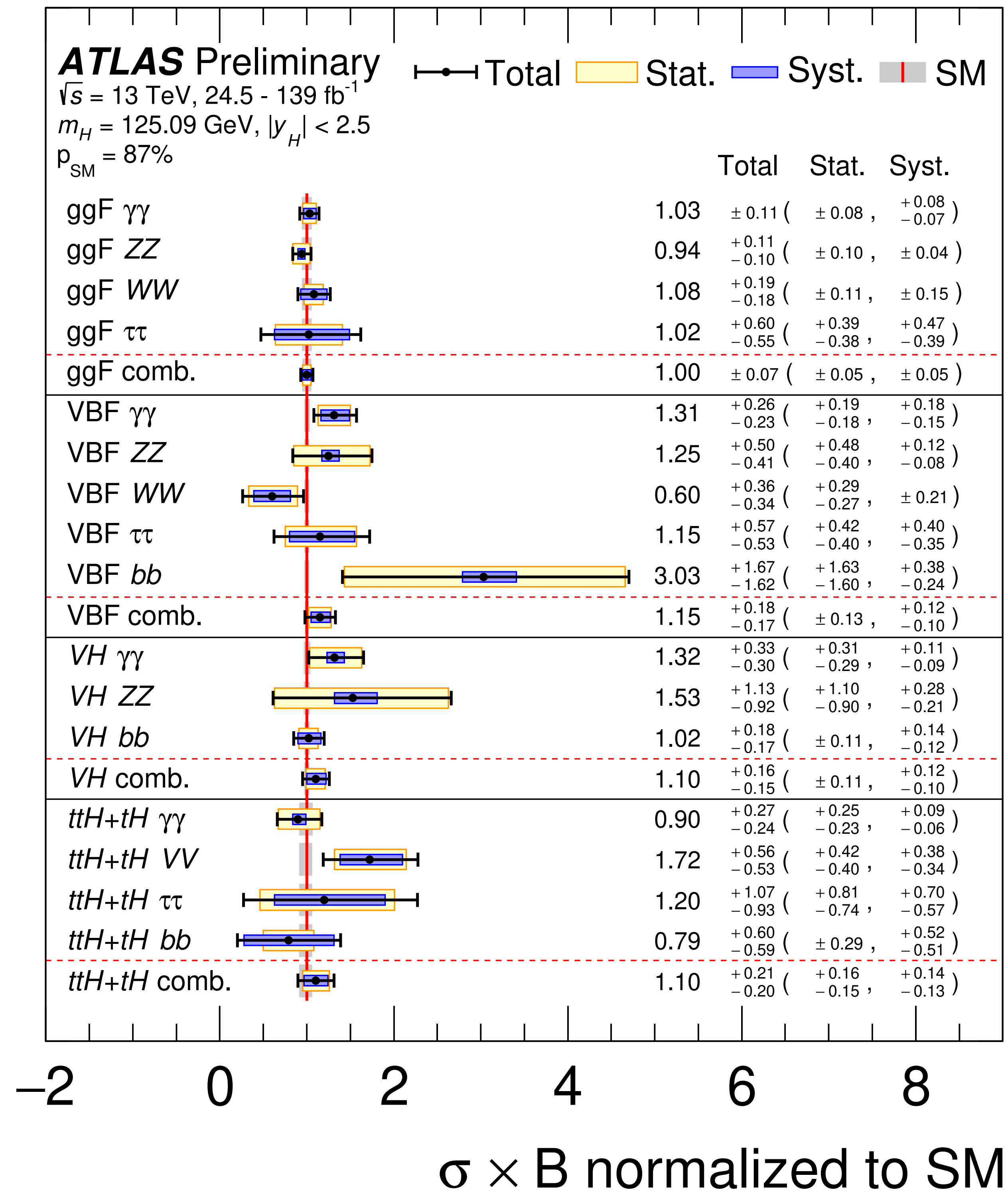

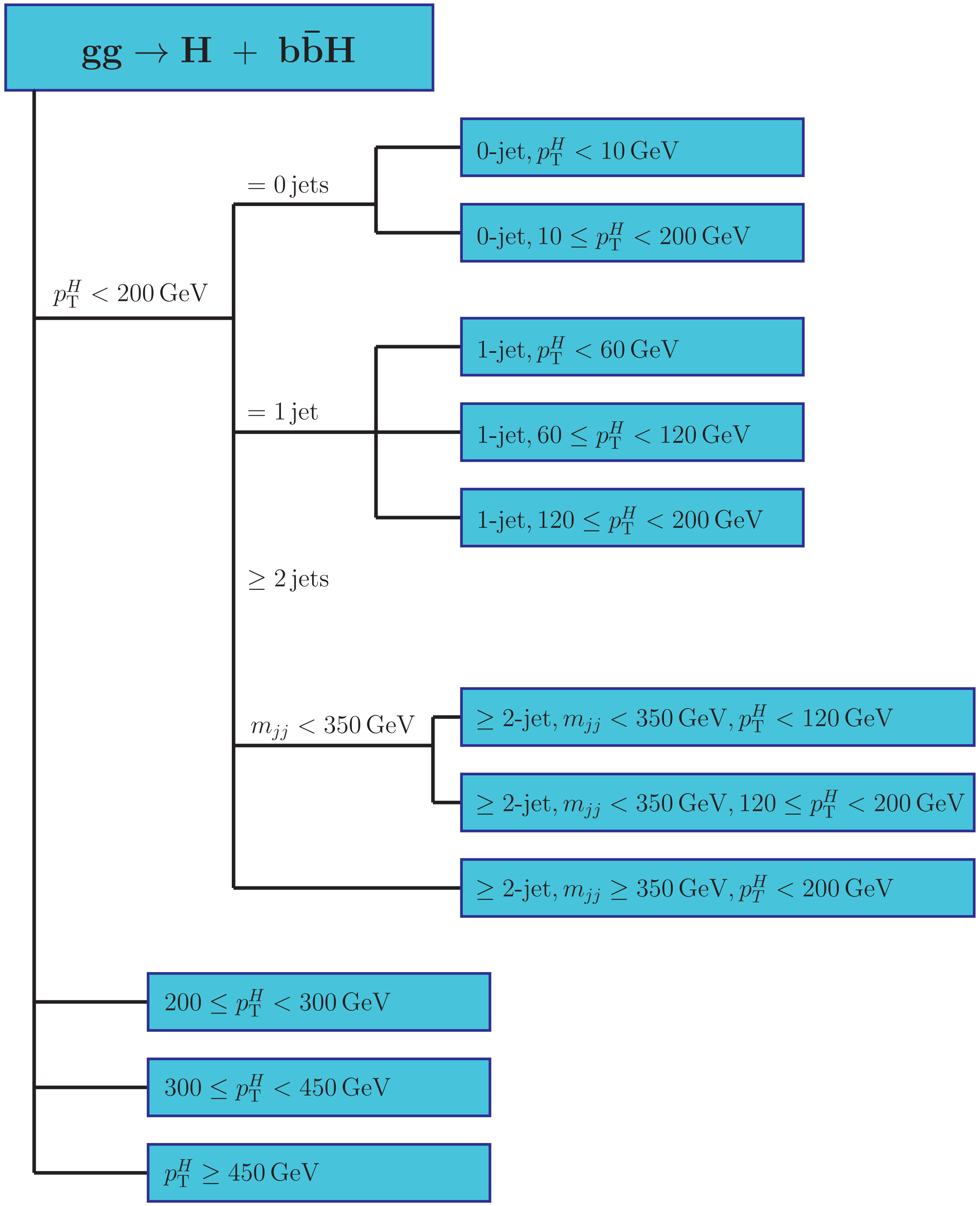

- Measure mutually exclusive phase-spaces in agreement with theory and LHC experiments
  - In terms of kinematics of the Higgs or associated objects in productions.
  - Sensitivity to deviations from SM.
  - Avoidance of large modelling uncertainties.
  - Approximate experimental sensitivity.

- Advantage of complementary sensitivity in production from different final states:
  - $m_{\rm jj} > 450$ GeV from $H \to WW^*$
  - High $p_T{}^H$ from $H \to bb$

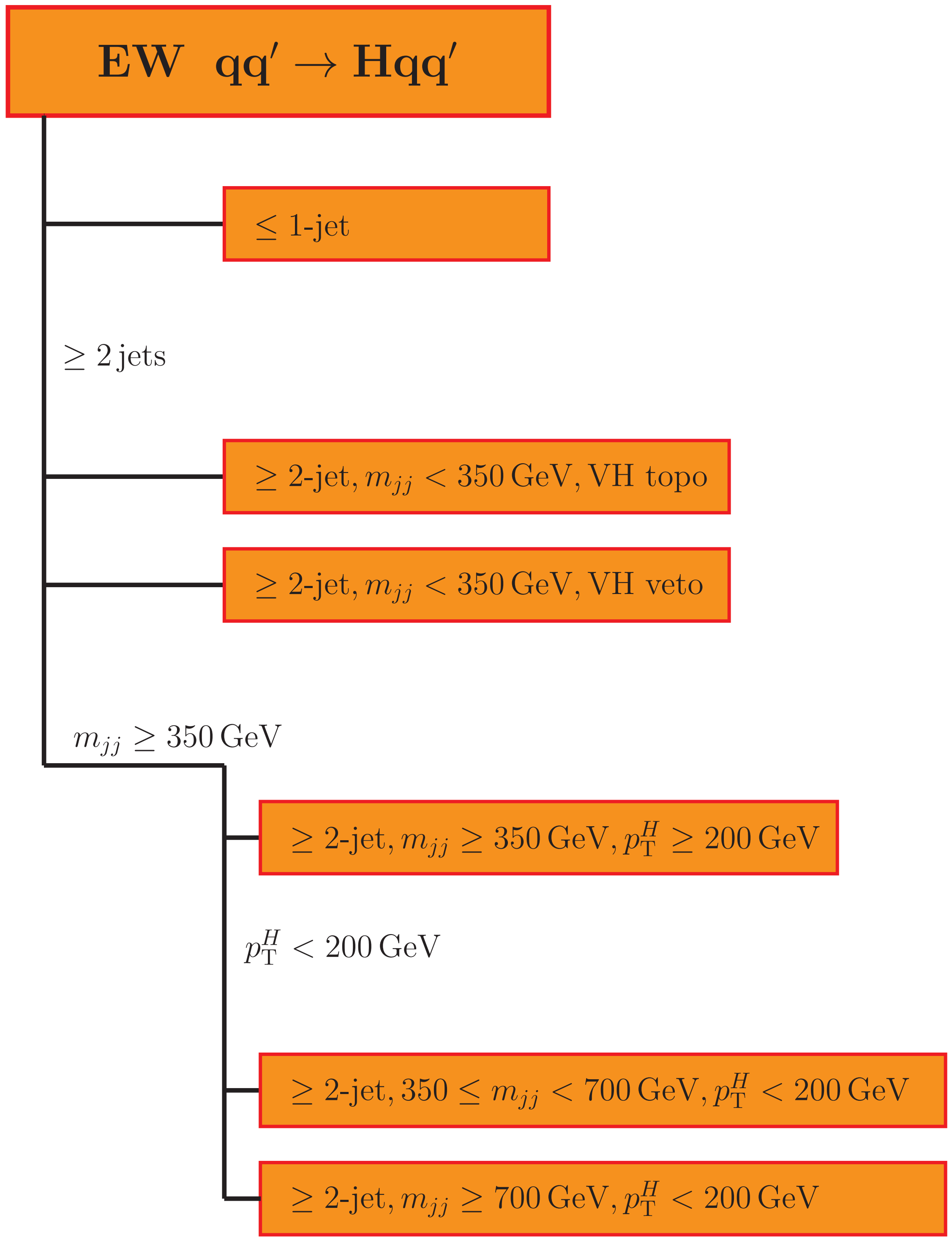

- Measure mutually exclusive phase-spaces in agreement with theory and LHC experiments
  - In terms of kinematics of the Higgs or associated objects in productions.
  - Sensitivity to deviations from SM.
  - Avoidance of large modelling uncertainties.
  - Approximate experimental sensitivity.

- Advantage of complementary sensitivity in production from different final states:
  - $m_{jj} > 450$ GeV from $H \to WW^*$
  - High p_T^H from $H \to bb$

Production modes

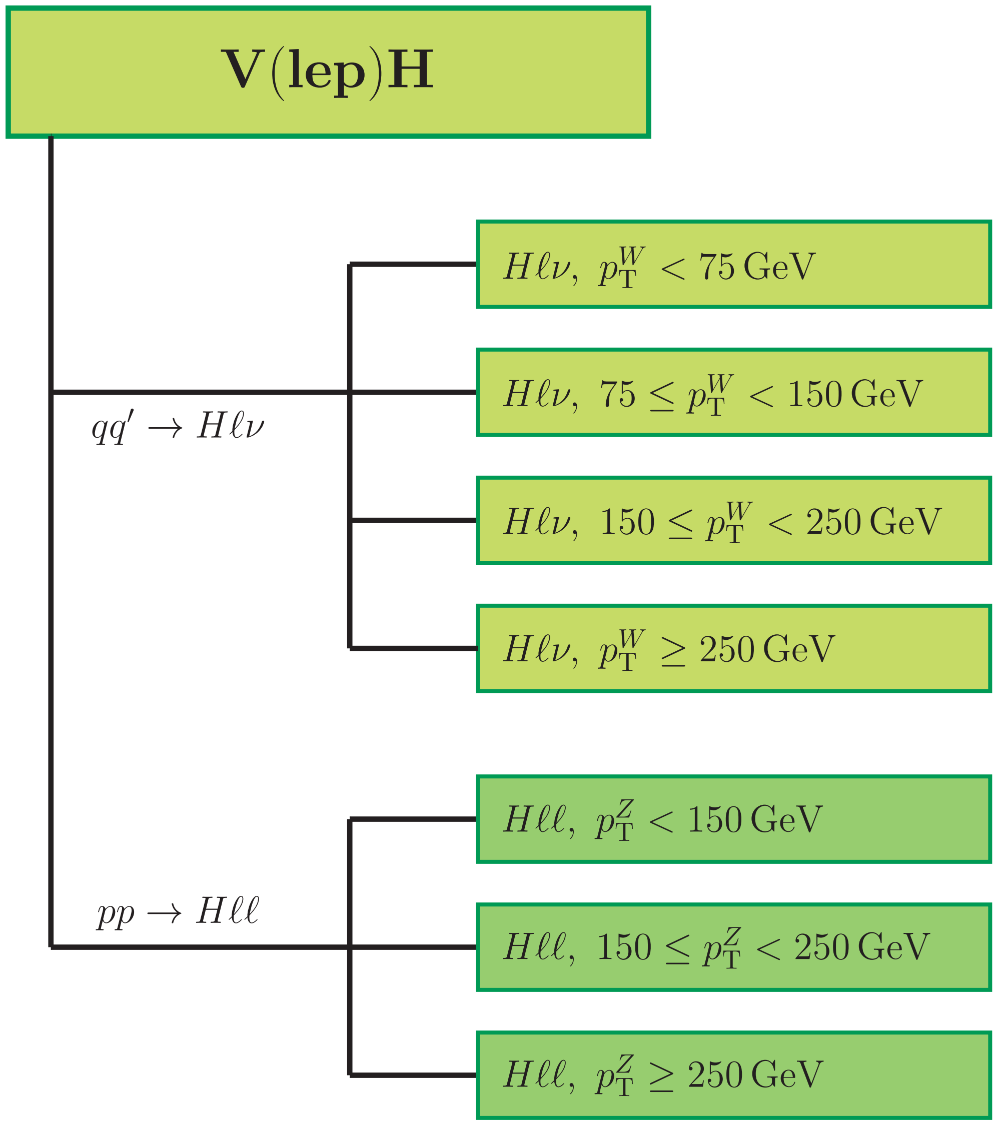

- Measure mutually exclusive phase-spaces in agreement with theory and LHC experiments
  - In terms of kinematics of the Higgs or associated objects in productions.
  - Sensitivity to deviations from SM.
  - Avoidance of large modelling uncertainties.
  - Approximate experimental sensitivity.
- Advantage of complementary sensitivity in production from different final states:
  - $m_{jj} > 450$ GeV from $H \to WW^*$
  - High $p_T{}^H$ from $H \to bb$

Production modes

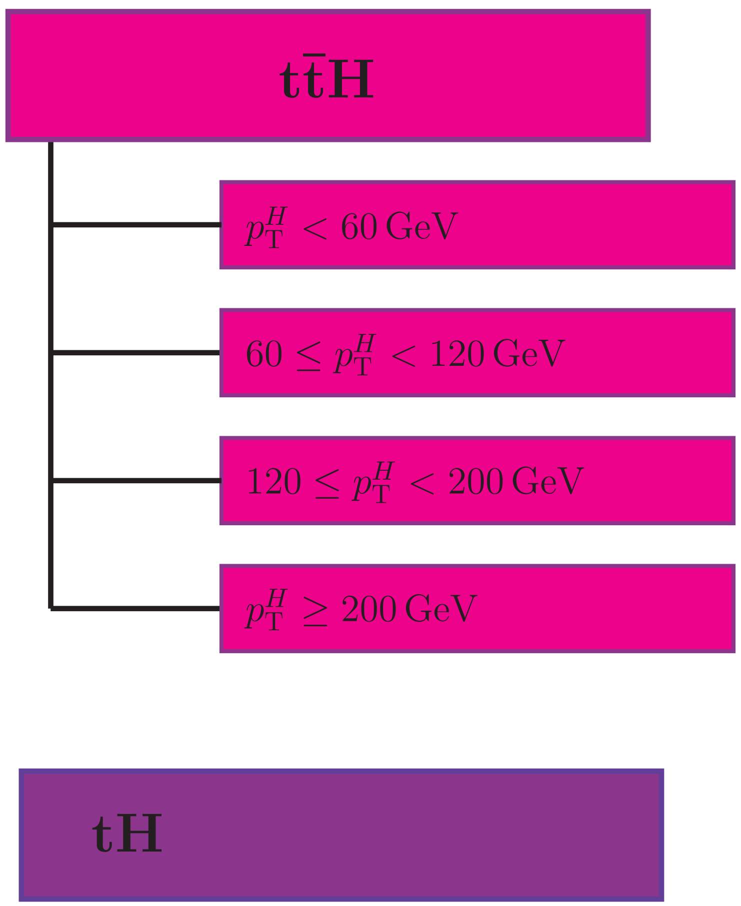

- Measure mutually exclusive phase-spaces in agreement with theory and LHC experiments
  - In terms of kinematics of the Higgs or associated objects in productions.
  - Sensitivity to deviations from SM.
  - Avoidance of large modelling uncertainties.
  - Approximate experimental sensitivity.

- Advantage of complementary sensitivity in production from different final states:
  - $m_{\mathrm{jj}} > 450\ \mathrm{GeV}$ from $H\to WW^{*}$
  - High $p_{\mathrm{T}}{}^{H}$ from $H\to bb$

- Strategy in measuring the cross section in these exclusive categories
  - Discussing here the example of the $H \to ZZ^*$

- Cut-based reconstruction-level categories,
  - maximising purity and minimising extrapolation to true phase-spaces.

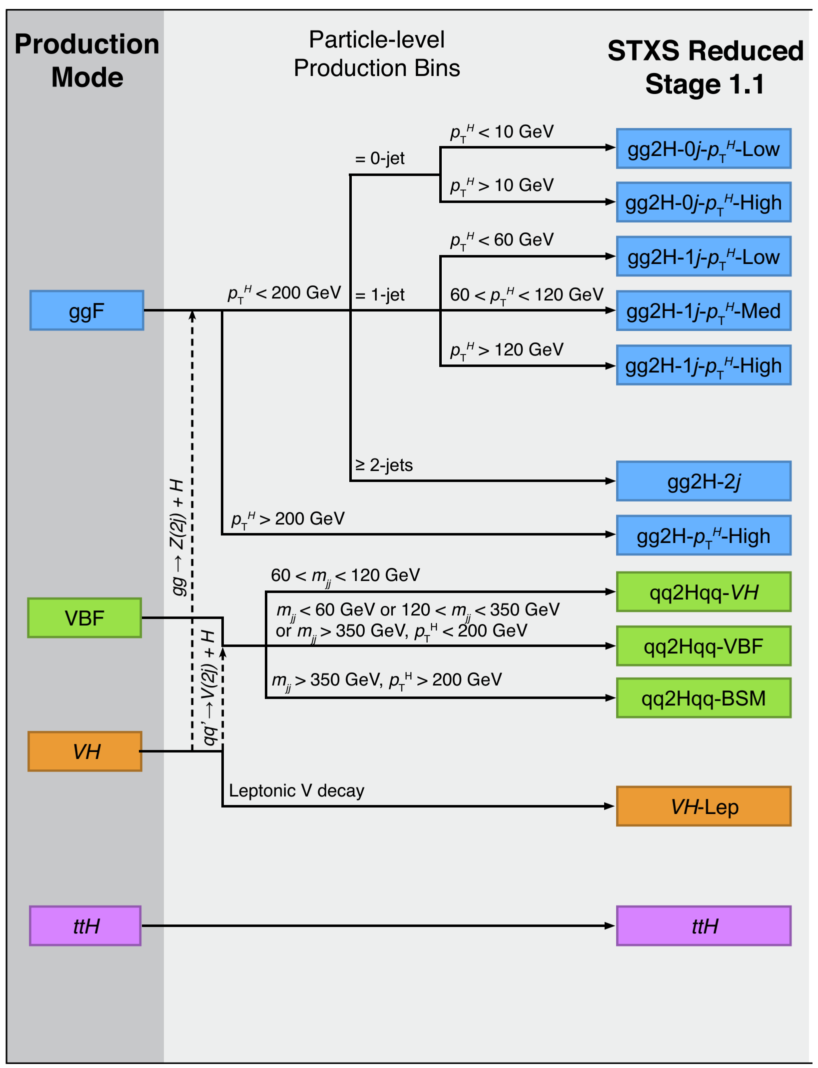

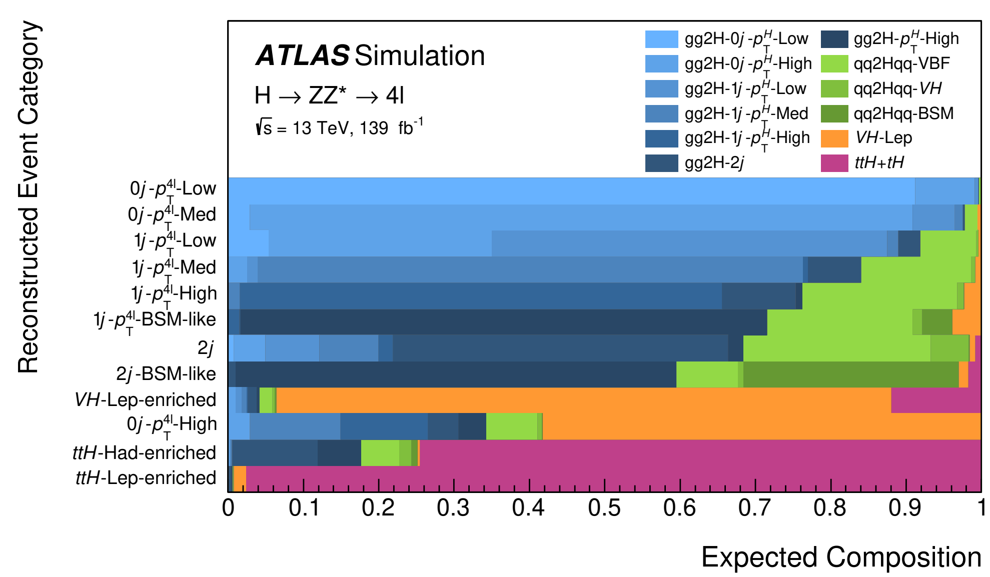

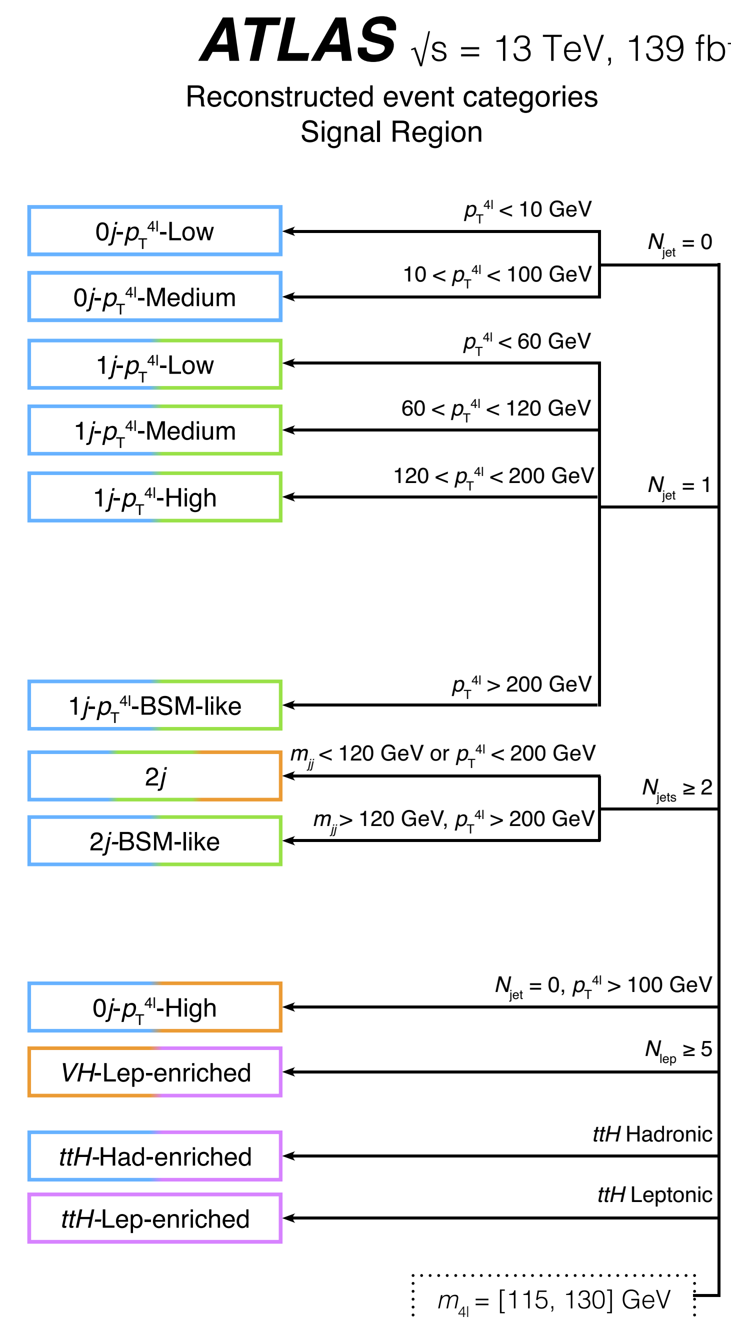

- Multi-output-node neural network discriminants in detector category.
  - Multidimensional fits on *n*-1dimensions on *n* output nodes per category.
- Backgrounds from data sidebands on resonant signal.
  - Performed as a function of the jet multiplicity to reduce higher order correction uncertainties.

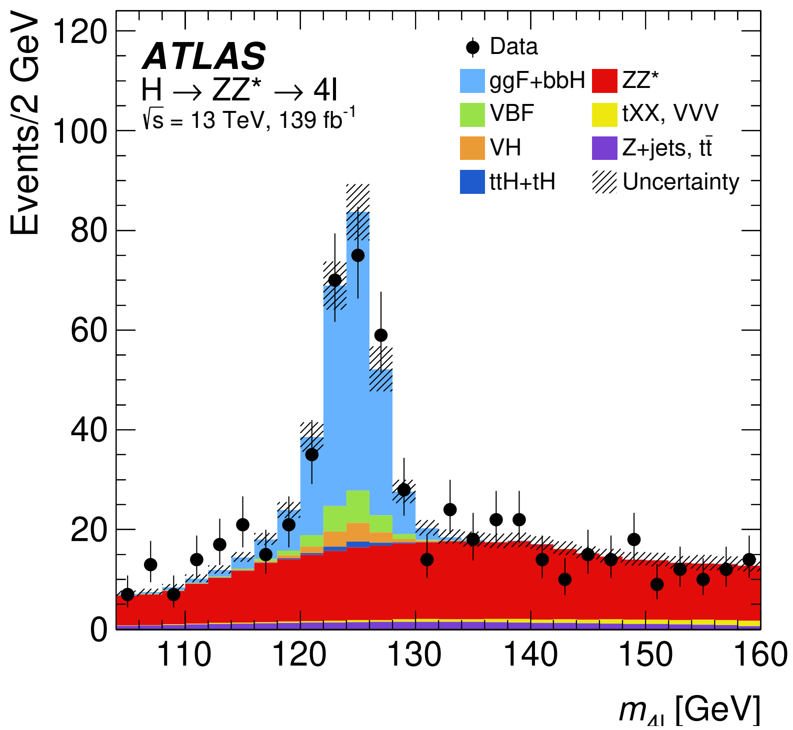

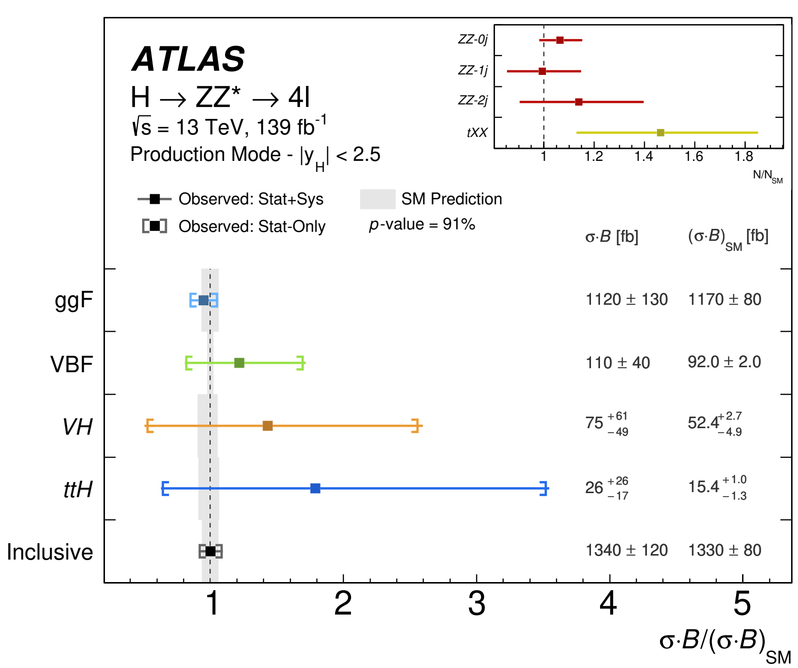

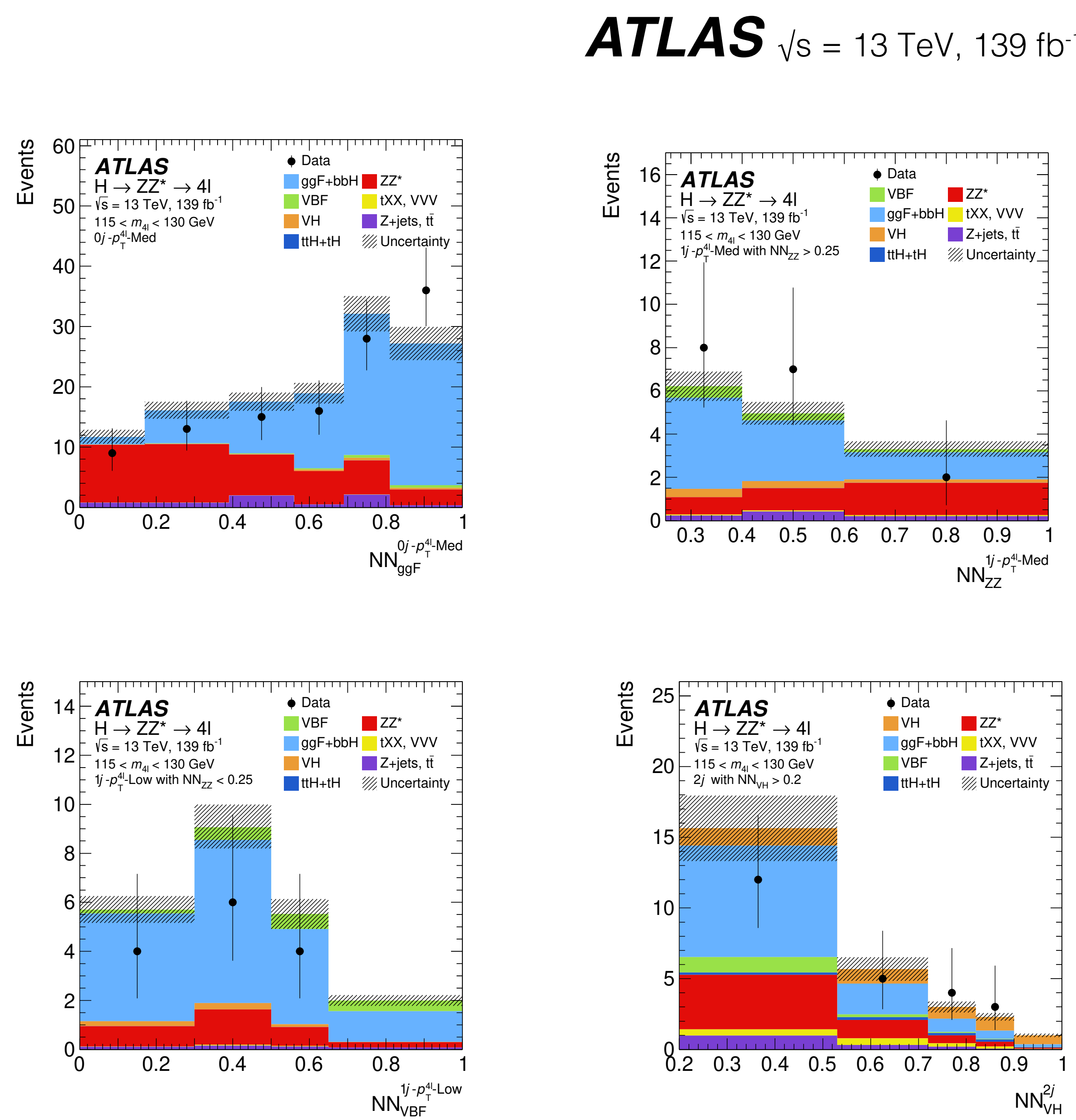

- Multi-output-node neural network discriminants in detector category.
  - Multidimensional fits on n-1 dimensions on n output nodes per category.
- Backgrounds from data sidebands on resonant signal.
  - Performed as a function of the jet multiplicity to reduce higher order correction uncertainties.

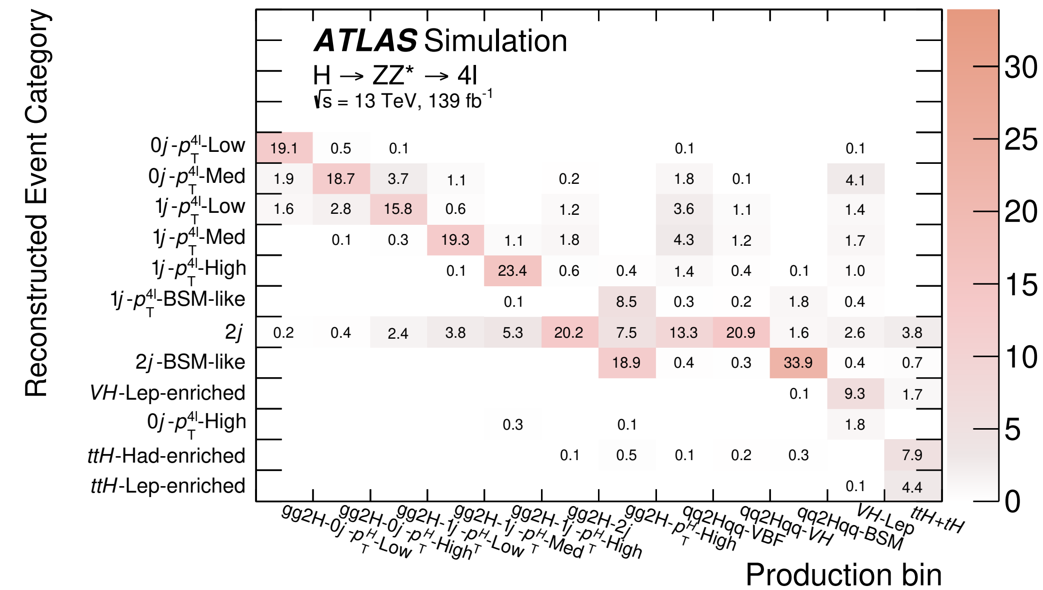

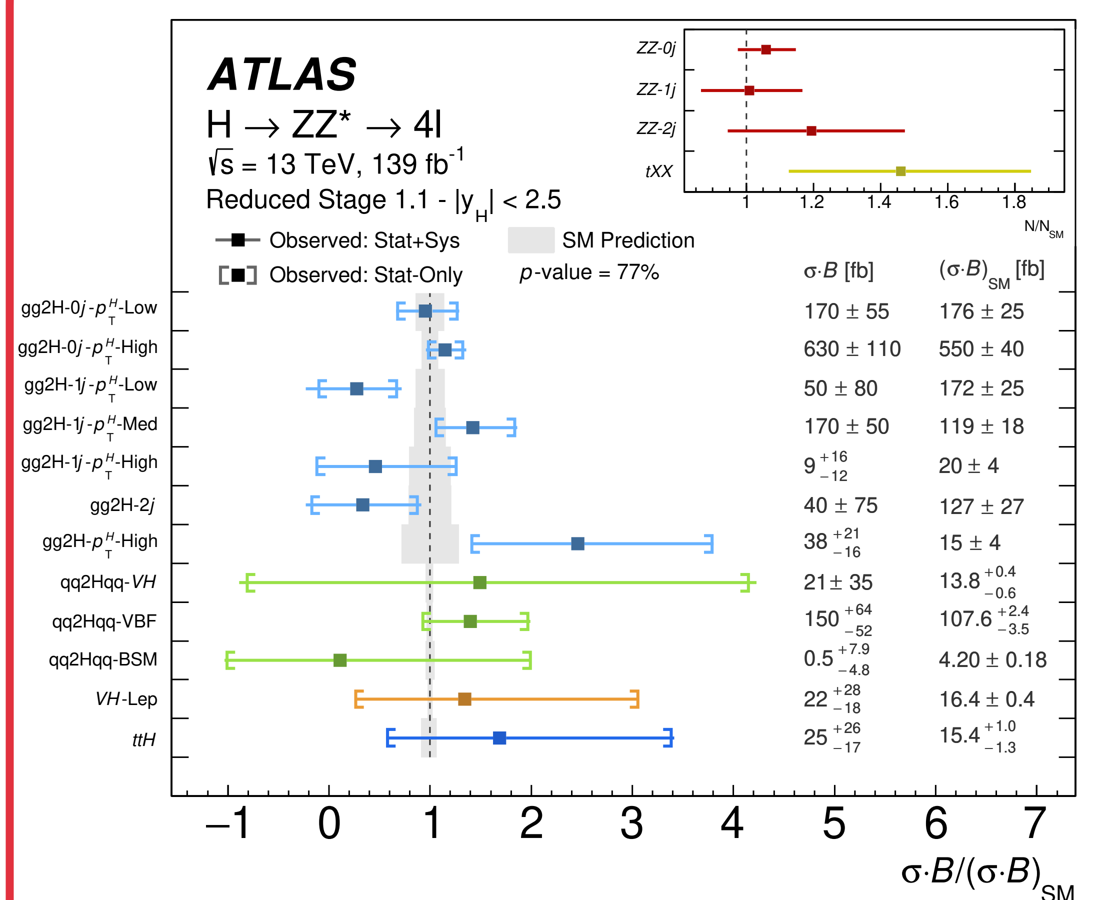

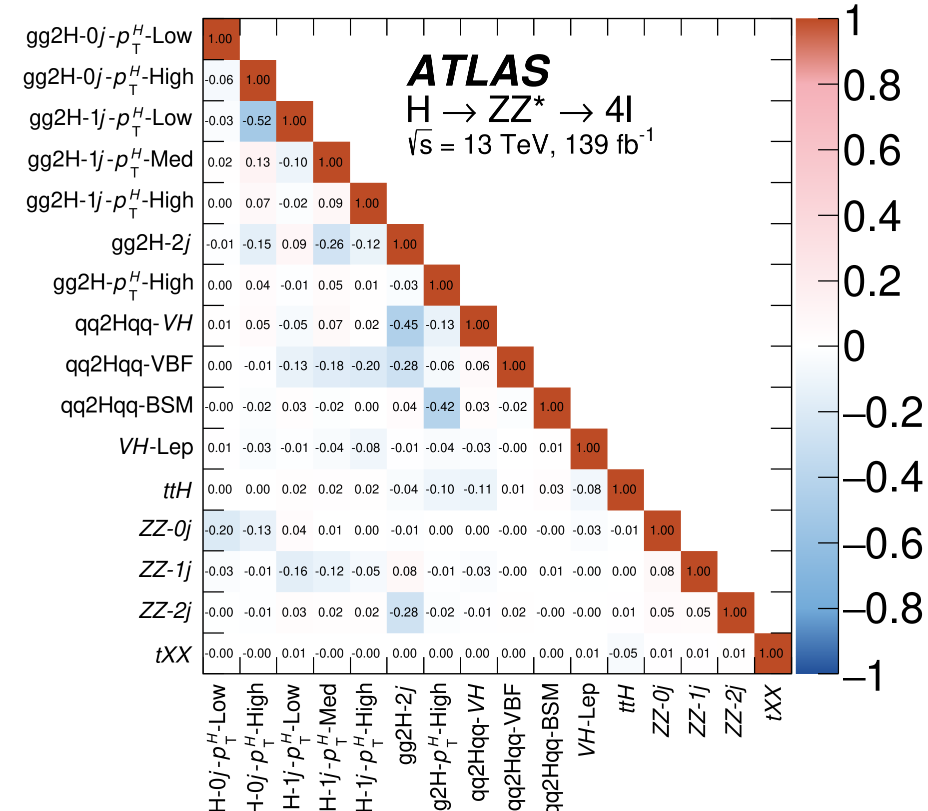

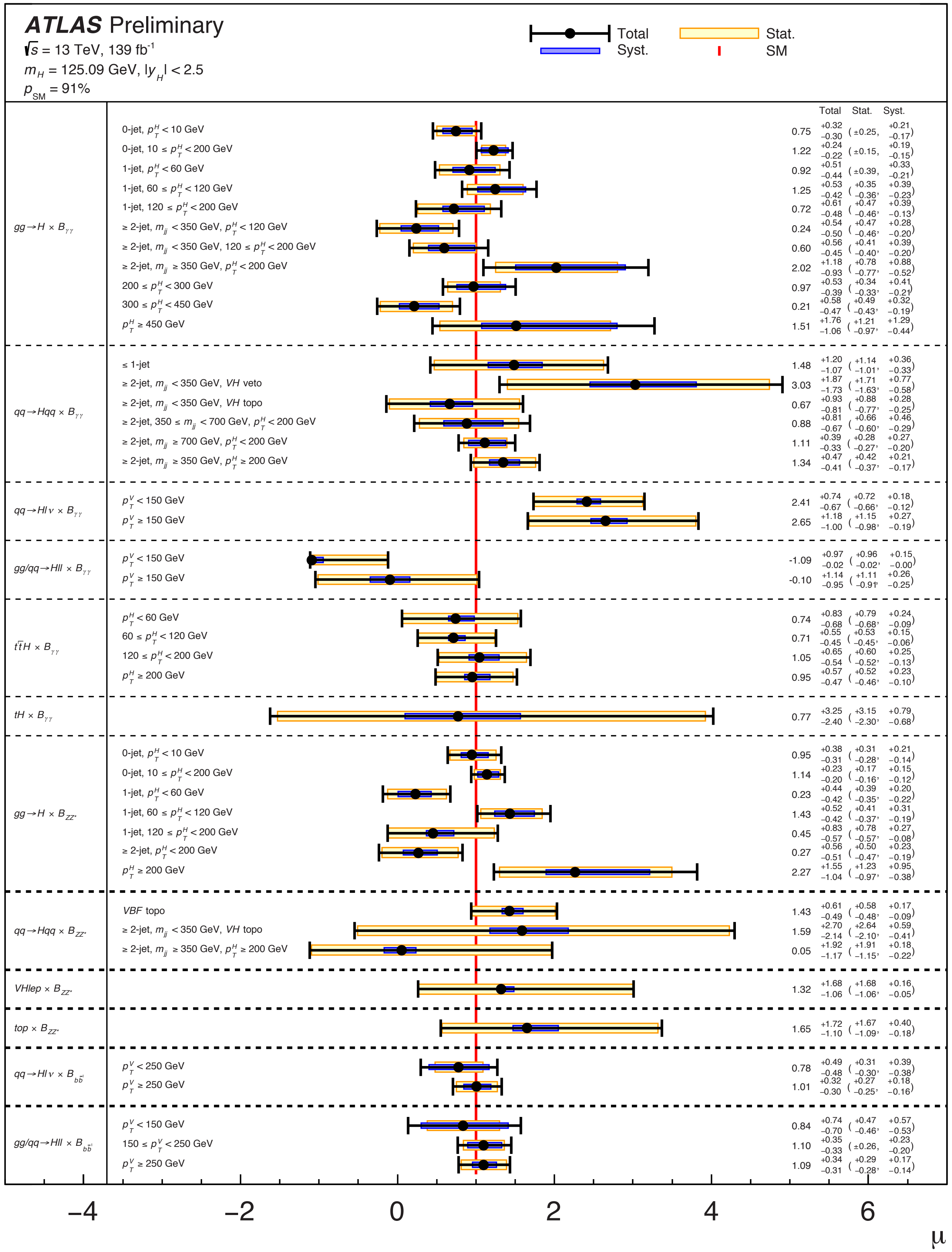

- Measure mutually exclusive phase-spaces in agreement with theory and LHC experiments
  - In terms of kinematics of the Higgs or associated objects in productions.
  - Sensitivity to deviations from SM.
  - Avoidance of large modelling uncertainties.
  - Approximate experimental sensitivity.

- Advantage of complementary sensitivity in production from different final states:
  - $m_{\mathrm{jj}} > 450$ GeV from $H \to WW^*$
  - High p_{T}^{H} from $H \to bb$

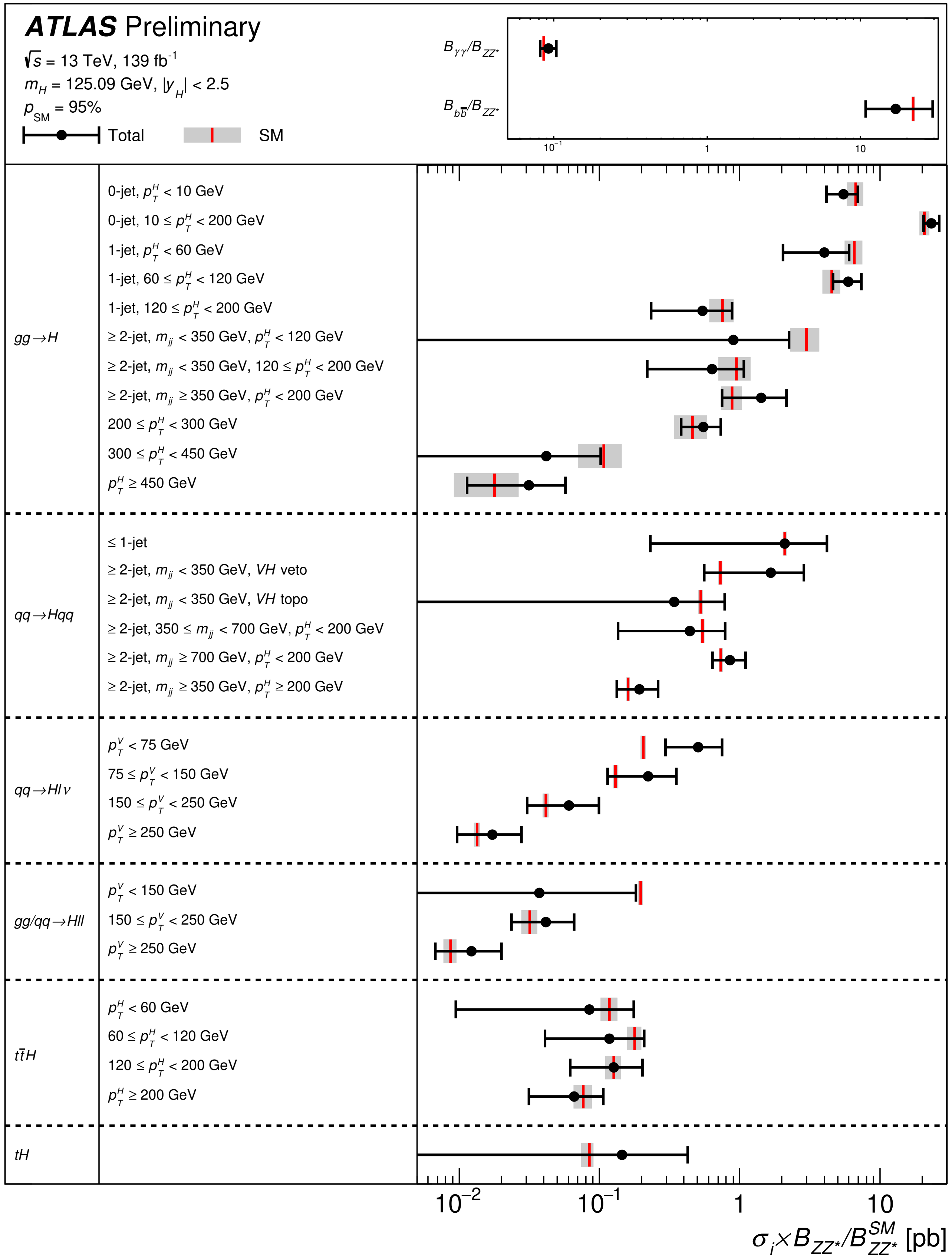

- Measure mutually exclusive phase-spaces in agreement with theory and LHC experiments
  - In terms of kinematics of the Higgs or associated objects in productions.
  - Sensitivity to deviations from SM.
  - Avoidance of large modelling uncertainties.
  - Approximate experimental sensitivity.

- Advantage of complementary sensitivity in production from different final states:
  - $m_{jj} > 450$ GeV from $H\to WW^*$
  - High $p_T{}^H$ from $H\to bb$

Couplings interpretations

- Interpretation of couplings cross sections in the context of new physics.
- Assuming production and decay are factorised

$$\sigma_i \times \mathrm{B}_f = \frac{\sigma_i(\boldsymbol{\kappa}) \times \Gamma_f(\boldsymbol{\kappa})}{\Gamma_H}$$

- Coupling strength modifiers

$$\kappa_j^2 = \frac{\sigma_j}{\sigma_j^{\mathrm{SM}}} \qquad \kappa_j^2 = \frac{\Gamma_j}{\Gamma_j^{\mathrm{SM}}}$$

$$\kappa_V = 1.03 \pm 0.03$$
$$\kappa_F = 0.97 \pm 0.07.$$

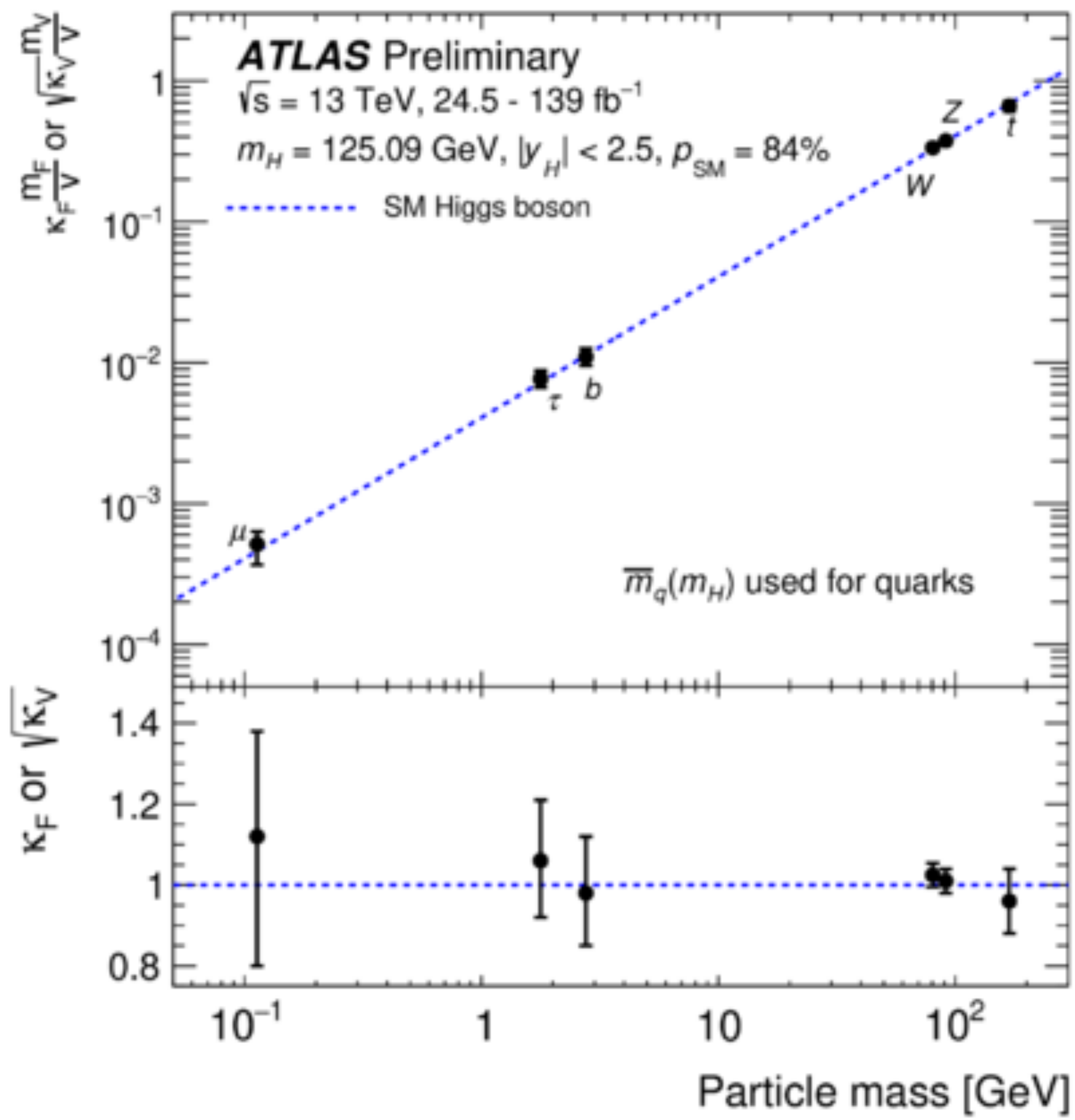

ATLAS-CONF-2019-005

- Results interpreted in the context of new physics:

$$\mathcal{L}_{\text{SMEFT}} = \mathcal{L}_{\text{SM}} + \sum_{i}^{N_{d6}} \frac{c_i}{\Lambda^2} \mathcal{O}_i^{(6)} + \sum_{j}^{N_{d8}} \frac{b_j}{\Lambda^4} \mathcal{O}_j^{(8)} + \ldots$$

  - Standard Model Effective Field Theory as the standard candle.
  - Probe for non-SM contributions to the tensor structure of the Higgs boson.

- Enhance sensitivity
  - by isolating dependencies in Wilson coefficients (c_i) allowing for simultaneous extraction through eigenvector decomposition of the dependencies.

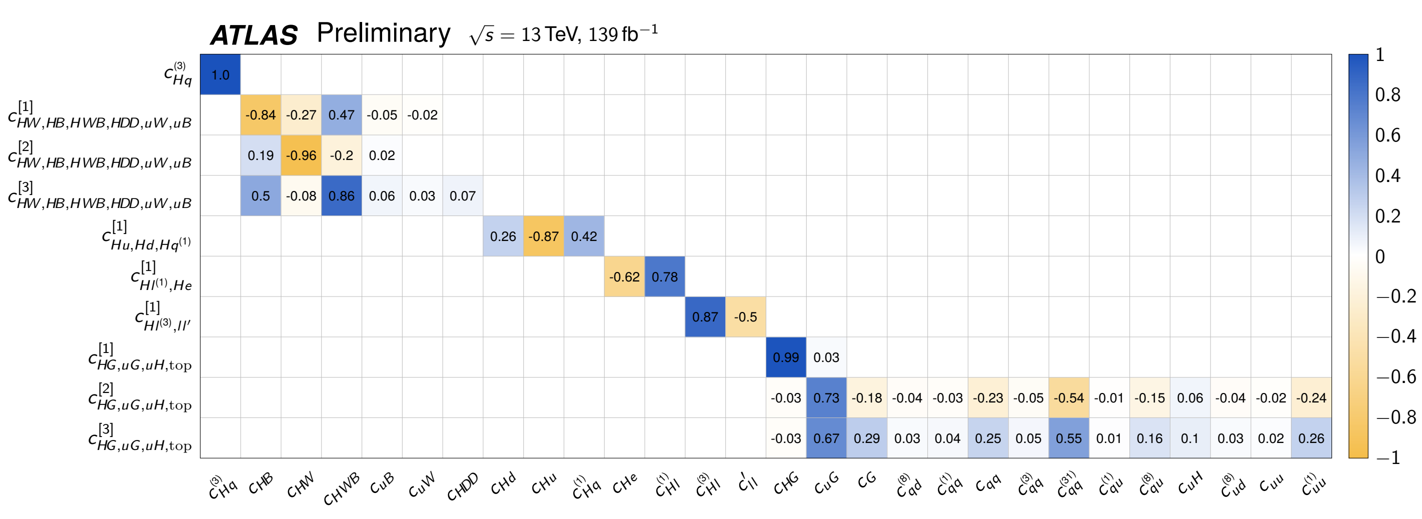

Coefficient	Operator	Example process
c_{HDD}	$(H^\dagger D^\mu H)^* (H^\dagger D_\mu H)$	
c_{HG}	$H^\dagger H\, G^A_{\mu\nu} G^{A\mu\nu}$	
c_{HB}	$H^\dagger H\, B_{\mu\nu} B^{\mu\nu}$	
c_{HW}	$H^\dagger H\, W^I_{\mu\nu} W^{I\mu\nu}$	
c_{HWB}	$H^\dagger \tau^I H\, W^I_{\mu\nu} B^{\mu\nu}$	
c_{eH}	$(H^\dagger H)(\bar{l}_p e_r H)$	
$c^{(1)}_{Hl}$	$(H^\dagger i \overleftrightarrow{D}_\mu H)(\bar{l}_p \gamma^\mu l_r)$	
$c^{(3)}_{Hl}$	$(H^\dagger i \overleftrightarrow{D}^I_\mu H)(\bar{l}_p \tau^I \gamma^\mu l_r)$	
c_{He}	$(H^\dagger i \overleftrightarrow{D}_\mu H)(\bar{e}_p \gamma^\mu e_r)$	
$c^{(1)}_{Hq}$	$(H^\dagger i \overleftrightarrow{D}_\mu H)(\bar{q}_p \gamma^\mu q_r)$	
$c^{(3)}_{Hq}$	$(H^\dagger i \overleftrightarrow{D}^I_\mu H)(\bar{q}_p \tau^I \gamma^\mu q_r)$	
c_{Hu}	$(H^\dagger i \overleftrightarrow{D}_\mu H)(\bar{u}_p \gamma^\mu u_r)$	
c_{Hd}	$(H^\dagger i \overleftrightarrow{D}_\mu H)(\bar{d}_p \gamma^\mu d_r)$	

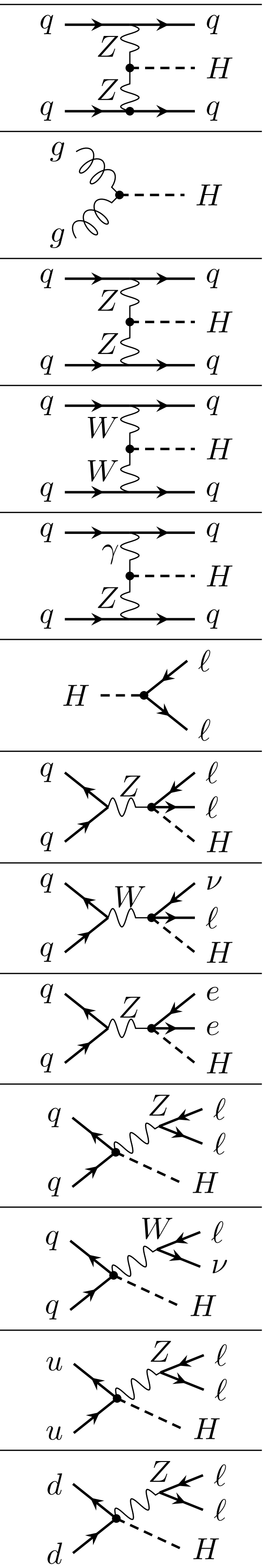

- Results interpreted in the context of new physics:

$$\mathcal{L}_{\mathrm{SMEFT}} = \mathcal{L}_{\mathrm{SM}} + \sum_{i}^{N_{d6}} \frac{c_i}{\Lambda^2} O_i^{(6)} + \sum_{j}^{N_{d8}} \frac{b_j}{\Lambda^4} O_j^{(8)} + \ldots$$

  - Standard Model Effective Field Theory as the standard candle.
  - Probe for non-SM contributions to the tensor structure of the Higgs boson.

- Account for BSM acceptance effects in kinematic observables of decay products

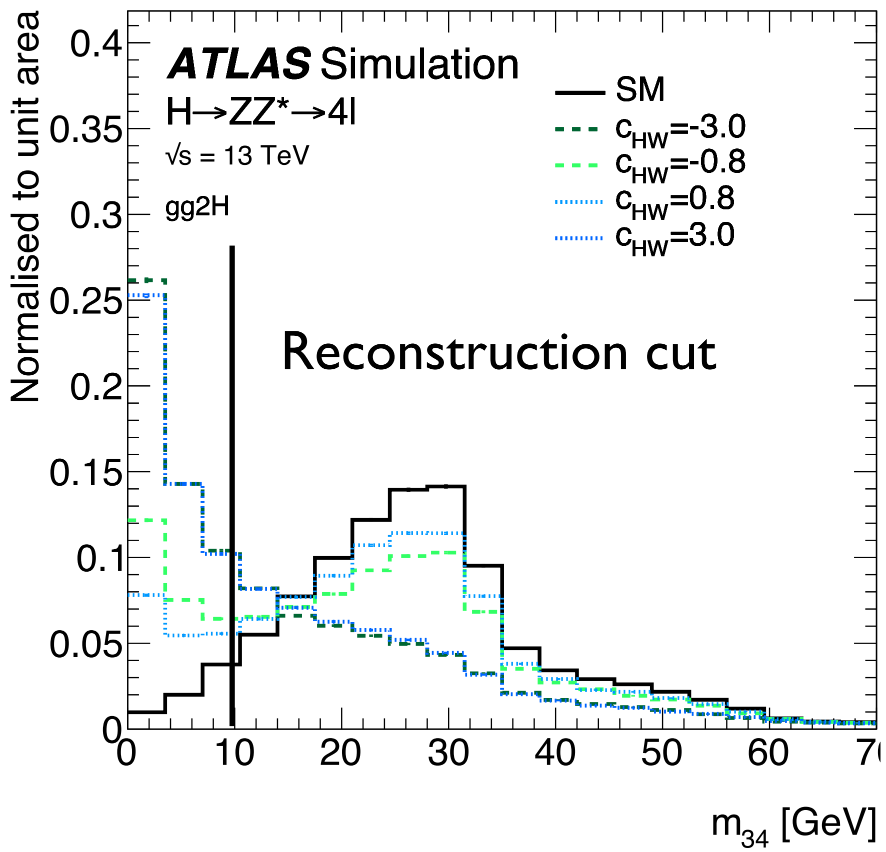

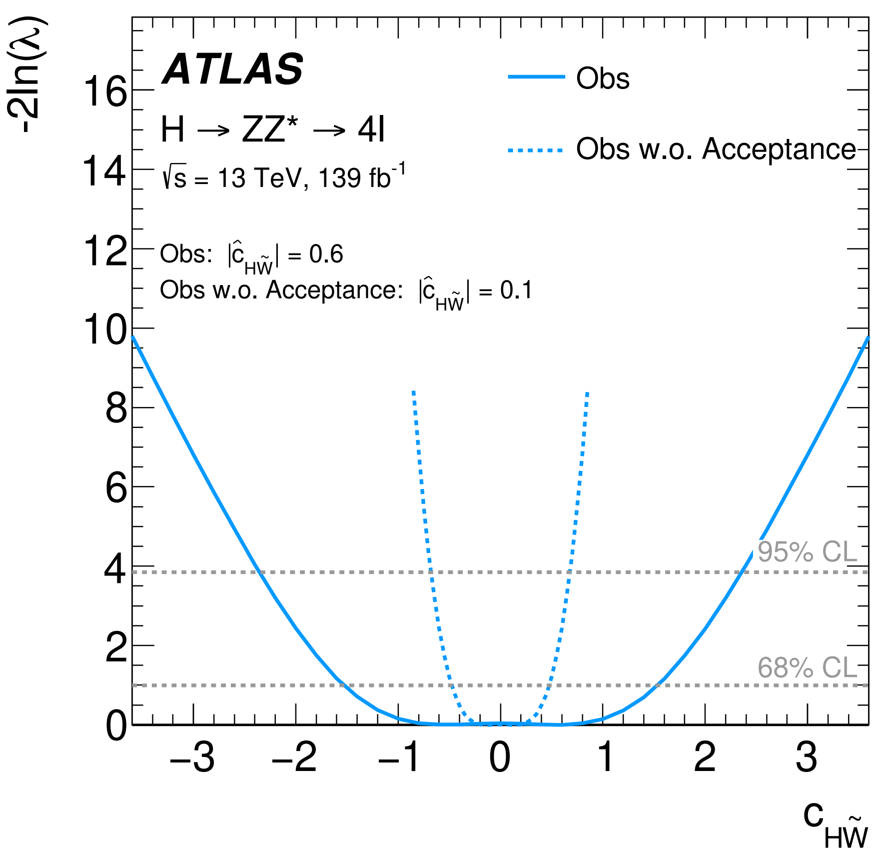

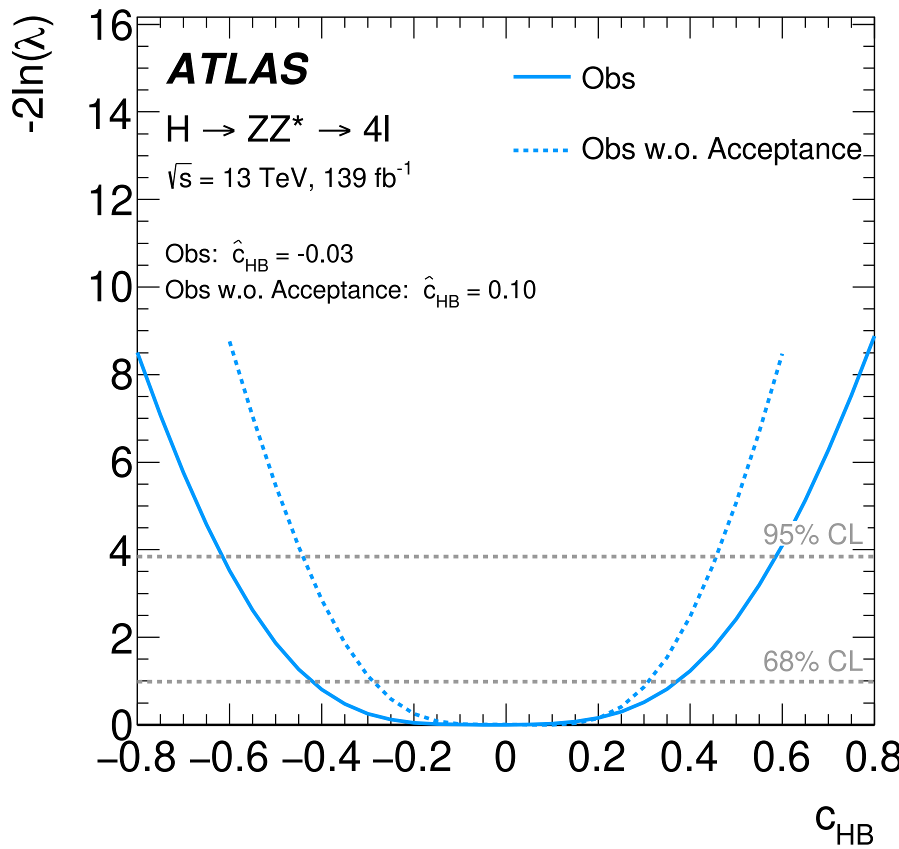

- Results interpreted in the context of new physics:
  - Results in both

$$\mathcal{L}_{\text{SMEFT}} = \mathcal{L}_{\text{SM}} + \sum_i^{N_{d6}} \frac{c_i}{\Lambda^2} \mathcal{O}_i^{(6)} + \sum_j^{N_{d8}} \frac{b_j}{\Lambda^4} \mathcal{O}_j^{(8)} + \ldots$$

    - linear approximation for dim-6 operators and,
    - linear plus quadratic approximation for general sensitivity to dim-8, suppressed by Λ^{-4}

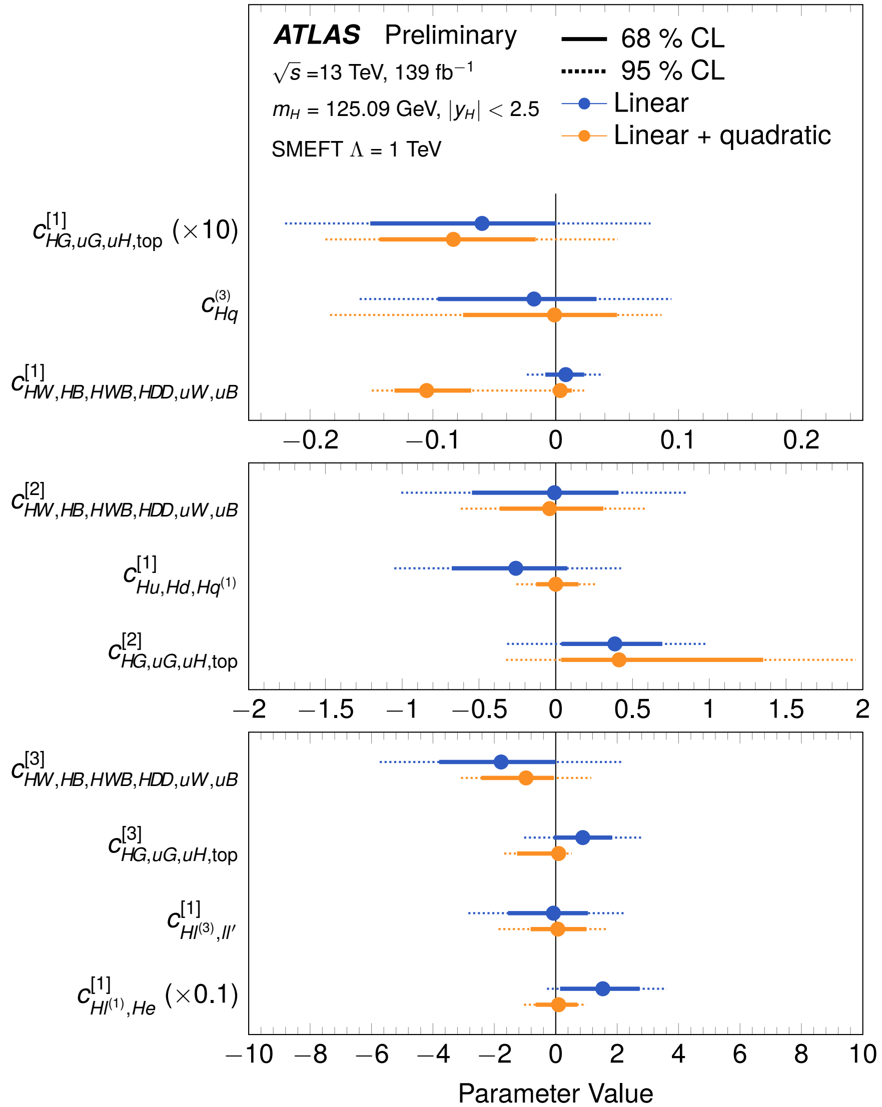

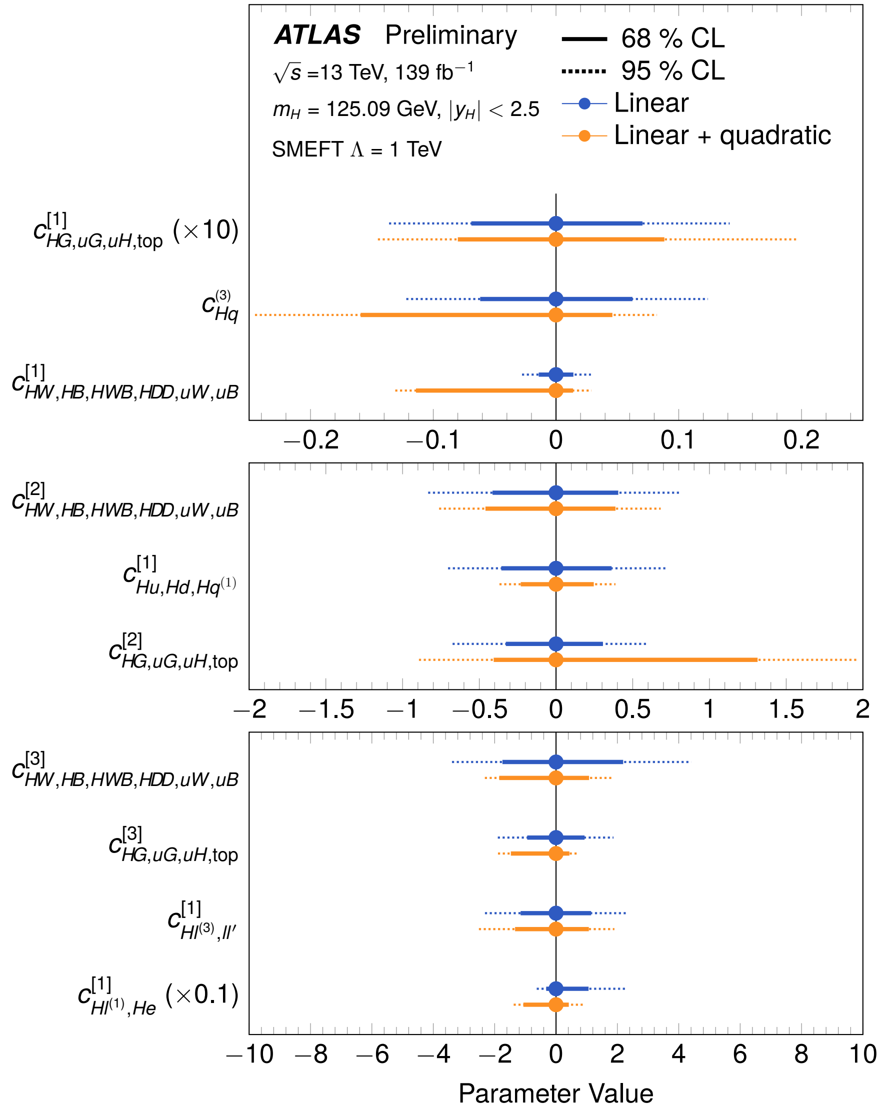

5. Differential cross section measurements

- At Run II sufficient statistics for constraining differential measurements
- Fiducial cross section definition
  - including detector efficiency (C) , detector acceptance (A) and branching $\mathscr{B}$

$$\sigma_{i,\mathrm{fid}} = \sigma_i \times A_i \times \mathcal{B} = \frac{N_{i,\mathrm{fit}}}{\mathcal{L} \times C_i}$$

  - Cuts mimicking reconstruction selection:

    (i) Model independent result.

    (ii) No extrapolation beyond measurable phase-space

- In diboson channels, resonant peak over smooth background
  - Good resolution on final-state particles, in particular in $H \rightarrow 4\ell$, $\gamma\gamma$
- Unfolding performed within the signal extraction fit
  - Via detector response inversion.
  - Reduces further any model assumptions in disentangling for detector effects

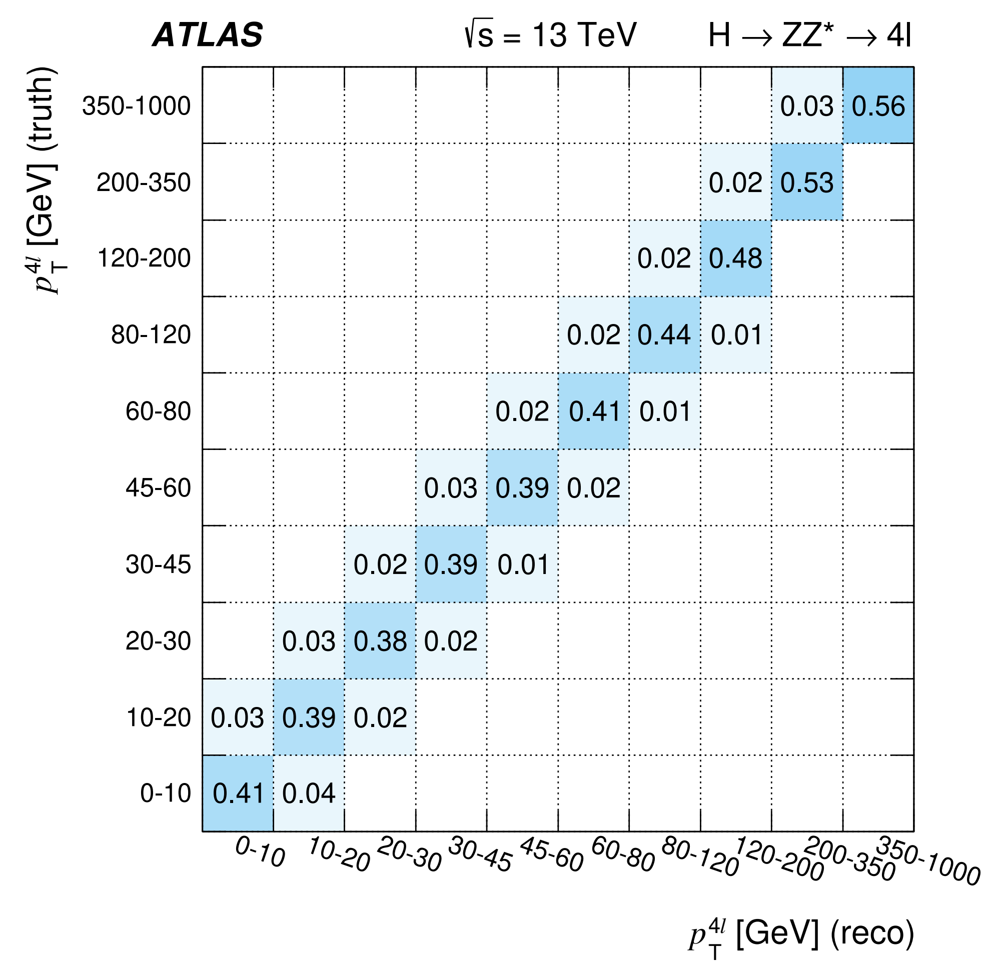

- Inclusive fiducial cross sections:

$$H \to \gamma\gamma \quad 60.4 \pm 6.1\ \text{(stat.)} \pm 6.0\ \text{(exp.)} \pm 0.3\ \text{(theo.)}\ \text{fb}$$

  - SM predictions of 3.33 ± 0.15 fb ($H \to ZZ$) and 63.5 ± 3.3 fb ($H \to \gamma\gamma$)

- For ZZ also cross section per final state
  - Eventually sensitivity to final state interference (10%) in same flavour quadruplets

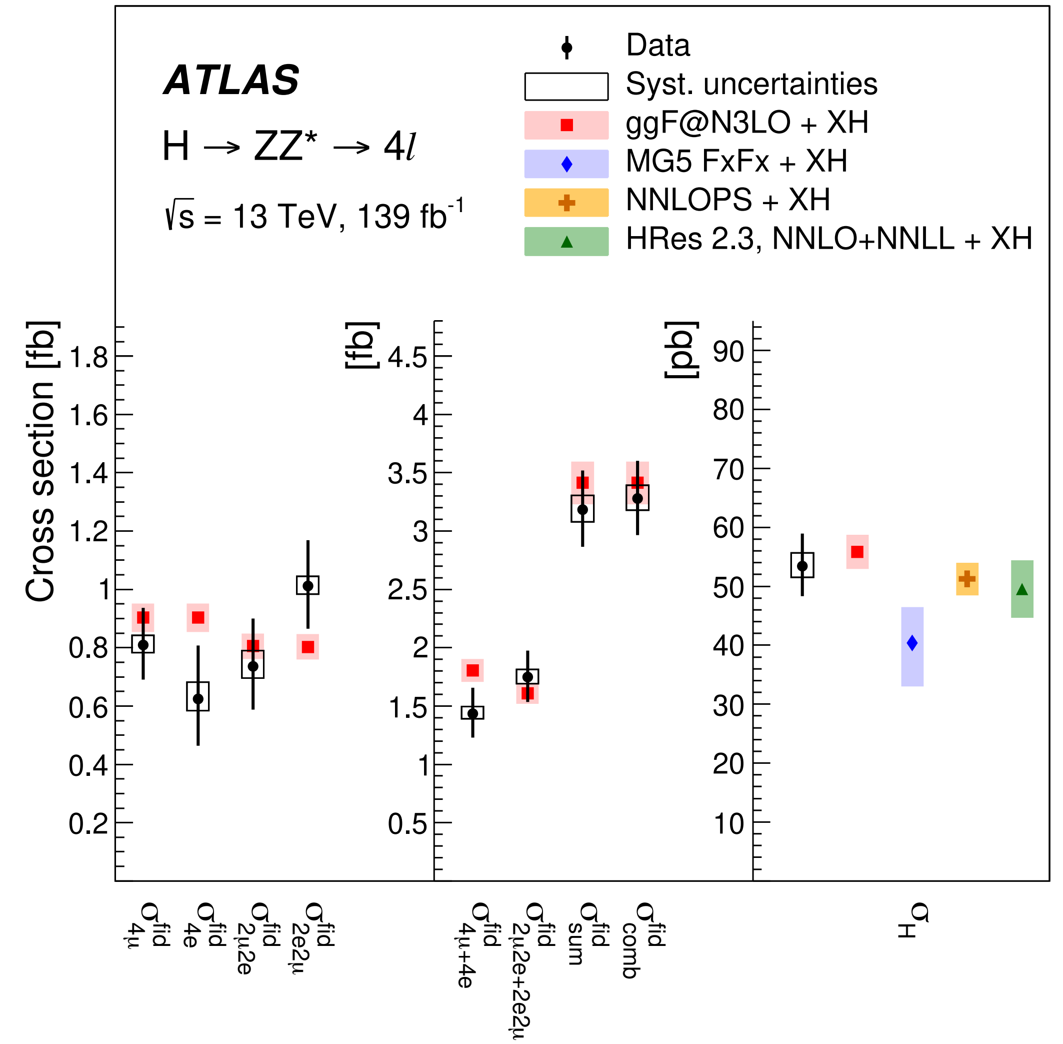

- In H→4ℓ m_{12} vs m_{34}: sensitivity to contact interactions:
  - ε_R, ε_L and κ: flavour universal modifiers of the contact terms between H, Z and leptons (arXiv:1504.04018)
    - ✦ Angular distributions unaffected: same Lorentz structure as SM term.

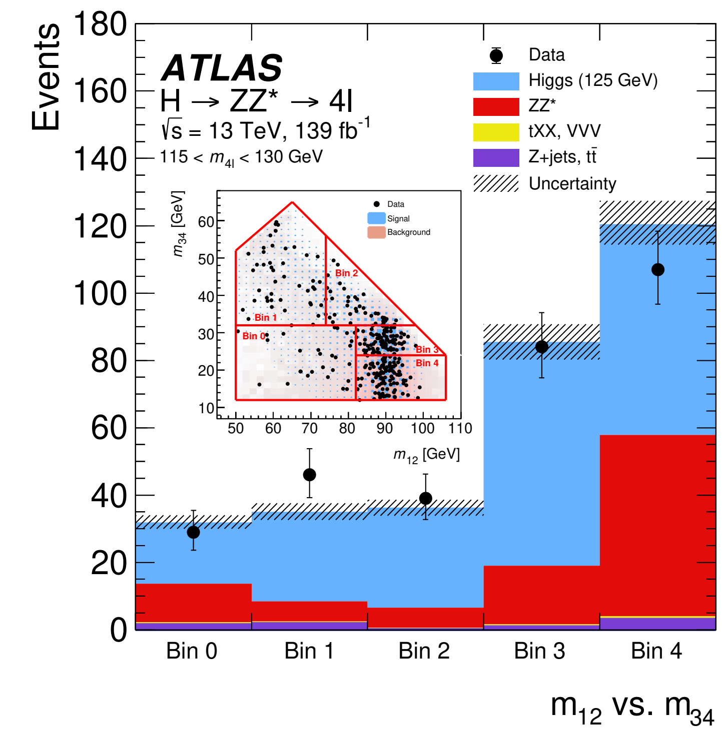

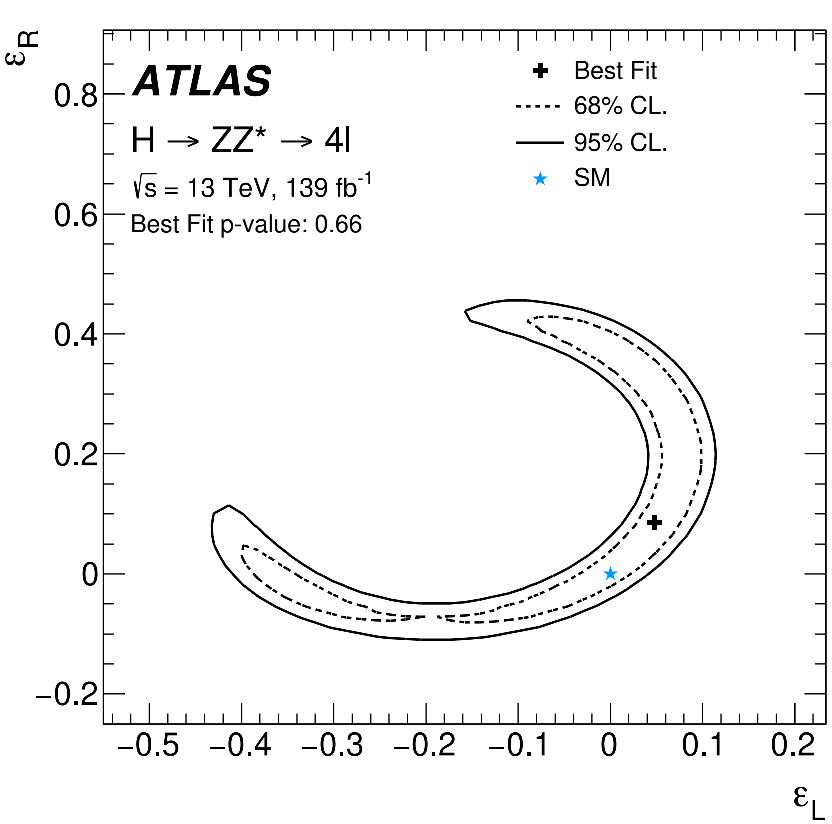

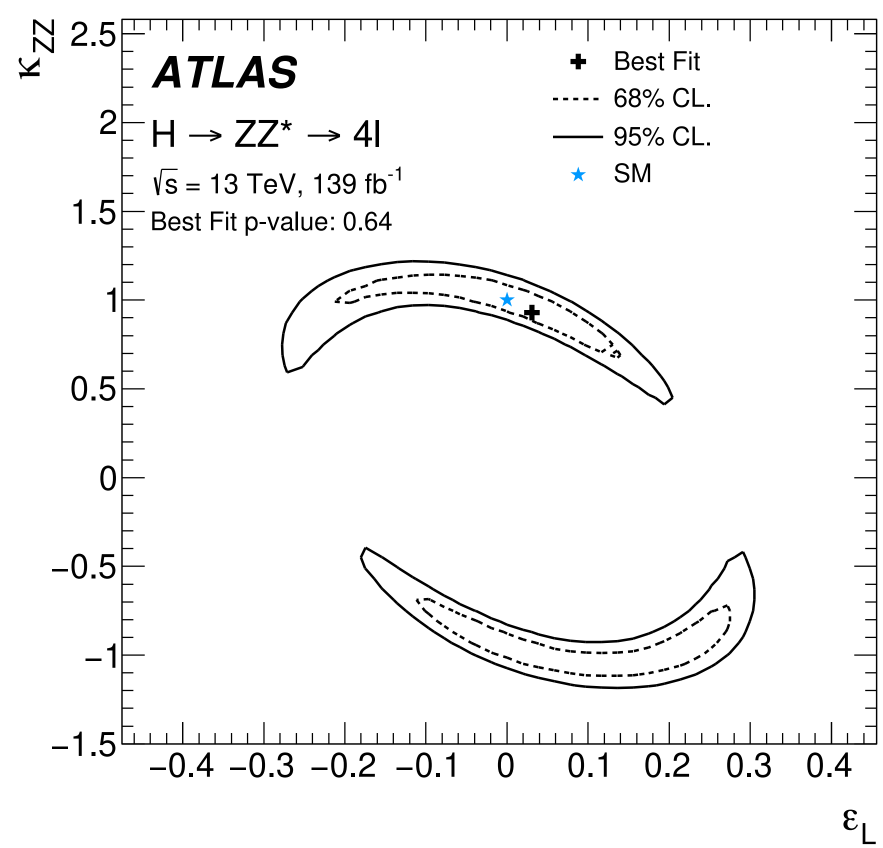

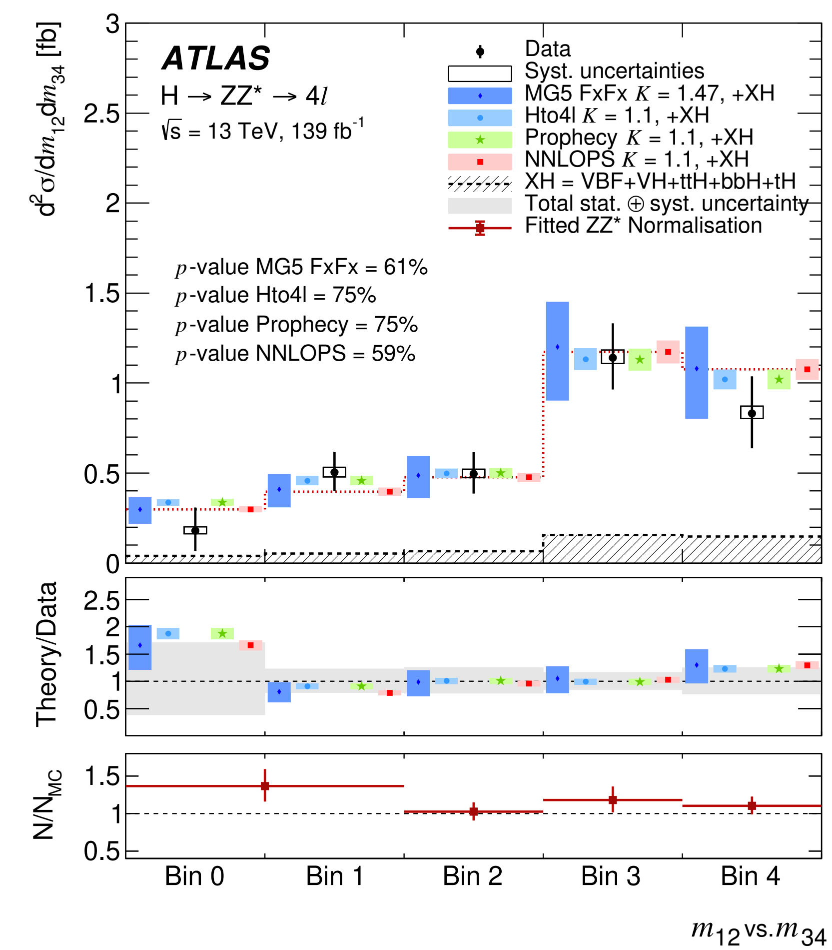

- 4ℓ: isolate signal under the Higgs resonant peak ($115 < m_{4\ell} < 130$).
- $\gamma\gamma$ cross section extracted from resonant peak over the $\gamma\gamma$ continuum.
- Higgs boson $p_{T,4\ell(\gamma\gamma)}$ and rapidity ($y_{4\ell(\gamma\gamma)}$) probe.
  - $p_{T,4\ell(\gamma\gamma)}$: Lagrangian structure of H interactions, Yukawa couplings
  - $y_{4\ell(\gamma\gamma)}$: Sensitivity to proton's parton density functions.

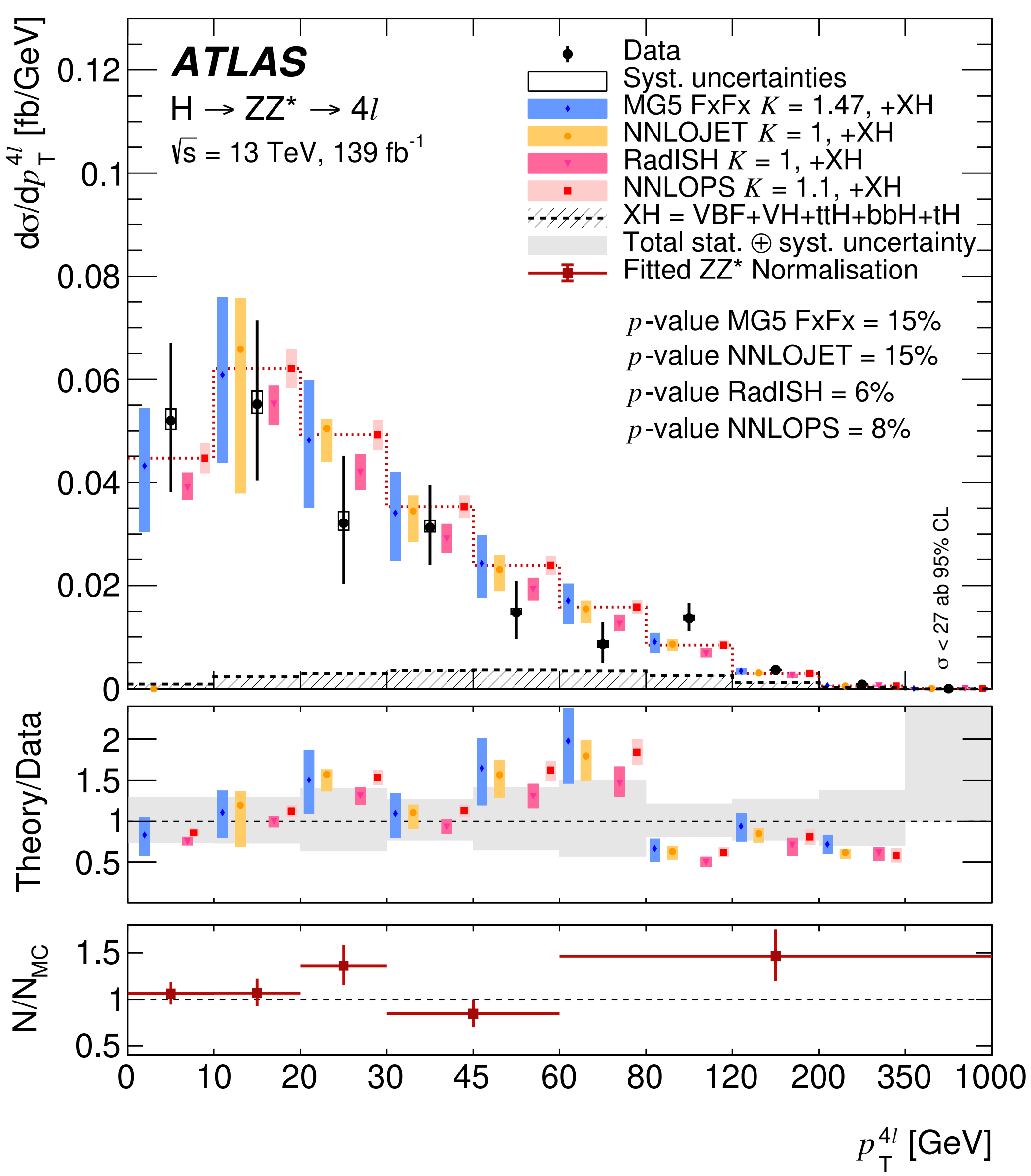

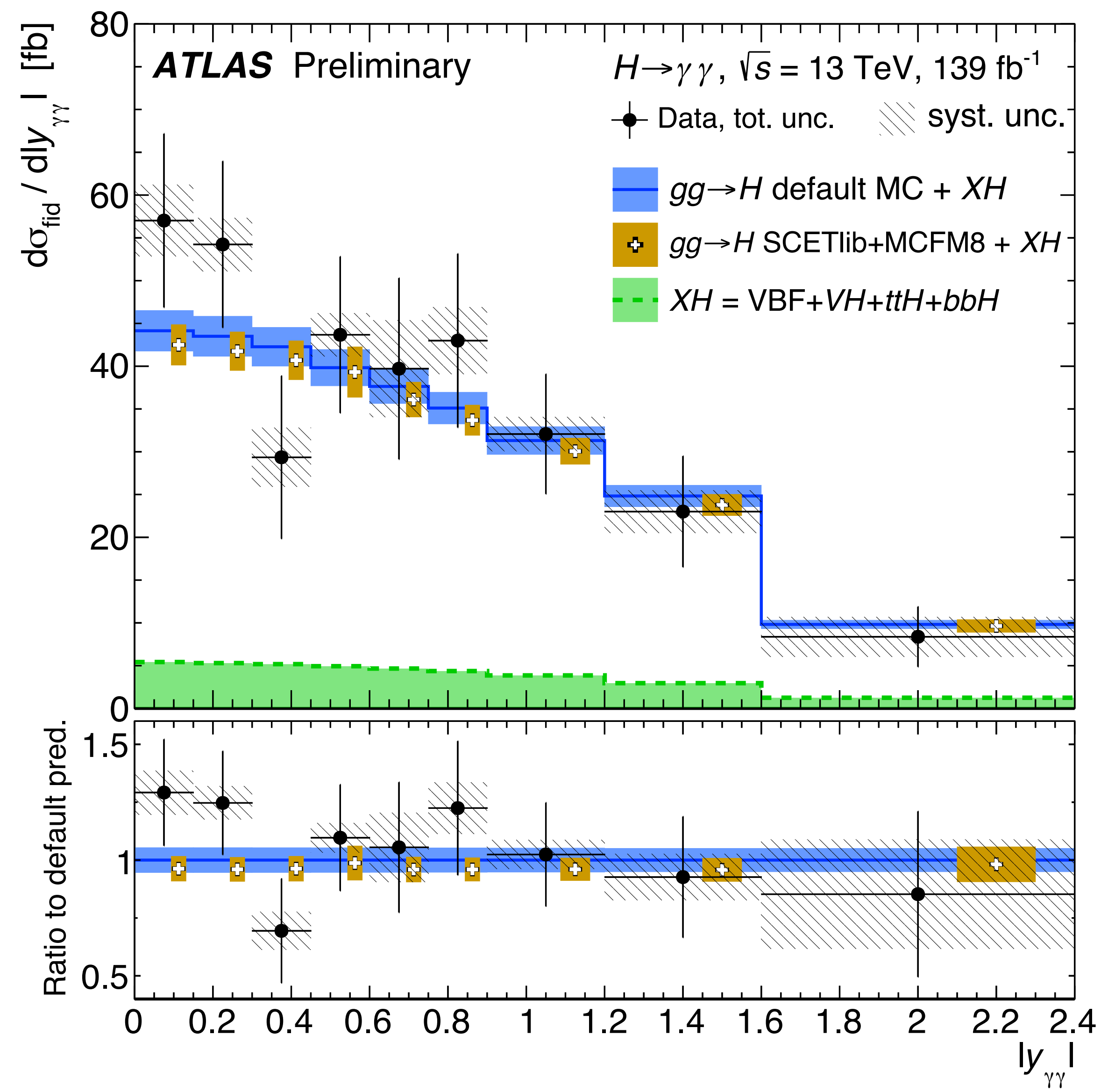

- At Run II sufficient statistics for constraining differential measurements
  - Increased precision needed to disentangle effects from higher-order corrections from observables spectra:
    - Ex Higgs p_T as a function of jet vetos

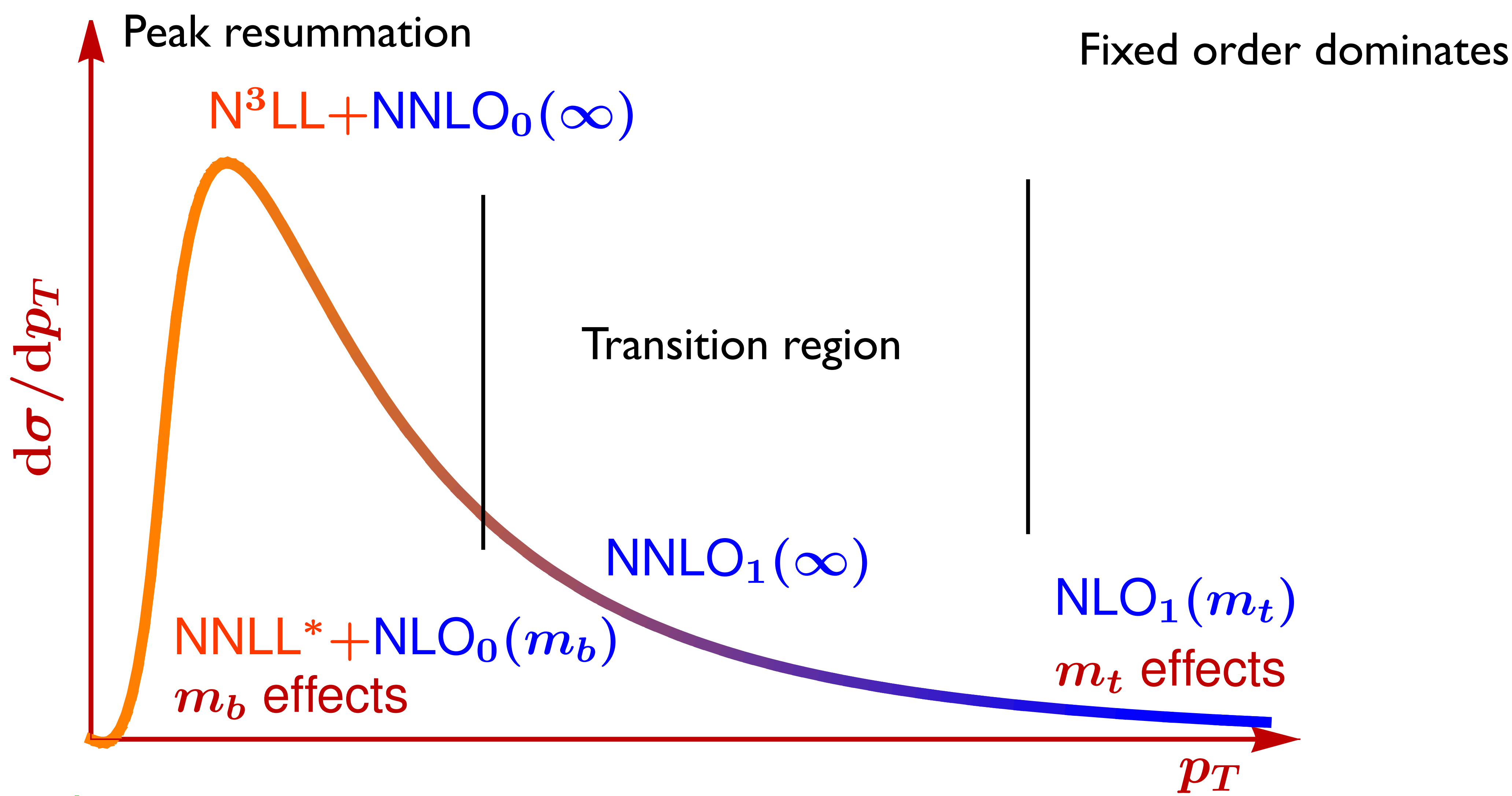

Depiction adapted from F. Tackmann

Differential cross section

- At Run II sufficient statistics for constraining differential measurements
  - Increased precision needed to disentangle effects from higher-order corrections from observables spectra:
    - Ex Higgs p_T as a function of jet vetos
    - State of the art predictions in these regions start being published.

Peak resummation

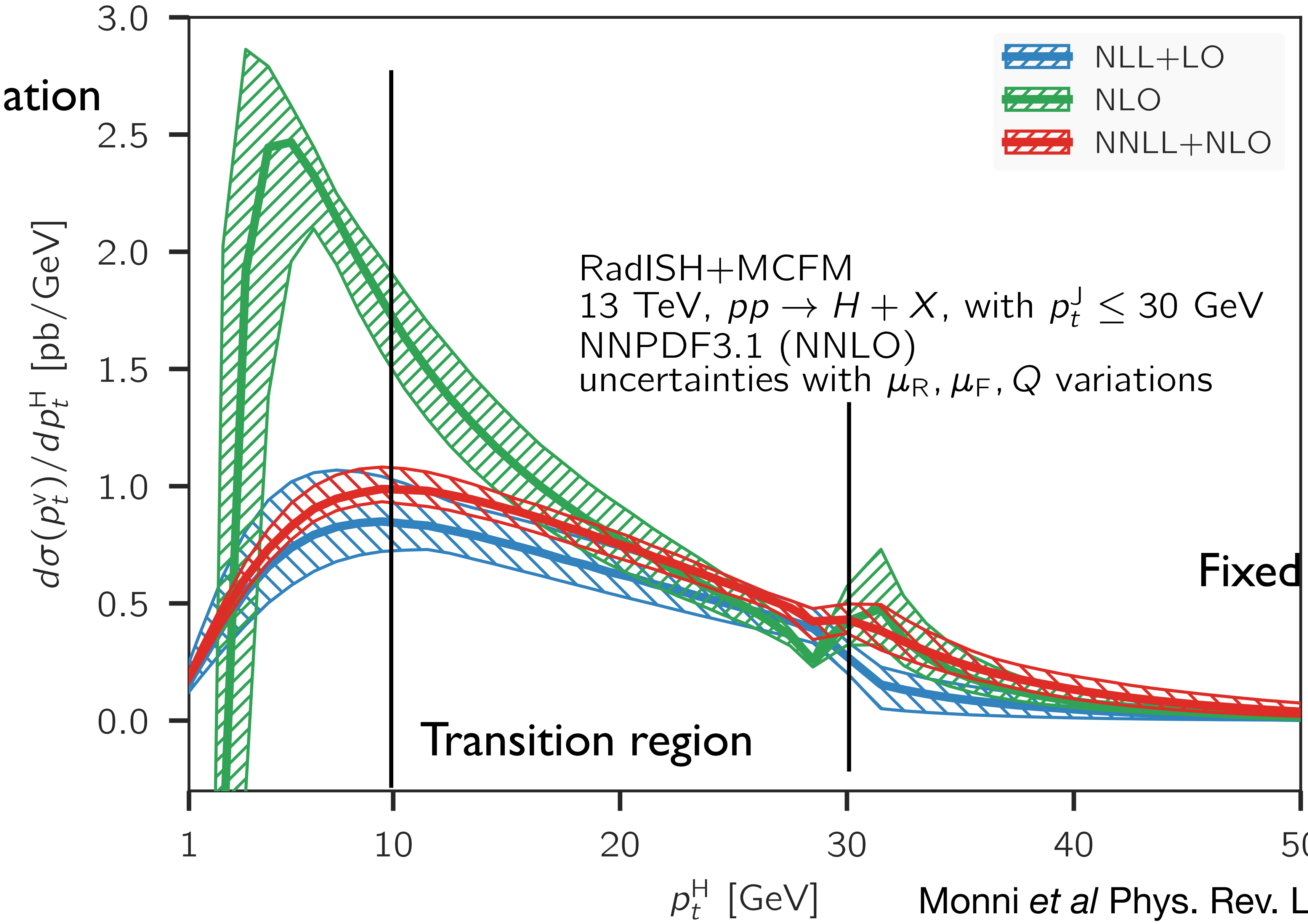

Fixed order dominates

Monni *et al* Phys. Rev. Lett. 124, 252001 (2020)

- Increased precision needed to disentangle effects from higher-order corrections from observables spectra:
  - Measurements at Run-2 competitive on these state-of-the art predictions
    - Ex RADISH and NNLOJET.

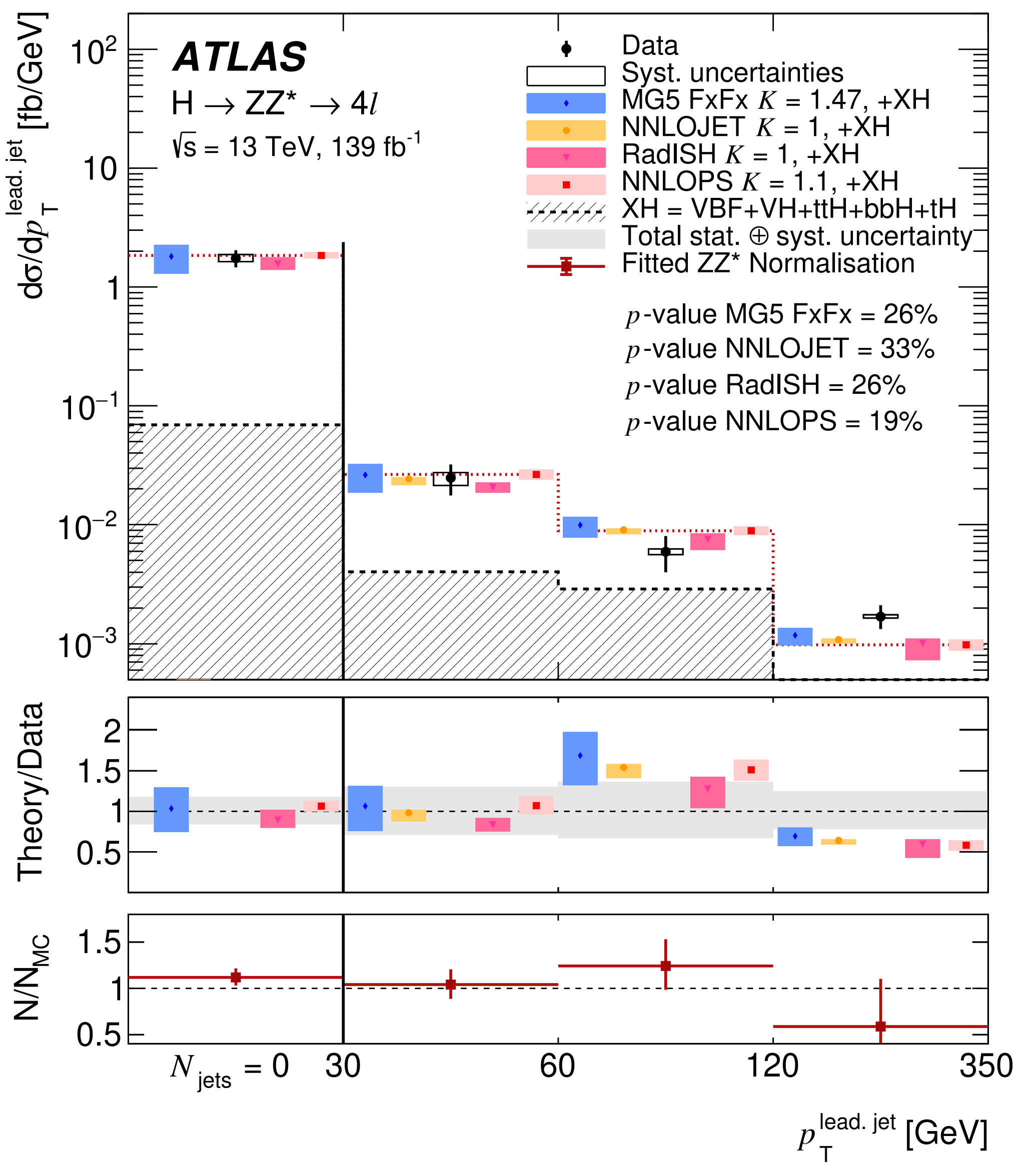

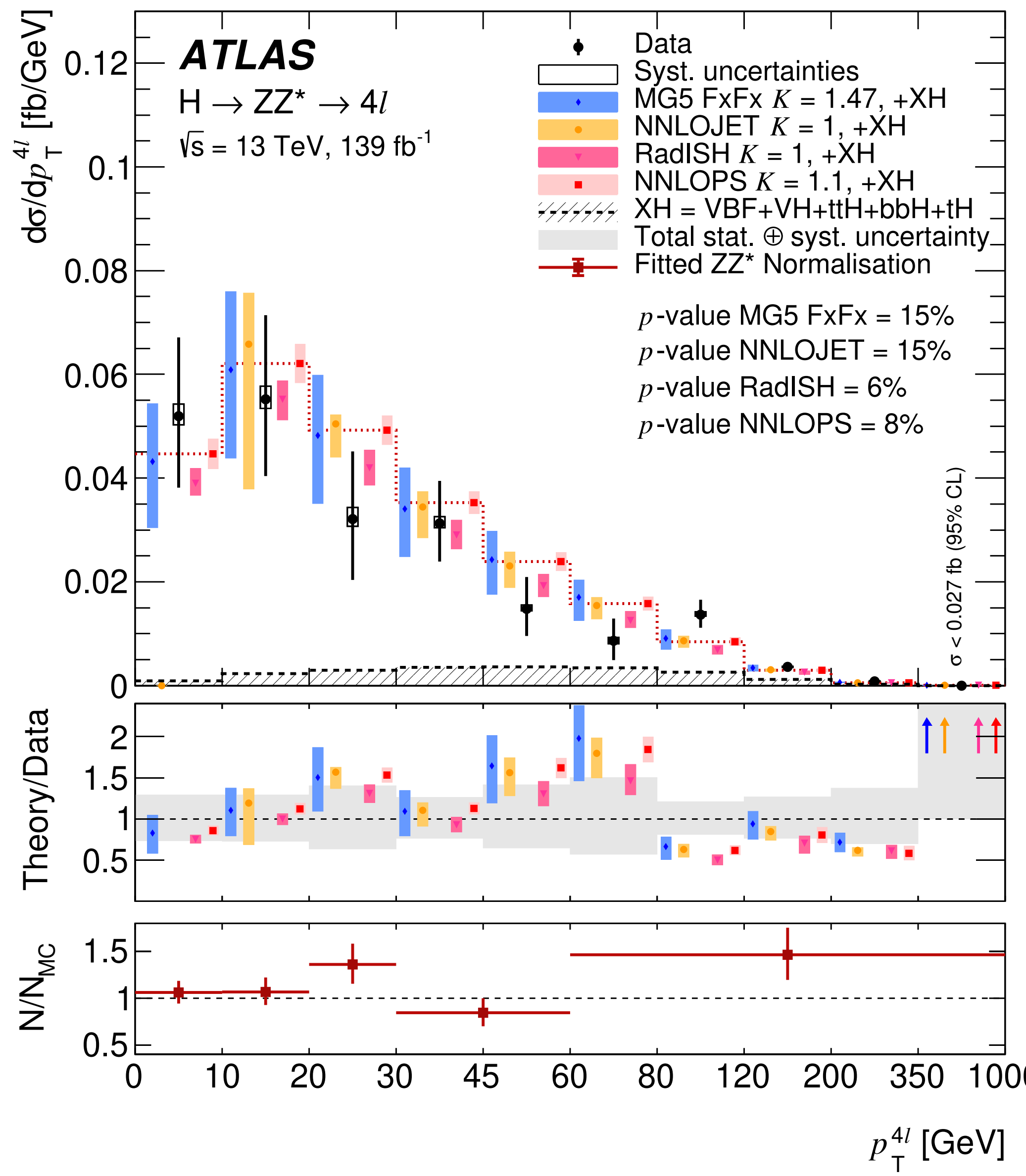

- Double differential $\mathrm{d}^2\sigma/\mathrm{d}p_{\mathrm{T}}\mathrm{d}N_{\mathrm{J}}$:
  - Probe the Higgs production mode
  - *N*j = 0 dominated buy ggF production
  - *N*j > 1 VBF enriched production

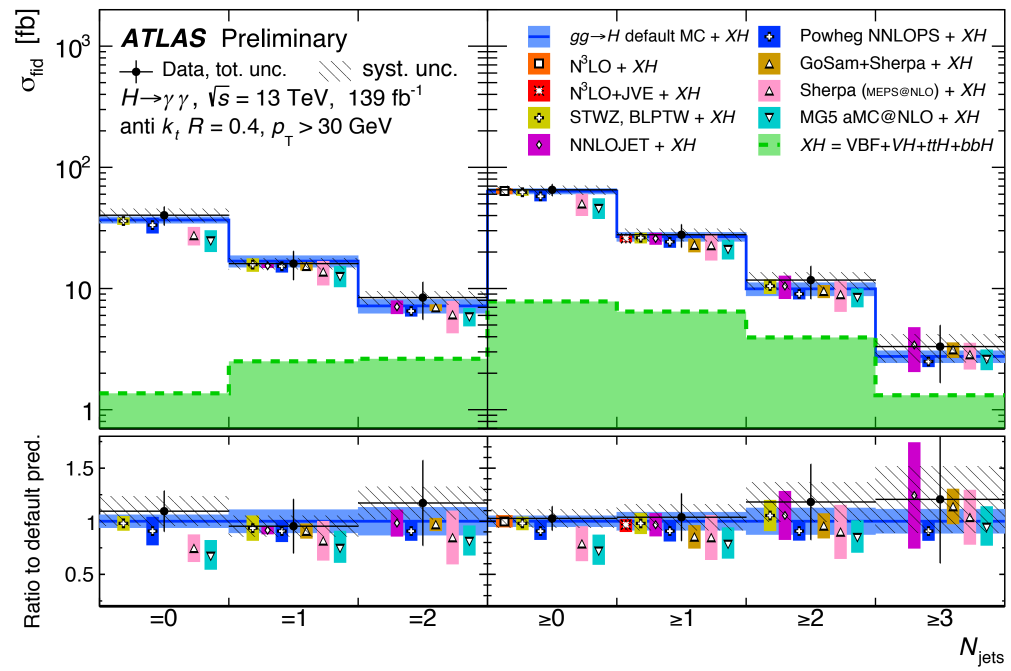

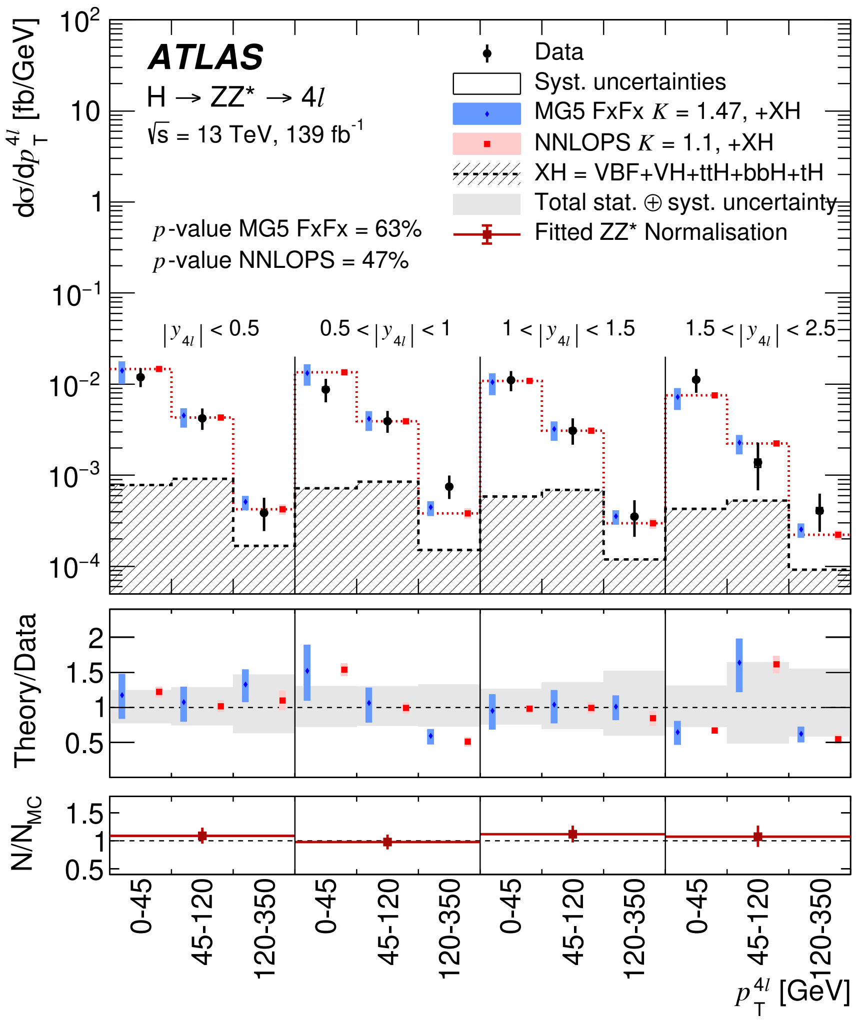

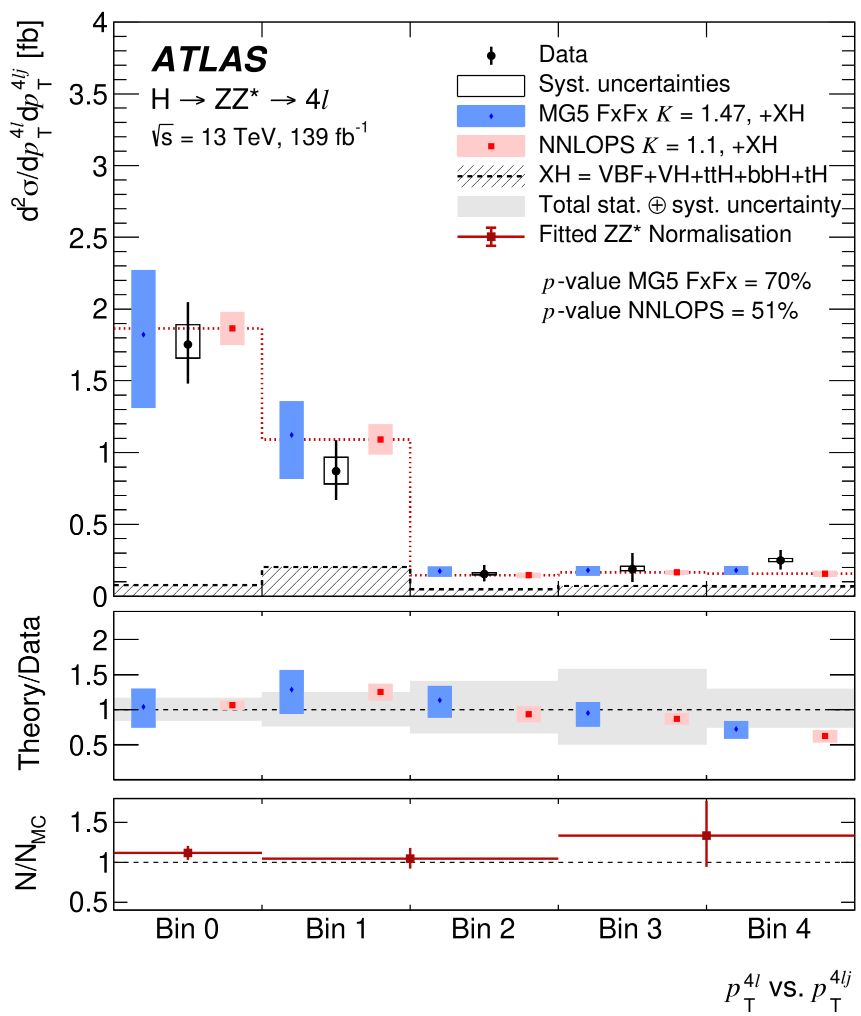

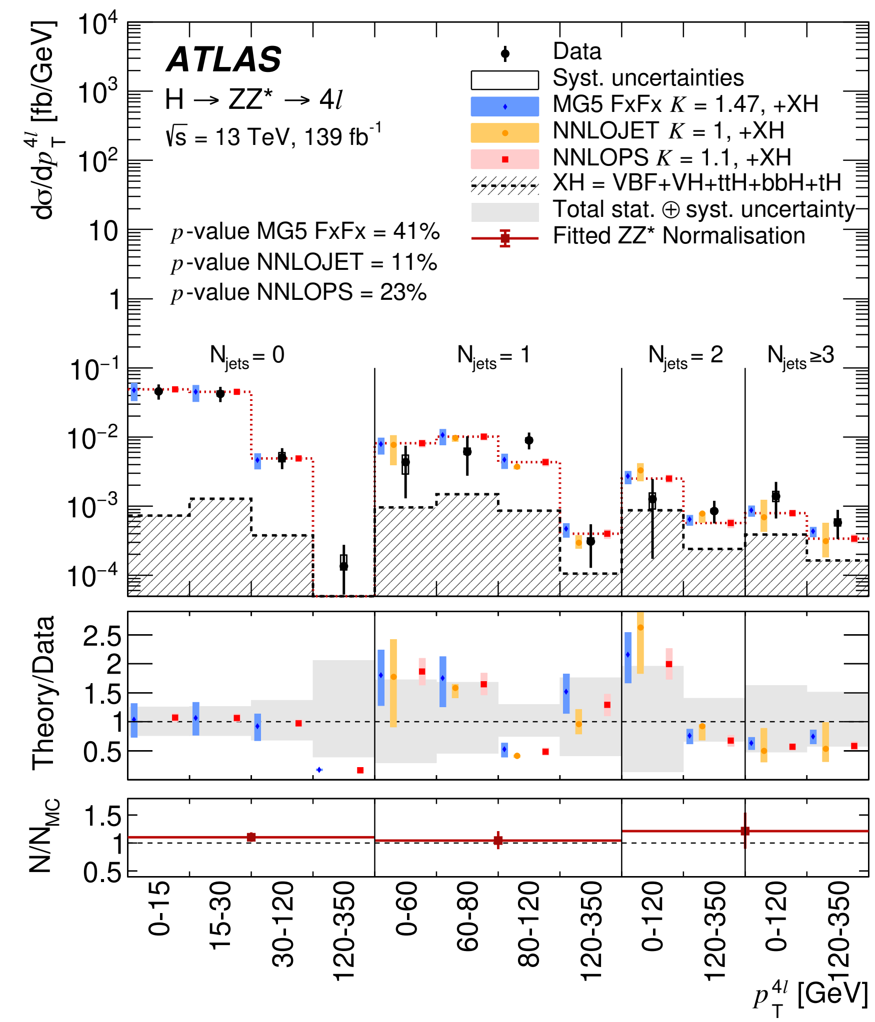

6. Conclusions

Conclusion

- Higs physics provide an excellent picture for
  - Searches for new phenomena resonant at higher scales.
  - Searches for deviations to theory within the scales of the experiment.

- Run II first results of ATLAS in the study of Higgs boson properties
  1. Measurement of m_H at 2 per mille precision level.
  2. Fiducial cross section measurements, sensitivity to several distributions
  3. Production mode analysis and template cross section measurements.

- Presented only a selection results full set

`https://twiki.cern.ch/twiki/bin/view/AtlasPublic/HiggsPublicResults`

Additional material

- Study of the the $m_{4\ell}$ spectrum and Offshell H production

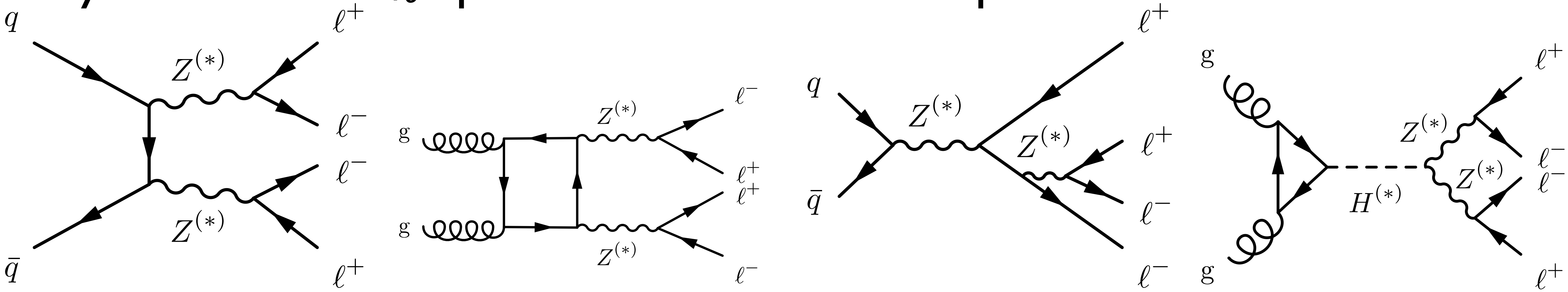

- $m_{4\ell}$ ranges from single Z resonance, including H production up to ZZ production
- Extraction of the BR($Z \to 4\ell$)

Measurement	$\mathcal{B}_{Z\to4\ell}/10^{-6}$
ATLAS, $\sqrt{s}$ = 7 TeV and 8 TeV [8]	4.31±0.34(stat)±0.17(syst)
CMS, $\sqrt{s}$ = 13 TeV [6]	4.83 $^{+0.23}_{-0.22}$(stat) $^{+0.32}_{-0.29}$(syst)±0.08(theo)±0.12(lumi)
ATLAS, $\sqrt{s}$ = 13 TeV	**4.70 ± 0.32(stat) ± 0.21(syst) ± 0.14(lumi)**

- Offshell Higgs production, enhanced at 350 GeV because of top-quark loops in ggF
  - Including interference between H and ZZ productions.
- Above ~ $2m_Z$ enhancements of qq→ZZ and gg→ZZ.

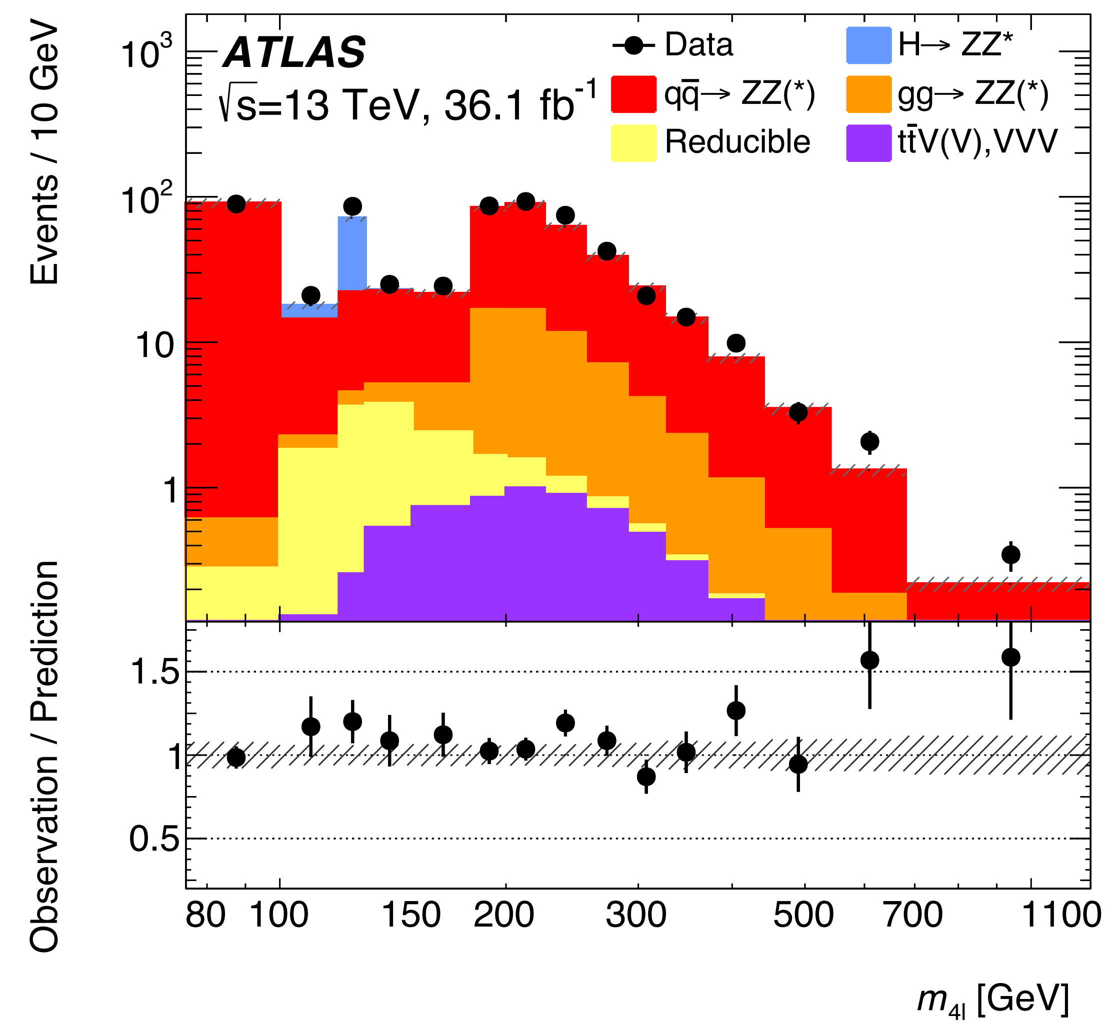

arXiv:1902.05892

- Study of the the $m_{4\ell}$ spectrum and Offshell H production

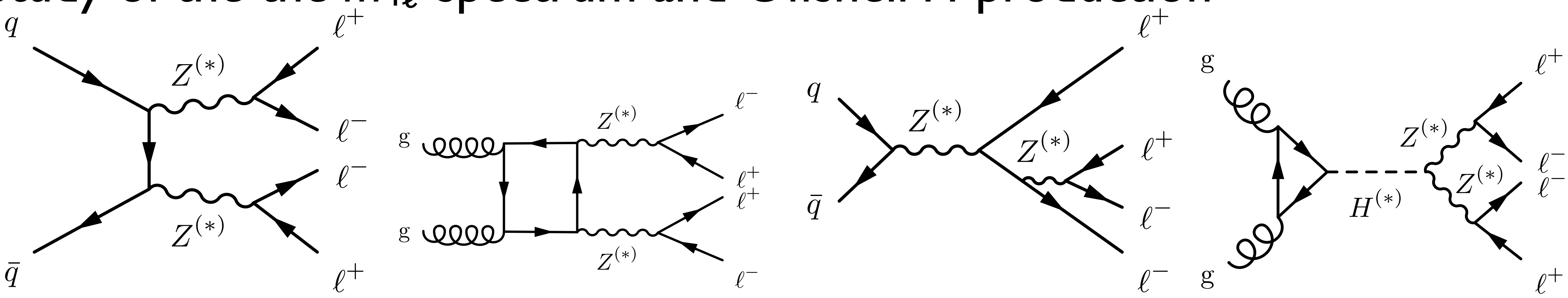

  - $m_{4\ell}$ ranges from single Z resonance, including H production up to ZZ production
  - Extraction of the BR($Z \to 4\ell$)

Measurement	$\mathcal{B}_{Z\to 4\ell}/10^{-6}$
ATLAS, $\sqrt{s}$ = 7 TeV and 8 TeV [8]	4.31±0.34(stat)±0.17(syst)
CMS, $\sqrt{s}$ = 13 TeV [6]	$4.83\ ^{+0.23}_{-0.22}$(stat) $^{+0.32}_{-0.29}$(syst)±0.08(theo)±0.12(lumi)
ATLAS, $\sqrt{s}$ = 13 TeV	**4.70 ± 0.32(stat) ± 0.21(syst) ± 0.14(lumi)**

  - Offshell Higgs production, enhanced at 350 GeV because of top-quark loops in ggF
    - Including interference between H and ZZ productions.
  - Above ~ $2m_Z$ enhancements of qq→ZZ and gg→ZZ.

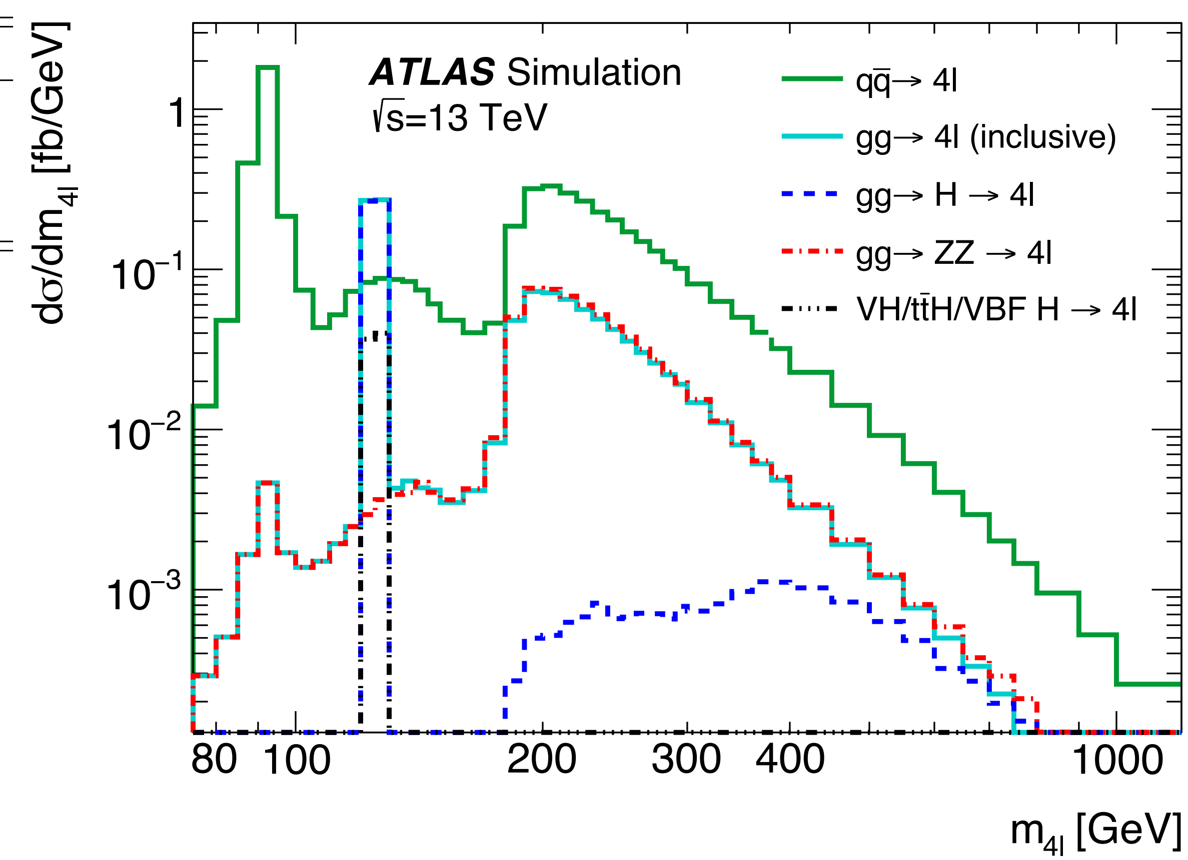

4ℓ mass spectrum — Differential cross section

- Study of the the $m_{4\ell}$ spectrum and Offshell H production

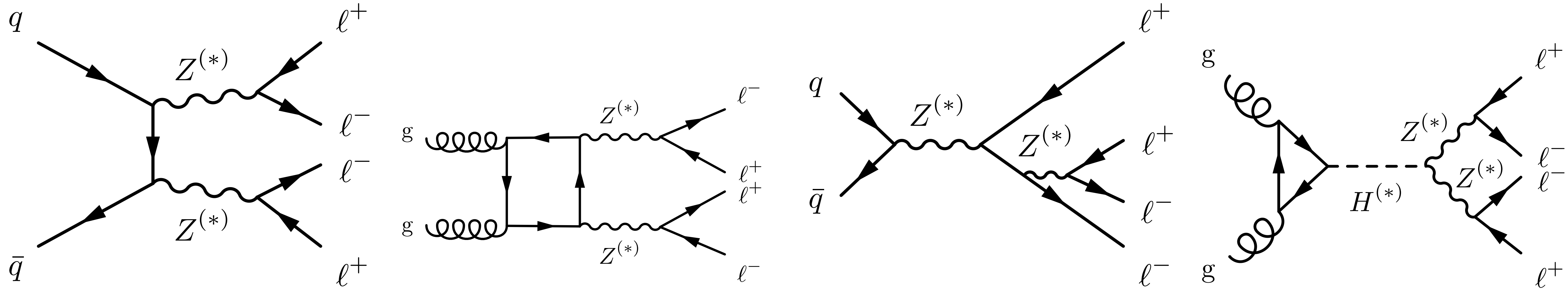

  - $m_{4\ell}$ ranges from single Z resonance, including H production up to ZZ production
  - Extraction of the BR(Z→ 4ℓ)

Measurement	$\mathcal{B}_{Z\to 4\ell}/10^{-6}$
ATLAS, $\sqrt{s}$ = 7 TeV and 8 TeV [8]	4.31±0.34(stat)±0.17(syst)
CMS, $\sqrt{s}$ = 13 TeV [6]	4.83 $^{+0.23}_{-0.22}$(stat) $^{+0.32}_{-0.29}$(syst)±0.08(theo)±0.12(lumi)
ATLAS, $\sqrt{s}$ = 13 TeV	**4.70 ± 0.32(stat) ± 0.21(syst) ± 0.14(lumi)**

  - Offshell Higgs production, enhanced at 350 GeV because of top-quark loops in ggF
    - Including interference between H and ZZ productions.
  - Above ~ 2m_Z enhancements of qq→ZZ and gg→ZZ.

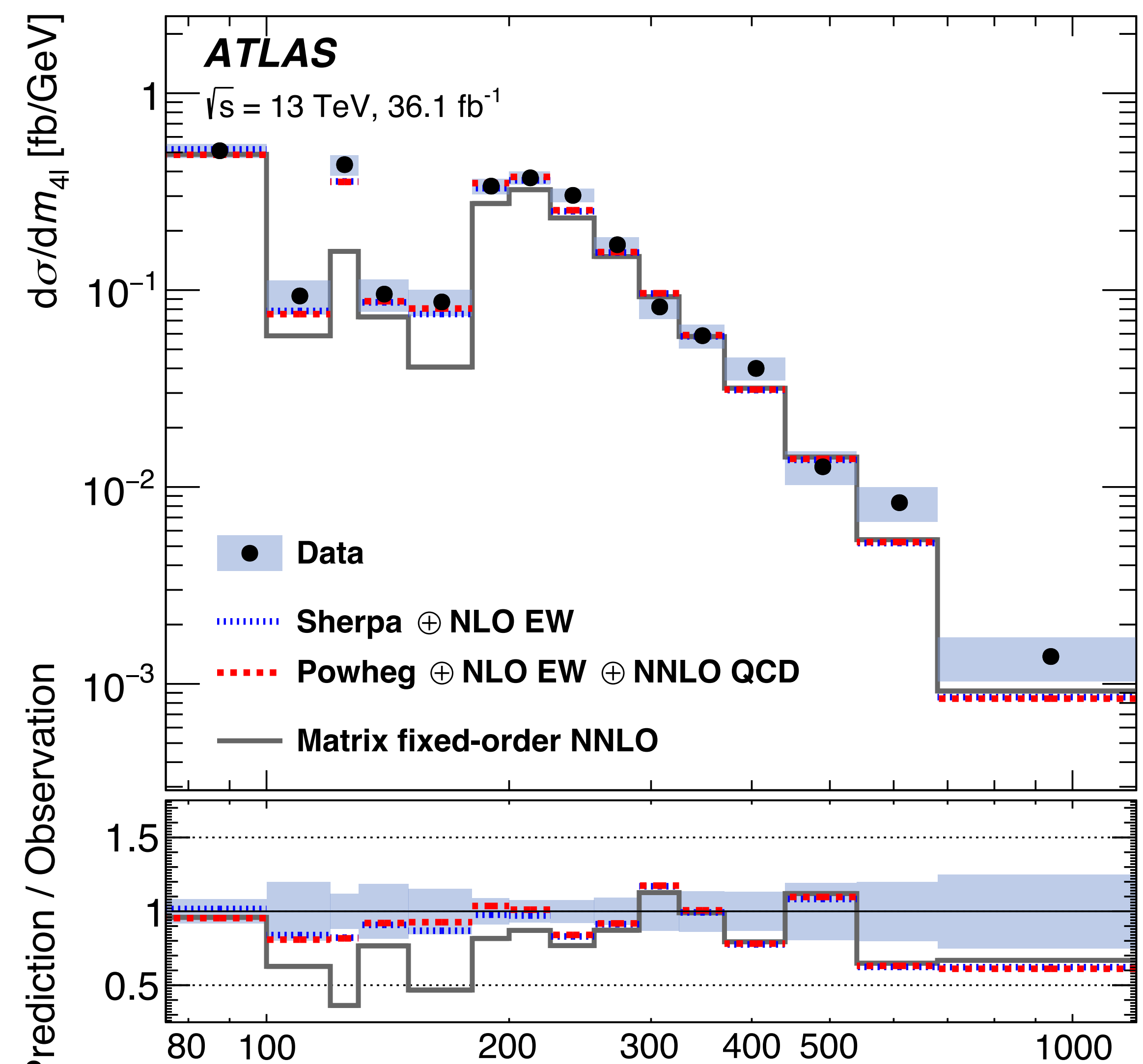

arXiv:1902.05892

4ℓ mass spectrum — Differential cross section

arXiv:1902.05892

- Study of the the $m_{4\ell}$ spectrum and off-shell H production

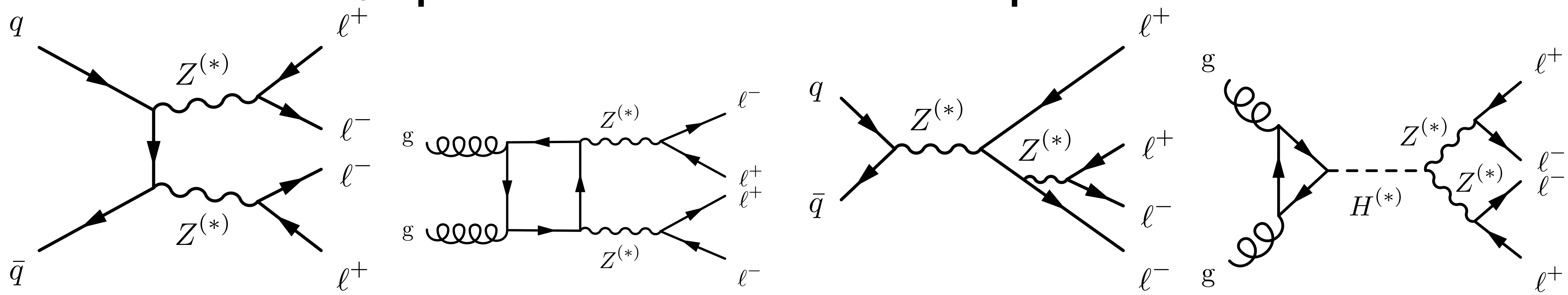

  - Offshell Higgs production, enhanced at 350 GeV because of top-quark loops in ggF
  - Measured upper limit on width combining 4ℓ and $\ell\bar{\ell}\nu\bar{\nu}$
  - Limit Γ_H possibile from the off-shell to on-shell event yield ratio R_{gg}
    - ✦ on-shell event yields ~ $k^2_{\mathrm{g,on\text{-}shell}} / \Gamma_H$, while off-shell ~ $k^2_{\mathrm{g,off\text{-}shell}}$

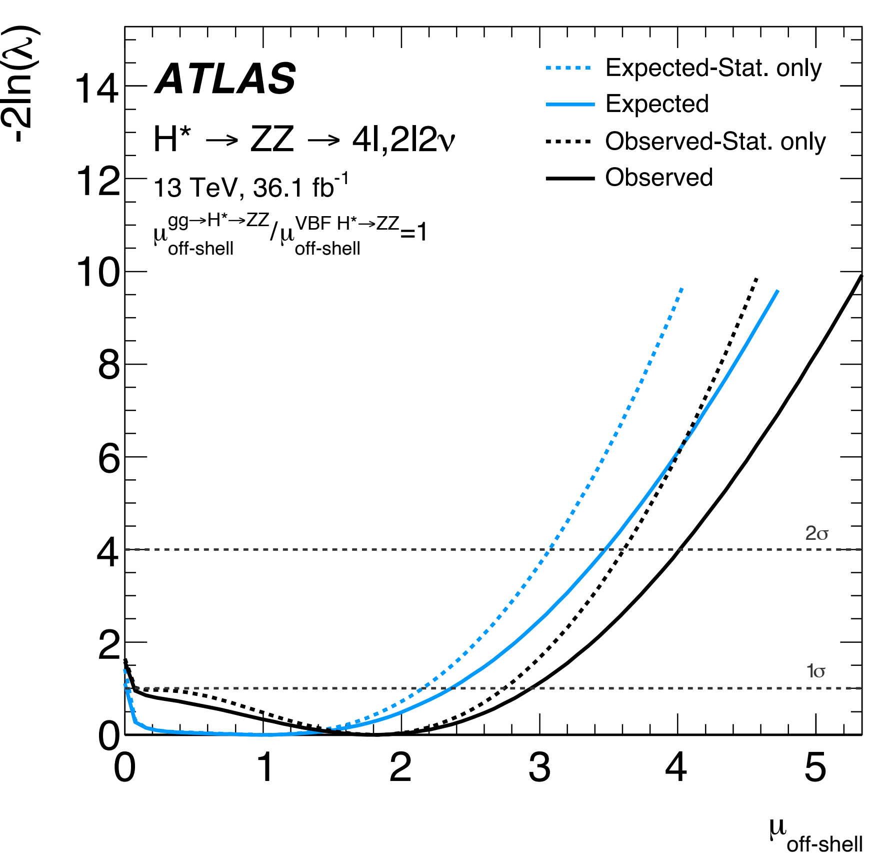

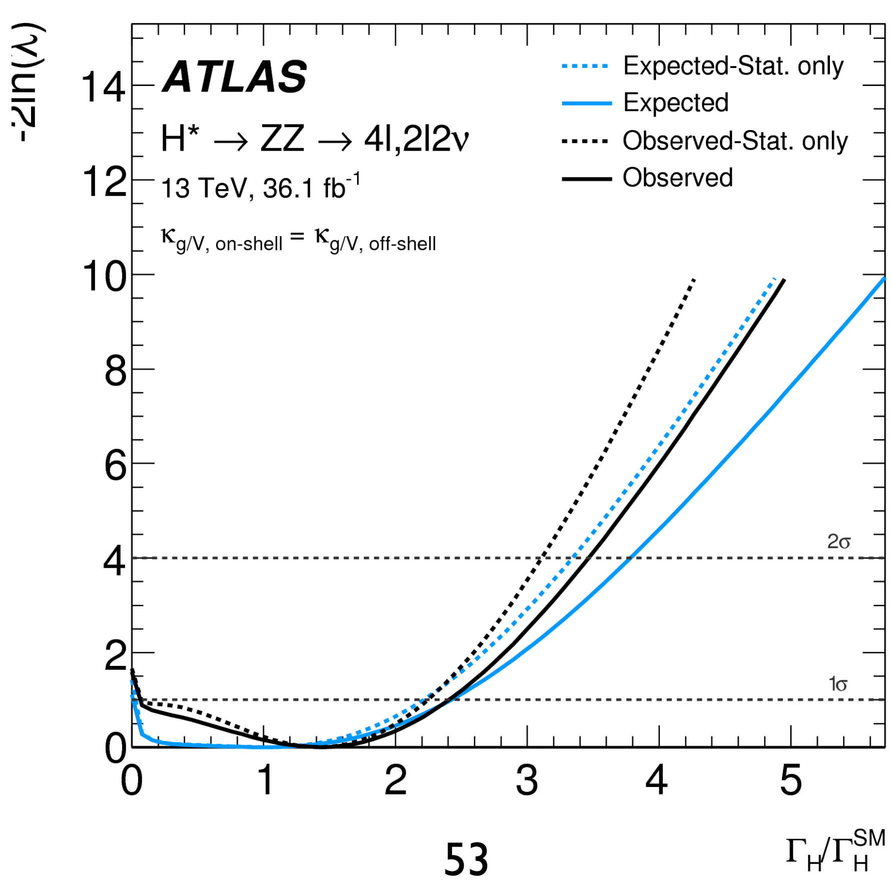

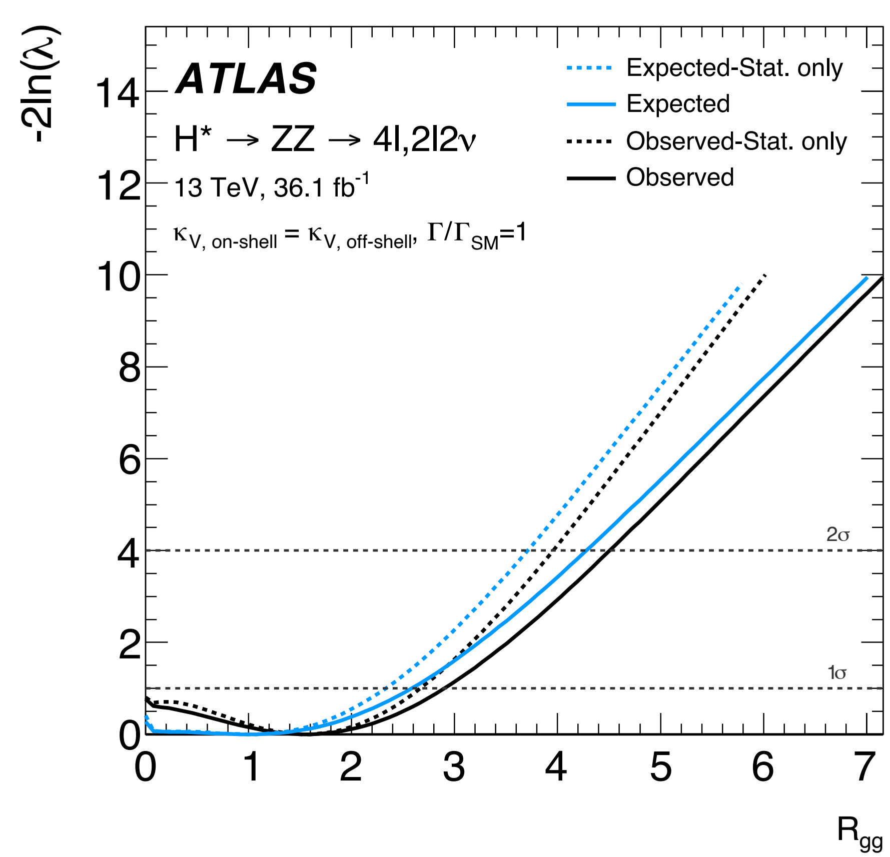

- Electrons (e).
  - Isolated objects clustered from calorimeter energy deposits with associated ID track.
  - $E_T > 7$ GeV, $|\eta| < 2.47$ and $|z_0 \sin(\vartheta)| < 0.5$ mm

- Muons (μ).
  - Combined track fit of Inner Detector and Muon Spectrometer hits,
  - $p_T > 5$ GeV, $|\eta| < 2.7$ $|z_0 \sin(\vartheta)| < 0.5$ mm of "loose or medium quality"
  - Isolated objects

- Jets (j).
  - Energy deposit grouping with *infra*-red safe algorithm:
  - $p_T > 25$ GeV and $|\eta| < 4.5$
    - ✦ Clustering with anti-k_T, $R=0.4$

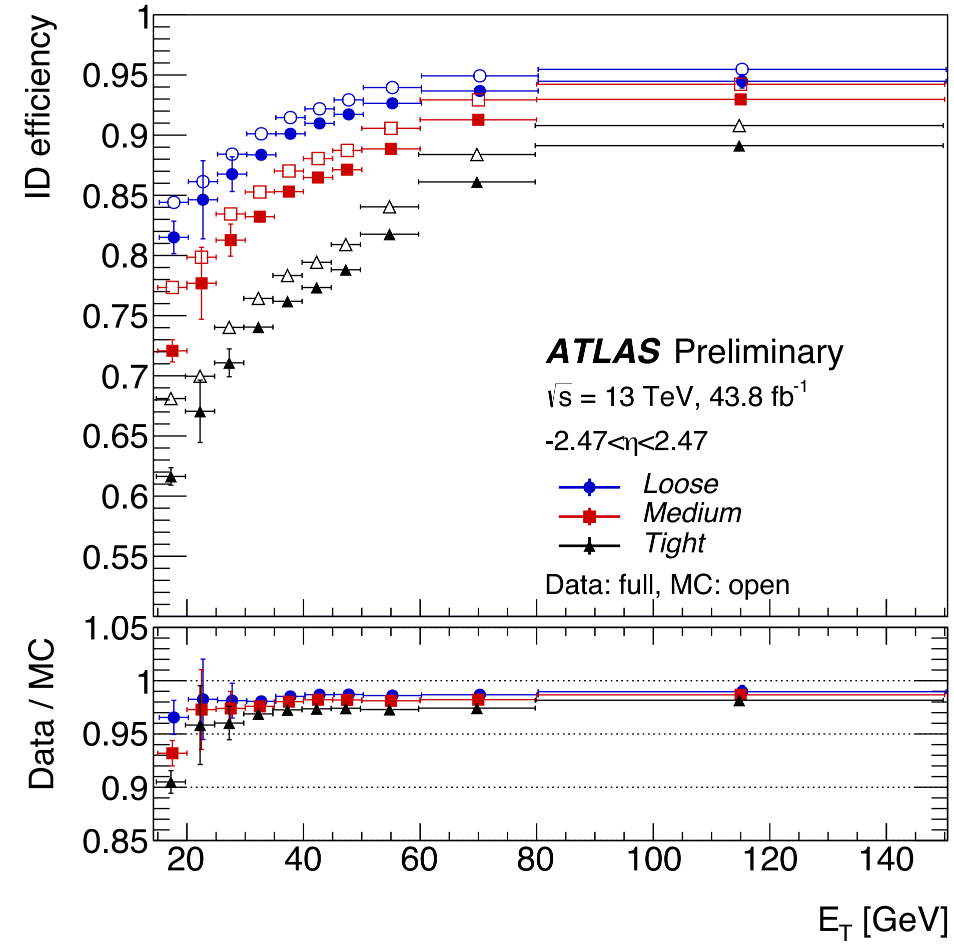

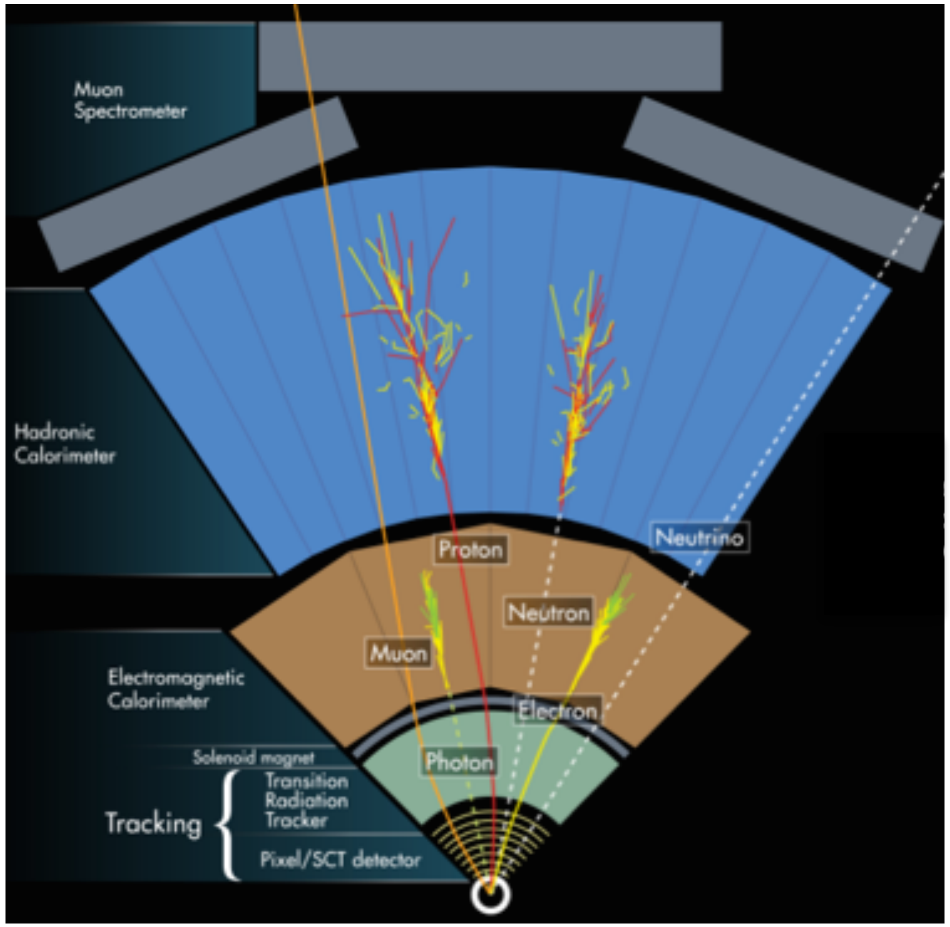

Object selection

- **Electrons (e).**
  - Isolated objects clustered from calorimeter energy deposits with associated ID track.
  - $E_T > 7$ GeV, $|\eta| < 2.47$ and $|z_0 \sin(\vartheta)| < 0.5$ mm

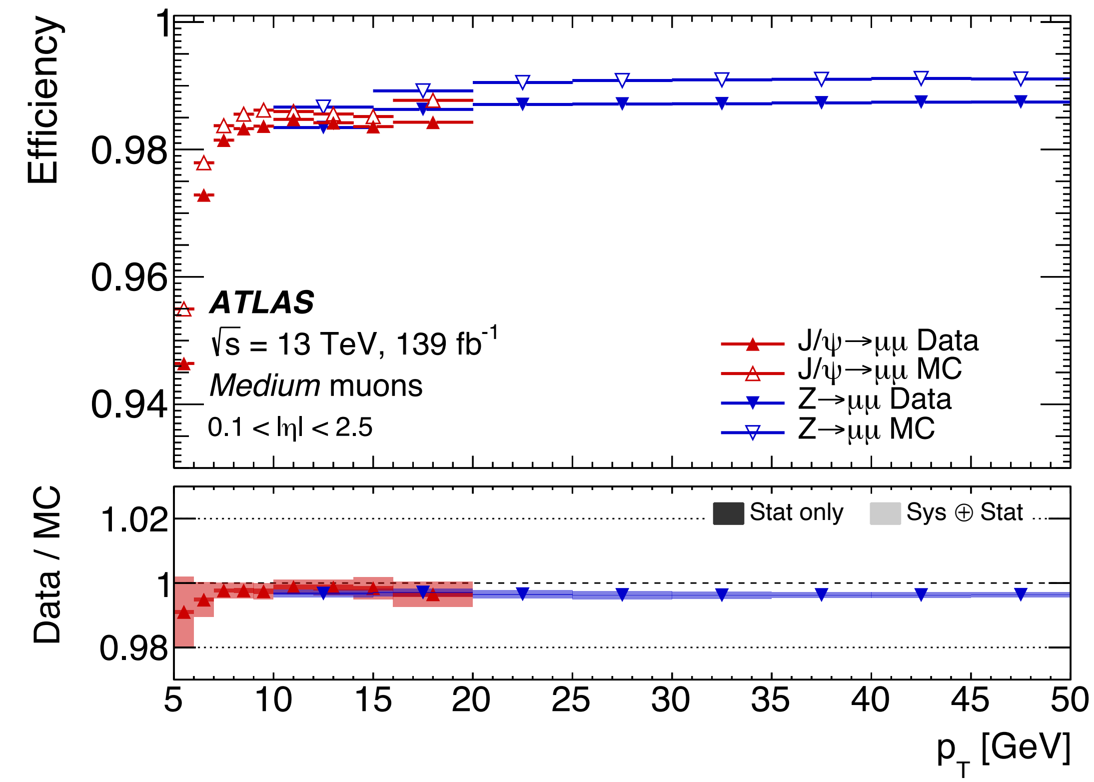

- **Muons (μ).**
  - Combined track fit of Inner Detector and Muon Spectrometer hits,
  - $p_T > 5$ GeV, $|\eta| < 2.7$ $|z_0 \sin(\vartheta)| < 0.5$ mm of "loose or medium quality"
  - Isolated objects

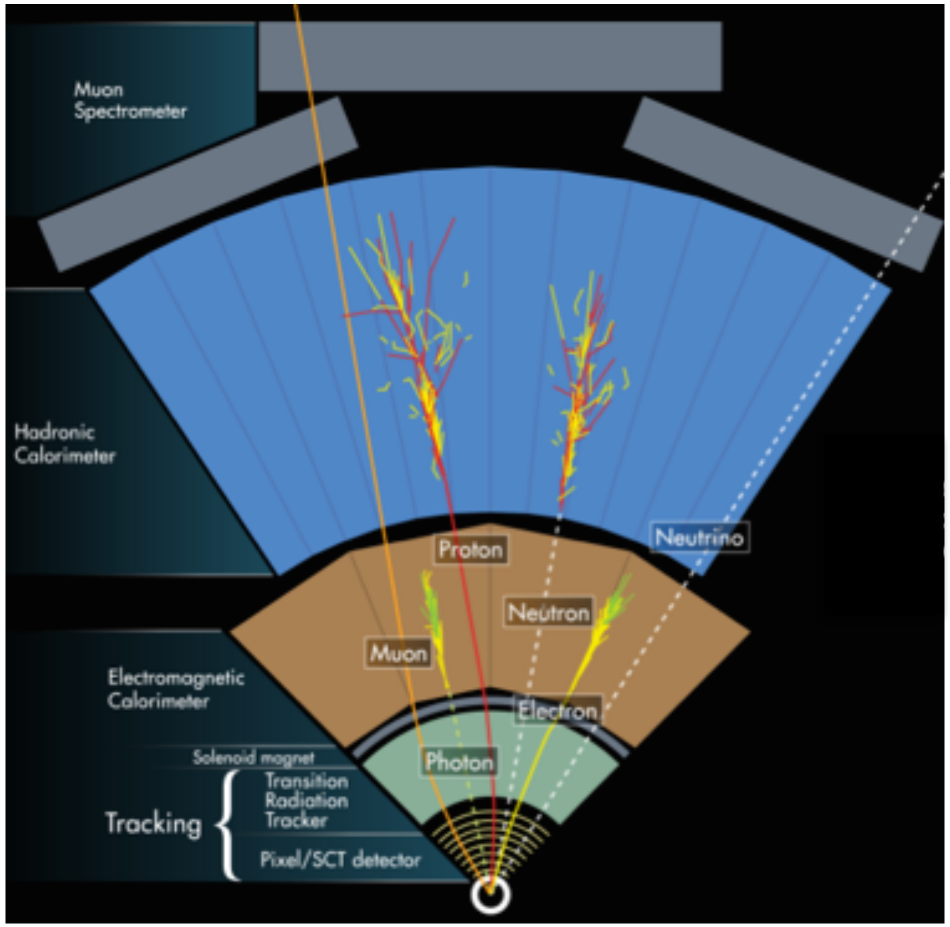

- **Jets (j).**
  - Energy deposit grouping with *infra*-red safe algorithm:
  - $p_T > 20$ GeV and $|\eta| < 4.5$
    - ✦ Clustering with anti-k_T, R=0.4

- Electrons (e).
  - Isolated objects clustered from calorimeter energy deposits with associated ID track.
  - $E_T > 7$ GeV, $|\eta| < 2.47$ and $|z_0 \sin(\vartheta)| < 0.5$ mm

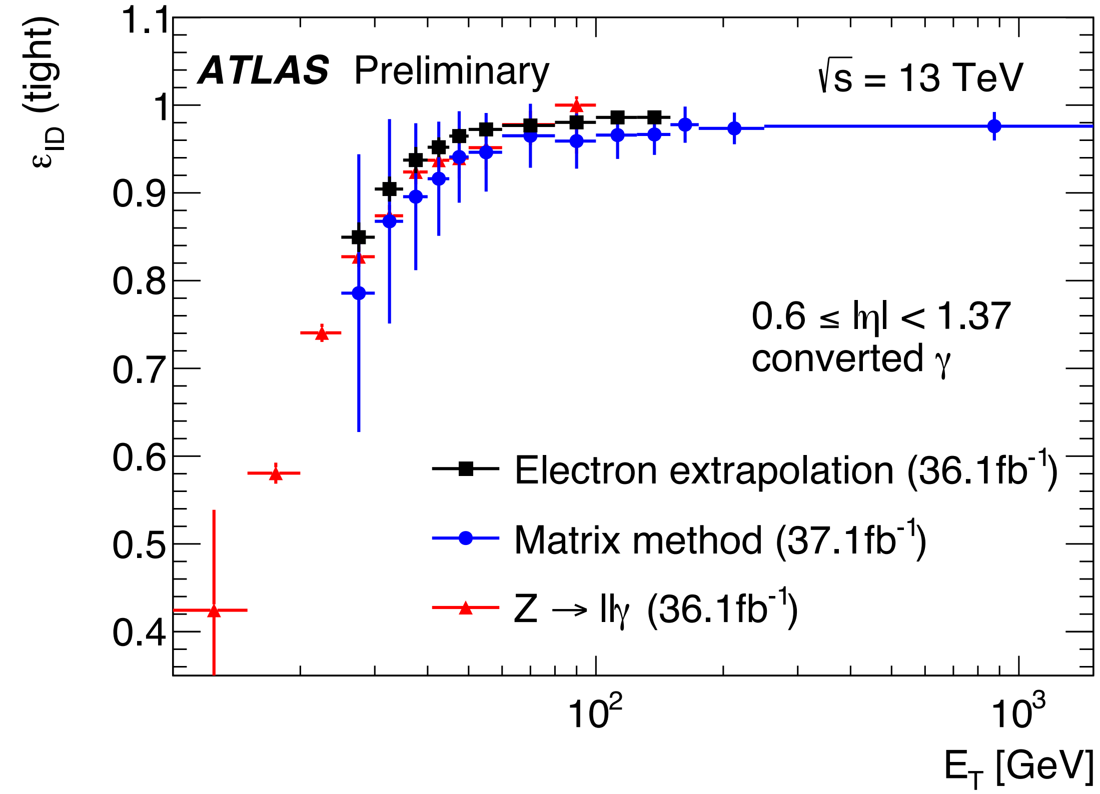

- Muons (μ).
  - Combined track fit of Inner Detector and Muon Spectrometer hits,
  - $p_T > 5$ GeV, $|\eta| < 2.7$ $|z_0 \sin(\vartheta)| < 0.5$ mm of "loose or medium quality"
  - Isolated objects

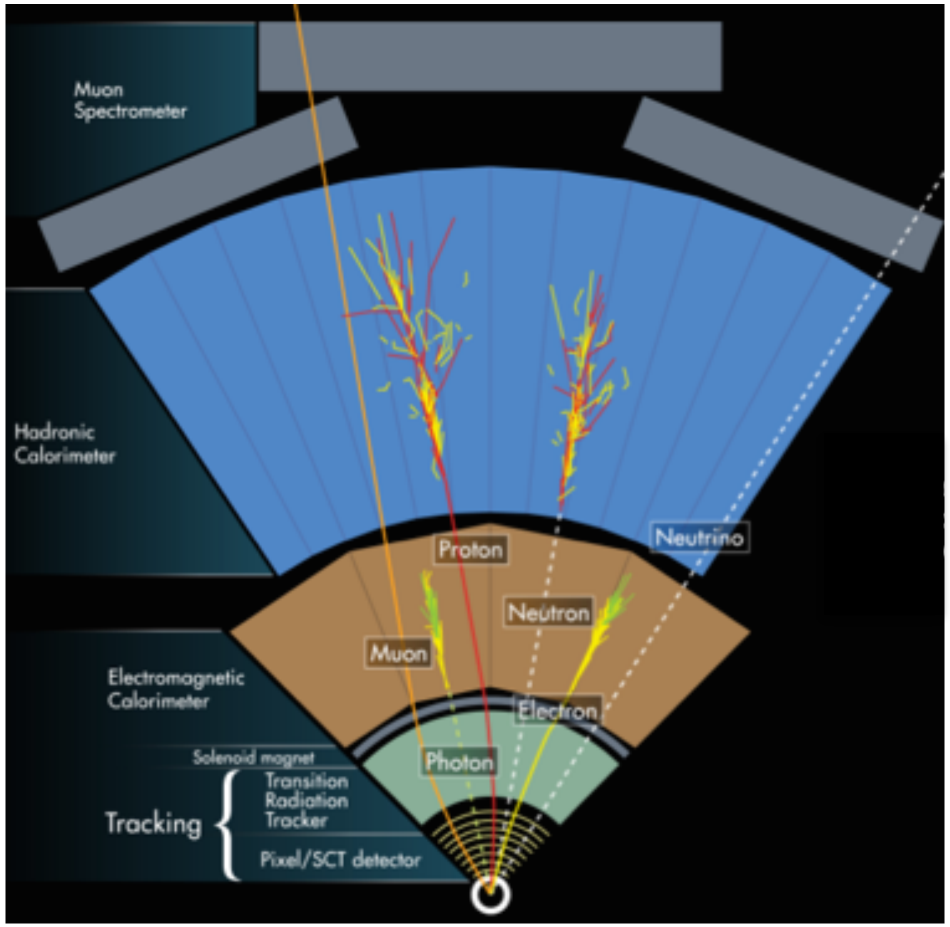

- Photons (γ).
  - Clustering of calorimeter energy deposits.
  - Identified with rectangular cuts on shower shapes.

- **Electrons (e).**
  - Isolated objects clustered from calorimeter energy deposits with associated ID track.
  - $E_T > 7$ GeV, $|\eta| < 2.47$ and $|z_0 \sin(\vartheta)| < 0.5$ mm

- **Muons (μ).**
  - Combined track fit of Inner Detector and Muon Spectrometer hits,
  - $p_T > 5$ GeV, $|\eta| < 2.7$ $|z_0 \sin(\vartheta)| < 0.5$ mm of "loose or medium quality"
  - Isolated objects

- **Jets (j).**
  - Combined from energy deposits in calorimeters and charged particles momenta
  - $p_T > 20$ GeV and $|\eta| < 4.5$
    - ✦ Clustering with anti-k_T, $R=0.4$

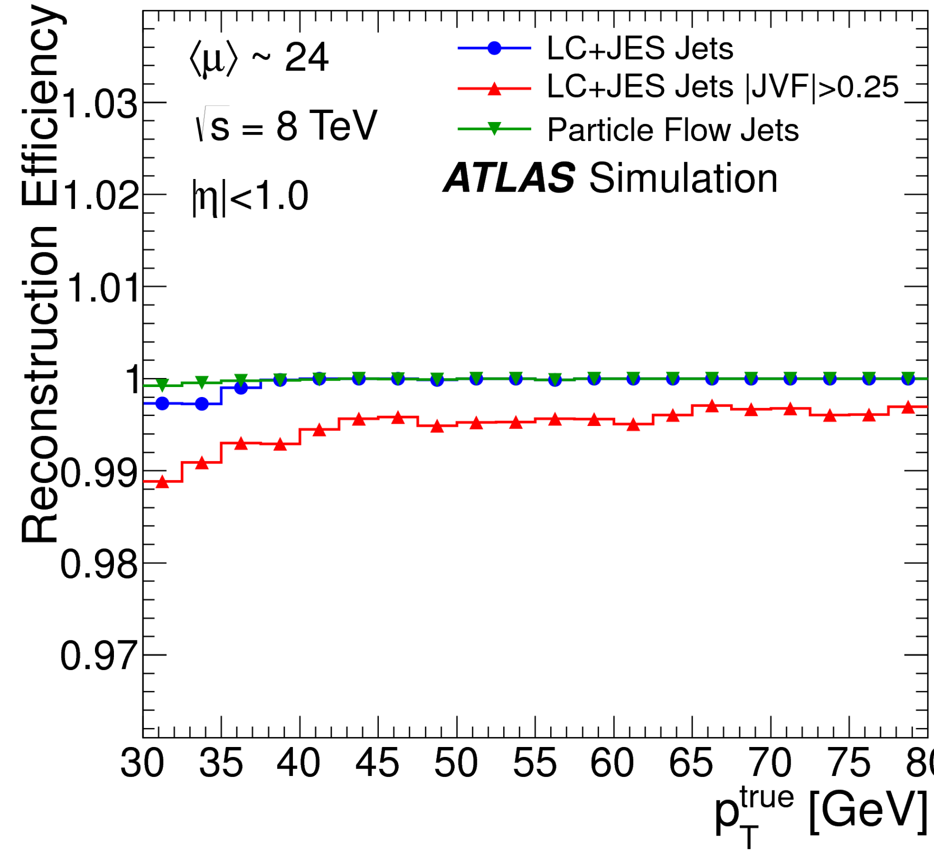

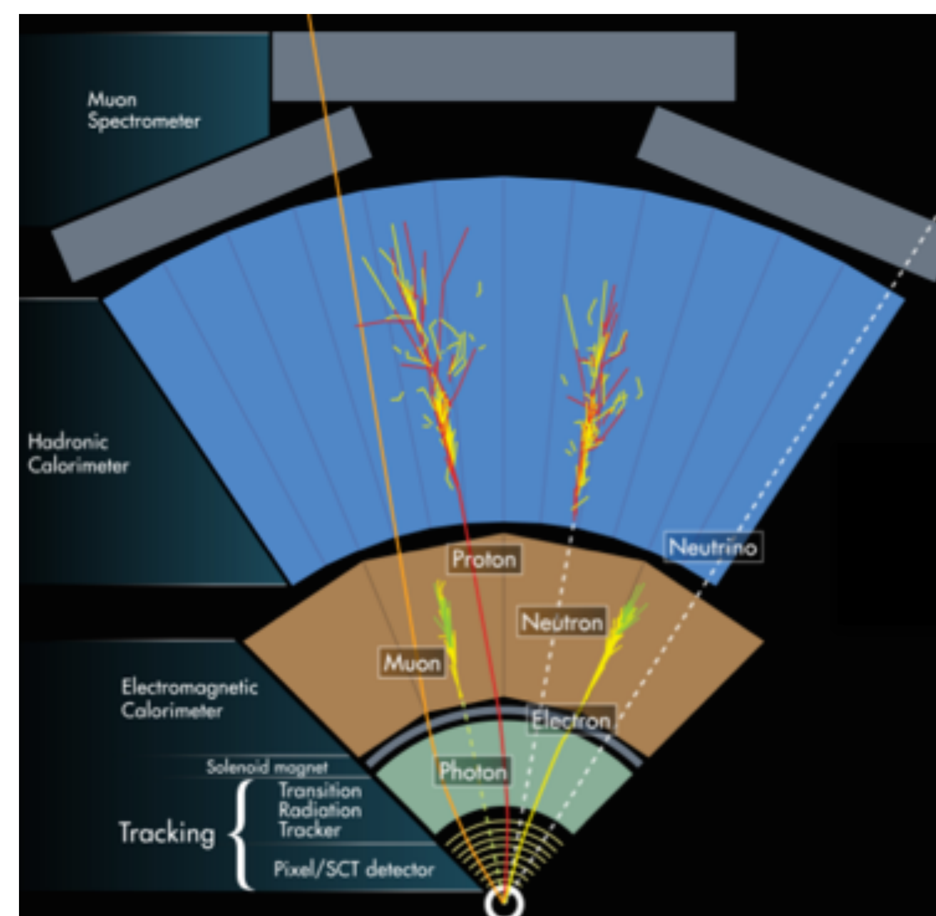

Object selection

- Electrons (e).
  - Isolated objects clustered from calorimeter energy deposits with associated ID track.
  - E_T > 7 GeV, $|\eta|$ < 2.47 and $|z_0 \sin(\vartheta)|$ < 0.5 mm

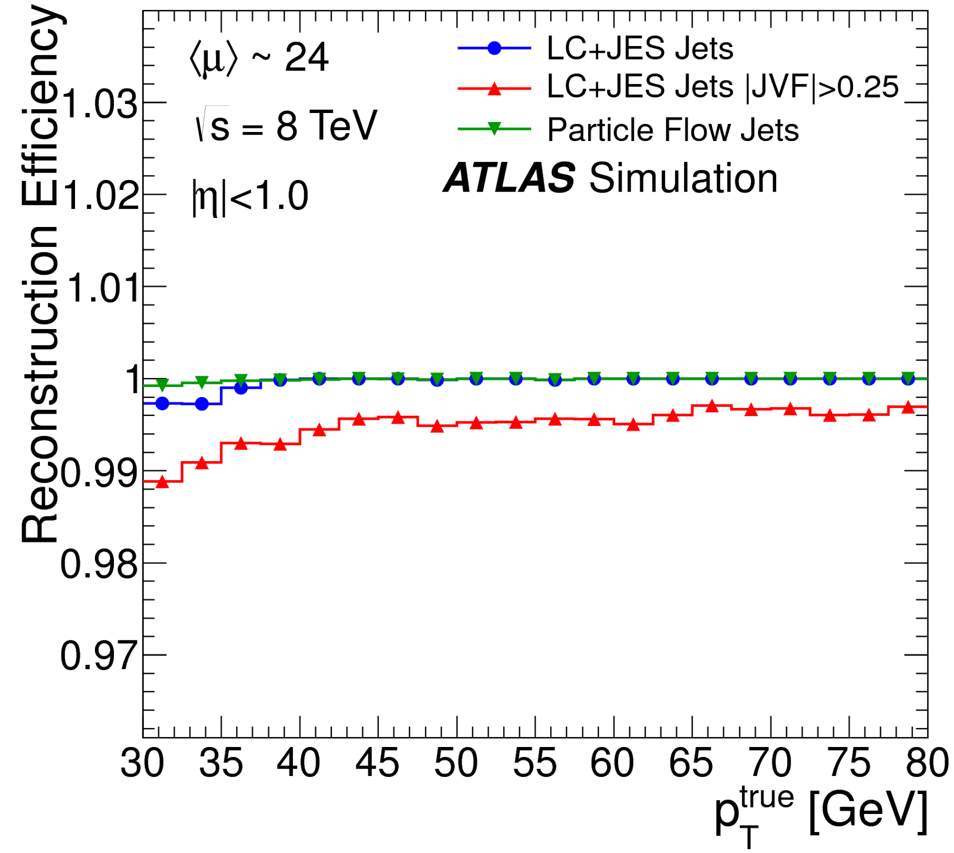

- Muons (μ).
  - Combined track fit of Inner Detector and Muon Spectrometer hits,
  - p_T > 5 GeV, $|\eta|$ < 2.7 $|z_0 \sin(\vartheta)|$ < 0.5 mm of "loose or medium quality"
  - Isolated objects

- Missing transverse energy ($E_T^{\rm miss}$).
  - Inferred from transverse momentum imbalance

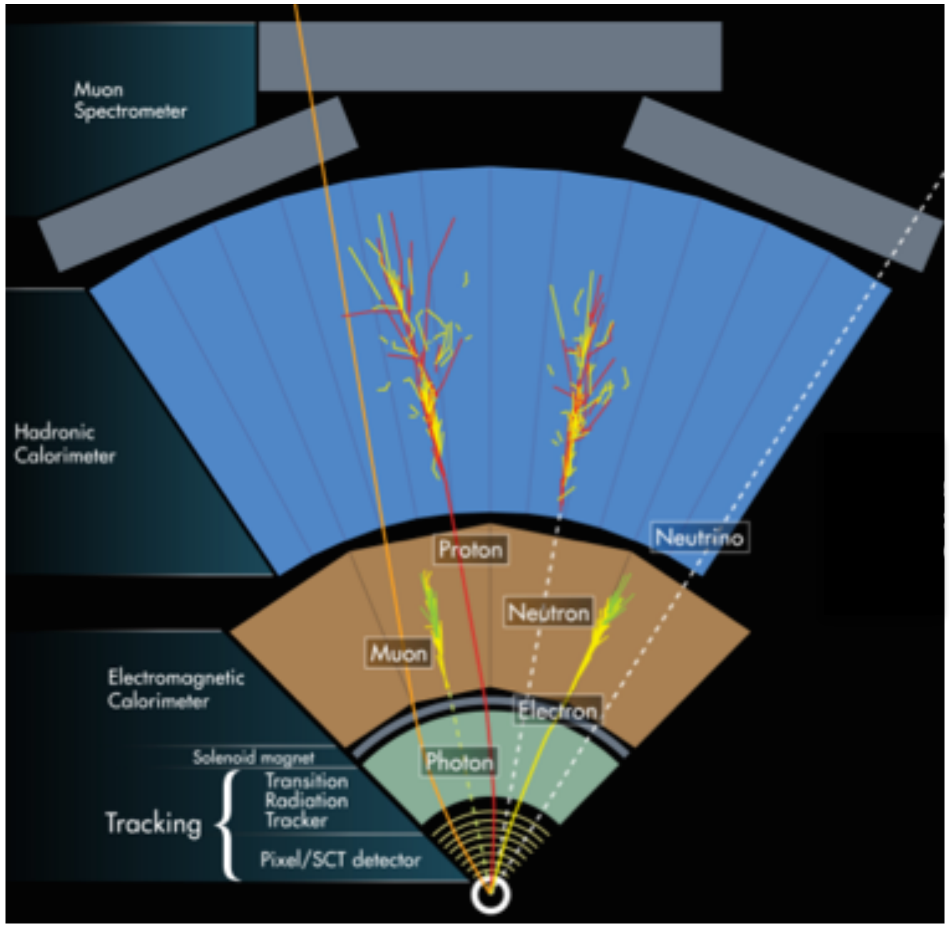

Couplings interpretations

- Interpretation of couplings cross sections in the context of new physics.
- Assuming production and decay are factorised

$$\sigma_i \times \mathrm{B}_f = \frac{\sigma_i(\boldsymbol{\kappa}) \times \Gamma_f(\boldsymbol{\kappa})}{\Gamma_H}$$

$$\kappa_V = 1.03 \pm 0.03$$
$$\kappa_F = 0.97 \pm 0.07.$$

- Coupling strength modifiers

$$\kappa_j^2 = \frac{\sigma_j}{\sigma_j^{\mathrm{SM}}} \qquad \kappa_j^2 = \frac{\Gamma_j}{\Gamma_j^{\mathrm{SM}}}$$

- BSM contributions in loops and decays
  - k_g and k_γ measured with all other modifiers fixed to SM value.
  - Both hypotheses of invisible decays (B_{inv} and B_{und} floating, with k_F=k_V=1) and no invisible decays (B_{inv}= B_{und}=0).

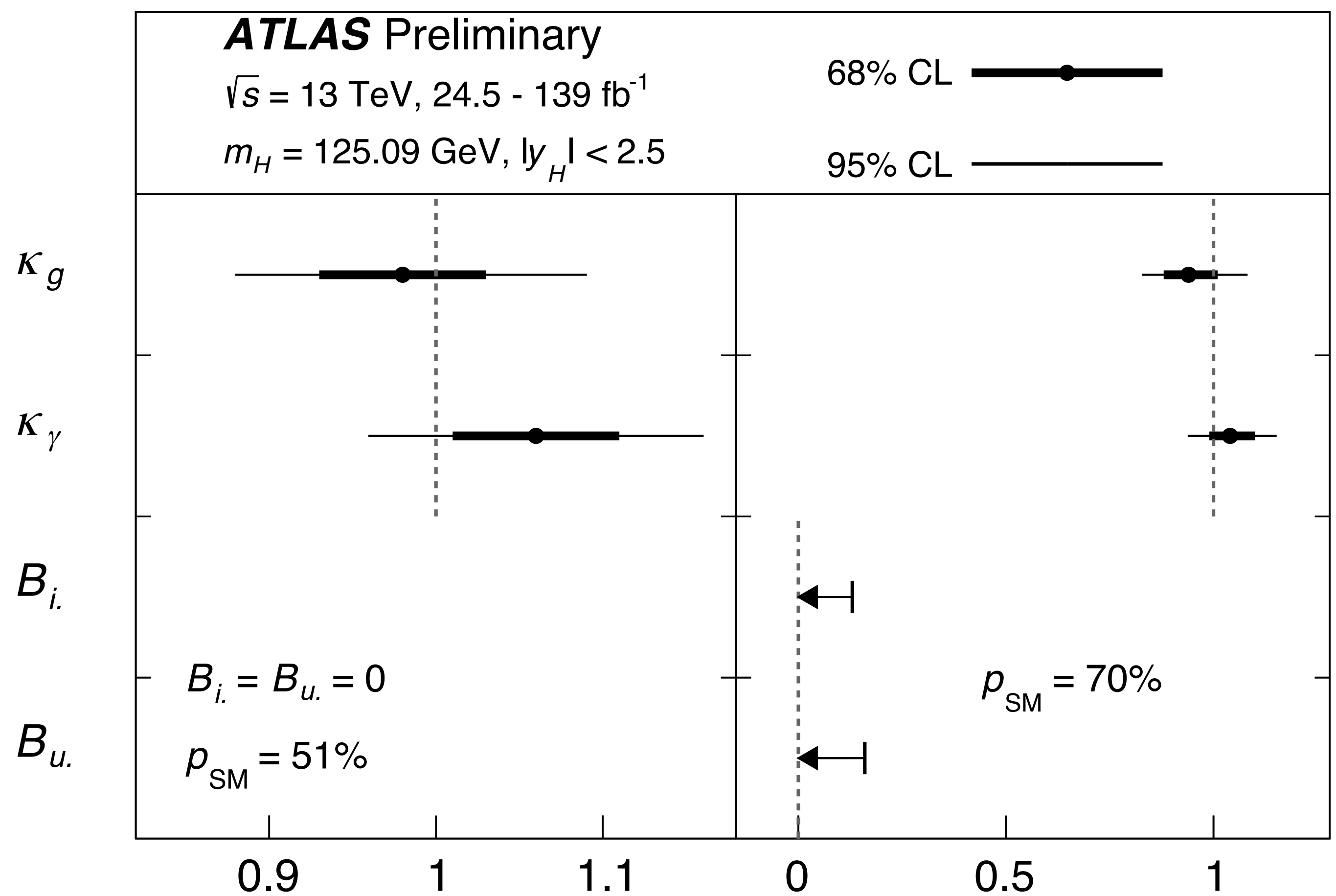

ATLAS-CONF-2019-005

- $WW^* \rightarrow e\nu\mu\nu$ selection
  - Two isolated leptons $p_T(\ell)$ > 22 GeV and $p_T(\ell)$ > 15 GeV
  - E_T^{miss} > 20 GeV
  - Neural network for VBF production
- Neural network for VBF production
- Background estimation:

Based on data

1. Non resonant WW production
2. $t\bar{t}$ production
3. Drell-Yan: $Z \rightarrow \tau^+\tau^-$
4. Hadrons misidentified as leptons:
   - W+jets $t\bar{t}$ and WZ production

Based on simulation

5. $ZZ^*, WZ, W\gamma(^*)$ production in
6. Single-top-quark (Wt) production

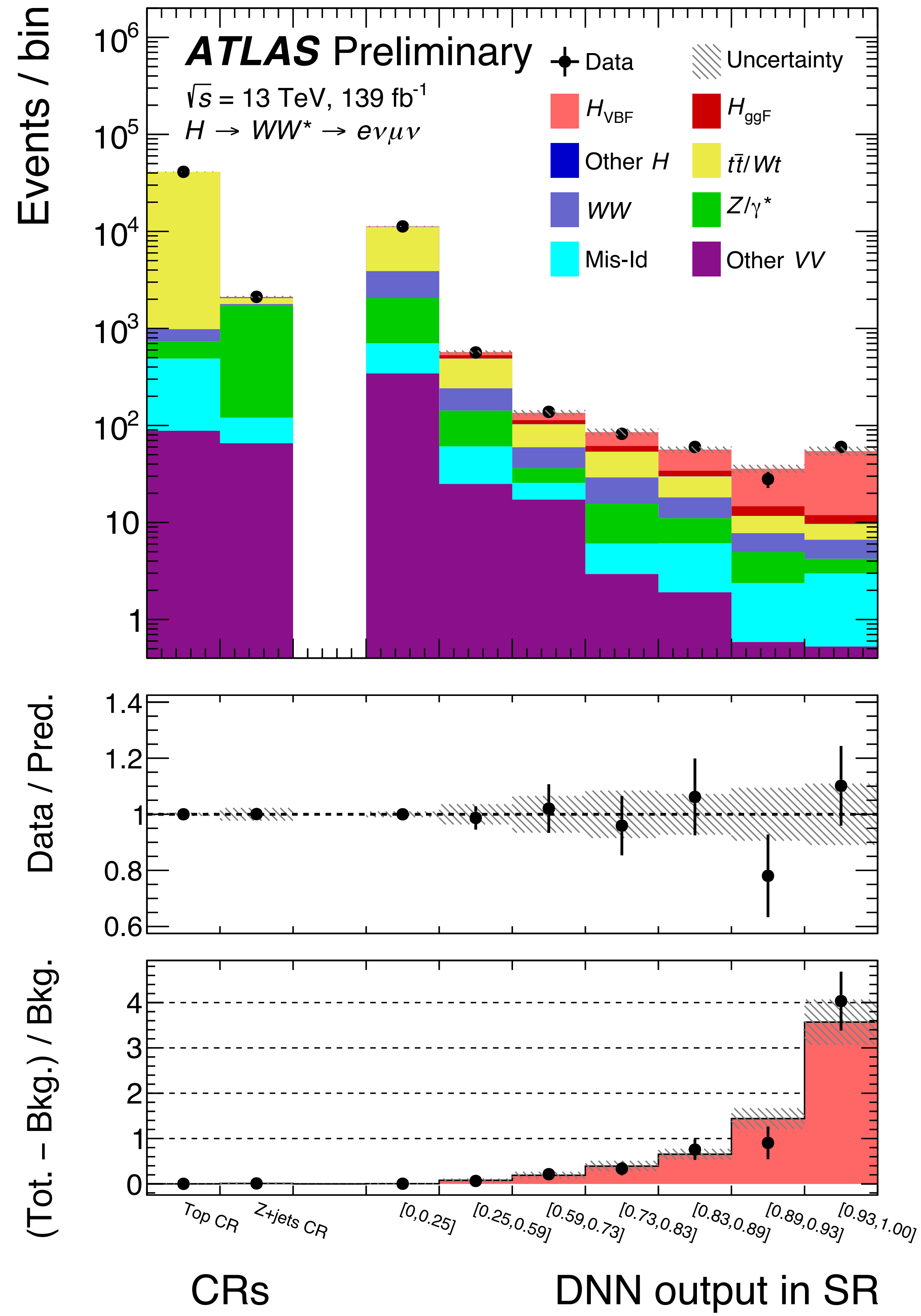

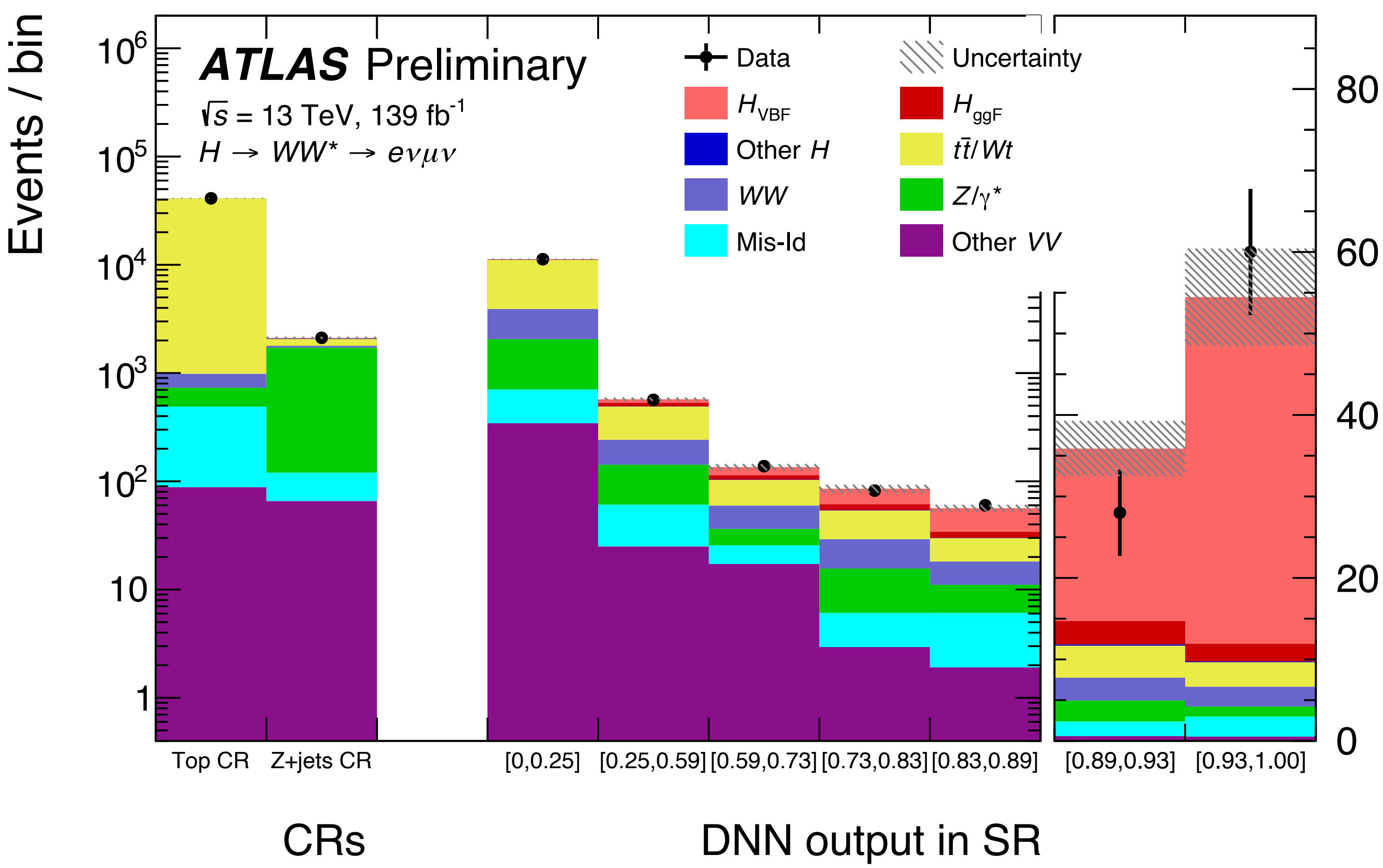

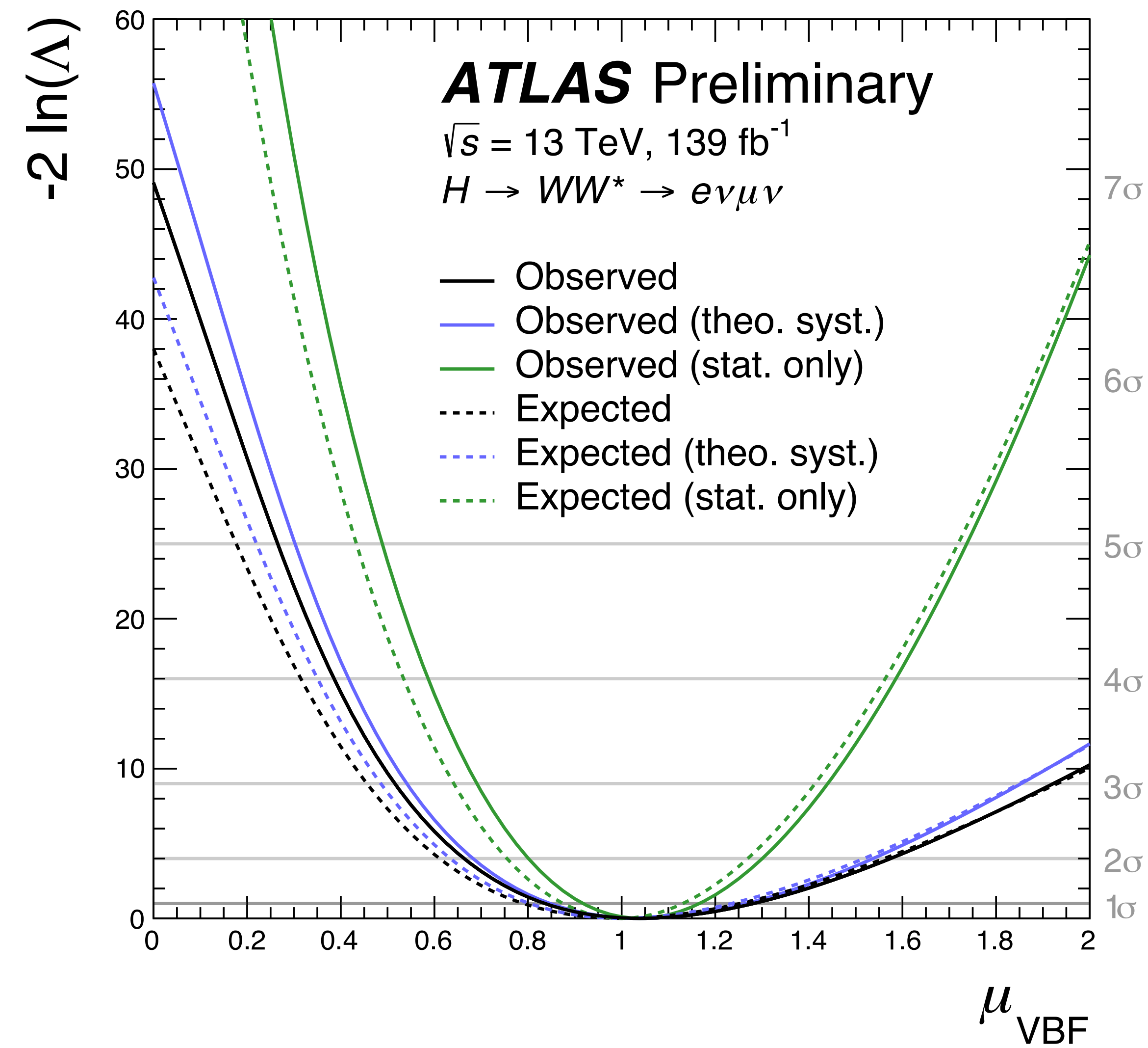

- Measured production cross section $0.85 \pm 0.1(\text{stat})\ ^{+0.17}{}_{-0.13}\ (\text{sys})\ \text{pb}$
  - Significance of the signal observed of 7.0 σ
    - 6.2σ expected for m_{H} = 125 GeV.

$ZZ^* \rightarrow 4\ell$ Reconstruction and selection

- $ZZ^* \rightarrow 4\ell$ ($\ell = \mu, e$) selection:
  - Isolated leptons with: $p_T(\ell)$ > 20 GeV , 15 GeV 10 GeV and 5 (7) GeV
  - Leading pair: pair closest to m_Z,
  - Vertex refit: χ^2 cut at 99.5% signal efficiency
  - Final state photon emission recovered

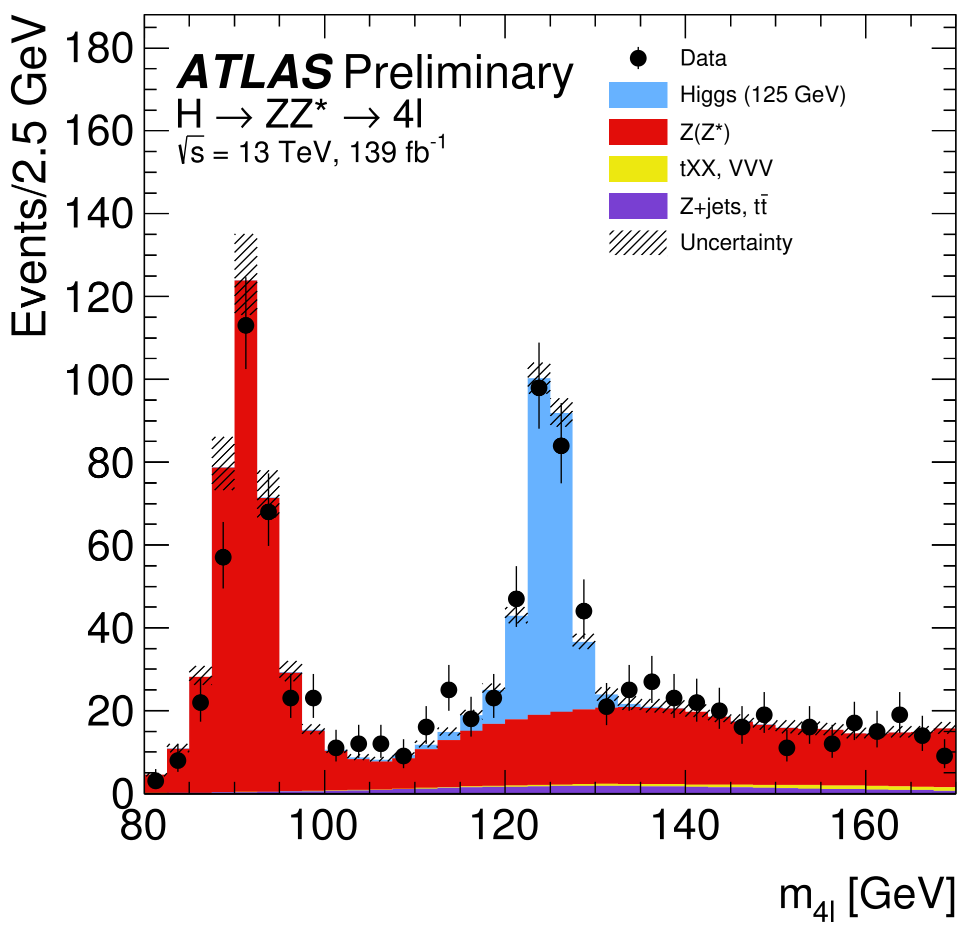

- Background estimation

1. ZZ^* production in 4ℓ (dominant)
   - From $q\bar{q}$ annihilation and gg fusion (subdominant)
2. Hadrons misidentified as leptons:
   - Z+jets $t\bar{t}$ and WZ production
   - Extrapolation to signal region making use of simulation

Based on data

3. ZZZ, WZZ and WWZ (small).

Based on simulation

Reconstruction and selection

- Diphoton event selection
  - At least two photon with E_T> 25 GeV
  - Highest E_T pair forms candidate.
  - Vertex identification with Neural Network
    - Vertex within 0.3 mm for 79% of ggH events.

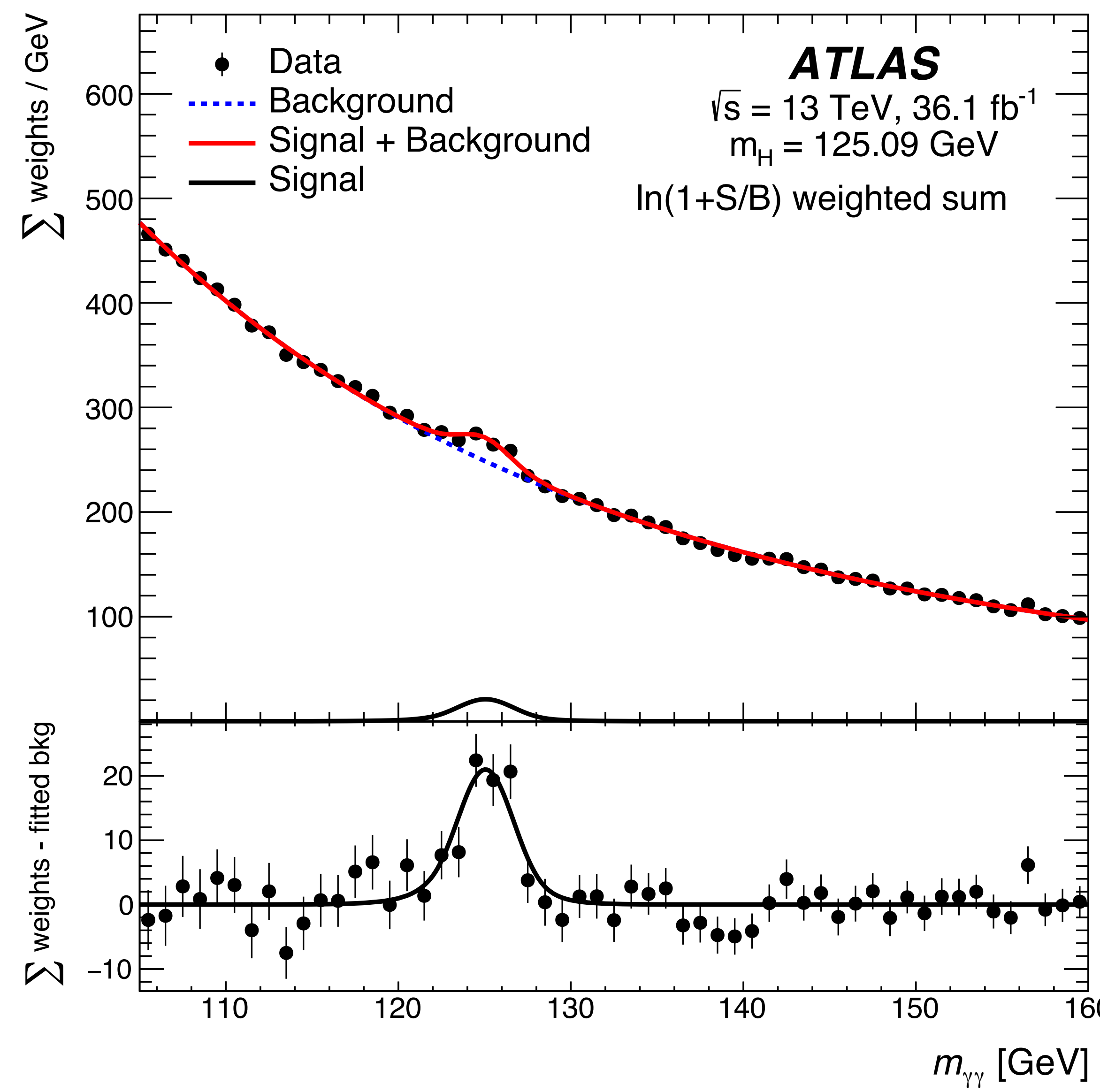

- Background estimation
  - Entirely estimated from data
  - Prompt photons: maximum likelihood fit to $m_{\gamma\gamma}$ spectrum
  - Jets misidentified as photons: from control sample

$WW^* \to \ell\bar{\nu}\bar{\ell}\nu$ Reconstruction and selection

- $WW^* \to e\nu\mu\nu$ selection
  - Two isolated leptons $p_T(\ell) > 22$ GeV and $p_T(\ell) > 15$ GeV
  - $E_T^{miss} > 20$ GeV
- Signal-to-background discriminants
  - Trasnverse mass (m_T) for ggF production and Boosted Decision Tree (BDT) for VBF production
- Background estimation

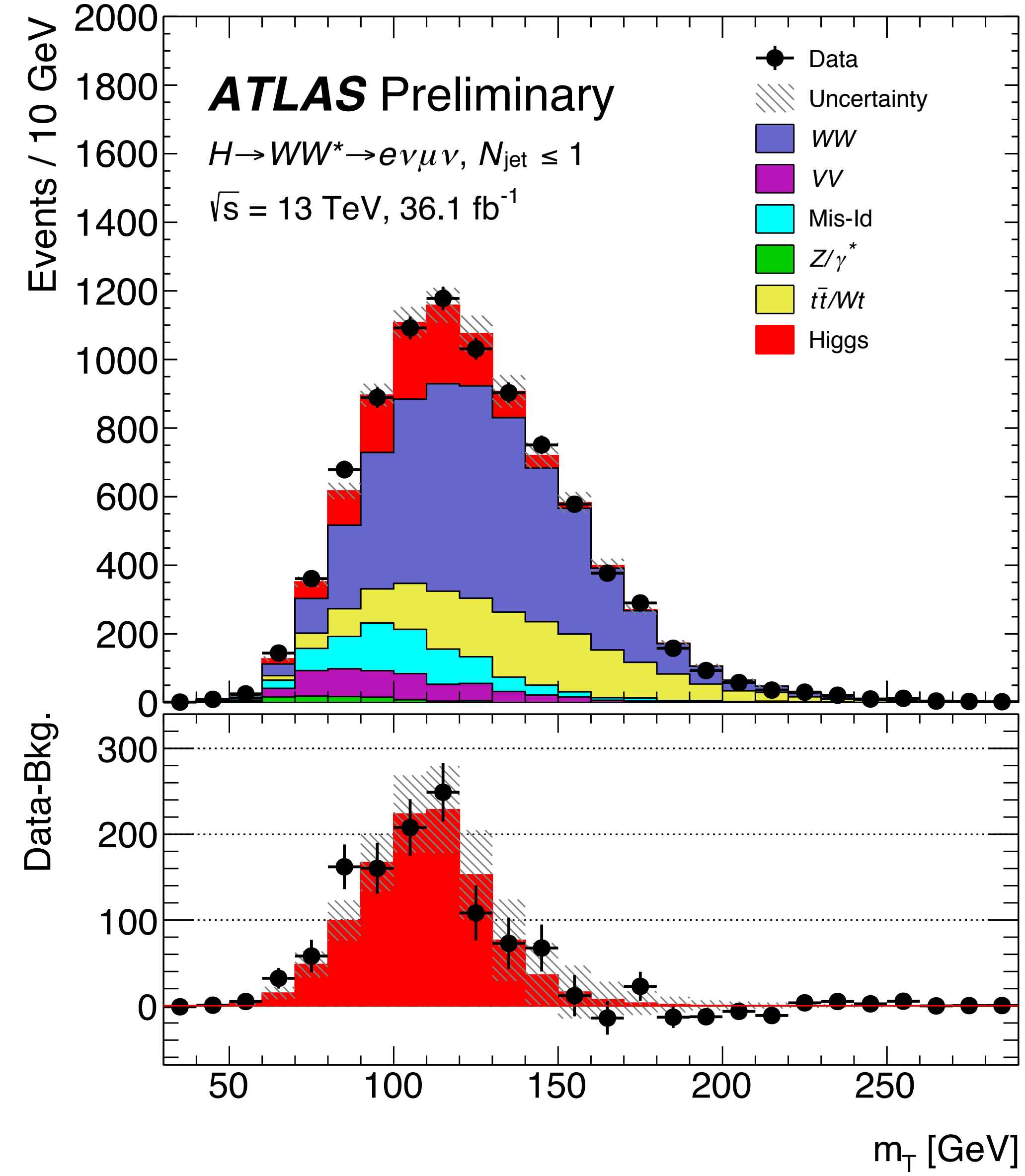

1. Non resonant *WW* production
2. $t\bar{t}$ production
3. Drell-Yan: $Z \to \tau^+\tau^-$
4. Hadrons misidentified as leptons:
   - W+jets $t\bar{t}$ and WZ production

Based on data

5. ZZ^*, WZ, $W\gamma(*)$ production in
6. Single-top-quark (Wt) production

Based on simulation

E_T(e/γ) resolution

- Good energy calibration necessary for increased precision on m_H
  - Two step approach: i) material energy loss and ii) global calorimetric scale from $Z \to ee$ data
- Total scale uncertainty of at 40 GeV at the per-mille level.

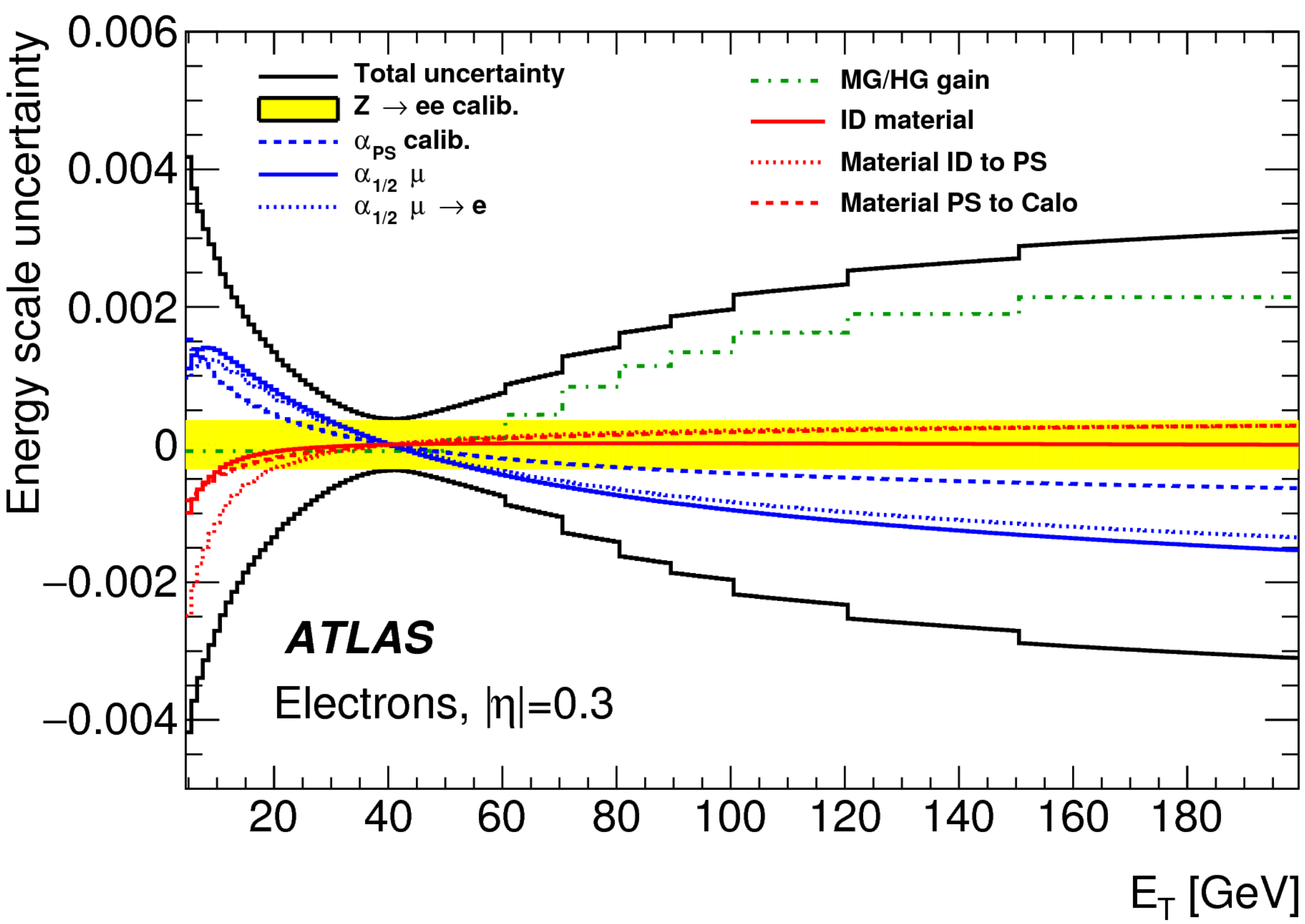

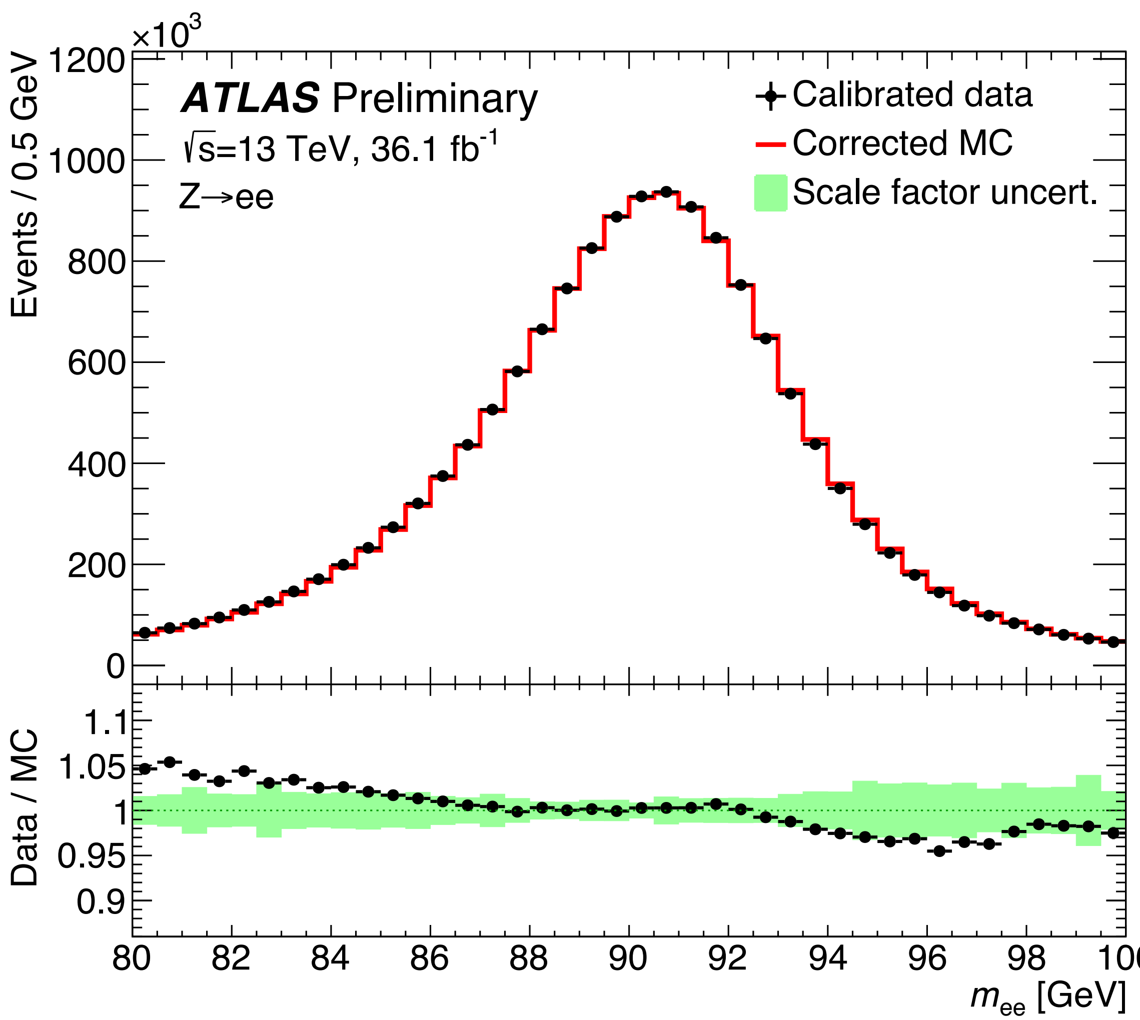

$E_T(e/\gamma)$ resolution

- Good energy calibration necessary for increased precision on m_H
  - Two step approach: i) material energy loss and ii) global calorimetric scale from $Z \to ee$ data
- Total scale uncertainty of at 40 GeV at the per-mille level.

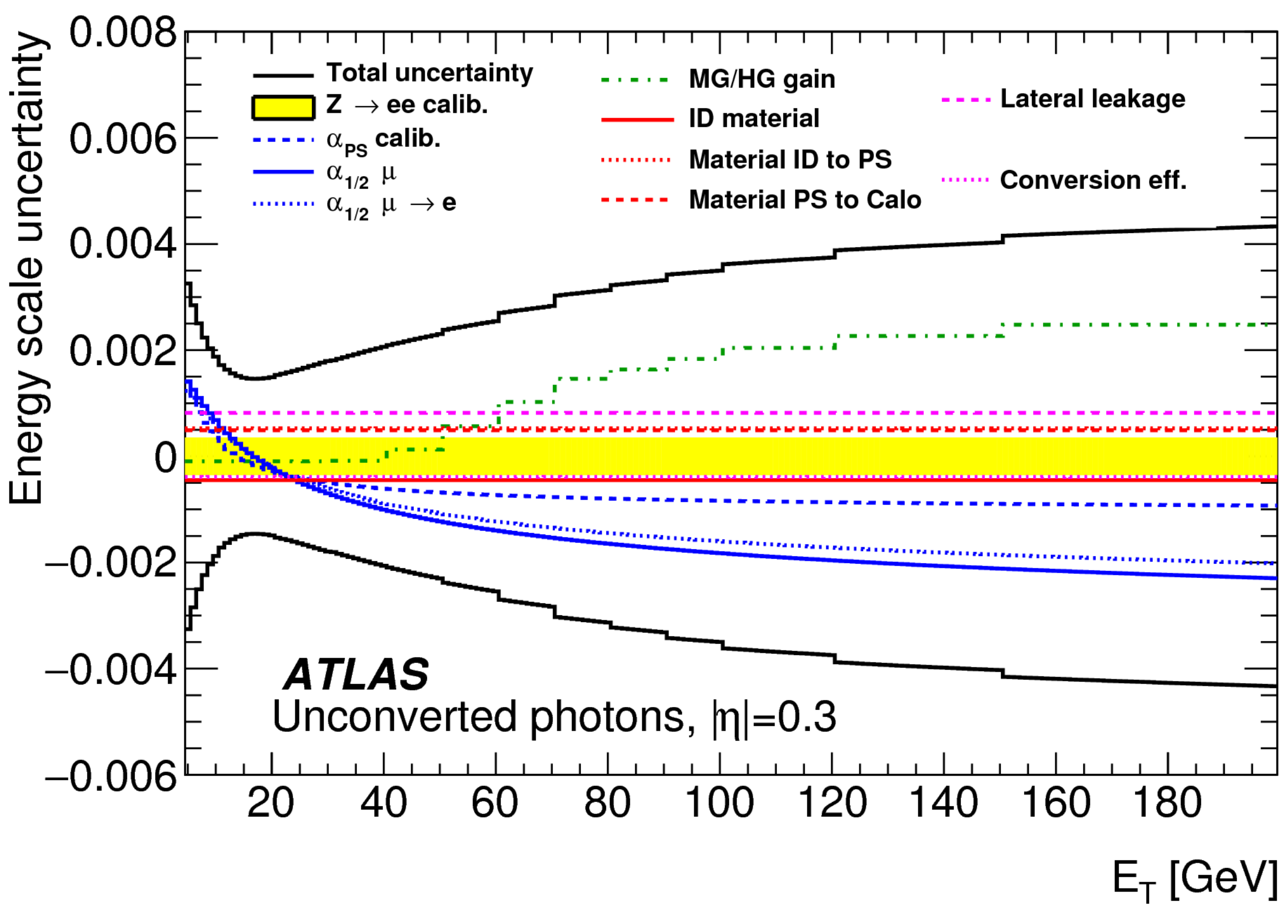

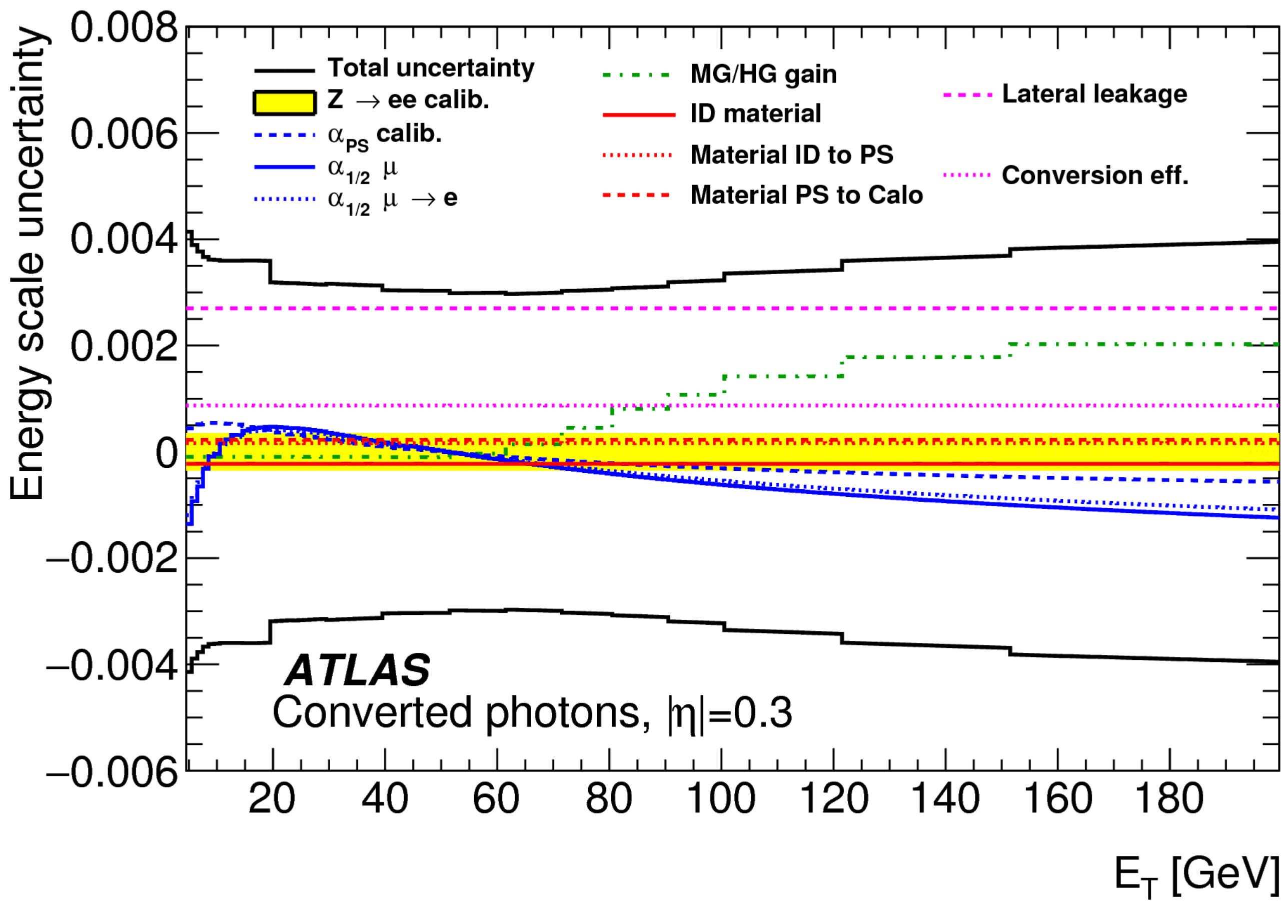

- $H\to\gamma\gamma$ updated result at Run II.
  - Analytical function in kinematic and detector categories.
  - Reduction of uncertainty through categorisation of events as a function of resolution and signal significance.

arXiv:1806.00242

- Expected statistical uncertainty of 0.21 GeV and 0.34 GeV systematic uncertainty

$$\boxed{m_H^{\gamma\gamma} = 124.93 \pm 0.40\ (\pm 0.21\ \text{stat only})\ \text{GeV}}$$

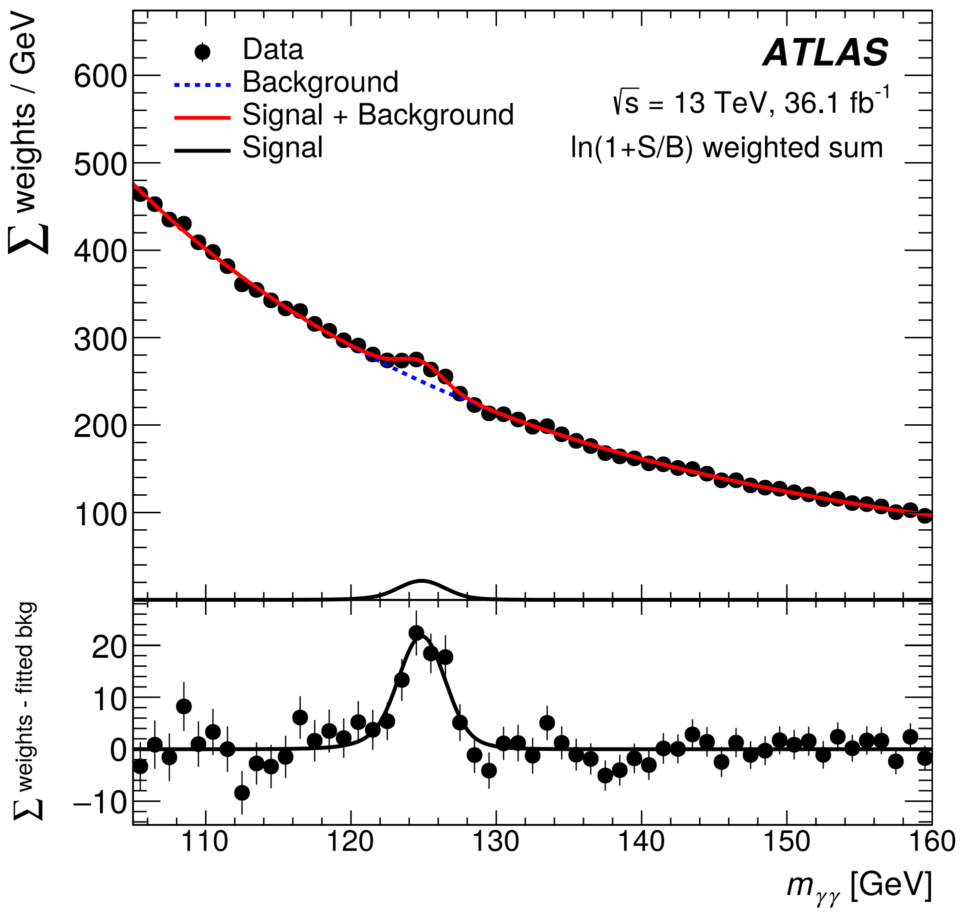

Source	Systematic uncertainty in m_H [MeV]
EM calorimeter response linearity	60
Non-ID material	55
EM calorimeter layer intercalibration	55
$Z \to ee$ calibration	45
ID material	45
Lateral shower shape	40
Muon momentum scale	20
Conversion reconstruction	20
$H \to \gamma\gamma$ background modelling	20
$H \to \gamma\gamma$ vertex reconstruction	15
e/γ energy resolution	15
All other systematic uncertainties	10

Introduction

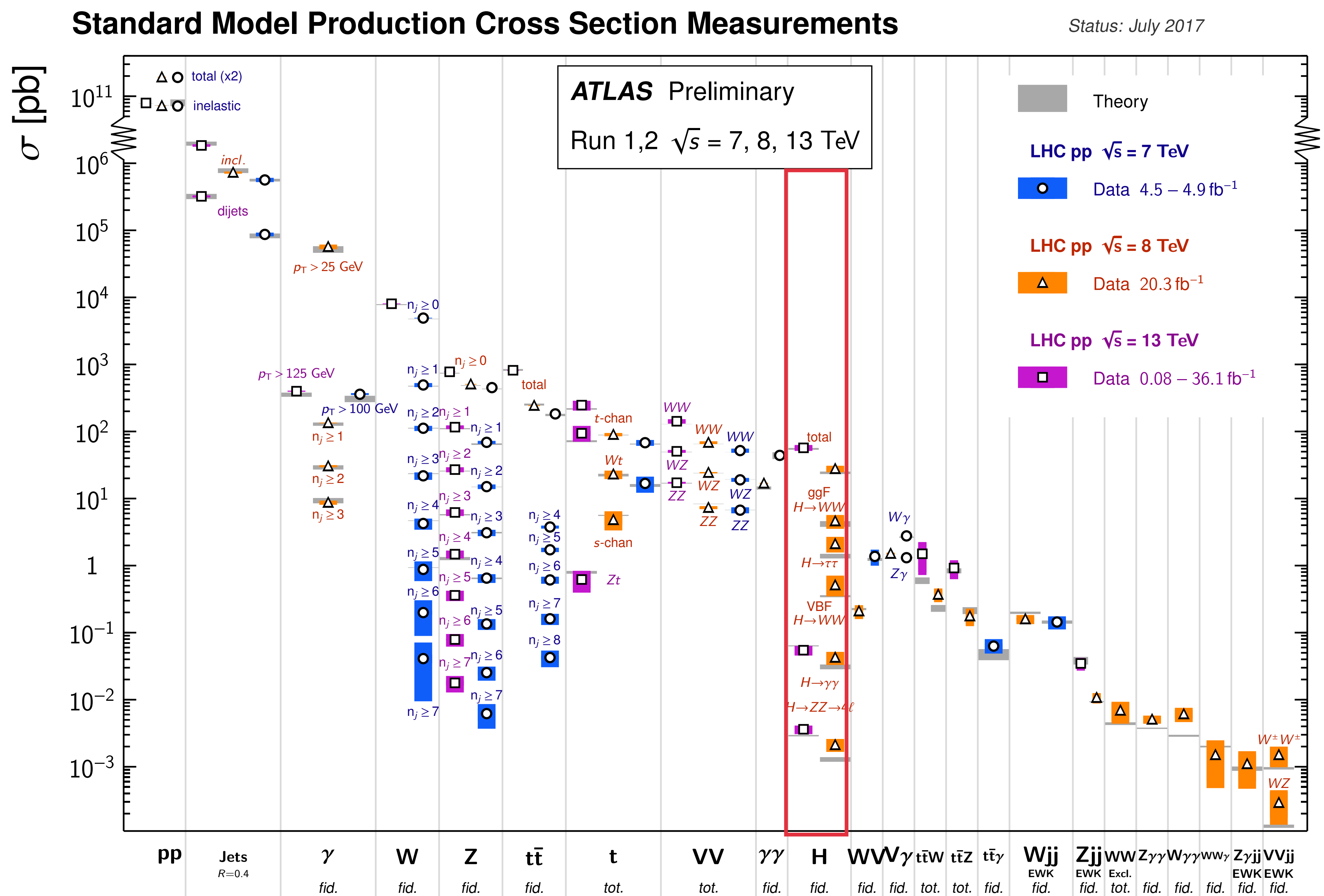

- Higgs boson decay channels considered in this talk :

(i) $H \rightarrow$ Dibosons ($ZZ^* \rightarrow 4\ell$, $WW^* \rightarrow \ell\bar{\nu}\bar{\ell}\nu$), and $\gamma\gamma$

(ii) $H \rightarrow$ fermions ($\tau\bar{\tau}$, $b\bar{b}$, $\mu\bar{\mu}$)

Di-Higgs production

- The Higgs boson can interact with itself through quadratic terms in the Higgs potential

$$\begin{aligned}\mathcal{L} = &-\frac{1}{4}F_{\mu\nu}F^{\mu\nu} \\ &+ i\bar{\Psi}\not{D}\psi \\ &+ D_\mu\Phi^\dagger D^\mu\Phi - \boxed{V(\Phi)} \\ &+ \bar{\Psi}_L\hat{Y}\Phi\Psi_R + h.c.\end{aligned} \quad \Rightarrow \quad V(\Phi) \sim -\mu^2(\Phi^\dagger\Phi) + \lambda(\Phi^\dagger\Phi)^2$$

  - About 500 times suppression of $\sigma(gg\rightarrow H)$ (48.5 pb) / $\sigma(gg\rightarrow HH)$ (~33.4 fb)
  - Destructive interference between the terms proportional to the κ_t^2 and the product of κ_t and κ_λ

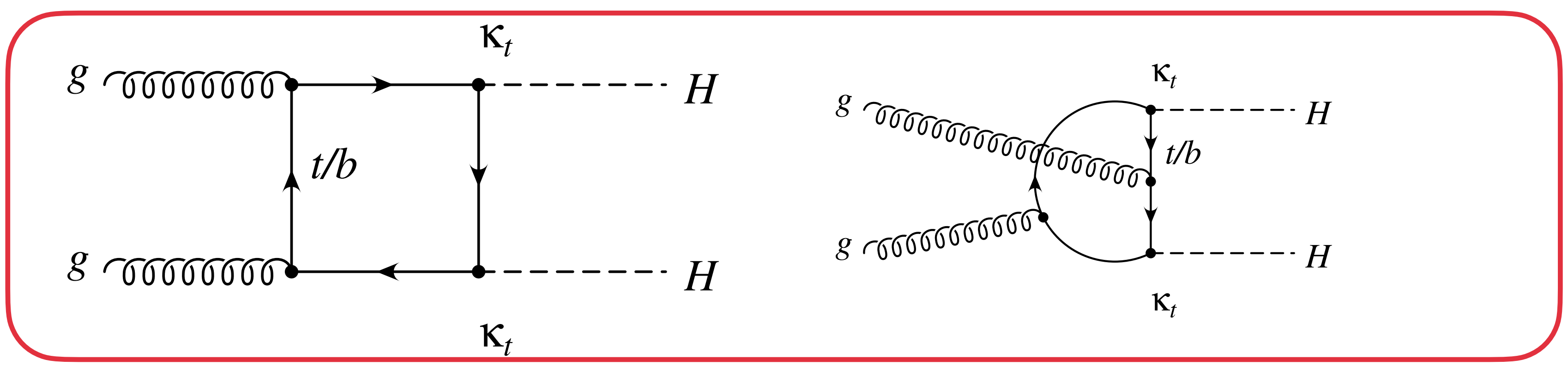

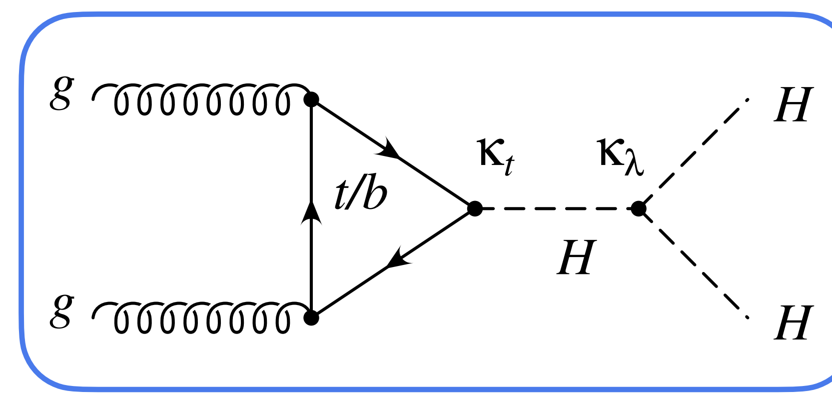

  - Single Higgs process do not depend on the trilinear self (λ_{HHH}) coupling at LO but are needed for the NLO EW corrections.

- Indirect constraint with comparing NLO EW dependant λ_{HHH} *effects*

ATL-PHYS-PUB-2019-009

Di-Higgs production

- Modified Higgs production cross section and branching rations to account for NLO EW corrections (K^i_{EW} and C^f)

$$\mu_i(\kappa_\lambda, \kappa_i) = \frac{\sigma^{\rm BSM}}{\sigma^{\rm SM}} = Z_H^{\rm BSM}(\kappa_\lambda)\left[\kappa_i^2 + \frac{(\kappa_\lambda - 1)C_1^i}{K_{\rm EW}^i}\right]$$

$$\mu_f(\kappa_\lambda, \kappa_f) = \frac{{\rm BR}_f^{\rm BSM}}{{\rm BR}_f^{SM}} = \frac{\kappa_f^2 + (\kappa_\lambda - 1)C_1^f}{\sum_j {\rm BR}_j^{\rm SM}\left[\kappa_j^2 + (\kappa_\lambda - 1)C_1^j\right]}$$

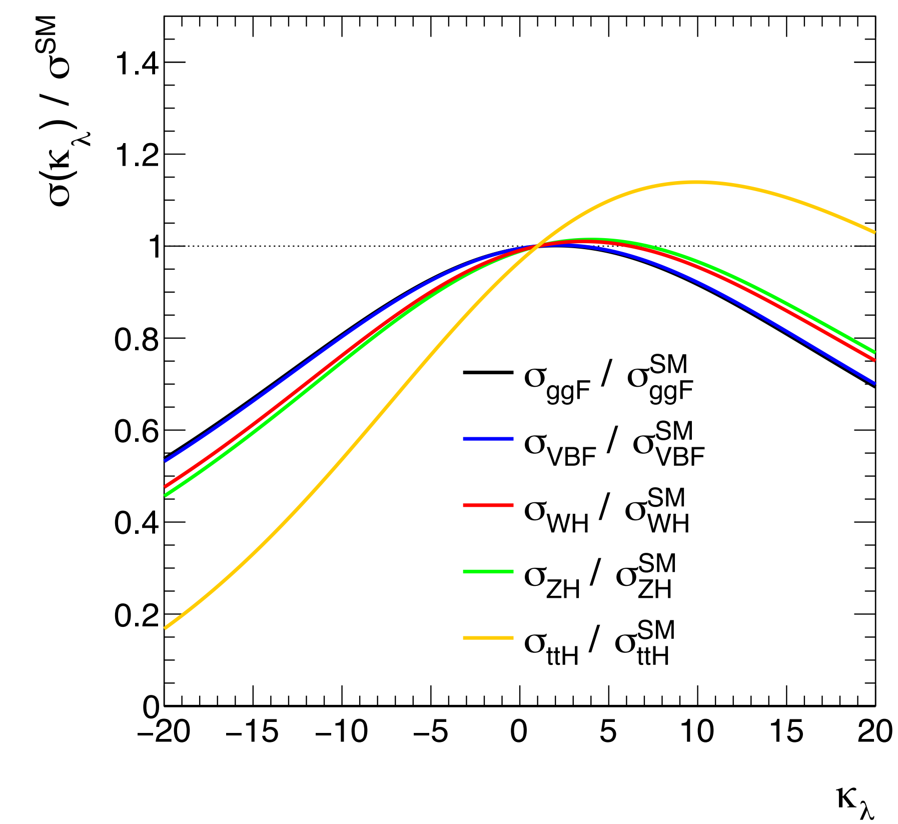

- Combined fit over Higgs STXS combination

$$\kappa_\lambda = 4.0^{+4.3}_{-4.1} = 4.0^{+3.7}_{-3.6}\,(\text{stat.})\,^{+1.6}_{-1.5}\,(\text{exp.})\,^{+1.3}_{-0.9}\,(\text{sig. th.})\,^{+0.8}_{-0.9}\,(\text{bkg. th.})$$

  - 95% C.L. -3.2 < κλ < 11.9 comparable over direct HH searches (-5.0 < κλ < 12.1)

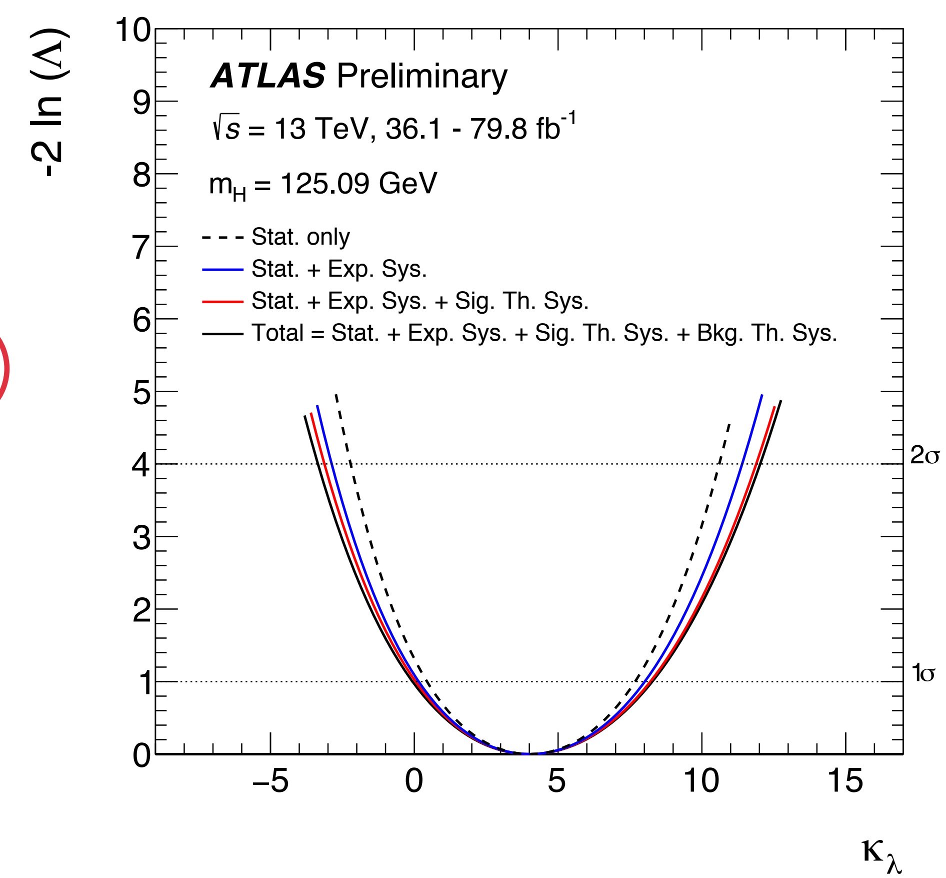

- 4ℓ: isolate signal under the Higgs resonant peak ($115 < m_{4\ell} < 130$).
- $\gamma\gamma$ cross section extracted from resonant peak over the $\gamma\gamma$ continuum.
- Higgs boson $p_{T,4\ell(\gamma\gamma)}$ and rapidity ($y_{4\ell(\gamma\gamma)}$) probe.
  - $p_{T,4\ell(\gamma\gamma)}$: Lagrangian structure of H interactions, Yukawa couplings
  - $y_{4\ell(\gamma\gamma)}$: Sensitivity to proton's parton density functions.

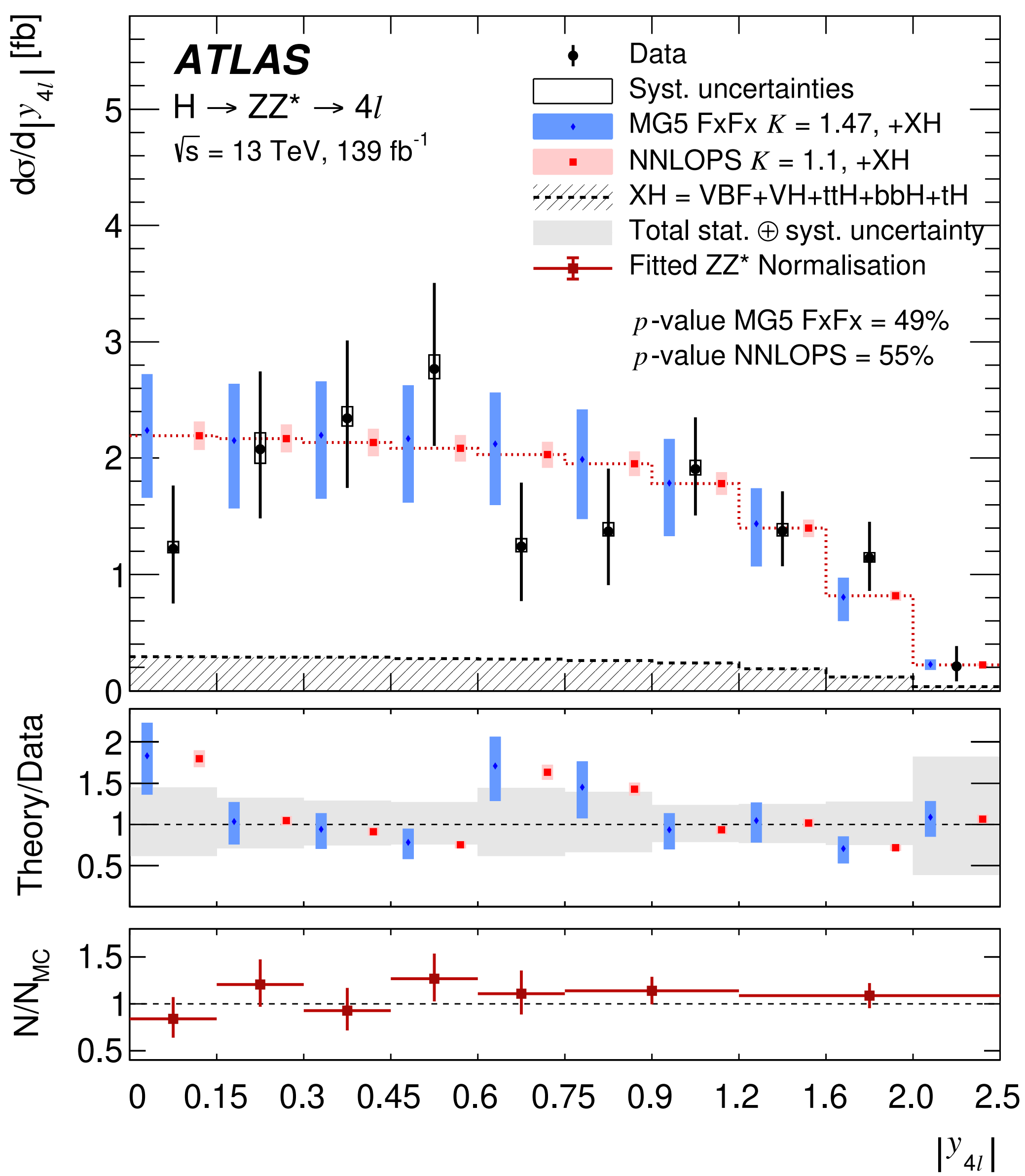

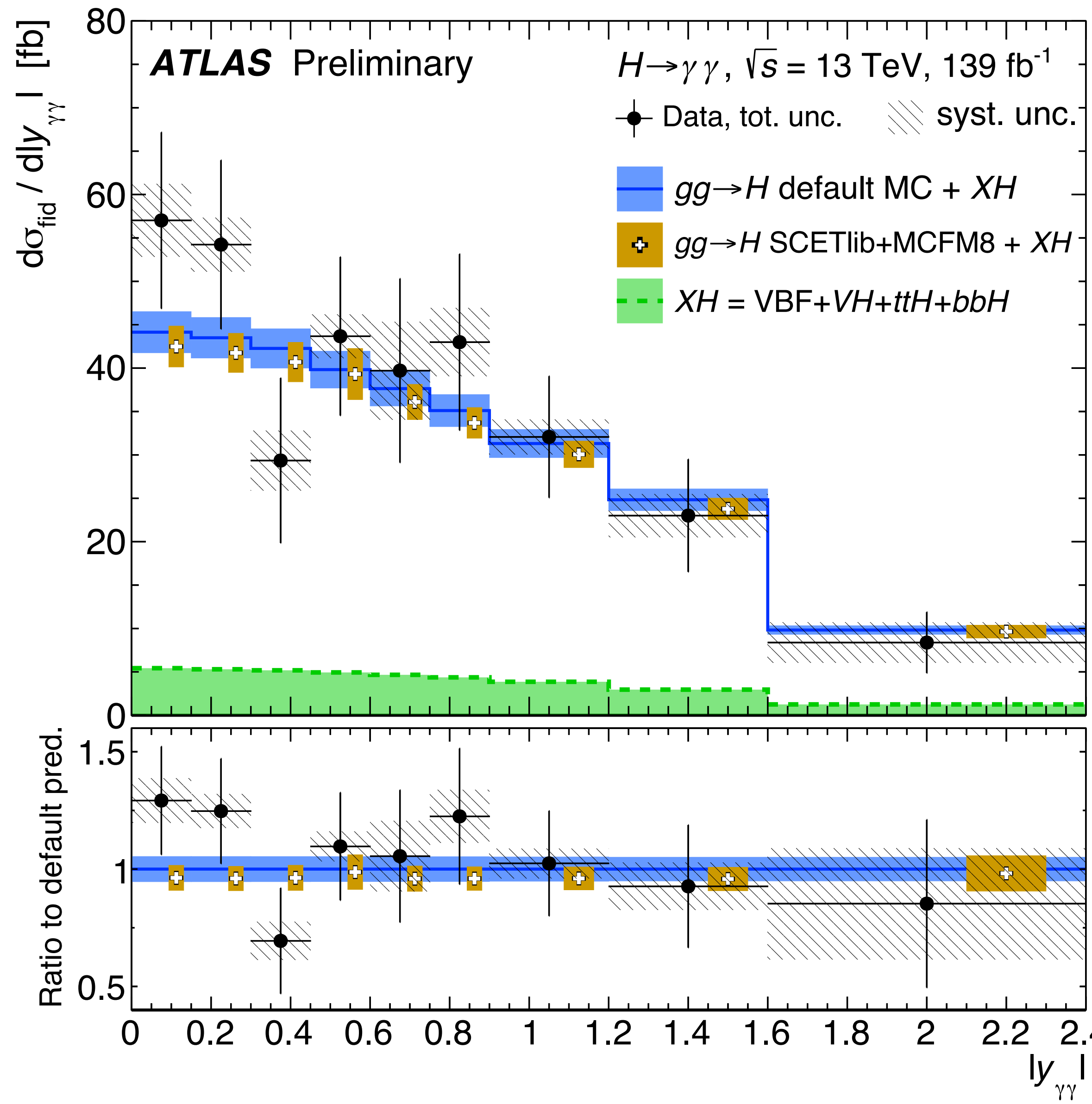

Physics objects definition and selection criteria.

Object selection

- Electrons (e).
  - Isolated objects clustered from calorimeter energy deposits with associated ID track.
  - $E_T > 7$ GeV, $|\eta| < 2.47$ and $|z_0 \sin(\vartheta)| < 0.5$ mm

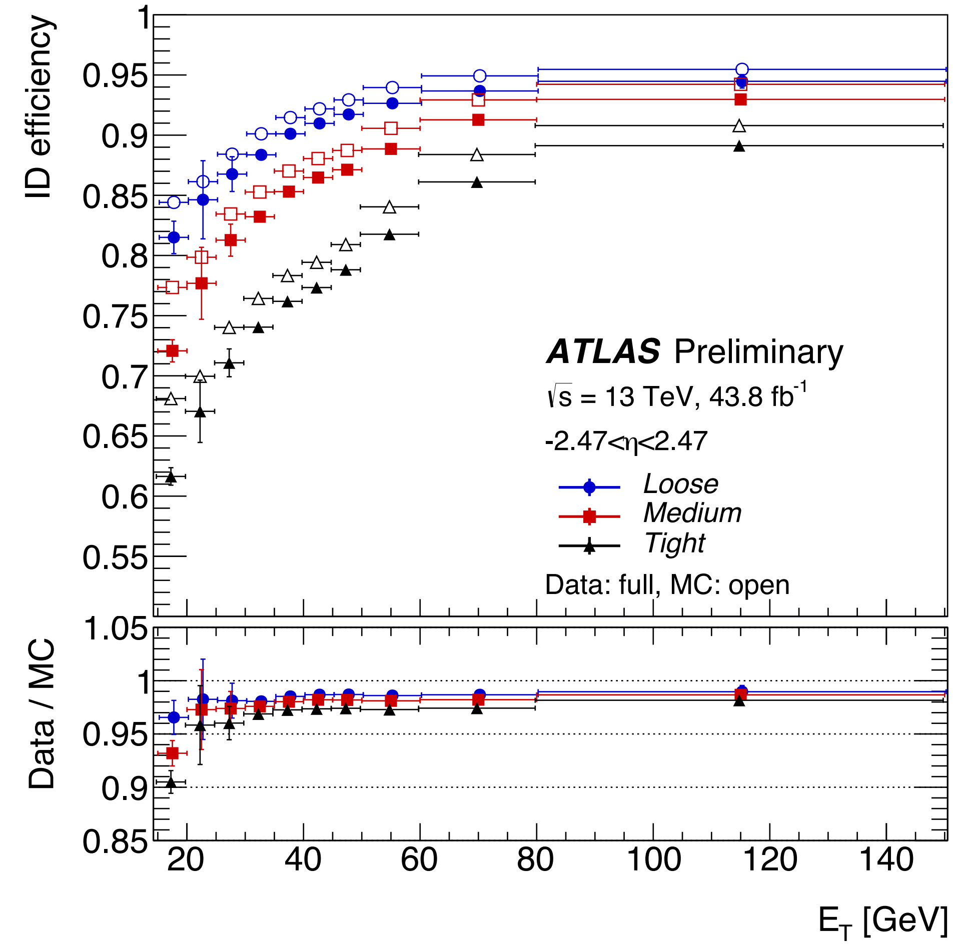

- Muons (μ).
  - Combined track fit of Inner Detector and Muon Spectrometer hits,
  - $p_T > 5$ GeV, $|\eta| < 2.7$ $|z_0 \sin(\vartheta)| < 0.5$ mm of "loose or medium quality"
  - Isolated objects

- Jets (j).
  - Energy deposit grouping with *infra*-red safe algorithm:
  - $p_T > 20$ GeV and $|\eta| < 4.5$
    - ✦ Clustering with anti-k_T, $R=0.4$

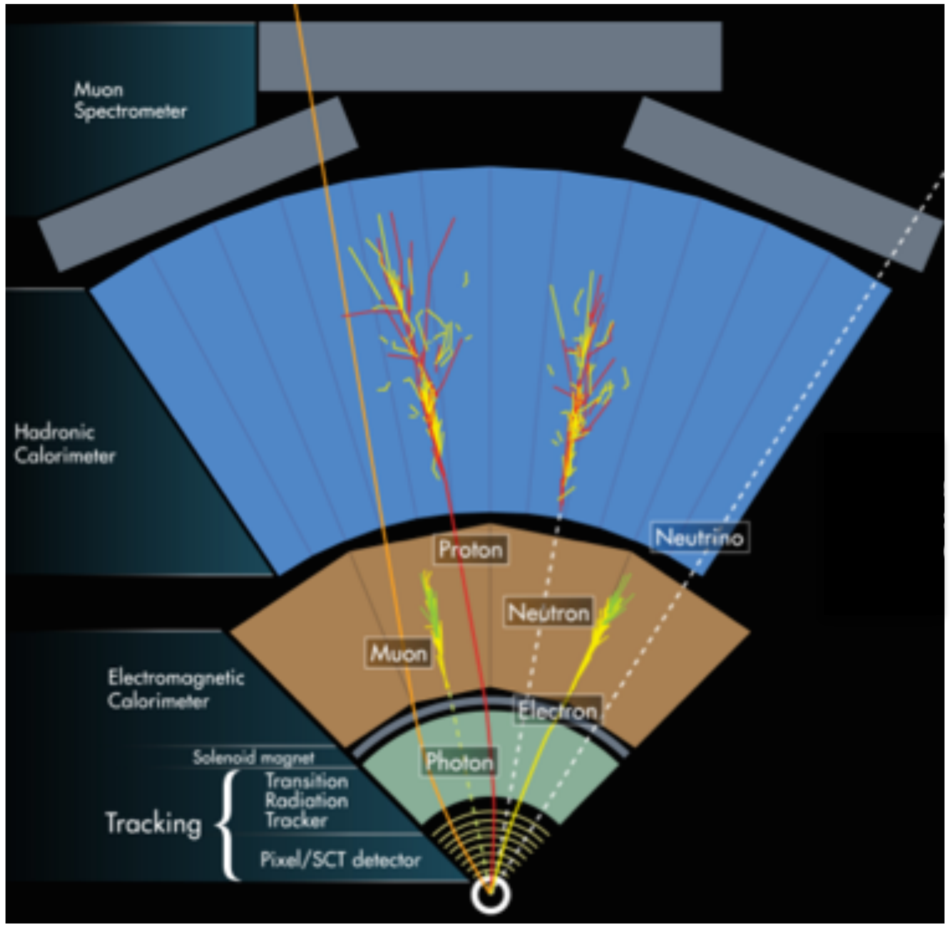

Object selection

- Electrons (e).
  - Isolated objects clustered from calorimeter energy deposits with associated ID track.
  - $E_T > 7$ GeV, $|\eta| < 2.47$ and $|z_0 \sin(\vartheta)| < 0.5$ mm

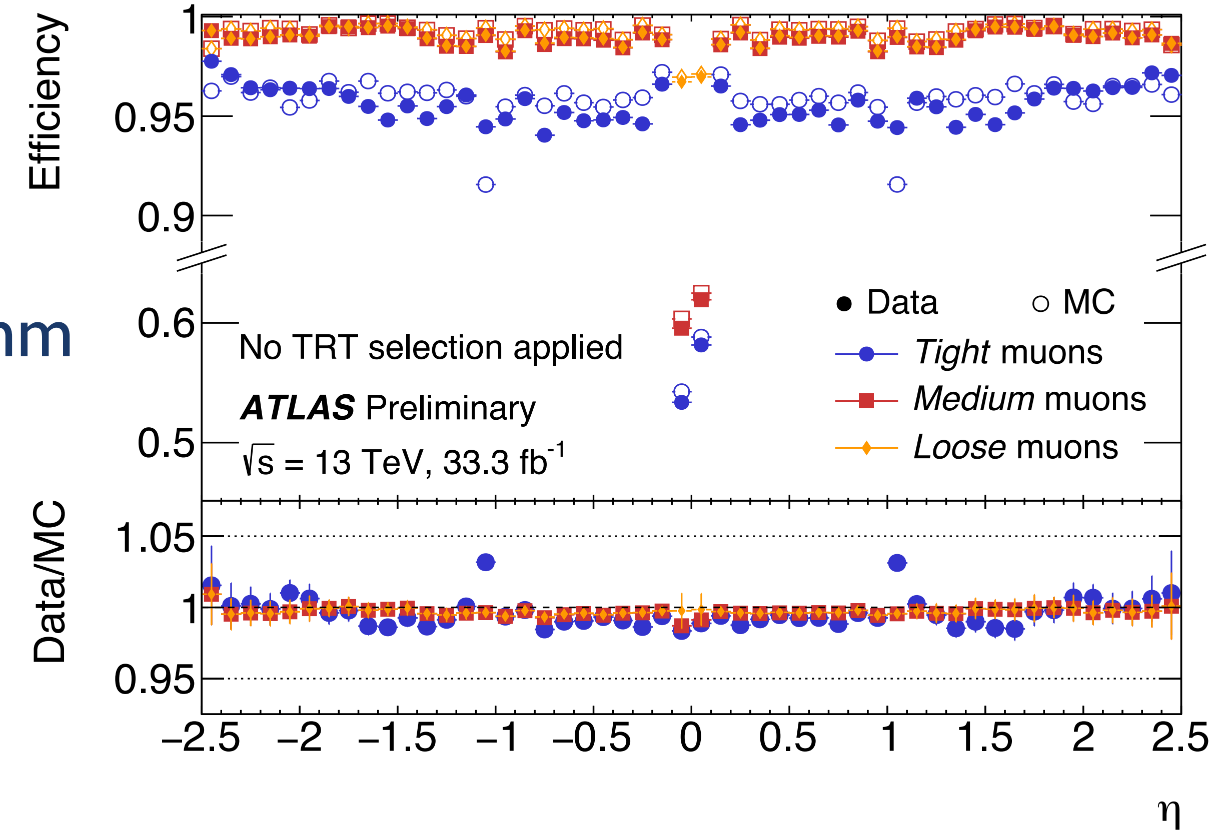

- Muons (μ).
  - Combined track fit of Inner Detector and Muon Spectrometer hits,
  - $p_T > 5$ GeV, $|\eta| < 2.7$ $|z_0 \sin(\vartheta)| < 0.5$ mm of "loose or medium quality"
  - Isolated objects

- Jets (j).
  - Energy deposit grouping with *infra*-red safe algorithm:
  - $p_T > 20$ GeV and $|\eta| < 4.5$
    - ✦ Clustering with anti-k_T, $R=0.4$

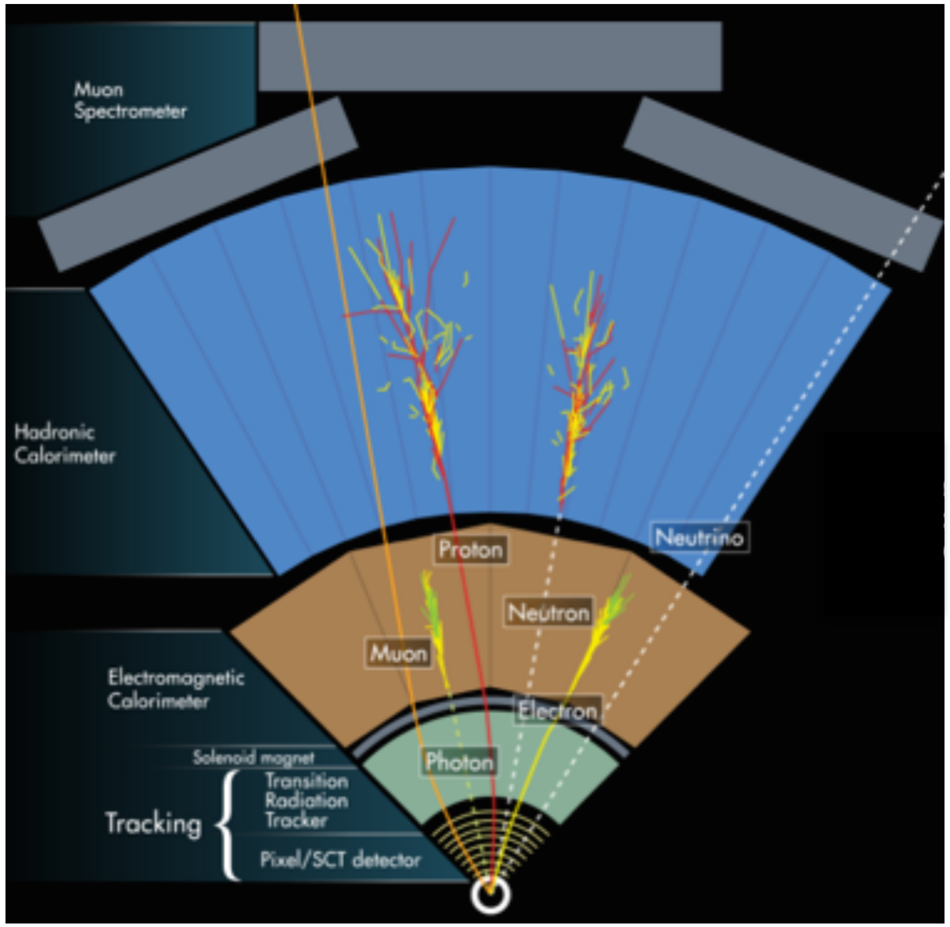

- Electrons (e).
  - Isolated objects clustered from calorimeter energy deposits with associated ID track.
  - $E_T > 7$ GeV, $|\eta| < 2.47$ and $|z_0 \sin(\vartheta)| < 0.5$ mm

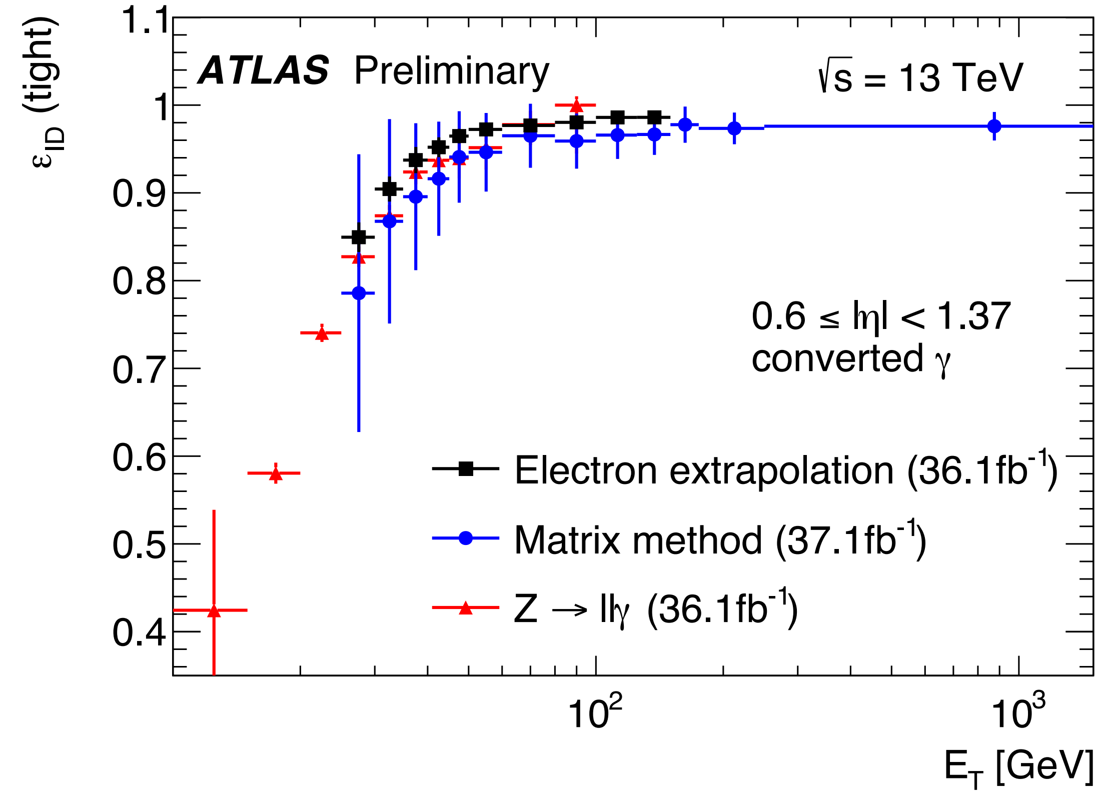

- Muons (μ).
  - Combined track fit of Inner Detector and Muon Spectrometer hits,
  - $p_T > 5$ GeV, $|\eta| < 2.7$ $|z_0 \sin(\vartheta)| < 0.5$ mm of "loose or medium quality"
  - Isolated objects

- Photons (γ).
  - Clustering of calorimeter energy deposits.
  - Identified with rectangular cuts on shower shapes.

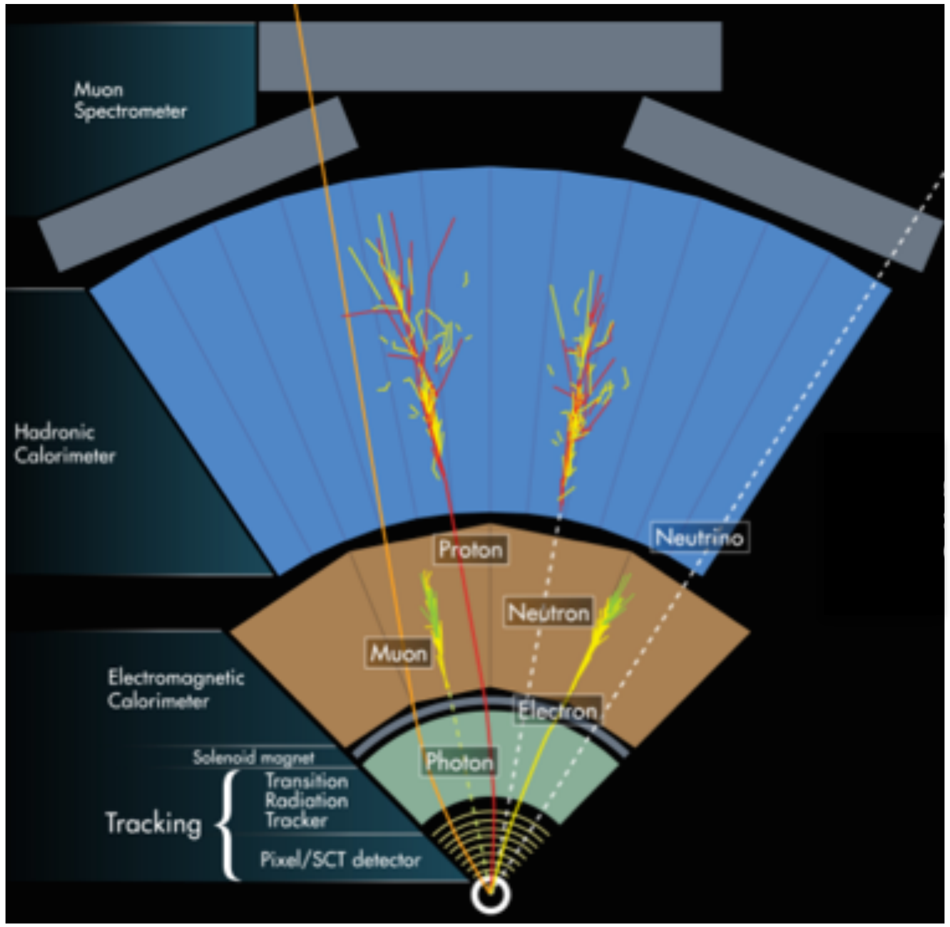

- **Electrons (e).**
  - Isolated objects clustered from calorimeter energy deposits with associated ID track.
  - $E_T > 7$ GeV, $|\eta| < 2.47$ and $|z_0 \sin(\vartheta)| < 0.5$ mm

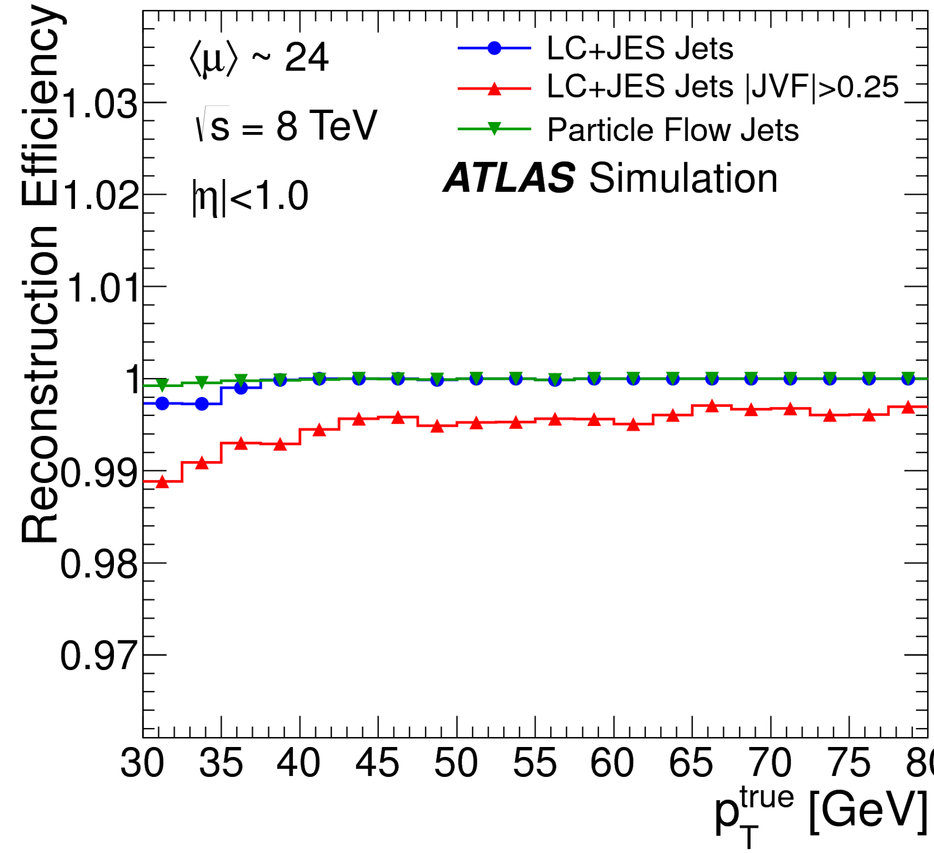

- **Muons (μ).**
  - Combined track fit of Inner Detector and Muon Spectrometer hits,
  - $p_T > 5$ GeV, $|\eta| < 2.7$ $|z_0 \sin(\vartheta)| < 0.5$ mm of "loose or medium quality"
  - Isolated objects

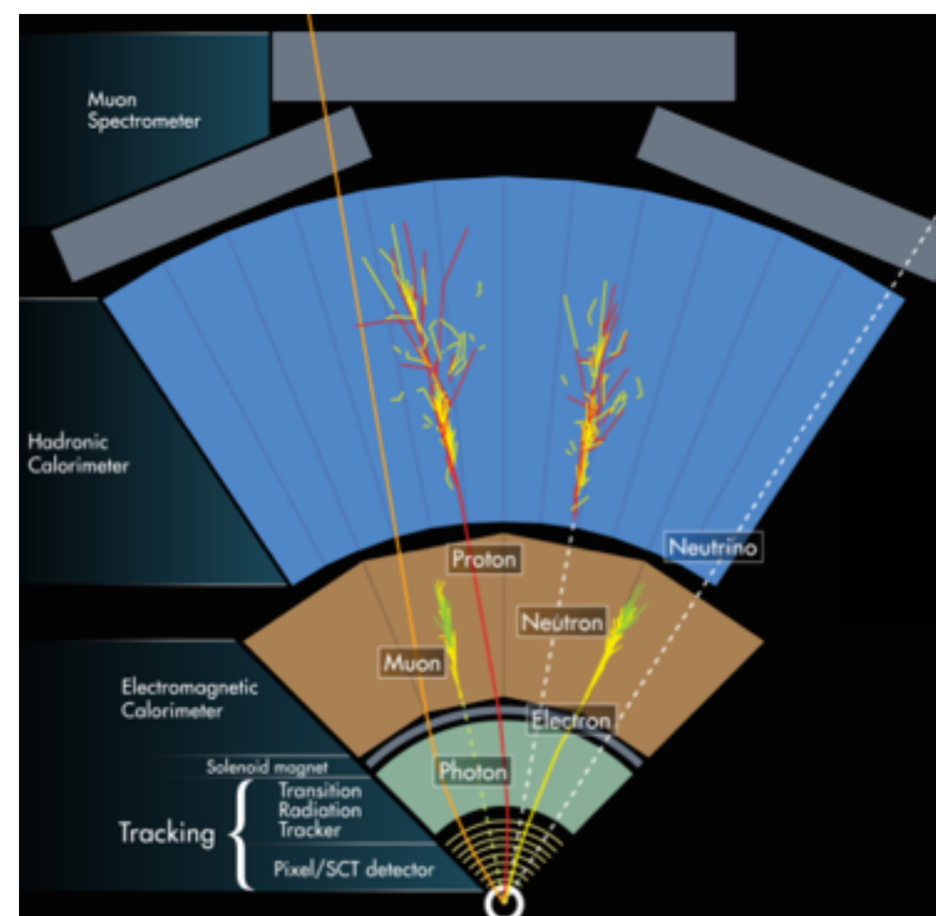

- **Jets (j).**
  - Energy deposit grouping with *infra*-red safe algorithm:
  - $p_T > 20$ GeV and $|\eta| < 4.5$
    - ✦ Clustering with anti-k_T, $R=0.4$

- Electrons (e).
  - Isolated objects clustered from calorimeter energy deposits with associated ID track.
  - $E_T > 7$ GeV, $|\eta| < 2.47$ and $|z_0 \sin(\vartheta)| < 0.5$ mm

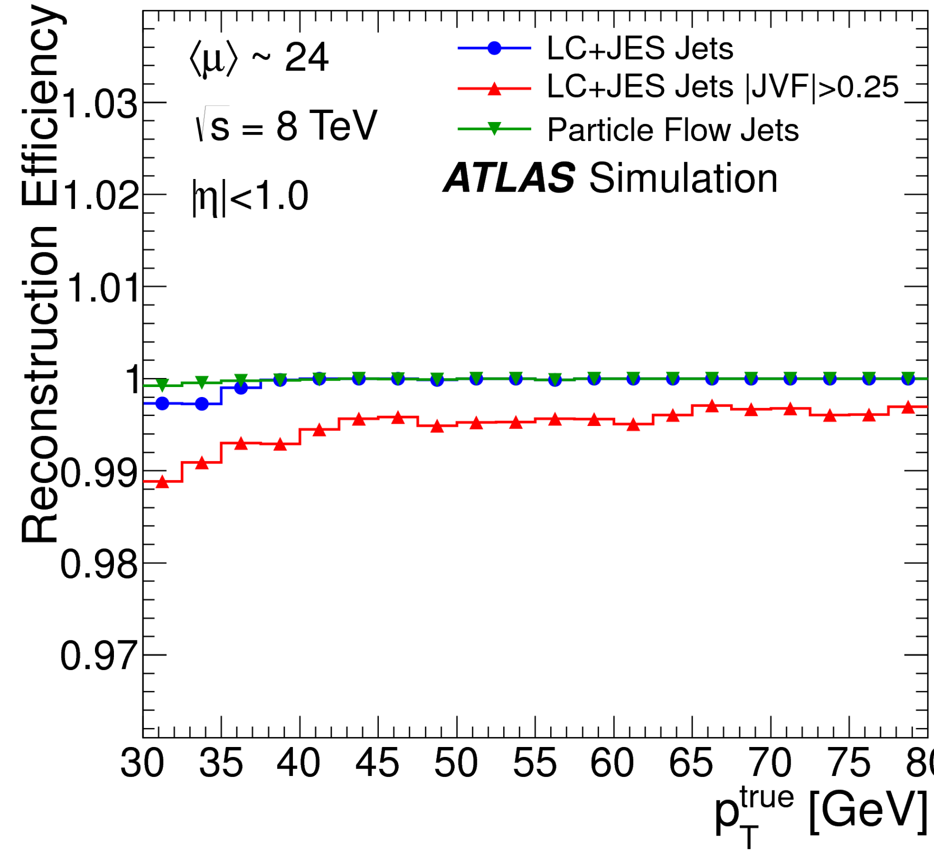

- Muons (μ).
  - Combined track fit of Inner Detector and Muon Spectrometer hits,
  - $p_T > 5$ GeV, $|\eta| < 2.7$ $|z_0 \sin(\vartheta)| < 0.5$ mm of "loose or medium quality"
  - Isolated objects

- Missing transverse energy (E_T^{miss}).
  - Inferred from transverse momentum imbalance

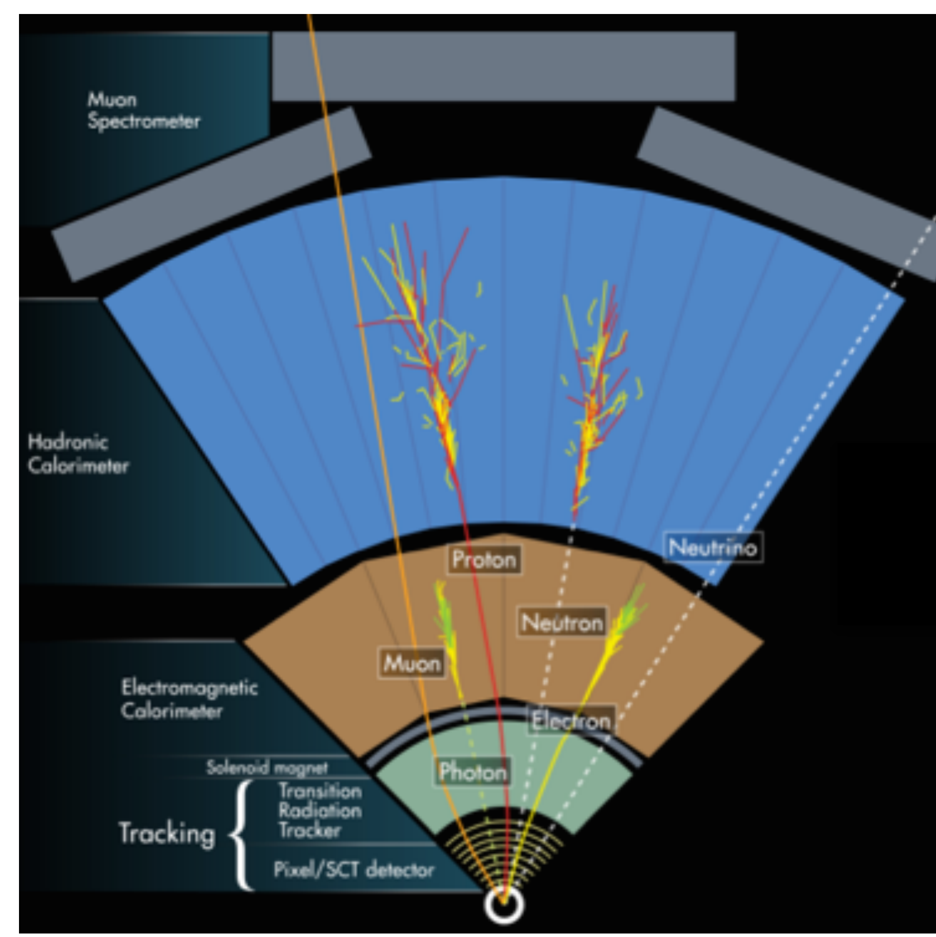

Run I status

- ATLAS run I precision on m_H of 0.33%
  - combined measurement from $H\to\gamma\gamma$ and $H\to ZZ^*\to 4\ell$.

Channel	Mass measurement [GeV]
$H \to \gamma\gamma$	$125.98 \pm 0.42\,(\text{stat}) \pm 0.28\,(\text{syst}) = 125.98 \pm 0.50$
$H\to ZZ^*\to 4\ell$	$124.51 \pm 0.52\,(\text{stat}) \pm 0.06\,(\text{syst}) = 124.51 \pm 0.52$
Combined	$125.36 \pm 0.37\,(\text{stat}) \pm 0.18\,(\text{syst}) = 125.36 \pm 0.41$

  - For both channels dominated by statistical uncertainty

- Aim in improving significantly on δm_H
  - Expect 1.7 times more candidates, with 36 fb^{-1} at $\sqrt{s}$=13 TeV

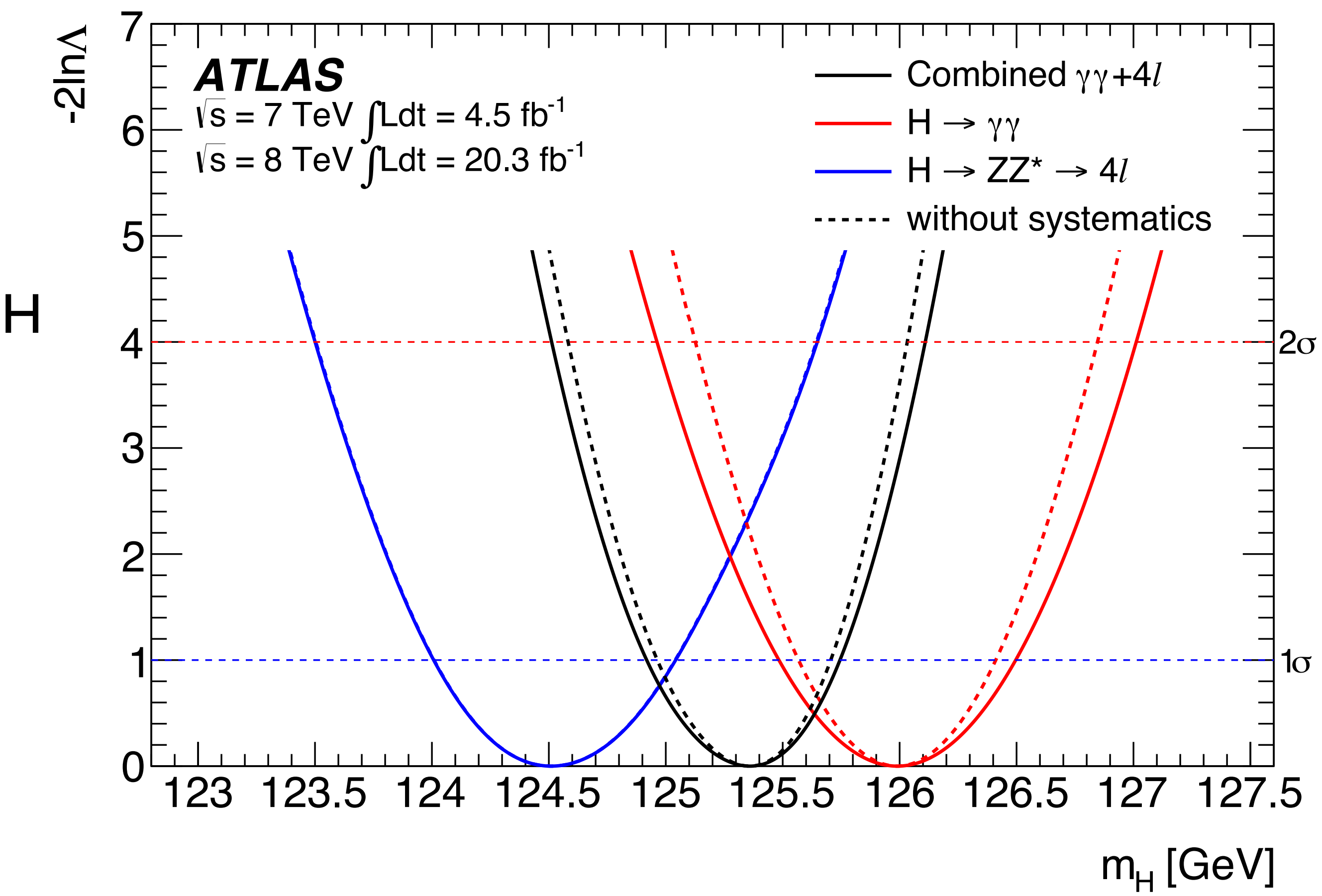

- Correction for local misalignments

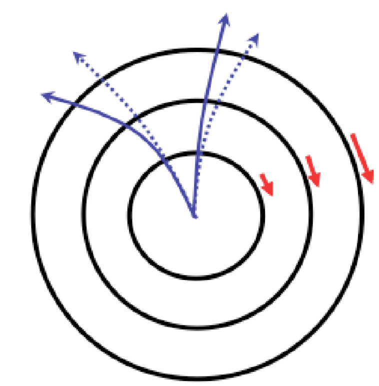

  - Charge dependent bias, with net effect of worsening resolution
  - In-situ correction based on Z→μμ data, recovers up to 5% in resolution.
  - Iteratively removing the bias δ_s:

$$p_T^{\mathrm{corr}}(\mu) = \frac{p_T^{\mathrm{bias}}(\mu)}{1 - q(\mu)\delta_s(\eta,\phi)p_T^{\mathrm{bias}}(\mu)}$$

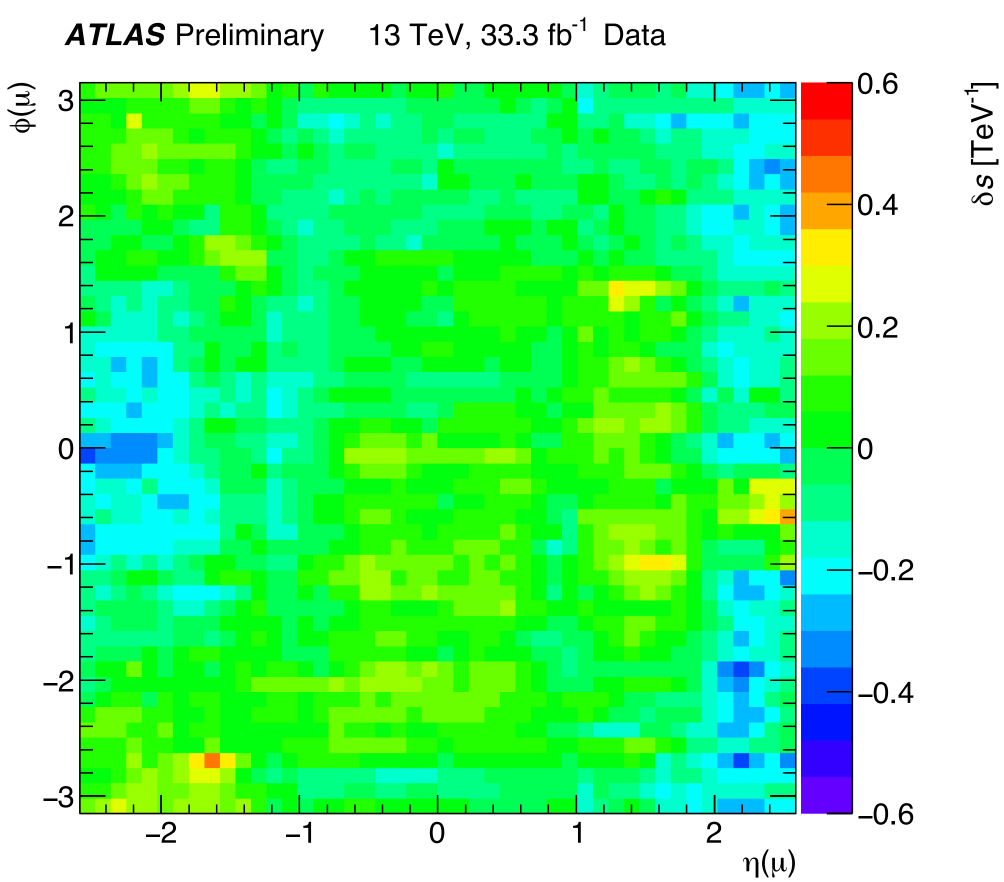

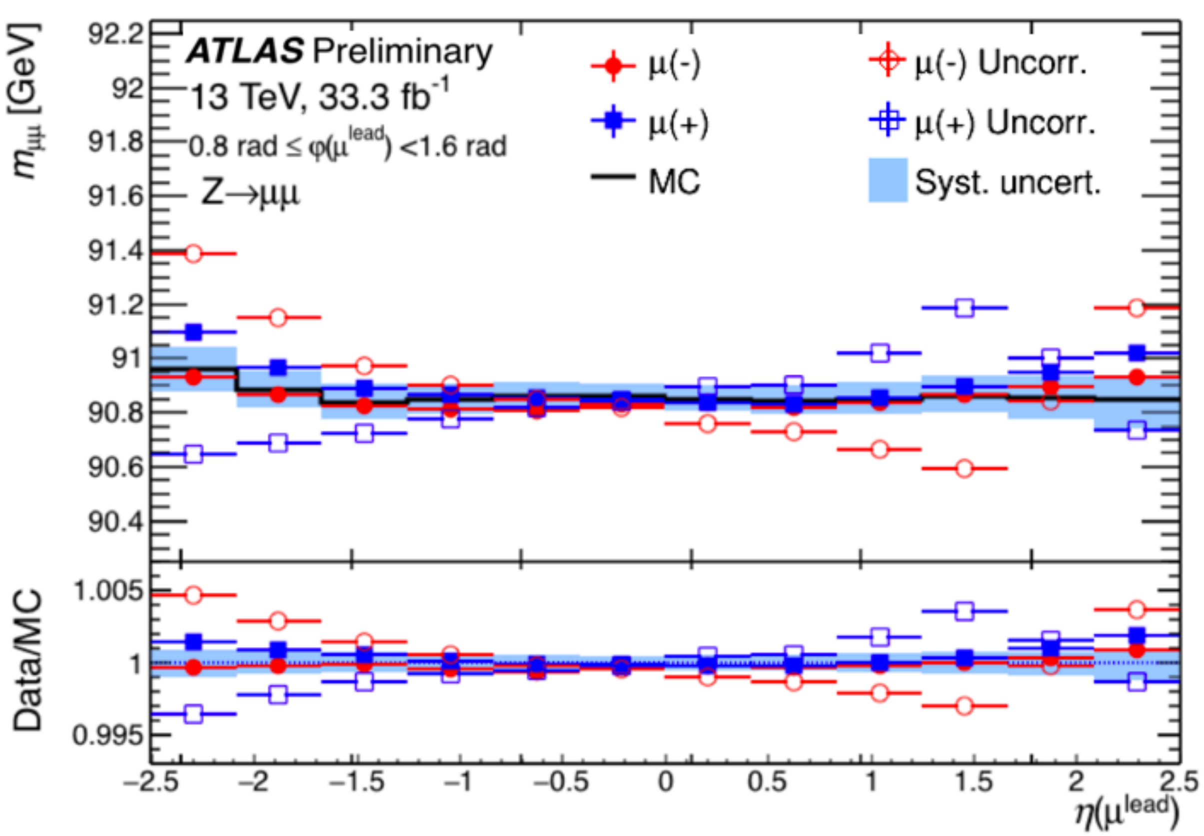

- ATLAS run I precision on m_H of 0.33%
  - combined measurement from $H\rightarrow\gamma\gamma$ and $H\rightarrow ZZ^*\rightarrow 4\ell$.

Channel	Mass measurement [GeV]
$H \rightarrow \gamma\gamma$	$125.98 \pm 0.42\,(\text{stat}) \pm 0.28\,(\text{syst}) = 125.98 \pm 0.50$
$H \rightarrow ZZ^* \rightarrow 4\ell$	$124.51 \pm 0.52\,(\text{stat}) \pm 0.06\,(\text{syst}) = 124.51 \pm 0.52$
Combined	$125.36 \pm 0.37\,(\text{stat}) \pm 0.18\,(\text{syst}) = 125.36 \pm 0.41$

  - For both channels dominated by statistical uncertainty

- Compatibility within 2.0 σ
  - *p*-value of about 0.05.

- Aim in improving significantly on δm_H
  - Expect 1.7 times more candidates, with 36 fb^{-1} at $\sqrt{s}$=13 TeV

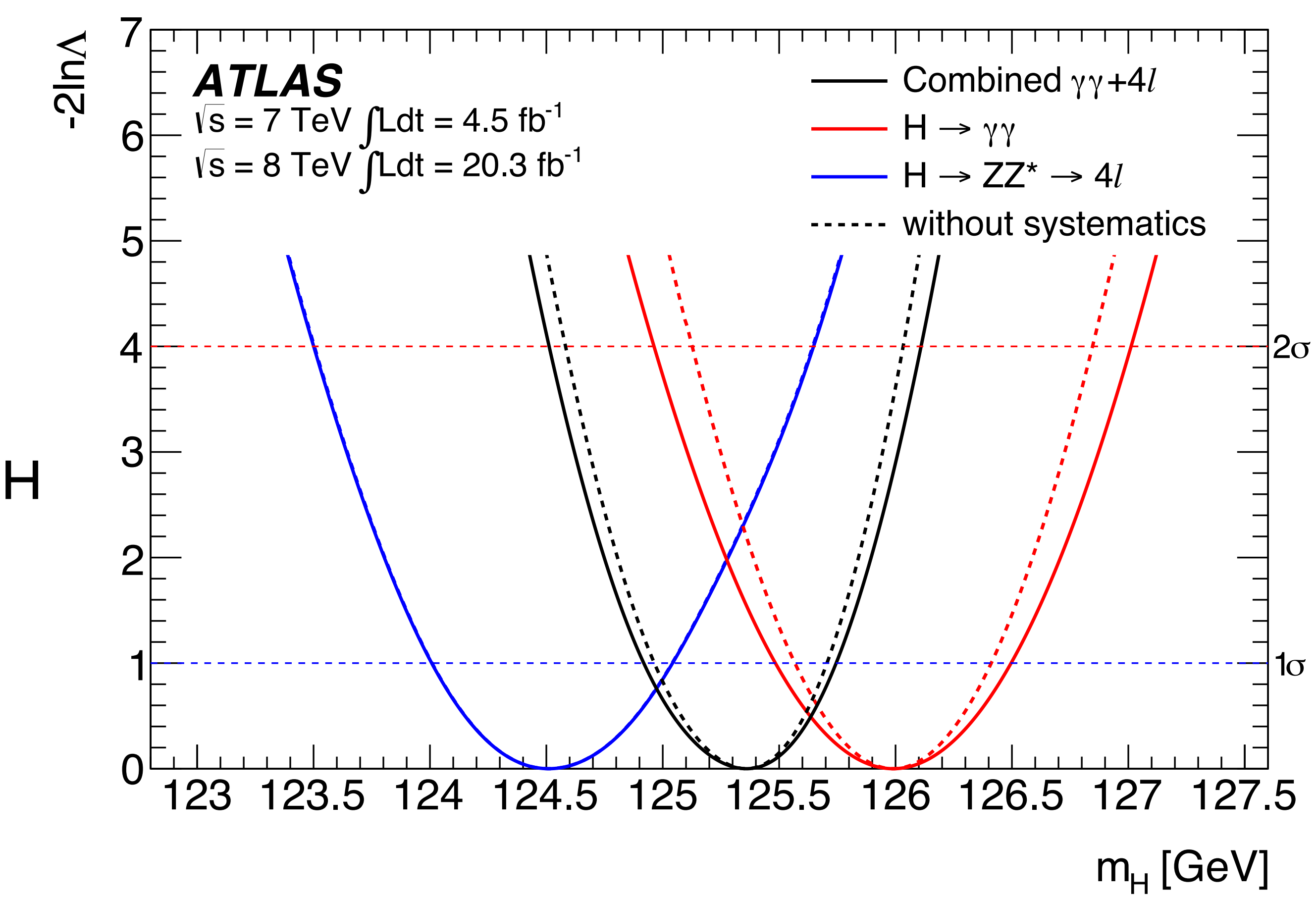

- $H\to\gamma\gamma$ updated result at Run II.
  - Analytical function in kinematic and detector categories.
  - Reduction of uncertainty through categorisation of events as a function of resolution and signal significance.

arXiv:1806.00242

- Expected statistical uncertainty of 0.21 GeV and 0.34 GeV systematic uncertainty

$$\boxed{m_H^{\gamma\gamma} = 124.93 \pm 0.40\ (\pm 0.21\ \text{stat only})\ \text{GeV}}$$

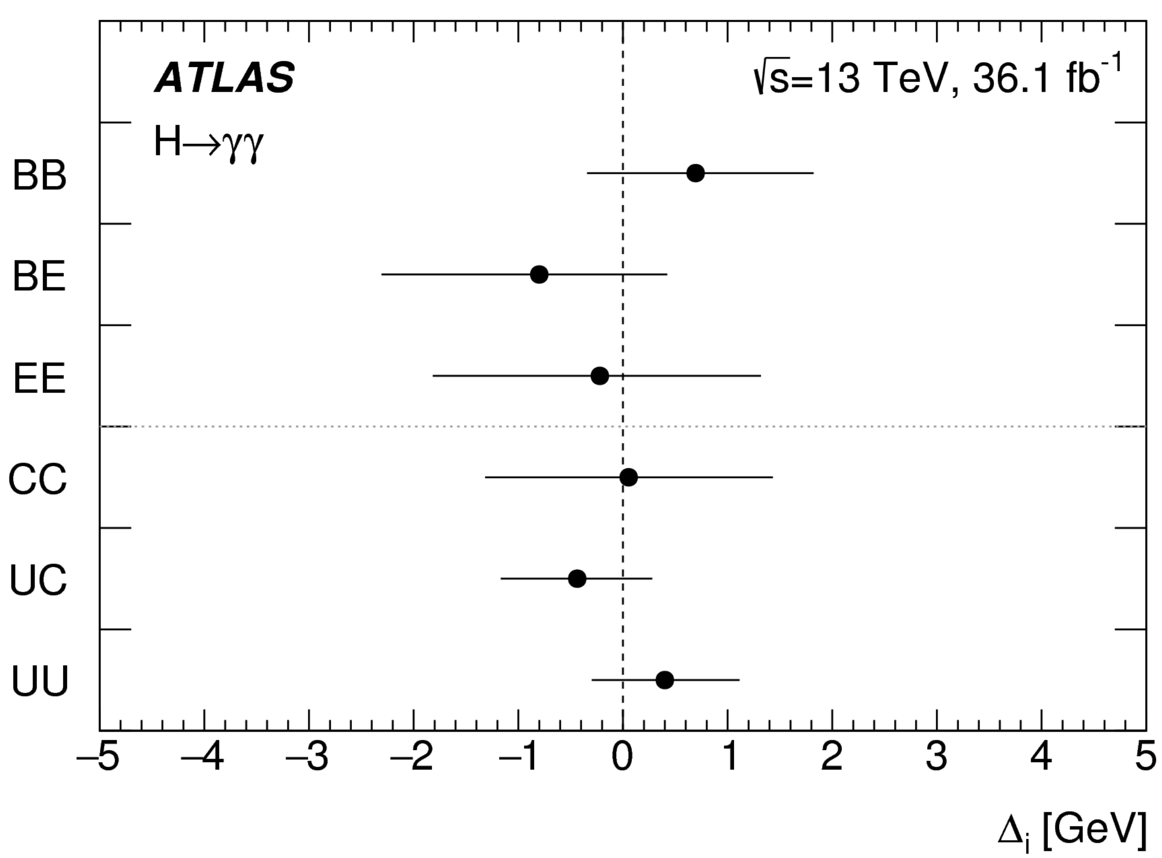

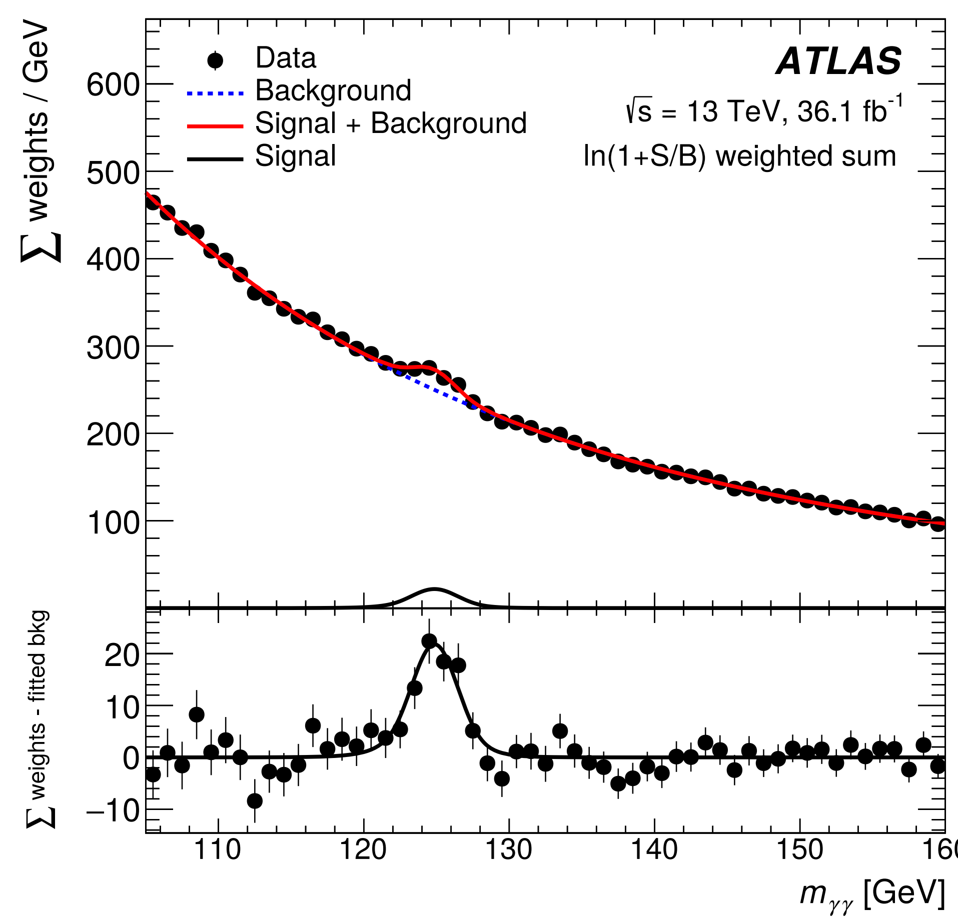

$H\to ZZ\to 4\ell$ results

Mass measurement

[arXiv:1806.00242](https://arxiv.org/abs/1806.00242)

- Final estimate from 4x4 simultaneous un-binned fit
  - Four kinematic categories and four final states
- Good agreement between channels.
- Systematic uncertainty of 50 MeV

Systematic effect	Uncertainty on $m_H^{ZZ^*}$ [MeV]
Muon momentum scale	40
Electron energy scale	26
Pile-up simulation	10
Simulation statistics	8

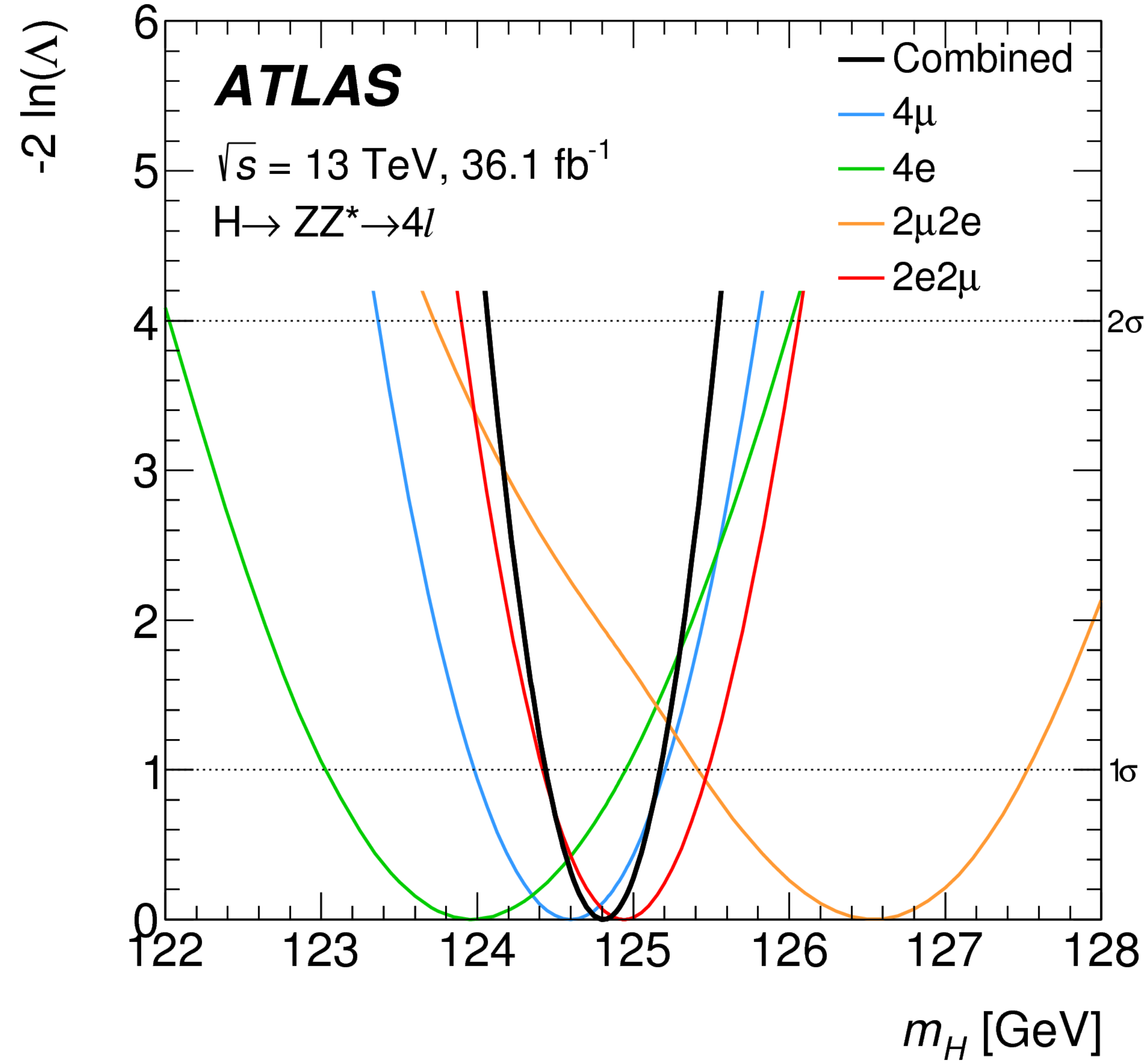

- Result:
  - 25% improved precision with respect to Run I ATLAS Combination.

$$\boxed{m_H^{ZZ^*} = 124.79 \pm 0.36 \ (\pm 0.05 \text{ stat only}) \text{ GeV}}$$

ATLAS-CONF-2018-018

- $ZZ^* \to 4\ell$ ($\ell = \mu$,e) selection:
  - Isolated leptons with: $p_T(\ell)$ > 20 GeV , 15 GeV 10 GeV and 5 (7) GeV
  - Leading pair: pair closest to m_Z,
  - Vertex refit: χ^2 cut at 99.5% signal efficiency
  - Final state photon emission recovered

Final state	Signal	ZZ^* background	Other backgrounds	Total expected	Observed
4μ	40.5 ± 1.7	19.0 ± 1.1	1.71 ± 0.10	61.2 ± 2.0	64
$2e2\mu$	28.2 ± 1.2	13.3 ± 0.8	1.38 ± 0.10	42.8 ± 1.4	64
$2\mu2e$	22.1 ± 1.4	9.2 ± 0.9	2.99 ± 0.09	34.3 ± 1.7	39
$4e$	21.1 ± 1.4	8.6 ± 0.8	2.90 ± 0.09	32.5 ± 1.6	28
Total	112 ± 5	50 ± 4	8.96 ± 0.12	171 ± 6	195

$$115 \text{ GeV} < m_{4\ell} < 130 \text{ GeV}$$

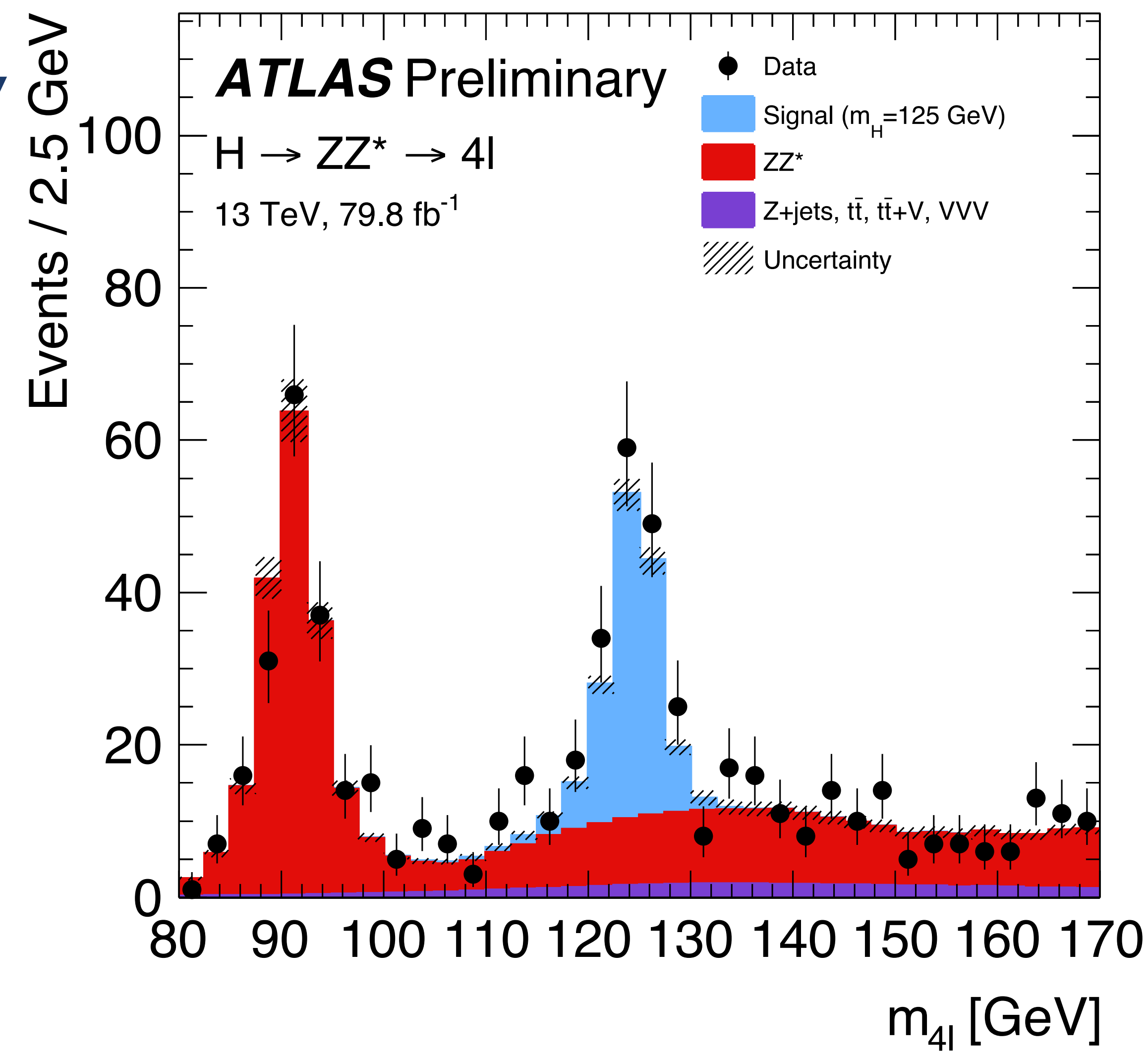

- Background estimation

Based on simulation

1. ZZ^* production in 4ℓ (dominant)
   - From $q\bar{q}$ annihilation and gg fusion (subdominant)
2. ZZZ, WZZ and WWZ (small).

3. Hadrons misidentified as leptons:
   - Z+jets $t\bar{t}$ and WZ production
   - Extrapolation to signal region making use of simulation

Based on data

Reconstruction and selection

ATLAS-CONF-2018-028

- Diphoton event selection
  - At least two photon with E_T> 25 GeV
  - Highest E_T pair forms candidate.
  - Vertex identification with Neural Network
    - Vertex within 0.3 mm for 79% of ggH events.

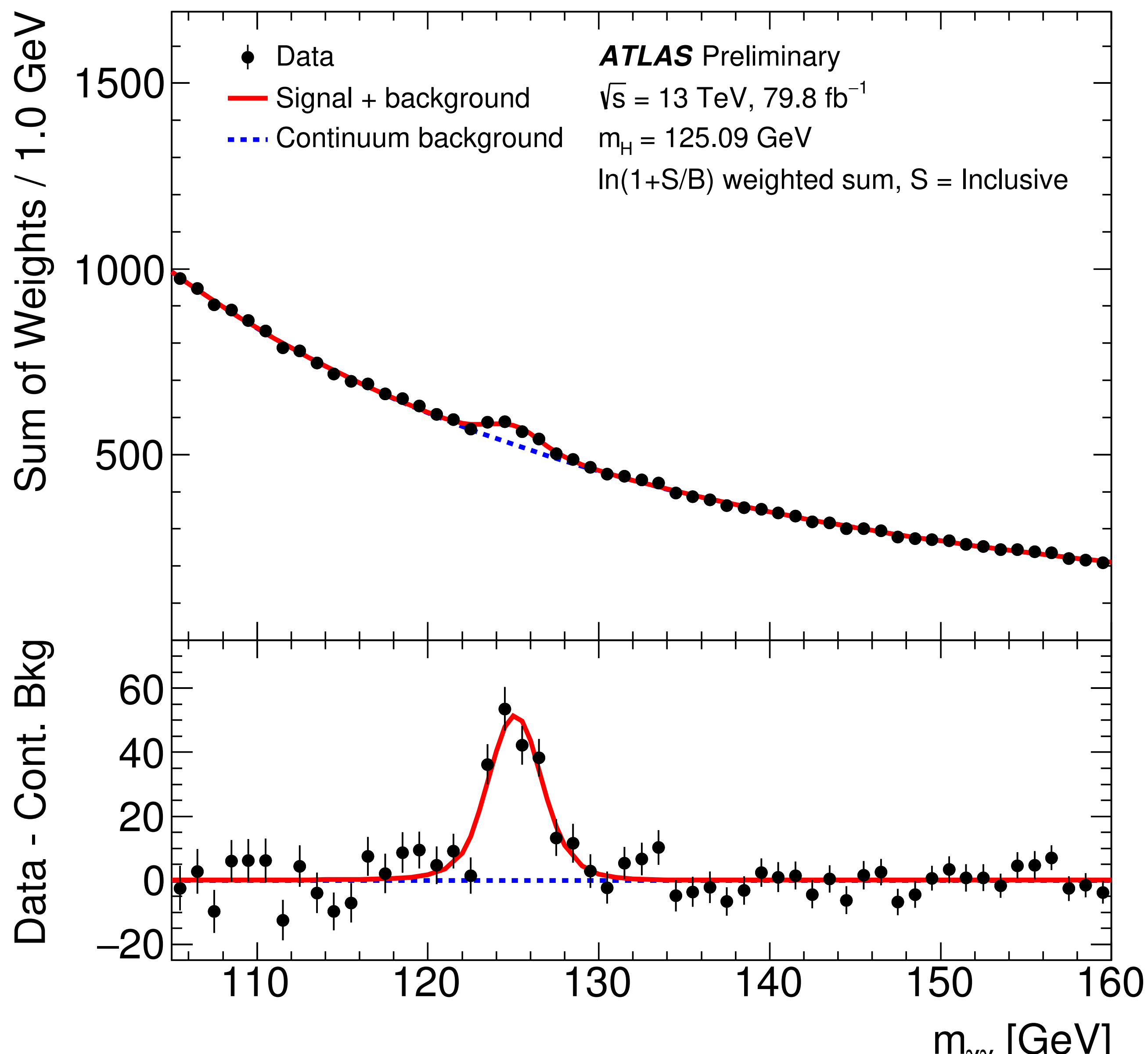

- Background estimation
  - Entirely estimated from data
  - Prompt photons: maximum likelihood fit to $m_{\gamma\gamma}$ spectrum
  - Jets misidentified as photons: from control sample

Reconstruction and selection

arXiv:1808.09054

- $WW^* \to e\nu\mu\nu$ selection
  - Two isolated leptons $p_T(\ell) > 22$ GeV and $p_T(\ell) > 15$ GeV
  - $E_T^{miss} > 20$ GeV
- Signal-to-background discriminants
  - Trasnverse mass (m_T) for ggF production and neural network for VBF production

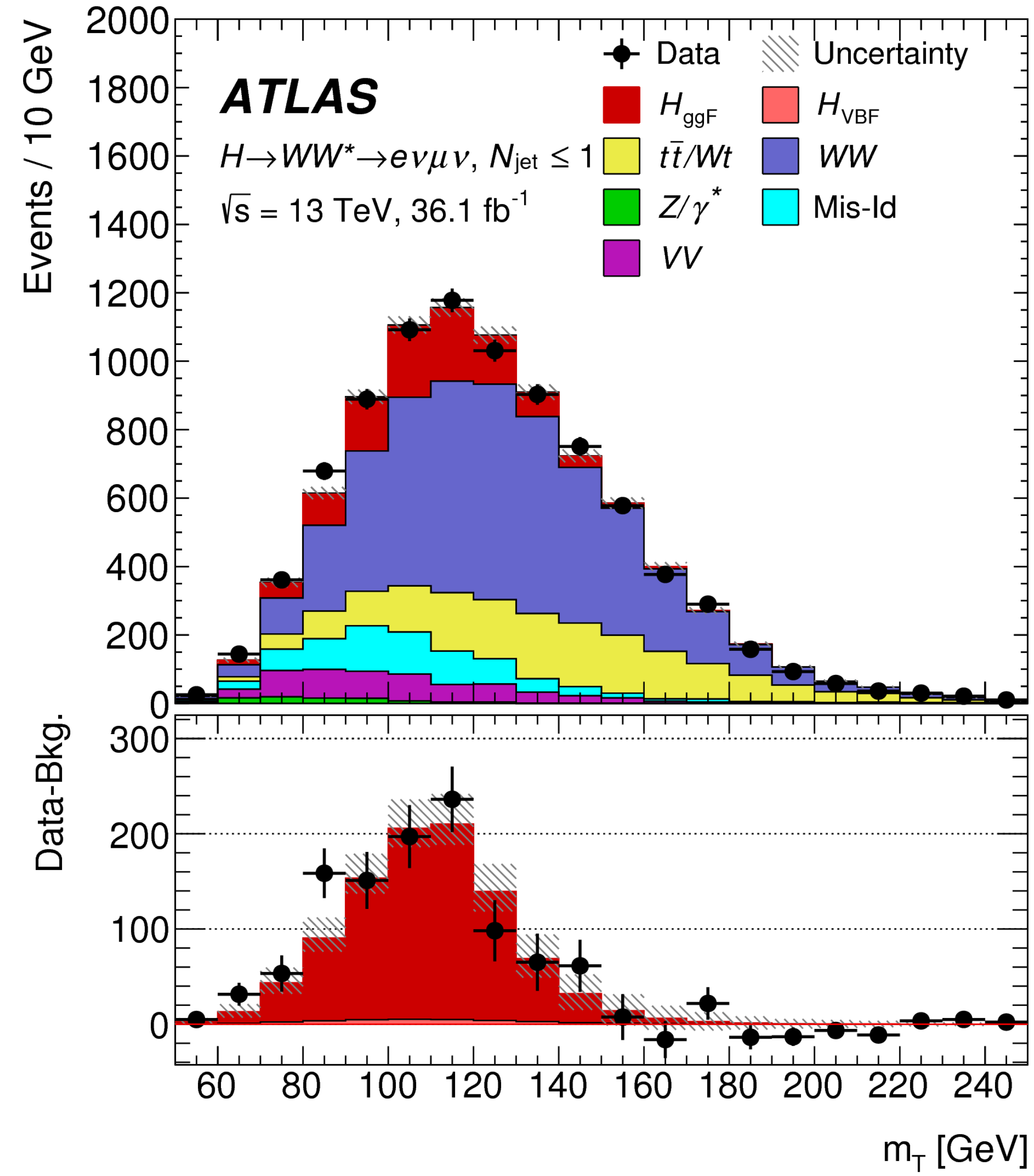

- Background estimation **Based on data**

1. Non resonant WW production
2. $t\bar{t}$ production
3. Drell-Yan: $Z \to \tau^+\tau^-$
4. Hadrons misidentified as leptons:
   - W+jets $t\bar{t}$ and WZ production

5. ZZ^*, WZ, $W\gamma(^*)$ production in
6. Single-top-quark (Wt) production

Based on simulation

Strategy — Production mode

- Cut based classification of events into category.
  - Ex. Jet multiplicity (ggF), m_{jj} for (VBF) and b-tagging ($t\bar{t}H$)
- and multivariate analysis (BDT) to discriminate contributions.
  - $gg\mathrm{F}$ from ZZ^{*}, VBF from $gg\mathrm{F}$, $\mathrm{VH(had)}$ from all.
  - Variables: $p_{\mathrm{T},4\ell}$, KD, η_{j}, $\Delta\eta_{\mathrm{jj}}$, $p_{\mathrm{T},j}$ etc.
- Detector and theoretical uncertainties

(i) Luminosity 3.2%

(ii) Lepton Identification <2%

(iii)Pileup ~2%

(iv)Jet Energy Scale (3%-7%)

(v) Jet Energy Resolution (2%-4%)

(i) μ_R and μ_F about 4% to 30%

(ii) ggF prediction in N_J categories.

(iii)(BSM only NLO/LO prediction)

Differential cross section

- Double differential measurements as a function of rapidity and p_T
- As well as matrix element discriminant between ZZ and H
  - MCFM-based.
- Comparisons with NLO EW and NLO EW and NNLO QCD predictions.

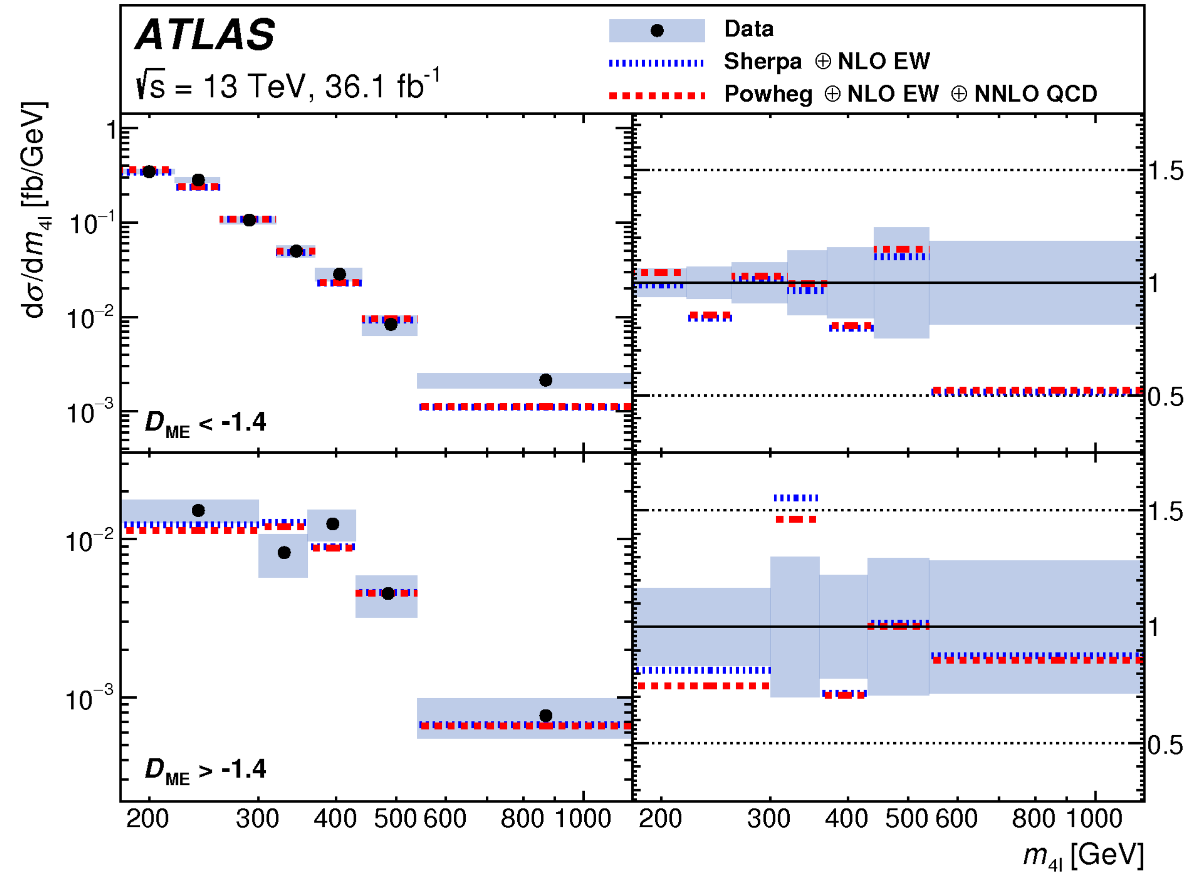

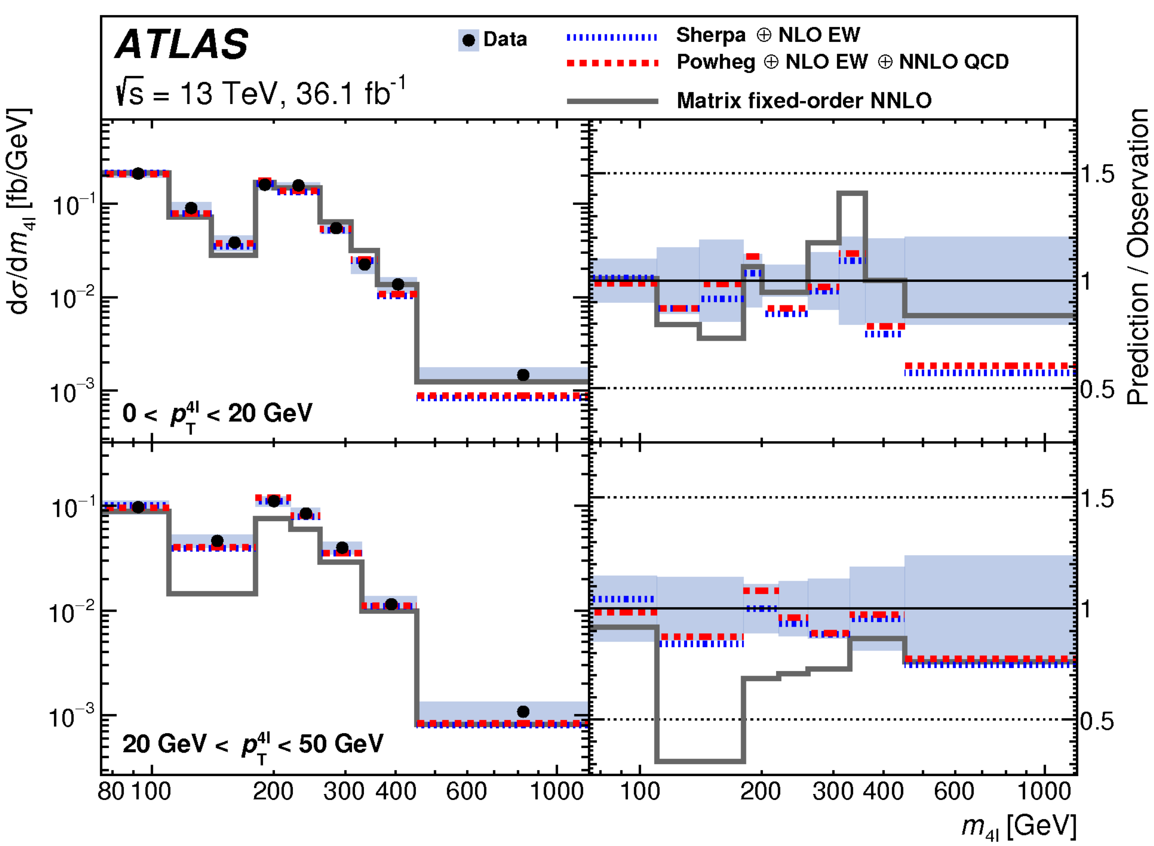

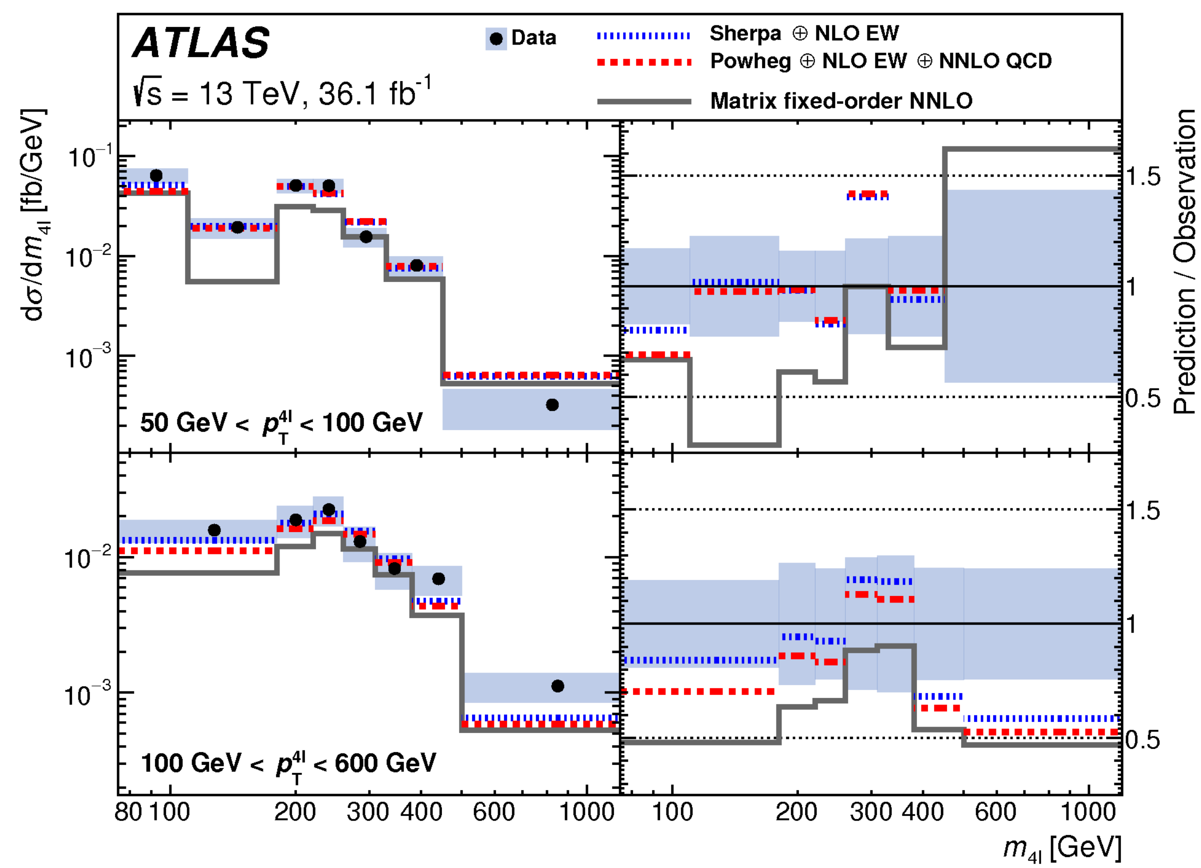

Higgs boson kinematics

- Higgs boson $p_{T,4\ell}$ and rapidity ($y_{4\ell}$) probe:
  - $p_{T,4\ell}$: Lagrangian structure of H interactions.

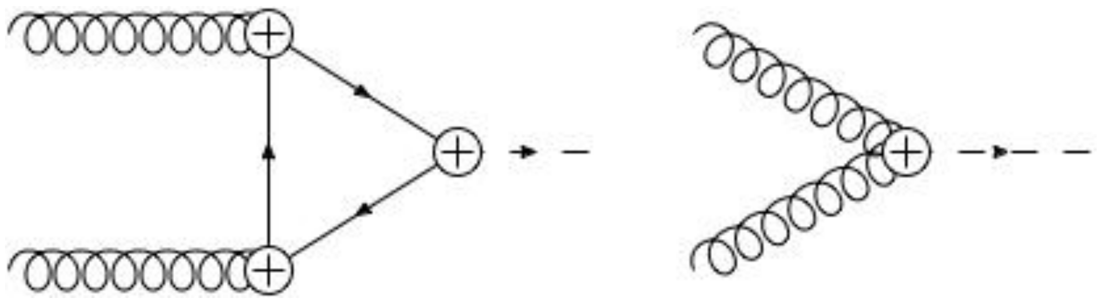

- Small perturbations to SM: dimension 6 operators most effective approach.

$$\frac{c_1}{\Lambda^2}\mathcal{O}_1 \rightarrow \frac{\alpha_S}{\pi v} c_g h G^a_{\mu\nu} G^{a,\mu\nu}\,,$$

c_g: ggH contact interaction

$$\frac{c_2}{\Lambda^2}\mathcal{O}_2 \rightarrow \frac{m_t}{v} c_t h \bar{t} t\,,$$

$$\frac{c_3}{\Lambda^2}\mathcal{O}_3 \rightarrow \frac{m_b}{v} c_b h \bar{b} b\,,$$

c_t: t and b Yukawa couplings

$$\frac{c_4}{\Lambda^2}\mathcal{O}_4 \rightarrow c_{tg}\underbrace{\frac{g_S m_t}{2v^3}(v+h)G^a_{\mu\nu}(\bar{t}_L\sigma^{\mu\nu}T^a t_R + h.c)}_{}$$

c_{tg}: dipole-moment, g-t interaction

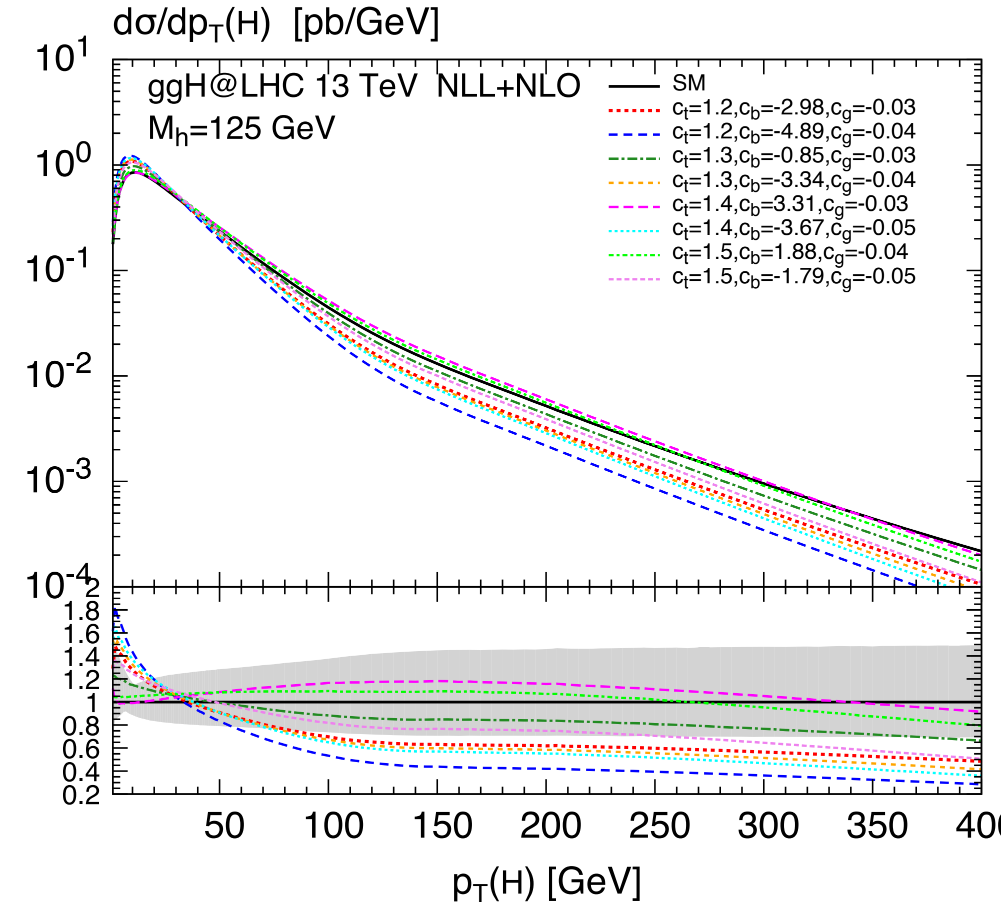

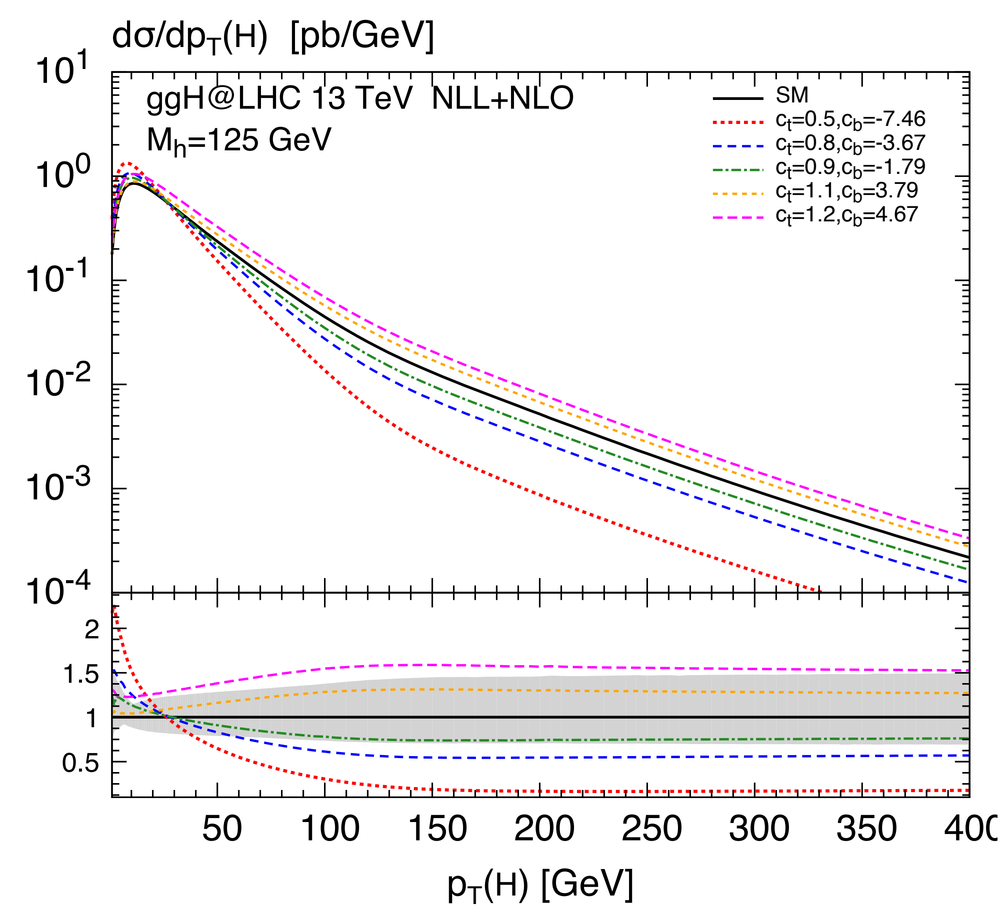

Grazzini *et al.* `arXiv:1612.00283`

- Simultaneous fit to the ggF and VBF categories.
  - Over m_T for ggF and BDT response for ggF
  - Extraction of ggF and VBF total cross sections

$$\mu_{\mathrm{ggF}} = 1.21^{+0.12}_{-0.11}(\mathrm{stat.})^{+0.18}_{-0.17}(\mathrm{sys.})$$

$$\mu_{\mathrm{VBF}} = 0.62^{+0.30}_{-0.28}(\mathrm{stat.}) \pm 0.22(\mathrm{sys.})$$

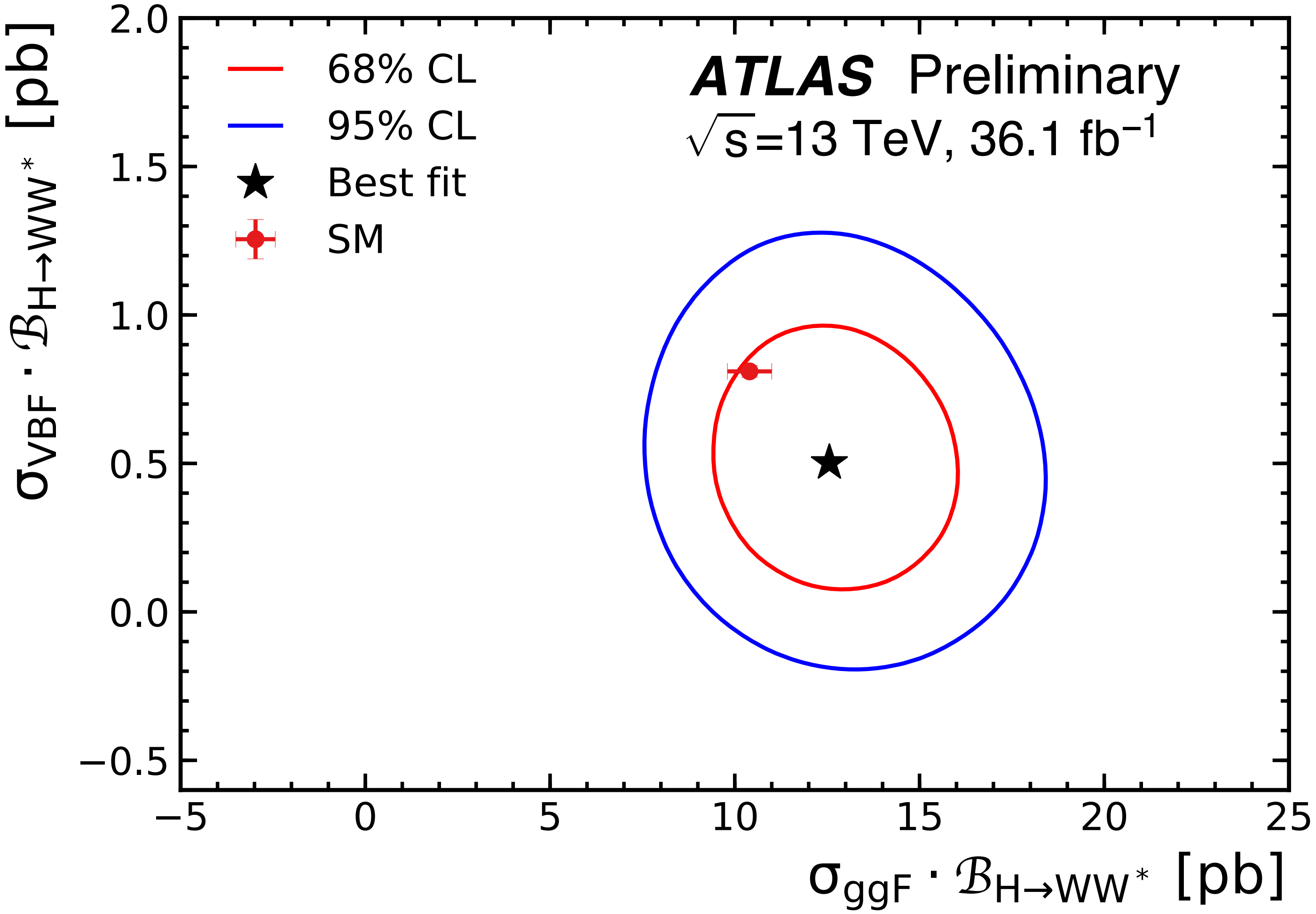

- Significances of 6.3 σ and 1.8 σ for ggF and VBF, respectively

$ZZ\rightarrow 4\ell$ and $\ell\bar{\ell}\nu\bar{\nu}$

- Searches for spin-0 and spin-2 resonances in the $ZZ\rightarrow 4\ell$ and $\ell\bar{\ell}\nu\bar{\nu}$ final states.
  - Upper limits for Type-I and II two-Higgs double models (spin-0) and for RS models (spin-2)
  - Separate sensitivity for ggF and VBF productions (both ATLAS and CMS)
    - ✦ Typical VBF selection: at least two jets with $p_T(j) > 30$ GeV, $\Delta\eta > 3.3$ and $m_{jj} > 400$ GeV
- Resonances searched in $m_{4\ell}$ and m_T
  - Analytical parametrisation of signal.
  - *h*-*H* interference taken into account in the large width approximation

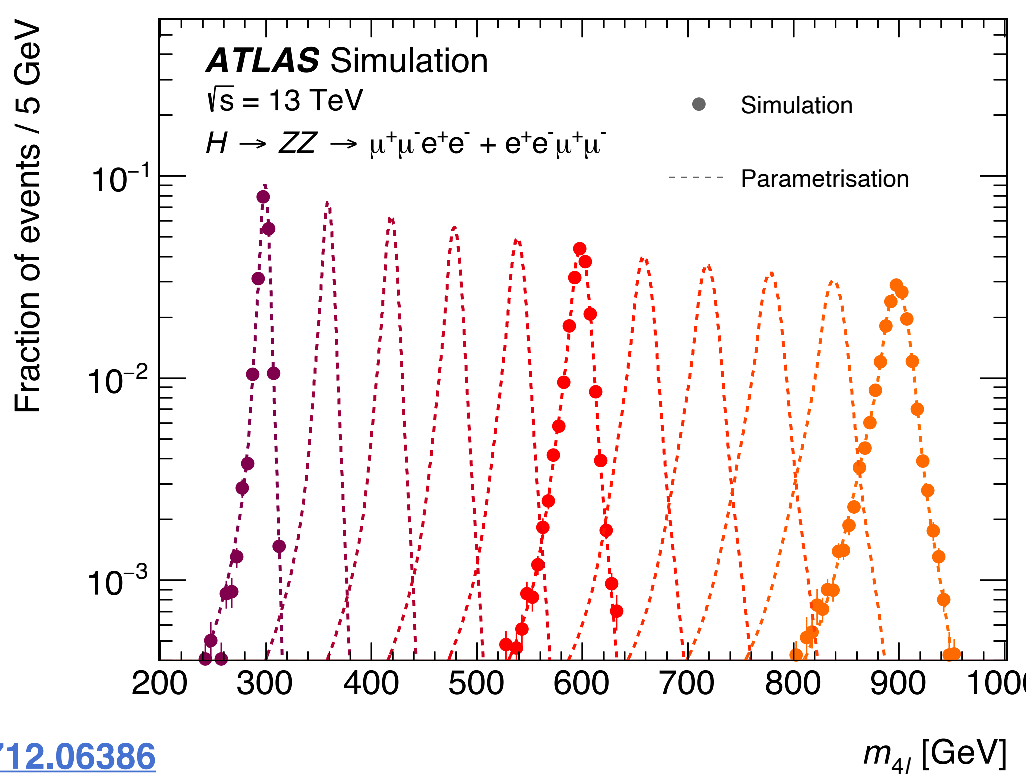

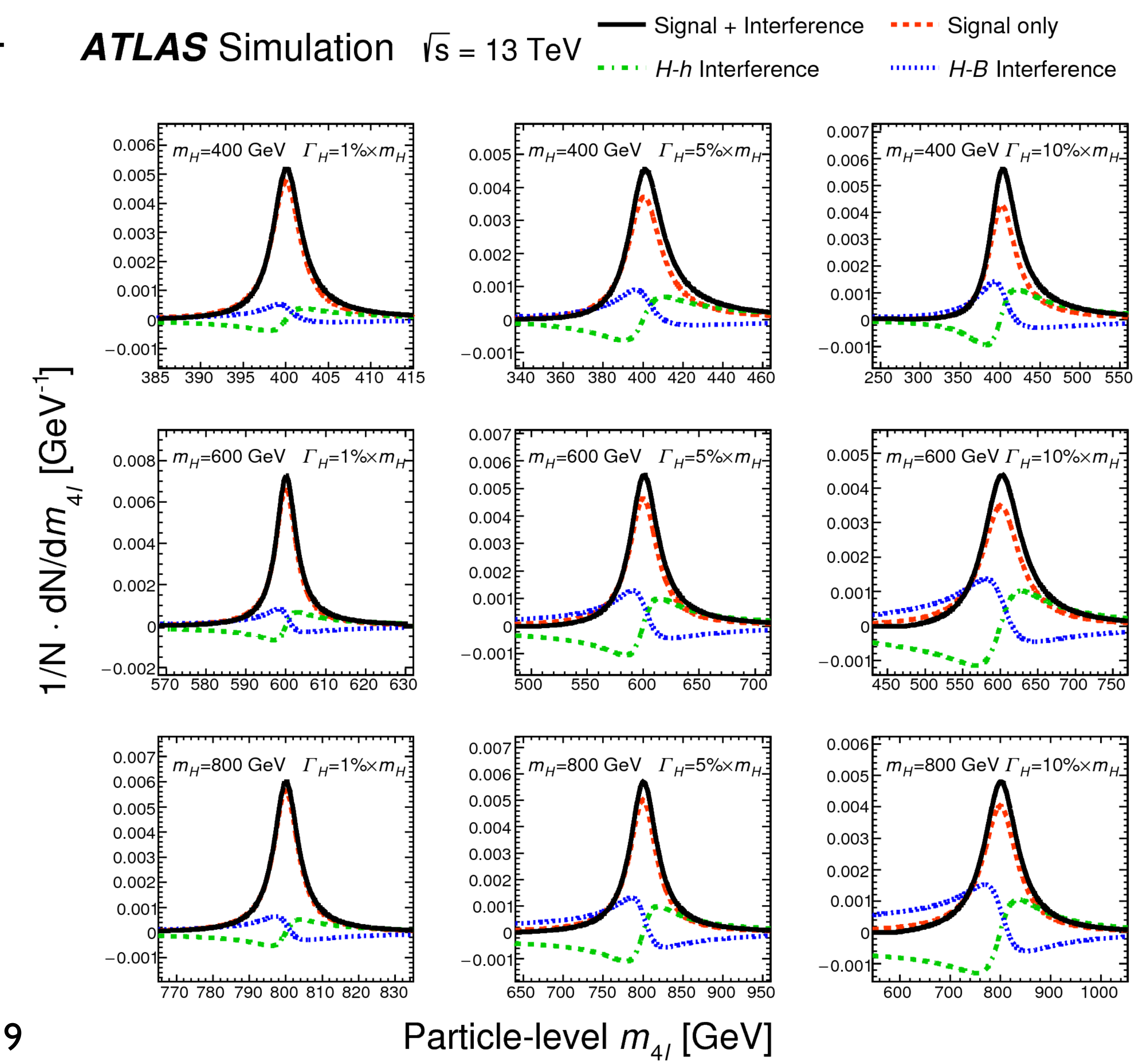

arXiv:1712.06386

$ZZ\rightarrow 4\ell$ and $\ell\bar{\ell}\nu\bar{\nu}$

- Searches for spin-0 and spin-2 resonances in the $ZZ(\rightarrow 4\ell$ and $\ell\bar{\ell}\nu\bar{\nu})$ channel
- Spin-0 resonance limits
  - Narrow width: 0.68 pb at m_H= 242 GeV to 11 fb at m_H= 1.2 TeV
  - Large width as a function of 1%, 5% and 10% of m_H

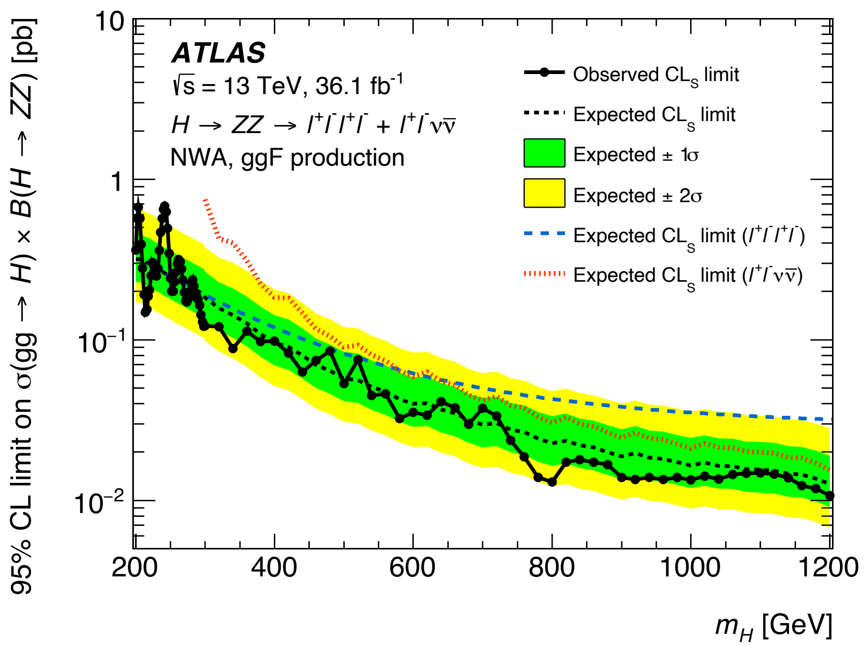

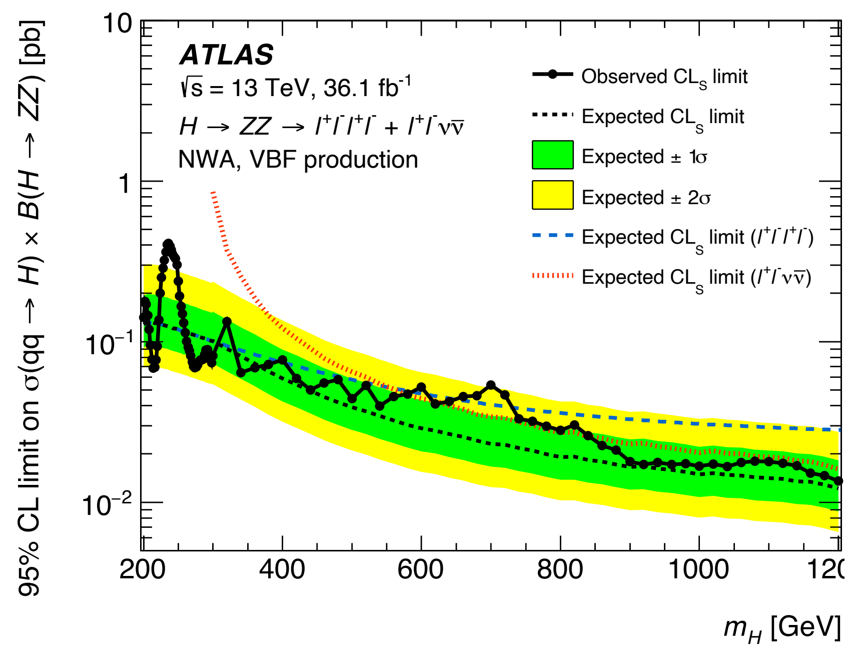

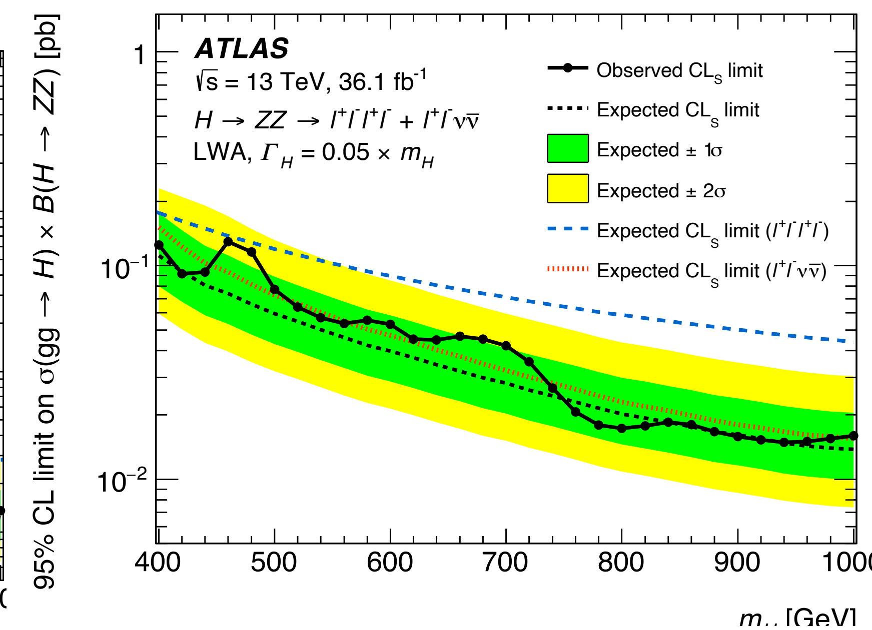

- Interpretation in context of 2HDM
  - No direct coupling of Higgs to leptons, only Type II and I considered.
  - Relative ggF to VBF rates fixed to 2HDM predictions for *m_H= 200 GeV.*
    - ✦ *NWA valid across wide range and maximal experimental sensitivity*

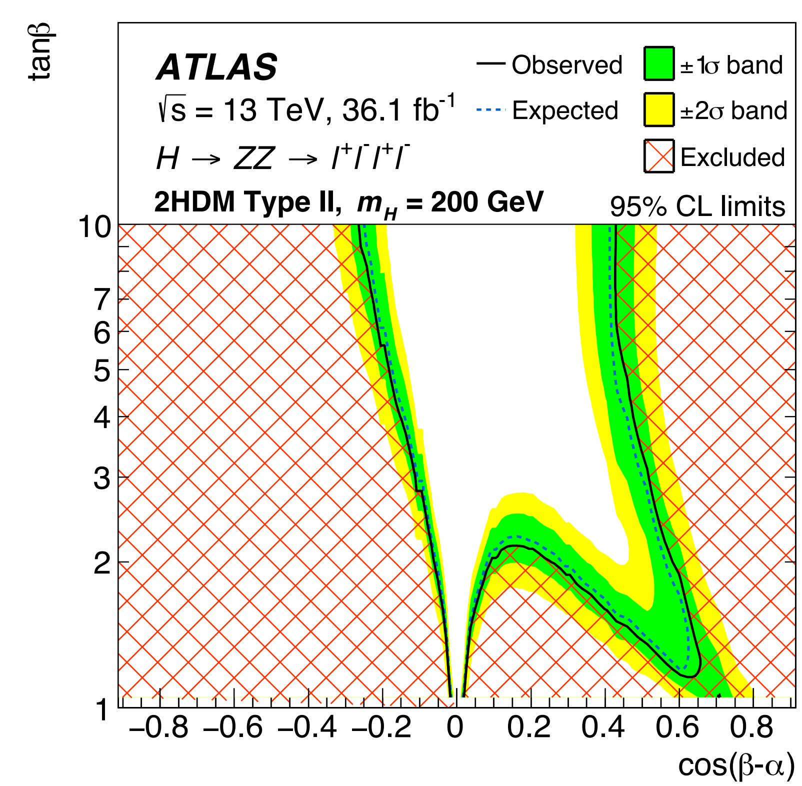

arXiv:1712.06386

- Improved statistical sensitivity
  - reduced correlations between production modes.
- Statistical and systematic uncertainties of the same size.

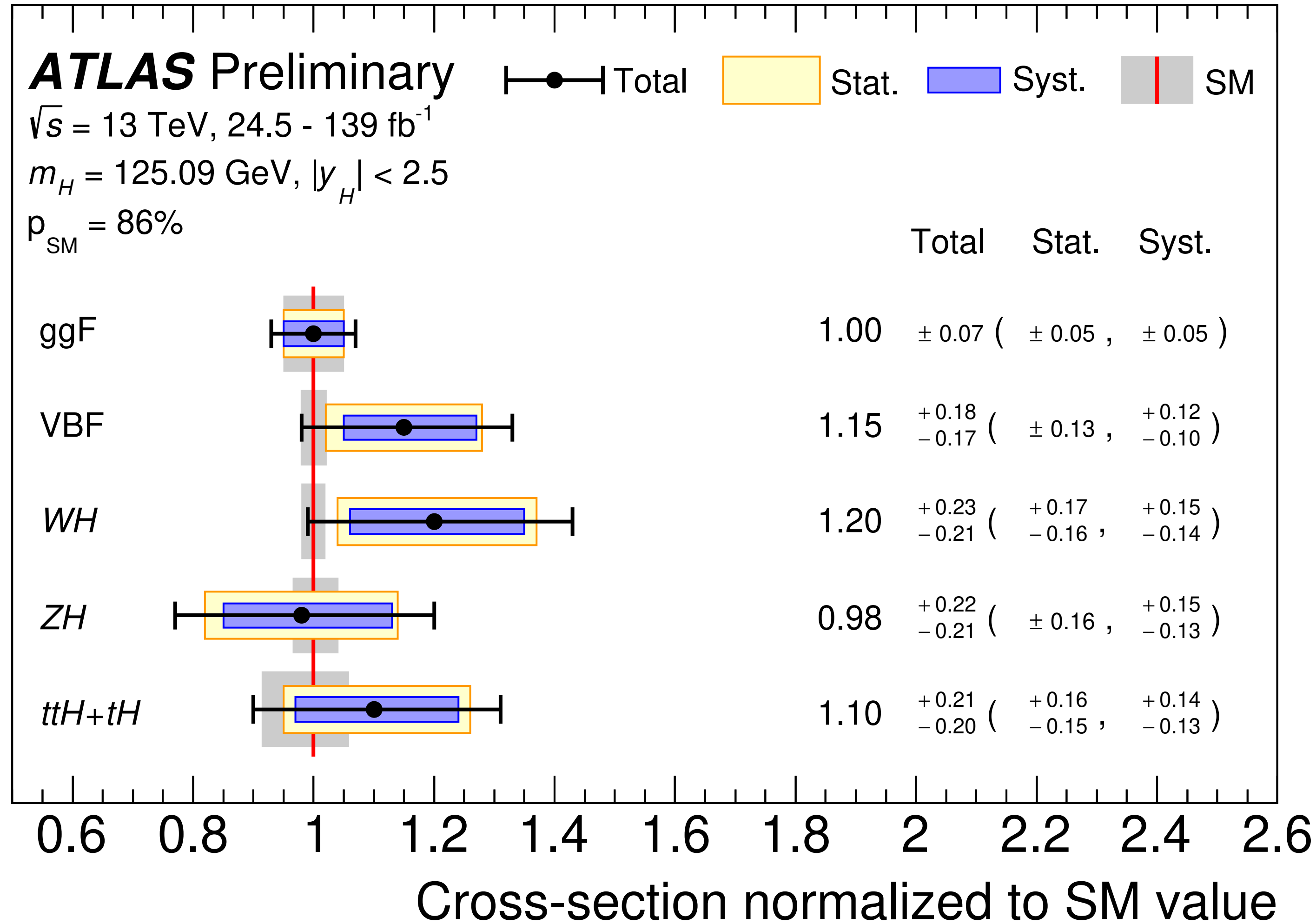

Process ($\lvert y_H \rvert < 2.5$)	Value [pb]	Uncertainty [pb] Total	Stat.	Syst.	Exp.	Sig. Th.	Bkg. Th.	SM pred. [pb]
ggF	44.7	± 3.1	± 2.2	± 2.2	$^{+1.8}_{-1.7}$	$^{+1.0}_{-0.9}$	$^{+0.9}_{-0.7}$	44.7 ± 2.2
VBF	4.0	± 0.6	± 0.5	± 0.4	$^{+0.3}_{-0.2}$	± 0.3	± 0.1	$3.51\ ^{+0.08}_{-0.07}$
WH	1.45	$^{+0.28}_{-0.25}$	$^{+0.20}_{-0.19}$	$^{+0.18}_{-0.17}$	$^{+0.13}_{-0.12}$	$^{+0.08}_{-0.06}$	$^{+0.10}_{-0.09}$	1.204 ± 0.024
ZH	0.78	$^{+0.18}_{-0.17}$	± 0.13	$^{+0.12}_{-0.10}$	$^{+0.08}_{-0.07}$	$^{+0.07}_{-0.05}$	± 0.06	$0.797\ ^{+0.033}_{-0.026}$
$t\bar{t}H + tH$	0.64	± 0.12	± 0.09	± 0.08	$^{+0.06}_{-0.05}$	$^{+0.03}_{-0.02}$	± 0.05	$0.59\ ^{+0.03}_{-0.05}$